THE UNIVERSITY
of EDINBURGH

REGULATION OF SKELETAL MINERALISATION BY PHOSPHO1

Dean Alexander Houston

This thesis is presented for the degree of Doctor of Philosophy at The University of Edinburgh

2016

Declaration

I declare that this thesis has been composed entirely by the candidate, Dean Alexander Houston. This work has not previously been submitted for any other degree or professional qualification. I have done all the work, unless acknowledged otherwise. All sources of information have been acknowledged.

Dean Alexander Houston

Acknowledgments

I would firstly like to thank my supervisors Prof. Colin Farquharson and Dr Vicky MacRae for their outstanding supervision and advice throughout my PhD. My primary supervisor, Colin, has not only given me tremendous academic support but is also the reason I have had so many fantastic experiences over the past four years. For these reasons I must pay him a special thank you.

A big thank you must be paid to all the members of the bone biology group, past and present, who helped introduce me to the world of bone and who have always been on hand to provide support, troubleshooting advice and laughter. In particular, I would like to thank Dr Katherine Staines for her words of ‘motivation’ over the past two years. Dr Ross Dobie, Dr Karla Oldknow, Dr Carmen Huesa and Elaine Seawright are due thanks for showing me the ways of the lab in the early years and for their daily humour and assistance. I am also grateful to all the people within The Roslin Institute who have given me advice during my time here.

Finally, I must acknowledge my incredible friends, mother, grandmother and partner, Rachel. They have put up with, and supported me through this demanding period and their love and encouragement has been greatly appreciated.

Abstract

PHOSPHO1 is a skeletal specific phosphatase whose activity towards the lipid metabolites, phosphocholine (PCho) and phosphoethanolamine (PEth), results in the generation of inorganic phosphate (P_i) within matrix vesicles (MV). PHOSPHO1 activity is essential for the initiation of biomineralisation. The genetic ablation of *Phospho1* results in severe hypomineralisation of the skeleton and dentition. Neutral sphingomyelinase 2 (nSMase2, encoded by the *Smpd3* gene) catalyses the breakdown of the membrane lipid sphingomyelin to generate ceramide and PCho. Similar hypomineralisation of the skeleton is noted in the *Smpd3*$^{-/-}$ mouse. This observation led to the hypothesis that nSMase2 and PHOSPHO1 work in tandem for the generation of P_i within MV.

Despite knowledge of the phenotype associated with the absence of *Phospho1* or *Smpd3*, little is known about the expression profiles of these genes during the initiation of extracellular matrix (ECM) mineralisation, or the regulation of these genes. This thesis characterised the expression of *Phospho1*, *Smpd3* and other key genes associated with ECM mineralisation in *in vitro* models of mineralisation under exogenous phosphatase substrate-free conditions. Additionally, building on preliminary work in osteocytes, the regulation of *Phospho1* and *Smpd3* by parathyroid hormone (PTH) was investigated both *in vitro* and *in vivo*.

Characterisation of MC3T3 osteoblast-like cell cultures, primary calvarial osteoblast and embryonic metatarsal organ cultures similarly revealed simultaneous and striking increases in the expression of PHOSPHO1 and nSMase2 prior to the onset of ECM

mineralisation. In *Phospho1*$^{-/-}$ cell and organ cultures, ECM mineralisation was markedly diminished, and nSMase2 expression was notably reduced.

The parathyroid hormone (PTH) regulation of *Phospho1* and *Smpd3* in osteocytes was confirmed in MC3T3 osteoblast-like cell cultures. *Phospho1* and *Smpd3* mRNA expression was strongly and rapidly (within 15 minutes) inhibited by PTH. Experiments with cycloheximide revealed that this was a direct effect not requiring protein synthesis. Further experimentation utilising the adenylyl cylase agonist, Forskolin and the PKA inhibitor, PKI (5-24), identified the cAMP-PKA signalling pathway as the mediator of the effects of PTH on *Phospho1* and *Smpd3* expression. In contrast, however, primary calvarial osteoblasts, human subchondral bone osteoblasts and murine embryonic metatarsal cultures all displayed an upregulation of *Phospho1* expression in response to a 24 h exposure to PTH. Although informative, these findings highlighted the need to investigate the PTH regulation of *Phospho1 in vivo*.

The administration of PTH (80 µg/kg) enhanced the expression of *Phospho1* and *Smpd3* within 6 h and after 14 and 28-day intermittent exposure in the distal femur of male wild-type mice. The expression of the transcription factors, *Runx2* and *Trps1*, which have been implicated in the regulation *Phospho1* were similarly upregulated by these PTH exposures. I hypothesised that the upregulation of *Phospho1* could provide a novel mechanism explaining the osteoanabolic effects of intermittent PTH (iPTH). Bone microarchitecture in response to iPTH was assessed in the tibiae of WT and *Phospho1*$^{-/-}$ mice by micro computed tomography. The absence of *Phospho1* limited the anabolic effects of PTH in cortical bone but not in the metaphyseal trabecular bone.

The work described within this thesis provides further evidence of the cooperative functions of nSMase2 and PHOSPHO1 in the initiation of skeletal mineralisation. The potent regulation of these enzymes *in vivo* by PTH offers an additional explanation of the anabolic effects of iPTH and forms part of an emerging body of evidence seeking to understand the regulation of these enzymes.

Lay summary

Despite appearances, the bone and cartilage which comprise the vertebrate skeleton are incredibly dynamic tissues. Bone is a composite material, comprising a flexible and durable collagenous scaffold onto which a calcium and phosphorous based mineral is deposited which provides strength and rigidity to the skeleton. This mineralisation of bone ensures that the skeleton can carry out its primary functions as a store of the essential minerals, calcium and phosphorous, as a protective armour to the vital organs and, as a resilient point of attachment for the body's musculature.

In 1999, an enzyme specific to the skeleton, named PHOSPHO1, was discovered. PHOSPHO1 is involved in the generation of a key component of the mineral phase of bone, phosphorous. As such, PHOSPHO1 is essential for successful mineralisation of the skeleton. Studies utilising genetically modified mice revealed that the absence of PHOSPHO1 gives rise to an inadequately mineralised skeleton which results in bowing of the long bones and greenstick fractures. Despite our understanding of the function of this enzyme, little is known about how and when, the gene which encodes the PHOSPHO1 enzyme is turned on and off (i.e. its expression).

In this thesis, I have developed and characterised models of skeletal mineralisation, utilising cells and indeed whole bones derived from new born or embryonic mice. These models revealed that *Phospho1* is expressed in advance of the mineralisation events, highlighting its importance in facilitating this process. In addition, this thesis provides the first evidence that parathyroid hormone, a major regulator of calcium levels in the body and important therapeutic in the treatment of osteoporosis, can potently regulate the expression of *Phospho1* in the bones of mice.

The findings of this thesis help to expand the knowledge surrounding the process of mineralisation. This knowledge helps not only our understanding of bone mineralisation pathologies, but also those of vascular mineralisation. In addition, my findings that parathyroid hormone enhances *Phospho1* expression may provide a novel explanation for the therapeutic success of this agent in the treatment of low bone mass.

Publications

Original peer reviewed publications

Houston DA, Myers K, Little K, Hopkinson M, Pitsillides AA, Millan JL, MacRae VE, Staines KA and Farquharson C (2016). PHOSPHO1 modulates the osteoanabolic effects of intermittent PTH. In preparation.

Houston DA, Staines KA, MacRae VE and Farquharson C (2016). Culture of Murine Embryonic Metatarsals: A Physiological Model of Endochondral Ossification. *Journal of Visualized experiments*, 118.

Houston DA, Myers K, MacRae VE, Staines KA and Farquharson C (2016). The expression of PHOSPHO1, nSMase2 and TNAP is coordinately regulated by continuous PTH exposure in mineralising osteoblast cultures. *Calcified tissue international and Musculoskeletal Research,* 99(5): 510-24

Huesa C[*], **Houston DA**[*], Kiffer-Moreira T, Yadav MM, Millan JL and Farquharson C (2015). The Functional co-operativity of Tissue-Nonspecific Alkaline Phosphatase (TNAP) and PHOSPHO1 during initiation of Skeletal Mineralization. *Biochemical and Biophysical Reports,* 1(4): 196-201.

Javaheri B, Carriero A, Staines KA, Chang YM, **Houston DA**, Oldknow KJ, Millan JL, Kazeruni BN, Salmon P, Shefelbine S, Farquharson C and Pitsillides AA (2015). Phospho1 deficiency transiently modifies bone architecture yet produces consistent modification in osteocyte differentiation and vascular porosity with ageing. *Bone* 8:277-291.

*Denotes joint first authorship

Review articles

Cui L, **Houston DA**, Farquharson C and MacRae VE (2016). Characterisation of matrix vesicles in skeletal and soft tissue mineralisation. *Bone* 87:147-58.

Published abstracts

Houston DA, Myers K, MacRae VE, Anish AK, Pitsillides AA, Millan JL, Staines KA and Farquharson C (2016). Does PHOSPHO1 regulates bone's response to PTH?

Frontiers in Bone Research (in press). The Bone Research Society (Liverpool), oral communication.

Houston DA, Myers K, MacRae VE, Millan JL, Staines KA and Farquharson C (2015). Contrasting effects of parathyroid hormone on PHOSPHO1 and alkaline phosphatase expression during osteoblast mineralization. *Journal of Bone and Mineral Research* (2015). The American Society of Bone and Mineral Research (Seattle), poster presentation.

Houston DA, Myers K, MacRae VE, Millan JL, Staines KA and Farquharson C (2015). Differential effects of parathyroid hormone on key regulators of osteoblast mineralisation. *Endocrine Abstracts 38:P7*. The Society of Endocrinology (Edinburgh), poster presentation.

Houston DA, Myers K, MacRae VE, Millan JL, Staines KA and Farquharson (2015). Differential effects of PTH on key regulators of osteoblast mineralisation. *Frontiers in Bone Research.* The Bone Research Society (Edinburgh), poster presentation.

Houston DA, Millan JL, Huesa C, MacRae VE and Farquharson C (2014). Understanding the roles of PHOSPHO1 and SMPD3 in the initiation of skeletal mineralisation. *Frontiers in Bone Research.* The Bone Research Society (Sheffield), oral communication.

Houston DA, Huesa C, Millan JL, MacRae VE and Farquharson C (2013). Development of novel model systems to reveal the role of PHOSPHO1 in the initiation of skeletal mineralisation. *Frontiers in Bone Research.* The Bone Research Society (Oxford), oral communication.

Awards

The Bone Research Society, New Investigator Award - **2016**

The Roslin Institute Student Day, Best Oral Presentation (runner up) - **2016**

The College of Medicine and Veterinary Medicine, Barnson Bequest Award - **2015**

Primer Design Student Sponsorship (Gold award) - **2013**

Travel grants

R(D)SVS, Birrell-Gray Travelling Scholarship – **2015**

The Bone Research Society, Travel Award – **2015**

Universitas 21, Graduate Research Conference Grant - **2014**

The Bone Research Society, Barbara Mawer Travelling Fellowship - **2014**

Abbreviations

βGP	β-glycerophosphate
µCT	Micro computed tomography
AC	Adenylyl cyclase
ADP	Adenosine diphosphate
ACP	Amorphous calcium phosphate
Anx	Annexins
ATF4	Activating transcription factor 4
Alpl	Tissue non-specific alkaline phosphatase (gene)
ANK	Progressive ankylosis
ANOVA	Analysis of variance
ASARM	Acidic serine- and aspartate- rich motif
ATP	Adenosine triphosphate
Atp5b	ATP synthase, H^+ transporting, mitochondrial F1 complex, beta polypeptide (gene)
Bglap	Bone gamma-carboxyglutamate protein (gene)
BLCs	Bone lining cells
BMD	Bone mineral density
BMP	Bone morphogenetic protein
BMU	Basic multicellular unit
BSA	Bovine serum albumin
BV/TV	Bone volume fraction
Ca^{2+}	Calcium
cAMP	Cyclic adenosine monophosphate
Cas9	CRISPR associated protein 9
cDNA	Complimentary DNA
Chkα/β	Choline kinase alpha/beta (genes)
CK	Choline kinase
CO_2	Carbon dioxide
cPTH	continuous PTH
CRISPR	clustered, regularly interspaced, short palindromic repeats
CREB	cAMP response element binding protein
CTX-1	C-terminal telopeptides of type I collagen
Cyp27b1	Cytochrome P450 family 27 subfamily B member 1 (gene)
DAB	Diaminobenzidine
DAG	Diacylglycerol
dH_2O	Distilled water
Dlx5	Distal-less homeobox 5
DMEM	Dulbecco's modified eagle medium
DMP1	Dentin matrix protein 1
DMSO	Dimethyl sulfoxide

DNA	Deoxyribonucleic acid
dNTP	deoxyribonucleotide triphophosphate
DTT	Dithiothreitol
ECM	Extracellular matrix
EDTA	Ethylenediaminetetraacetic acid
Enpp1	Ectonucleotide pyrophosphatase/ phosphodiesterase 1 (gene)
ENU	N-ethyl-N-nitrosurea mutagenesis
EV	Empty vector
FBS	Foetal bovine serum
FGF23	Fibroblast growth factor 23
FP1	FLAG-tagged PHOSPHO1
fro	*fragilitas ossium*
GACI	Generalised calcification of infancy
GPCR	G protein coupled receptor
HA	Hydroxyapatite
HAD	Haloacid dehalogenase
HBSS	Hank's balanced salt solution
HPP	Hypophosphatasia
HRP	Horseradish peroxidase
Ibsp	Bone sialoprotein (gene)
IFN-γ	Interferon gamma
IgG	Immunoglobulin G
Ihh	Indian hedgehog
iPTH	intermittent PTH
LC	liquid chromotography
LP	Lysophospholipids
LPC	Lysophosphatidylcholine
LRP	low-density lipoprotein receptor-related protein
MEPE	Matrix extracellular phosphoglycoprotein
MGP	Matrix gla protein
MOPS	3-(N-morpholino) propanesulfonic acid
mRNA	Messenger ribonucleic acid
MS	Mass spectrometry
MSC	Mesenchymal stem cells
MV	Matrix vesicle
NFW	Nuclease free water
nSMase2	Neutral sphingomyelinase 2
OCN	Osteocalcin
OPG	Osteoprotegerin
OPN	Osteopontin
PBS	Phosphate buffered saline
P1NP	procollagen type I N-terminal propeptide

PC	Phosphatidylcholine
PCho	Phosphocholine
PCR	Polymerase chain reaction
PE	Phosphatidylethanolamine
PEth	Phosphoethanolamine
PFA	Paraformaldehyde
PHOSPHO1	Phosphatase orphan 1
Pi	Inorganic phosphate
PI	Phosphatidylinositol
PiT	Inorganic phosphate transporter
PKI (5-24)	cAMP-dependent protein kinase inhibitor (5-24)
PMA	Phorbol myristate acetate
PPi	Inorganic pyrophosphate
PPI	Proton pump inhibitor
PS	Phosphatidylserine
PTH	Parathyroid hormone
PTH1R	Parathyroid hormone 1 receptor
PTHrP	Parathyroid hormone related peptide
PXE	Pseudoxanthoma elasticum
qPCR	Quantitative PCR
RANKL	Receptor activator of nuclear factor kappa B ligand
RIPA	Radio-immunoprecipitation assay
RNA	Ribonucleic acid
RNase	Ribonuclease
RT	Reverse transcription
Runx2	Runt-related transcription factor 2
SDS	Sodium dodecylsulphate
SEM	Standard error of the mean
SIBLING	Small integrin-binding ligand N-linked glycoprotein
SM	Sphingomyelin
Smpd3	Sphingomyelin phosphodiesterase 3 (gene)
SOST	Sclerostin
SOX9	Sex determining region Y-box 9
Sp7	Sp7 transcription factor 7 (encodes Osterix, gene)
Spp1	Secreted phosphoprotein 1 (gene)
T3	3,5,3'-triiodothyronine
TGFβ	Transforming growth factor beta
TNAP	Tissue non-specific alkaline phosphatase
Tb.Sp	trabecular separation
Tb.Th	trabecular thickness
Tb.N	trabecular number
Tb.Pf	trabecular pattern factor

TRAF-6	tumour necrosis factor receptor associated factor 6
Trps1	Transcriptional repressor GATA binding 1 (gene)
Vdr	Vitamin D receptor (gene)
WT	Wild-type

Table of contents

Chapter 1

Introduction

1.1. The structure and function of bone

Bone is often considered to be a lifeless, inert structure. This could not be further from reality. Bone is in fact a composite tissue which, through the tightly choreographed actions of numerous cell types, undergoes dynamic reconstruction throughout life. The combination of organic and inorganic material properties produces a flexible and durable, yet resistant and robust material which is capable of serving its many functions, such as in the protection of the vital organs, as a site of attachment for the musculature of the body and as an adaptable store of mineral ions (Farquharson and Staines, 2011). More recently, bone has been shown to be a systemic regulator of energy metabolism and reproduction, highlighting its role as an endocrine organ (Oldknow et al., 2015).

The mineralised extracellular matrix (ECM) of bone may take two distinct forms at the macro-level; cortical (compact), which forms the outer surface of flat bone and the shaft of the long bones, and trabecular (cancellous), found sandwiched between the compact bone of the flat bones and within the interior of the ends of long bones. Comprising around 80% of the total bone mass, cortical bone is composed or numerous osteons (Brandi, 2009). These osteons are formed from concentric rings of bone, or lamellae, surrounding a central Haversian canal through which vasculature, lymphatic and neural tissues penetrate to supply the bone. These microstructures afford cortical bone the ability to resist axial and torsional loads. Cancellous bone on the other hand, does not contain a Haversian system, but rather is composed of numerous thin trabeculae which exist in a highly organised 3D structure. The individual trabecular are arranged with respect to the prevailing mechanical loads acting on the bone

(Sommerfeldt and Rubin, 2001). The 3D structure of trabecular bone gives rise to a large surface area which allows cancellous bone to be more metabolically active than cortical bone. This results in a bone that is remodelled more quickly that compact bone.

1.2. Bone formation

1.2.1 Intramembranous ossification

Much of the vertebrate skull, the sternum, scapula and clavicle are derived through the process of intramembranous ossification (Franz-Odendaal, 2011). The sesamoid bones (*e.g.* the patella) and bone formation following some fractures types are also mediated by this process (Schindeler et al., 2008). Intramembranous ossification occurs directly via the condensation and differentiation of neural-crest derived mesenchymal osteochondroprogenitor cells. Primarily under the control of Runx2, these cells differentiate into osteoblasts which secrete and mineralise a collagenous ECM (Komori, 2010). Occasionally, osteoblasts become entrapped in this mineralised ECM and develop into osteocytes, although the majority continue to secrete osteoid which separates them from the mineralising tissue. The mesenchymal cells on the perimeter of the ossifying bone remain and form the periosteum (Franz-Odendaal, 2011).

1.2.2. Endochondral ossification

In contrast to intramembranous ossification, endochondral ossification involves the progressive replacement of a cartilage anlage with bone ECM which is subsequently mineralised. Endochondral ossification is the process by which the majority of the vertebrate skeleton is formed. The cartilage model of the prospective bone initially arises through the condensation of lateral plate mesoderm-derived mesenchymal precursor cells at the future sites of skeletal development (Provot and Schipani, 2005).

Under the influence of the transcription factor Sox9, cells within these condensations differentiate into chondrocytes that proliferate and secrete a type II collagen and proteoglycan-rich ECM (Kronenberg, 2003). Chondrocyte proliferation within the cartilage model supports its expansion. Chondrocytes then progress through morphologically distinct zones, regulated by endocrine and paracrine factors. Parathyroid hormone related peptide (PTHrP) and Indian hedgehog (Ihh) are the key regulators of this progression of chondrocytes through the zones of the growth plate. In the developing bone, PTHrP is synthesised exclusively by perichondral cells and chondrocytes at the epiphyses of the prospective bone (Kronenberg, 2006). PTHrP, acting through the PTH 1 receptor (PTH1R), simultaneously maintains chondrocyte proliferation whilst delaying their further differentiation. Only those chondrocytes sufficiently distant to the source of PTHrP production are able to initiate further differentiation. The differentiation of proliferative chondrocytes to pre-hypertrophic chondrocytes brings about the synthesis of Ihh (Kronenberg, 2005). Ihh acts to maintain the proliferative chondrocyte phenotype both directly, and indirectly through the upregulation of PTHrP in the epiphyseal chondrocytes. Furthermore, Ihh acts on the cells of the perichondrium stimulating their differentiation into osteoblasts (Kronenberg, 2003). These osteoblasts eventually form a bone collar extending around the cartilage anlage and ultimately form the periosteum. Thus, the PTHrP/Ihh feedback loop tightly controls the pool of proliferating chondrocytes in the growth plate and the site of formation of the bone collar. After cessation of proliferation, chondrocytes initiate a genetic program which stimulates a substantial volume expansion or hypertrophy. This hypertrophy is critical for longitudinal bone growth. In addition, hypertrophic chondrocytes direct the mineralisation of the surrounding ECM through

the release of specialised extracellular nano-structures, termed matrix vesicles (MVs)(Bonucci, 1967, Anderson, 1969) (see section 1.4.2.). Vascular invasion of the prospective bone is also regulated by hypertrophic chondrocytes which secrete vascular endothelial growth factor (Mackie et al., 2011). Blood vessel infiltration of the cartilaginous ECM allows the simultaneous invasion of osteoblasts, which secrete and mineralise a bone specific ECM utilising the existing chondrocyte ECM as a scaffold, and haematopoetically derived osteoclasts which resorb the chondrocyte remnants and much of the cartilaginous matrix (Mackie et al., 2008). These processes establish the primary ossification centre (Figure 1.1). Secondary ossification centres are later established at the epiphyses of the bone, demarcating two cartilaginous growth plates, which are responsible for the linear growth of the bone during postnatal life (Farquharson and Jefferies, 2000).

1.2.3. Appositional bone growth

Appositional growth, whereby osteoblasts, primarily in the diaphysis of the bone, form new bone on the perimeter of existing bone, thus increasing its width, is an essential process which allows bone to respond to the increasing mechanical pressures during early foetal and postnatal life (Carter et al., 1996). Periosteal osteoblasts lay down new bone in successive laminae. This occurs in tandem with endosteal bone resorption by osteoclasts. The net effect of these actions is an increase in bone mass and marrow cavity diameter. In humans, unlike longitudinal bone growth which ceases upon sexual maturity through the ossification and fusion of the growth plate (Farquharson and Jefferies, 2000), appositional bone growth has been observed by tetracycline

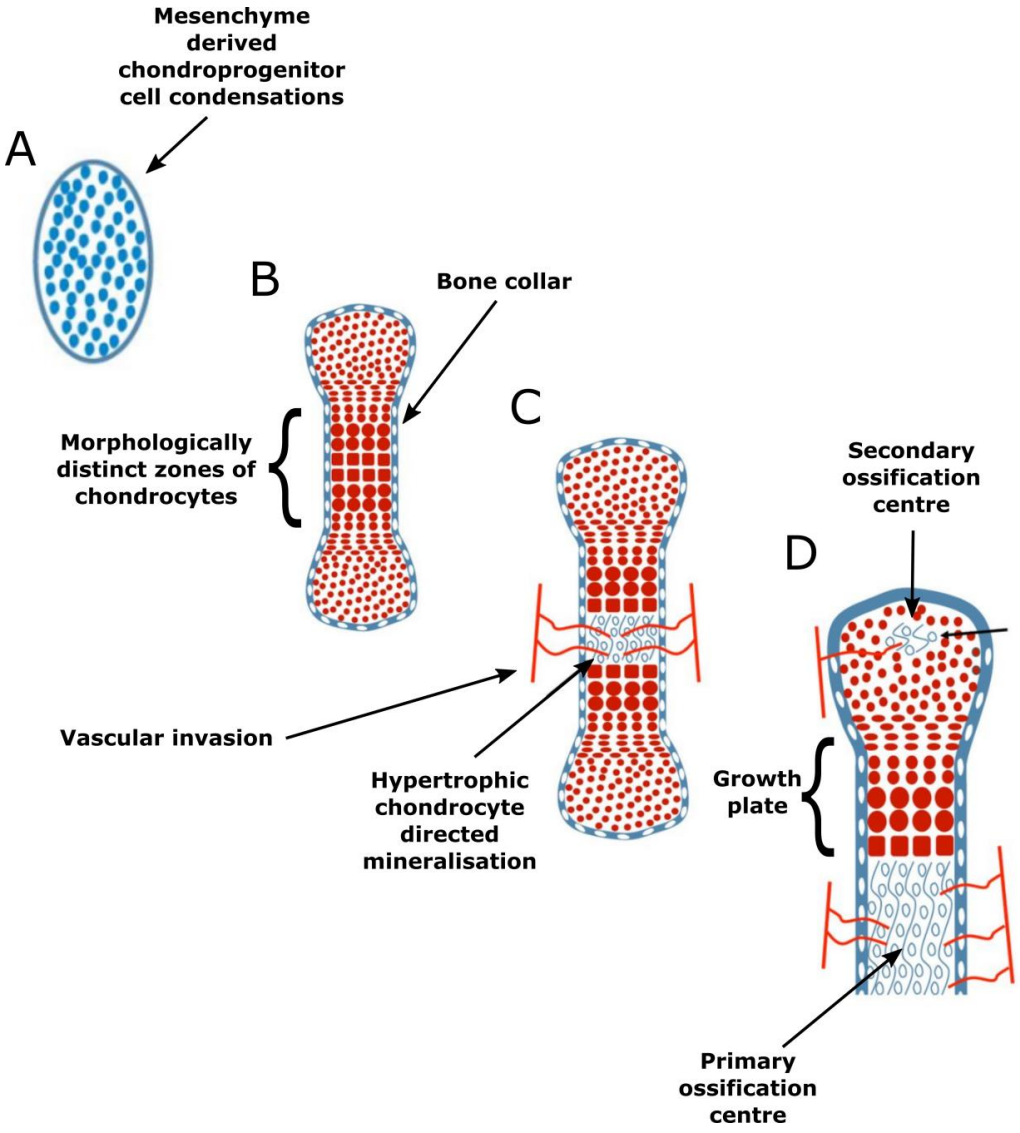

Figure 1.1. The process of endochondral ossification.

(A) Mesenchymal derived osteochondroprogenitor cells condense and aggregate at the site of the prospective bone, forming the cartilage anlage. **(B)** Endocrine and paracrine factors influence the development of morphologically distinct zones of chondrocytes at different stages of differentiation. Cells at the periphery of the condensations are directed to differentiate into osteoblasts, forming the bone collar and eventually the periosteum. **(C)** Hypertrophic chondrocyte mineralise their ECM through the release of MVs. Vascular invasion follows, bringing with it ECM resorbing osteoclasts. **(D)** The primary ossification centre is established through the resorbing actions of the osteoclasts and the formation and mineralisation of a bone ECM by osteoblasts. The founding of the secondary ossification centre, creates region of chondrocytes in the metaphysis which comprise the growth plate. Adapted from Kozhemyakina et al. (2015).

incorporation into newly mineralised bone in individuals in their 7th decade of life (Epker and Frost, 1966).

1.3. Bone modelling and remodelling

Maintenance of the mechanical and structural integrity of bone occurs throughout life by means of two processes; bone modelling and bone remodelling. Bone modelling, orchestrated by the independent actions of osteoblasts and osteoclasts, occurs primarily during growth, but also in the mature skeleton (Clarke, 2008). This process is essential for the adaptation of bone to variations in mechanical load, perhaps most strikingly exemplified in tennis players who display increased cortical thickness in the radius of their racket arm compared to the contralateral (and unloaded) arm (Calbet et al., 1998). The continued renewal of the skeleton occurs through the coupled and sequential actions of osteoclasts and osteoblasts. The process of remodelling occurs within temporary anatomical structures termed basic multicellular units (BMUs), comprising osteoclast resorption at its leading edge, followed by osteoid deposition and mineralisation by osteoblasts (Figure 1.2.) (Baron and Hesse, 2012). Remodelling may be either targeted (for the repair of micro-damage) or stochastic (for example in the procurement of calcium) and is tightly controlled at both an endocrine level and locally, by osteocytes (Hadjidakis and Androulakis, 2006). Disruption of bone remodelling can lead to pathologies of bone mass such as osteopetrosis, osteoporosis and Paget's disease.

1.3.1 Osteoblasts

Multipotent, self-renewing mesenchymal stem cells (MSC) found within the stroma of several mesenchymal tissues are the source of a number of cell types including:

adipocytes, chondrocytes, fibroblasts, myoblasts and importantly, osteoblasts (James, 2013). Despite their specialised role in the synthesis and subsequent mineralisation of the organic ECM of bone, osteoblasts possess only two transcripts which differentiate them from fibroblasts; *Runx2* and *Bglap* (bone gamma-carboxylate protein, or Osteocalcin (OCN)) (Ducy et al., 2000). The expression of the Runx2 transcription factor is essential in triggering the osteogenic genetic program of MSCs. The absence of Runx2 results in the complete absence of osteoblasts (Komori et al., 1997, Komori, 2010). Bone morphogenetic protein (BMP), transforming growth factor β (TGFβ), Wnt, and Ihh signalling are potent regulators of *Runx2* expression (Ducy et al., 2000). After lineage commitment, the actions of *Sp7* (encoding Osterix) and Wnt signalling advance the progression of precursors to the osteoblast phenotype, whilst simultaneously blocking the differentiation of chondrocytes (James, 2013). Maturation of osteoblasts is accompanied by significant production of ECM proteins (mainly type I collagen), tissue non-specific alkaline phosphatase (TNAP) and OCN. The secretory nature of osteoblasts is exemplified by their numerous mitochondria, Golgi, endoplasmic reticulum and ribosomes. Mature osteoblasts are cuboidal and reside on the surface of bone and are ultimately resigned to three different fates; apoptosis, quiescence or they become embedded in the bone matrix and differentiate into osteocytes (Maes et al., 2007, Kim et al., 2012). In addition to their role in bone formation, osteoblasts also orchestrate resorption through the expression of molecules which regulate osteoclast formation and activity (see section 1.3.2).

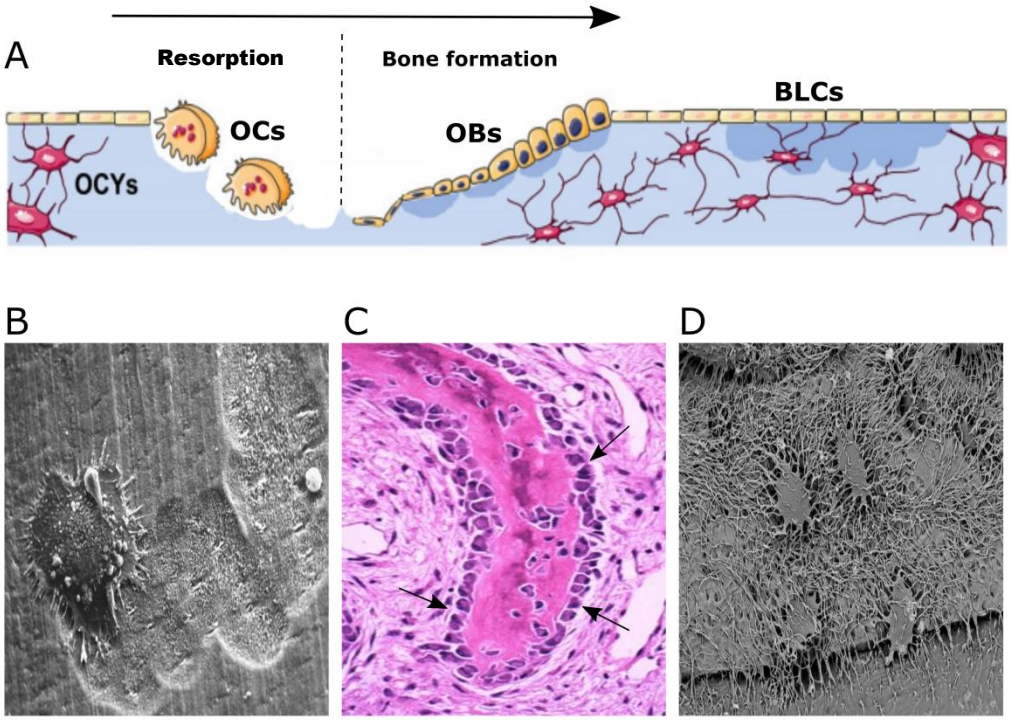

Figure 1.2. Bone remodelling and skeletal cell morphology

(A) Physiological bone remodelling involves both bone resorption and subsequent bone formation carried out by osteoclasts (OCs) and osteoblasts (OBs) respectively and orchestrated by the osteocytes (OCYs). Bone lining cells (BLCs). Adapted from Baron and Hesse (2012). **(B)** Electron micrograph of actively resorbing osteoclast **(C)** Cuboidal osteoblasts lining the surface of a newly formed trabecula. Adapted from de la Rosa, (2014). **(D)** Electron micrographs showing the extensive dendritic processes of osteocytes within bone. B & D provided from the bone research society by kind permission of Alan Boyde and Kevin Mackenzie.

1.3.2. Osteoclasts

Osteoclasts are large multinucleated cells which function to resorb mineralised bone and cartilage and together with osteoblasts are essential for remodelling of the skeleton. Partially committed, haematopoetically derived granulocyte-macrophage colony forming units are the precursors to osteoclasts (Zaidi et al., 2003, Yamashita et al., 2012). Osteoblasts and osteocytes, as well as stromal cells and T-lymphocytes secrete receptor activator of nuclear factor kappa B ligand (RANKL) which is a potent inducer of osteoclast activity and osteoclastogenesis. Binding of RANKL to the RANK receptor stimulates the recruitment of TNF receptor associated family 6 (TRAF-6) which triggers a number of downstream signalling pathways to initiate the osteoclast genetic program (Zaidi et al., 2003). Osteoblasts additionally control osteoclastogenesis through secretion of the RANKL decoy receptor, osteoprotegerin (OPG) (Simonet et al., 1997). The expression of the osteoclast regulatory molecules is tightly controlled by endocrine factors such as oestrogen and PTH (Zaidi et al., 2003). Also, the binding of the αvβ3 Integrin to amino-acid motifs within the bone matrix stimulates osteoclasts resorption (Teitelbaum, 2000). Through filamentous actin remodelling, polarized osteoclasts seal their perimeter onto the bone surface enclosing a ruffled membrane within the resorption lacunae. Acidification of this microenvironment to aid dissolution of hydroxyapatite (HA) mineral, is achieved through the actions of vacuolar H^+-ATPase and Cl^- channels which subsequently generate hydrochloric acid (Zaidi et al., 2003). The demineralised ECM is subsequently degraded by matrix metalloproteinases, tartate resistant acid phosphatase and the lysosomal cysteine protease, cathepsin K (Charles and Aliprantis). Extensive endocytosis at the ruffled border, traffics bone breakdown products to the osteoclasts

opposing surface (Stenbeck and Horton, 2004). Whilst it is yet to be established whether osteoclasts resorb bone in a targeted or stochastic manner during bone remodelling, it is clear that any disturbance of osteoclast formation and function can have profound effects on bone mass (Teitelbaum, 2000).

1.3.3. Osteocytes

Comprising up to 95% of the cellular component of bone, and one of the longest lived cells of the body, osteocytes are essential orchestrators of bone mass and systemic phosphate homeostasis (Bonewald, 2011). Although the precise genetic and molecular mechanisms are yet to be elucidated, subpopulations of osteoblasts on the bone surface are the osteocyte's precursor. The temporally regulated expression of key osteocyte markers leads to substantial morphological changes and embedding of the osteocyte within the mineralised ECM. The early osteocyte marker E11 (podoplanin) is believed to regulate these early morphological changes (Bonewald, 2011, Staines et al., 2016). Evidence is emerging that osteocytes actively invade the ECM, rather than being passively trapped (Prideaux et al., 2012). Residing in discrete lacunae, osteocytes use their dendritic processes to connect to adjacent osteocytes or the vasculature through so called canaliculi. Osteocytes transduce both mechanical and hormonal inputs into molecular signalling events which regulate bone remodelling by osteoblasts and osteoclasts (Dallas et al., 2013). Indeed, osteocytes as opposed to osteoblasts or stromal cells are the major source of RANKL and OPG, implicating a direct role in modulating bone resorption (Nakashima et al., 2011). The late osteocyte marker and potent Wnt signalling antagonist, sclerostin (SOST, encoded by the *Sost* gene) has attracted a lot of attention with regard to its role in regulating bone mass. SOST inhibits

low-density lipoprotein receptor-related protein 5 (LRP5) mediated increases in bone mass, and its expression in osteocytes is modulated by mechanical loading and endocrine signalling (Robling et al., 2008, Kramer et al., 2010).

Osteocytes are powerful regulators of phosphate homeostasis and mineralisation through the expression of PHEX (phosphate-regulating gene with homologies to endopeptidases on the X chromosome**)**, and the SIBLING proteins (see section 1.5.1.1.), dentin matrix protein 1 (DMP-1) and matrix extracellular phosphoglycoprotein (MEPE) (Bonewald, 2011). The endocrine function of the osteocyte was confirmed in 2004 through characterisation of the fibroblast growth factor 23 (FGF-23) knockout mouse. *Fgf23* is highly expressed by osteocytes and its ablation results in elevated serum P_i and increased renal P_i reabsorption and 25-hydroxyvitamin D_3-1α-hydroxylase activity (Shimada et al., 2004). Increased circulating FGF-23 levels has been linked with the progression of chronic kidney disease (particularly the bone wasting phenotype) and vascular calcification (Bonewald and Wacker, 2013).

1.3.4. Endocrine regulation of bone remodelling.

Hormones are powerful regulators of bone remodelling and mineral homeostasis through their direct and indirect actions on bone cells. Indeed, their actions on the skeleton are so varied that they are beyond the scope of this thesis. In brief however, it is well accepted that the gonadal sex steroids are the primary regulators of bone remodelling in adults. Oestrogen in particular, through the loss of bone mass associated with its deficiency in post-menopausal women has been identified as having an influential role. Oestrogen deficiency leads to increased remodelling, with a net

resorptive effect, as the action of oestrogen at the skeleton is primarily to inhibit osteoclastogenesis (via enhanced osteoblast expression of OPG) (Hadjidakis and Androulakis, 2006, Walsh, 2015).

Glucocorticoids are catabolic to the skeleton, impairing the differentiation of osteoblasts through inhibition of Runx2 and BMP signalling. Furthermore, osteoclastogenesis and osteoclast survival are enhanced in part by an increase in RANKL expression (Canalis and Delany, 2002). Investigations into the precise role of dexamethasone on osteoblast differentiation have provided conflicting results and, thus, the mechanism of dexamethasone's action *in vitro* are still to be fully elucidated.

Leptin, originally classified as an energy regulating hormone, indirectly regulates bone remodelling via the sympathetic nervous system. Leptin knockout, or leptin receptor knockout mice are grossly obese and hypogonadal and yet they exhibit around three times more bone mass than control mice (Ducy et al., 2000). Further knockout studies revealed that the action of leptin on the sympathetic nervous system is transmitted to osteoblasts through the β2 adrenergic receptor. Receptor activation results in signalling cascades which ultimately result in the upregulation of RANKL expression and increased osteoclastogenesis and bone resorption (Karsenty, 2006).

The active thyroid hormone, 3,5,3′-L-triiodothyronine (T3), increases bone remodelling primarily through its actions on osteoblasts where its stimulates their differentiation and activity through numerous pathways (Williams, 2013). Importantly however, T3 also increases the expression of RANKL by osteoblasts, and patients with hyperthyroidism exhibit reduced bone mass (Britto et al., 1994).

One of the best characterised regulators of bone remodelling is (PTH). As a major focus of this thesis, PTH is discussed in more detail below.

1.3.5. Parathyroid hormone

PTH is a peptide hormone synthesised and secreted by the chief cells of the parathyroid glands. PTH mRNA encodes a 115 amino acid PreProPTH protein, which through two successive proteolytic cleavages at the amino terminal, is converted to the 84 amino acid protein of PTH (Potts Jr et al., 1982). PTH acts to elevate serum Ca^{2+} concentrations. A diverse range of cellular functions are mediated by Ca^{2+} and as such serum Ca^{2+} must be maintained within a very narrow range to prevent disturbance to these functions and pathophysiology (Brown, 2015). The calcium sensor receptor (a G-protein coupled receptor (GPCR)), expressed on the surface of the chief cells, detects perturbations in serum Ca^{2+} concentration and in response to hypocalcaemia induces the rapid release of secretory vesicles containing PTH (Brown, 2015). PTH acts on the target tissues of bone and kidney through interaction with the PTH1R, another GPCR. Ligand binding can induce either adenylate cyclase or phospholipase C directed signalling pathways (Figure 1.3.)(Gardella, 2015). It is generally recognised that only the first 34 amino acids are required for both the binding and signal inducing function of PTH (Pioszak and Xu, 2008). The classical actions of PTH are: i) increased reabsorption of Ca^{2+} in the thick ascending limb and distal convoluted tubule of the kidney, in part through the enhancement of transient receptor potential vanilloid 5 (TRPV5) expression. ii) increased activity of 1α-hydroxylase enzyme which catalyses the conversion of 25(OH)VitD_3 to the 100-fold more potent 1,25$(OH)_2$Vitamin D_3 (Vitamin D) in the proximal tubule of the kidney. Vitamin D acts on the intestine to

increase reabsorption of Ca^{2+} and phosphate. iii) increased mobilisation of Ca^{2+} (and phosphate) from the mineral stores of bone by increasing bone remodelling (Potts, 2005, Revollo and Civitelli, 2015). These actions of PTH are hierarchal in the response to low calcium levels. By far the fastest mechanism to restore serum Ca^{2+} levels is via increased reabsorption in the kidney whereas increased resorption and mobilisation of mineral from bone is the last line of defence against low circulating calcium levels (Revollo and Civitelli, 2015).

Osteoblasts and osteocytes are regarded as the primary cell types eliciting the effects of PTH in bone. Osteoclasts have been shown to express the PTH1R *in vitro*, although a number of studies have failed to show their activation by PTH (Dempster et al., 2005). The effects of PTH on bone are truly pleiotropic and depend, in part, on the duration of exposure. A greater understanding of these effects came in large through pre-clinical and clinical studies of PTH administration and pathologies of PTH secretion (Poole and Reeve, 2005, Silva and Kousteni, 2015). Indeed, the intermittent exposure to low doses of PTH is anabolic to the skeleton, whereas the continuous exposure to elevated serum PTH leads to osteocatabolic effects (Silva and Bilezikian, 2015).

The anabolic effects of PTH have been established over a number of years utilising various animal models and more recently, extensive clinical trials (Neer et al., 2001, Rubin et al., 2002, Langdahl and Harsløf, 2011). The evidence from these studies now favours the use of low-dose intermittent administration of PTH to induce the anabolic effects on the skeleton. The method of administration potently stimulates trabecular bone formation and significantly reduces the risk of non-vertebral fractures (Silva and

Bilezikian, 2015). These anabolic effects are enacted through signalling pathways which modulate osteoblasts and osteocytes. The result is a plethora of effects (discussed in more detail in Chapter 5) which include, but are not limited to, the increased recruitment, differentiation, activity and survival of osteoblasts alongside the inhibition of *Sost* expression by osteocytes. Indeed during the initial months of PTH therapy, there is a significant rise in bone formation markers (typically serum procollagen type I N-terminal propeptide (P1NP)) without an accompanying rise in bone resorption markers (Lindsay et al., 2016). This bone modelling phase is described as the anabolic window and is limited by a concomitant rise in bone resorption; the two processes eventually becoming more aligned and thus the expansion of bone mass is stemmed (Pazianas, 2015).

The increases in BMD reported in the literature, highlight a role for the skeletal phosphatases which have been shown to be essential in the mineralisation process.

1.4. Matrix mineralisation

The material properties of bone are dictated by its two primary components, the collagenous ECM and the hydroxyapatite (HA) mineral deposited within and upon that. The interaction of these elements creates a rigid yet fracture resillient material. Alterations to the intricate structure of the collagen-mineral composite can have a harmful impact on bone strength, particularly in old age and disease. Mineralisation process is governed by physicochemical and biochemical factors which regulate the deposition of HA within the ECM (Millán, 2012). If the process is not properly regulated, the result can be too little of the mineral or too much - either of which can

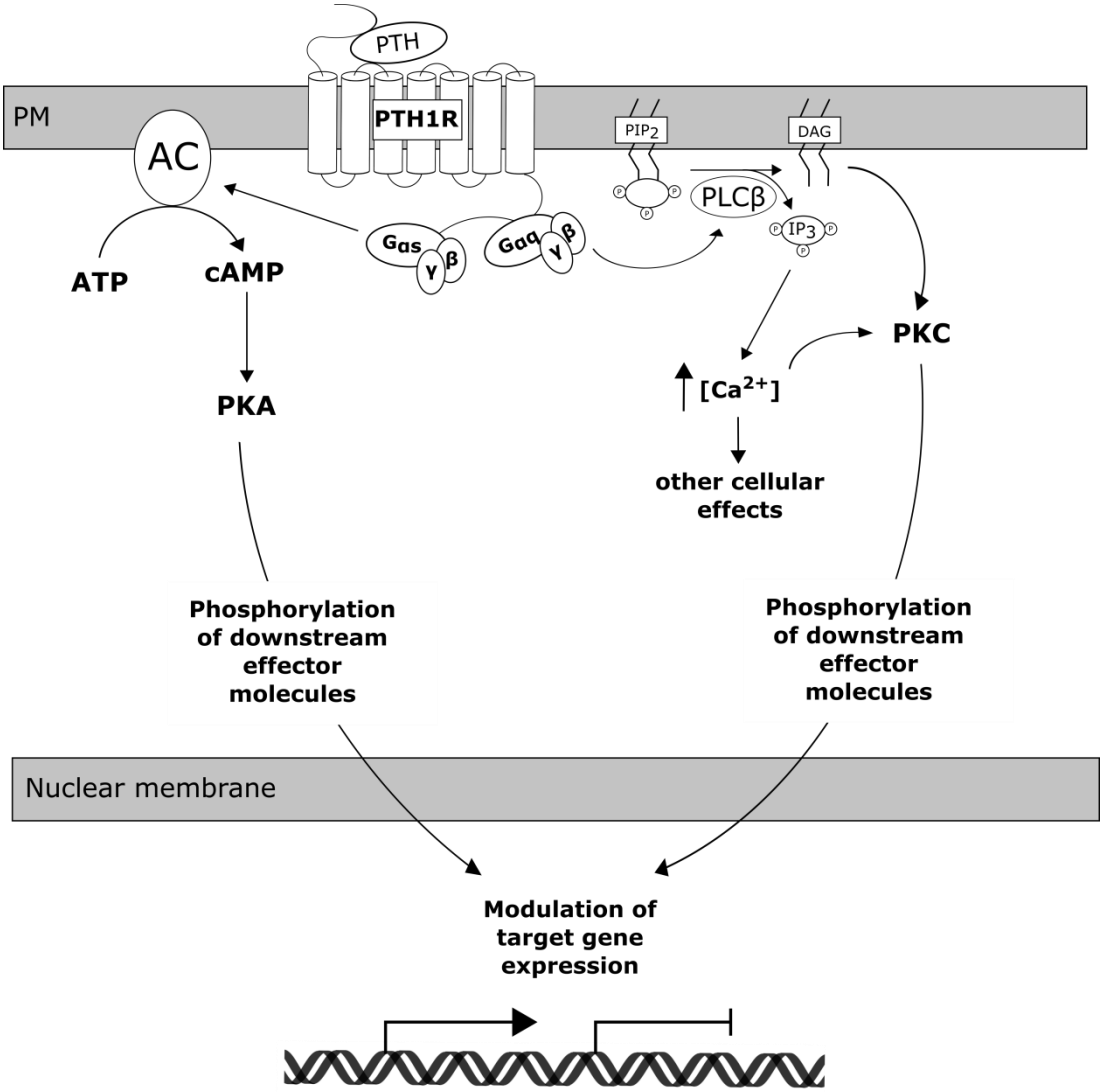

Figure 1.3. Schematic representation of the classical downstream signalling pathways induced by PTH.

Ligand binding to the PTH1R can activate either the cAMP/PKA signalling pathway (through stimulation of adenylyl cyclase (AC)) or the PKC signalling pathway (through the stimulation of phospholipase C β (PLCβ) and production of diacylglycerol (DAG) and inositol triphosphate (IP_3)). PKA and PKC can phosphorylate a range of downstream effector proteins. These proteins can translocate to the nucleus and modulate the expression of target genes through interaction with the DNA.

compromise bone health. Unfortunately, many aspects of the mineralisation process remain poorly understood, however, through studying the molecular players in the mineralisation process, we have the opportunity to gain a better understanding of the mechanism of mineralisation and what happens when the process goes awry. Suchknowledge is imperative for the identification of therapeutic targets against disorders of this process.

1.4.1. The role of collagen in matrix mineralisation

Type I collagen is the principal component of the mineralised tissue of bone, dentin and cementum. It has long been accepted that the collagenous matrix not only provides a scaffolding for mineral propagation, but the stereochemistry of the collagen molecule and the fibrillary network is capable of nucleating HA (Glimcher, 1987, Landis and Jacquet, 2013). This is perhaps the most accepted mechanism explaining the initial nucleation of apatite crystals within the ECM and has been extensively examined. Type I collagen comprises around 85-90% of the ECM of mineralised tissues of mammals and is constructed from three peptide chains, stabilised in a triple helical collagen molecule by hydroxylation of proline and lysine residues (Landis and Silver, 2008). These collagen molecules (300 nm in length) self-assemble in the extracellular space into microfibrils. In 2D, this assembly possess results in 40nm ‘hole’ regions between the ends of adjacent helices. Layers of these microfibrils are crosslinked in such a manner that the hole regions line up creating channels within the now 3D collagen fibril (Landis and Jacquet, 2013). The stereo-configuration of the collagen fibril results in charged amino acid residues flanking the hole regions which promotes the infiltration of Ca^{2+} and P_i from the extracellular fluids and which act as potential

nucleation sites (Landis and Silver, 2008, Nudelman et al., 2010). Newly formed, thin, plate-like crystals of HA are organised such that their c-axis is parallel with the associated collagen molecule. Growth of apatite crystals occurs preferentially along the axis of the collagen helices (Figure 1.4.) (Landis, 1999). Non-collagenous proteins, in particular negatively charged proteins are implicated as facilitators of amorphous calcium phosphate (ACP) movement into the collagen fibril prior to its nucleation within the hole sites (Landis et al., 1993, Nudelman et al., 2010). For example, in the absence of the negatively charged, aspartate rich region of Dentin Matrix Protein 1 (DMP1), mineral formation of collagen matrices only occurs in the extrafibrillar environment (Nudelman et al., 2010). Other mechanisms for the initiation of ECM mineralisation may exist (see 1.4.2) and of note is the recent observation that mineral may be formed on the outside of the collagen fibrils where it forms elongated mineral plate structures (McNally et al., 2012).

1.4.2. The role of matrix vesicles in matrix mineralisation

Whilst many in the field of bone mineralisation see no alternative to the collagen mediated mechanisms of HA nucleation and propagation, others believe that the initiation of skeletal mineralisation occurs within membrane limited MVs. Ground breaking electron microscopy studies by Bonucci (1967) and Anderson (1967) were the first to identify and describe the presence of mineral crystals within ‘’roundish bodies’’ adjacent to collagen fibrils. We now know with hindsight, that the extracellular lipid staining at the mineralisation front of rat growth plates and foetal human mandibles described by Irving (1959), is the Ca^{2+}-binding, acidic phospholipids of the MV (Wuthier and Lipscomb, 2011). To date MVs have been

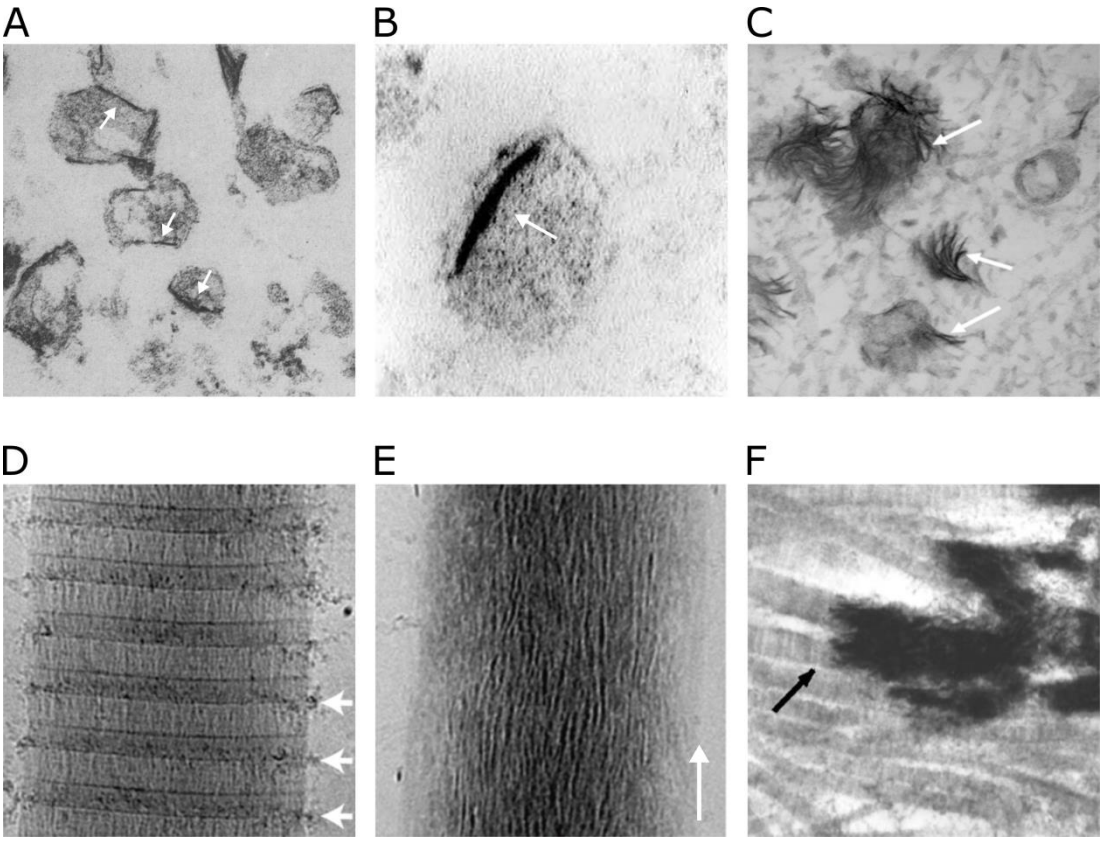

Figure 1.4. MV and collagen directed mineralisation observed by electron microscopy.

(A-B) Nucleation of ACP within MVs derived from bovine and rat growth plates (adapted from Ali et al. (1970) and Anderson et al. (2005a) respectively) **(C)** Eruption of the needle-like crystal of immature HA from the MV to the ECM (Millán, 2012). White arrows indicate the location of the HA crystals. **(D)** Localisation of ACP to the hole zones of collagen fibrils (Nudelman et al., 2010) **(E-F)** Apatite crystals propagate along the axis of the collagen fibrils (adapted from Nudelman et al. (2010) and Millán (2012) respectively). White arrow indicates the axis of the collagen fibrils. Black arrow indicates the electron dense HA crystals.

shown to be involved in the initiation of HA formation during growth plate mineralisation (Anderson, 1969), intramembranous ossification (Bernard and Pease, 1969), dentin mineralisation (Sisca and Provenza, 1972), antler calcification (Sayegh et al., 1974), and pathological calcifications of aortic valves, neoplasms and tendons (Kim, 1976, Sela and Bab, 1979). MVs are encapsulated by a trilaminar membrane and are typically around 100-400 nm in diameter. Their biogenesis from the parent cell is contested, with polarised budding and apoptotic cell membrane rearrangement both being offered as possible mechanisms (Cui et al., 2016). Although apoptotic bodies are capable of mineral accrual, morphological studies have shown that the osteoblast and growth plate chondrocyte membranes are intact post MV release. Furthermore, Kirsch et al. (2003) identified alizarin red staining in the chick growth plate, prior to any TUNEL staining, suggesting that MV release and mineralisation occurs prior to hypertrophic chondrocyte apoptosis. Proteomic characterisation of MVs from Saos-2 human osteosarcoma cells revealed 93% of the proteins are also present on the apical membrane of microvilli of the parent cell (Thouverey et al., 2009). This study also identified a number of cytoskeletal remodelling and vesicle trafficking proteins within microvilli, implicating a coordinated and active mechanism governing MV manufacture and release. Of interest, MV formation and release also appears to be spatially regulated. In the growth plate, they are only released from the lateral edges of the hypertrophic chondrocytes and not the apical and basal surfaces, this is consistent with sites of cartilage ECM mineralisation i.e. within the longitudinal septae and not the transverse septae of the growth plate (Reinholt and Wernerson, 1988). Although MVs share many of the same proteins and lipids with their parent cells, the precise composition is notably different (Genge et al., 2003, Xiao et al., 2009).

The trilaminar lipid membrane of MVs undergoes dynamic changes throughout the mineralisation process. Pioneering studies by Wu et al. (2002), examining the temporal changes in lipid composition of chick growth plate cartilage derived MVs, showed that MV membrane lipids underwent catabolism during *in vitro* calcification. In particular, phosphatidylinositol (PI), phosphatidylethanolamine (PE) and sphingomyelin (SM) were rapidly degraded, whereas phosphatidylcholine was degraded more slowly. Furthermore, the inner leaflet of MV membranes shows selective enrichment in the anionic phospholipid, phosphatidylserine (PS) where it is typically found as PS-Ca^{2+}-P_i complexes (Wu et al., 2002). *In vitro,* formation of PS-Ca^{2+}-P_i complexes show a potent ability to induce HA precipitation when incubated in synthetic cartilage lymph (Wu et al., 2009). Gain of function mutations in the PS synthase 1 gene, which catalyses the exchange of choline with serine on phosphatidylcholine (PC), has been shown to cause the rare Lenz–Majewski syndrome, which is associated with hyperostosis of the cranium, vertebrae and diaphysis of tubular bones (Sousa et al., 2014). As well as a particular lipid composition, MVs are also equipped with an arsenal of proteins which serve to aid the accumulation of calcium and modulation of P_i/ inorganic pyrophosphate (PP_i) levels.

The most abundant MV proteins are the Annexins (Anx), with particular enrichment in Anx A2, A5 and A6 (Golub, 2011). Their precise roles are yet to be fully elucidated, although clarification is coming from their 3D crystal structures. For example, Anx A5 contains a hydrophilic pore formed by a cluster of alpha helices, suggestive of an ion (Ca^{2+}) channelling role. Anx A6 on the other hand, possesses six Ca^{2+} binding sites (Wuthier and Lipscomb, 2011). To date, the primary role of Anx appears to be in the

nucleation of PS-Ca^{2+}-Pi complexes, *i.e.* to initiate the formation of ACP (Balcerzak et al., 2003). Of course, Ca^{2+} is only one component of ACP; MVs are also powerful modulators of the local P_i concentrations. The major MV regulators of intra and extravesicular P_i and PP_i are discussed in detail in section 1.5.2.

1.5. Regulators of matrix mineralisation

1.5.1. Extracellular matrix proteins

1.5.1.1. SIBLING proteins

Osteopontin (OPN), bone sialoprotein, MEPE, DMP-1 and dentin sialoprotein make up a group of non-collagenous extracellular mineralisation-regulating proteins termed SIBLING (small integrin-binding ligand N-linked glycoprotein) proteins (Staines et al., 2012). These proteins share a conserved arginine-glycine-aspartic acid (RGD) motif which mediates their cell attachment and signalling functions (Fisher and Fedarko, 2003). The conserved ASARM (acidic serine and aspirate rich motif) peptide region within this family of proteins appears to be the key determinant of their role in mineralisation (Rowe, 2012). In particular, it is the post-translational modifications of this motif, through enzymatic cleavage and phosphorylation, which dictates its function. Indeed, the ASARM peptide of OPN has been shown to inhibit the ECM mineralisation of osteoblast-like cells through the binding of HA (Addison et al., 2010). This inhibition of mineralisation is dependent on the number of phosphorylated serine residues, with non-phosphorylated ASARM peptide showing no inhibition of mineralisation (Addison et al., 2010). OPN has also emerged as a potent inhibitor of ectopic, pathological mineralisation (Giachelli, 2005). This effect was most clearly demonstrated by a study which showed the exacerbation of vascular calcification in

the matrix gla protein (MGP) null mouse through the simultaneous ablation of OPN (Speer et al., 2002). The phosphorylated ASARM peptide of MEPE has also been shown to inhibit the mineralisation of osteoblast-like cells and bone marrow stromal cell cultures (Addison et al., 2008, Martin et al., 2008). More recently, inhibition of ECM mineralisation by the phosphorylated, but not non-phosphorylated, MEPE-ASARM peptide in cultured murine embryonic metatarsals has been observed (Staines et al., 2012). To my knowledge, the ability of TNAP to dephosphorylate the OPN ASARM peptide as previously shown (Addison et al., 2007, Narisawa et al., 2013), has yet to be shown for other SIBLING protein derived ASARM peptides.

1.5.1.2. Bone morphogenetic proteins

Bone morphogenetic proteins (BMP), part of the TGFβ superfamily, are a group of multifunctional proteins which regulate osteo- and chondro-genesis as well as the self-renewal of embryonic stem cells (Xiao et al., 2007). Osteoprogenitors, osteoblasts and chondrocytes produce and secrete BMPs into the ECM of bone. BMP-2, -4, -5, -6, -7 and -9 display the greatest osteogenic capability, whereas BMP-3 strongly antagonises bone development (Hogan, 1996). Classically, BMPs induce the hetero-dimerisation of type I and type II BMP receptors (serine/threonine kinase receptors); phosphorylation of the type I component results in a downstream signalling cascade. Smads 1,5,8 are a common target of BMP signalling and their translocation to the nucleus, activates the transcription of target genes (Zhu et al., 2015). BMP signalling enforces differentiation of mesenchymal mutipotent stem cells to cells of either the osteogenic or chondrogenic lineage. Collagen synthesis and alkaline phosphatase and osteocalcin expression, markers of differentiated osteogenic cells, are all stimulated

by BMPs (Hogan, 1996). The osteogenic capacity of BMPs has now been harnessed in the clinic, in particular, for the acceleration of bone regeneration in fracture repair. For example, the delivery of recombinant human BMP-2 or BMP-7 significantly improves the quality and time to union of problematic non-union tibial fractures (Valentin-Opran et al., 2002, White et al., 2007). In recent years, the BMP coating of implants (for example, titanium femoral heads used in hip replacement surgery) has received attention in an attempt to improve their osseous integration (Agarwal and Garcia, 2015).

1.5.2. Phosphatases and phosphate transport in matrix mineralisation

The establishment, maintenance and management of the ratio between promoters and inhibitors of the biomineralisation process is central to physiological skeletal mineralisation. As a major component of the HA nanocrystals of vertebrate mineral, the regulation of P_i concentrations is vital. Contrastingly, PP_i has long been recognised as a potent inhibitor of mineralisation, obstructing the nucleation and propagation of HA (Russell and Fleisch, 1975). Disruption of the P_i:PP_i ratio leads to mineralisation pathologies characterised by hypo- or hyper- and ectopic- mineralisation phenotypes. Locally, during the initiation of skeletal mineralisation, phosphatase activity and P_i or PP_i transportation, are crucial in developing intra- and extra- vescicular environments conducive to mineralisation. The major players in this process are introduced below.

1.5.2.1. Tissue non-specific alkaline phosphatase

In 1923, Robison described the hydrolysis of a phosphoric acid monoester by an enzyme abundant in ossifying rabbit cartilage (Robison, 1923). The enzyme in question would later be identified as an alkaline phosphatase isozyme, tissue non-

specific alkaline phosphatase (TNAP). Encoded by the *ALPL* gene in humans, TNAP is preferentially expressed in bone, liver and kidney (Weiss et al., 1988). Osteoblasts, hypertrophic chondrocytes and odontoblasts express TNAP on their plasma membrane, and on the membrane of their shed MVs, by means of a glycosylphosphatidylinositol anchor (Millan, 2006). TNAP is the major extravesicular regulator of the PP_i/P_i ratio through its hydrolysis of PP_i and ATP (Ciancaglini et al., 2010). More recently, TNAP was additionally shown to dephosphorylate, and thus prevent, the HA-binding properties of OPN, highlighting TNAPs multifactorial role in promoting skeletal mineralisation (Addison et al., 2010, Narisawa et al., 2013). Loss of function, primarily missense mutations in one or both *ALPL* alleles, leads to the human condition known as hypophosphatasia (HPP) (Henthorn and Whyte, 1992, Whyte et al., 2015). HPP can present with a spectrum of severity, in part dictated by the precise mutation involved. The infantile and childhood HPP forms are the most severe and are characterised by severe dental and skeletal defects associated with hypomineralisation, alongside vitamin B_6-dependent seizures, nephrocalcinosis and muscle weakness (Whyte, 2010, Millán and Whyte, 2015). The *Alpl*$^{-/-}$ mouse developed by Narisawa et al. (1997), recapitulates the infantile HPP phenotype and has provided an essential model for the study of TNAP function in skeletal mineralisation. Correction of extracellular PP_i levels in the *Alpl*$^{-/-}$ mouse by concomitant ablation of either *Enpp1* or *ank* (the major providers of extracellular PP_i) restores the mineralisation defects and affirmed the accumulation of PP_i as the causative agent for the hypomineralisation observed in the absence of functional TNAP (Harmey et al., 2004).

Accrual of PP_i within the extracellular environment prevents the propagation of HA crystals formed within the confines of MVs. *Alpl*$^{-/-}$ mice are born with a normally mineralised skeleton, with hypomineralisation defects only becoming apparent around postnatal days 6-10 (Yadav et al., 2011). Furthermore, electron microscopy studies identified crystals of HA within MVs derived from patients with HPP and the *Alpl*$^{-/-}$ mouse (Anderson et al., 1997, Anderson et al., 2004). These findings highlight alternative mechanisms of generating a PP_i/P_i ratio conducive to mineral formation within the interior of MVs.

1.5.2.2. Nucleotide pyrophosphatase/ phosphodiesterase 1

Physiological mineralisation is a tightly regulated process. Disruption of the fine balance between promoters and inhibitors of mineralisation leads to pathological mineralisation. Whereas as TNAP positively promotes the mineralisation process through the hydrolysis of PP_i, the generation of PP_i by nucleoside pyrophosphatase/ phosphodiesterase 1 (NPP1), provides vital control to unrestrained mineralisation. NPP1 is a transmembrane protein highly expressed in osteoblasts, chondrocytes and their shed MVs (Bollen et al., 2000, Terkeltaub, 2006). NPP1 generates PP_i and P_i through cleavage of the pyrophosphate bonds in ATP and ADP respectively (Mackenzie et al., 2012a). As was the case for TNAP, the importance of NPP1 in regulating mineralisation was underlined through the study of human conditions, in this case, generalized arterial calcification of infancy (GACI) and pseudoxanthoma elasticum (PXE). Bi-allelic mutations in the *ENPP1* gene which results in the loss of function of NPP1 and low systemic levels of PP_i are the hallmark of GACI (Nitschke et al., 2012). The reduction in PP_i levels results in the catastrophic calcification of

arteries, with most children affected by this rare autosomal recessive condition dying within 6 months of life (Rutsch et al., 2000). Characterisation of mutant (*ttw/ttw*) and knock-out (*Enpp1*$^{-/-}$) mouse models emphasised the role of NPP1 in regulating skeletal and ectopic mineralisation. These mice exhibit intervertebral and peripheral joint hyperostosis, arterial and cartilage calcification alongside substantial changes to bone composition and structure (Okawa et al., 1998, Harmey et al., 2004). Interestingly, the calvariae of *Enpp1*$^{-/-}$ mice show hypermineralisation, whereas the long bones present with reduced trabecular and cortical bone mass, albeit with similarly reduced porosity, compared to WT animals (Anderson et al., 2005b, Hajjawi et al., 2014). These findings suggest a differential expression of *Enpp1* between the axial and appendicular skeleton. Consistent with this observation, restoration of the hypomineralised phenotype of *Alpl*$^{-/-}$ mice by simultaneous ablation of *Enpp1*, was effective in the calvariae and verterbrae, but not in the long bones (Anderson et al., 2005b). Evidence is emerging that loss of *Enpp1* may affect systemic regulators of skeletal mineralisation, as well as the classical local changes in PP_i levels. Serum levels and calvarial mRNA expression of *Fgf23* are increased in *Enpp1*$^{-/-}$ mice (Mackenzie et al., 2012b). As a phosphaturic hormone, increased FGF-23 may be a compensatory response to reduce the extent of excessive mineralisation through the elimination of P_i. Interestingly, hypophosphataemic rickets resulting from increased FGF-23 levels, has been observed in patients with *ENPP1* mutations (Lorenz-Depiereux et al., 2010). These findings highlight, the yet to be fully characterised, roles of skeletal mineralisation regulators in controlling whole body mineral homeostasis.

1.5.2.3. PHOSPHO1

Originally identified as a phosphatase enriched in chick hypertrophic chondrocytes (Houston et al., 1999), PHOSPHO1 provides a means of explaining the presence of HA within MVs lacking TNAP activity. PHOSPHO1 is a member of the functionally and evolutionary diverse, haloacid dehalogenase (HAD) superfamily of magnesium-dependent enzymes (Stewart et al., 2003). Amino acid sequence analysis of PHOSPHO1 from various organisms revealed the presence of two fully conserved aspartate residues at positions 43 and 123, which are proposed to be essential to the phosphohydrolase activity of this enzyme (Stewart et al., 2003). Early studies identified PHOSPHO1 in the mineralising regions of both embryonic and mature chick bone by immunohistochemistry and *in situ* hybridisation (Stewart et al., 2006). These findings were later established in the mouse, where PHOSPHO1 was again shown to be expressed in hypertrophic chondrocytes, metatphyseal trabecular bone, and the osteoblasts lining the bone forming surfaces of cortical bone (Roberts et al., 2007). *In vitro* recombinant human PHOSPHO1 exhibits high, specific activity towards two components of phospholipid metabolism, phosphocholine (PCho) and phosphoethanolamine (PEth). Sonicated, but not intact, *Alpl*$^{-/-}$ MVs are able to generate P_i during incubation with PCho or PEth, highlighting the localisation of PHOSPHO1 within MVs (Roberts et al., 2007). Also, analysis of the 267 amino acid long human PHOSPHO1 protein revealed the absence of a signal peptide. This suggests PHOSPHO1 to be a soluble cytoplasmic phosphatase (Stewart et al., 2003). To date, PHOSPHO1 has been identified in MVs derived from osteoblasts, chondrocytes, and odontoblasts (Houston et al., 2004, Roberts et al., 2007, McKee et

al., 2013), and a number of studies unequivocally provide evidence for its key role in intravesicular P_i generation.

Importantly for its proposed role in the initiation of MV mineralisation, PHOSPHO1 is expressed prior to the appearance of mineralisation. Small molecule compounds, such as lanzoprazole, that inhibit PHOSPHO1 activity reduce MV-mediated calcification and long bone mineralisation (Roberts et al., 2007, MacRae et al., 2010). Inhibition of ECM mineralisation has similarly been observed in vascular smooth muscle cell and embryonic metatarsal cultures treated with the potent and specific PHOSPHO1 inhibitor, MLS-0263839 (Kiffer-Moreira et al., 2013, Huesa et al., 2015). The pivotal role of PHOSPHO1 in bone mineralisation was recently highlighted by the generation and characterisation of the *Phospho1*$^{-/-}$ mouse. *Phospho1*$^{-/-}$ mice display severe bone and tooth abnormalities including hypomineralisation, bowed long bones, spontaneous fractures and scoliosis (Yadav et al., 2011, Huesa et al., 2011, Rodriguez-Florez et al., 2015, McKee et al., 2013). Javaheri et al. (2015) also detected raised numbers of osteocyte lacunae and Haversian canals in *Phospho1*$^{-/-}$ animals. Serum PP_i and phosphorylated-OPN levels are raised in *Phospho1*$^{-/-}$ mice, possibly explained through reduced *Alpl* expression. Despite this, the overexpression of *Alpl* does not significantly mitigate the skeletal pathologies of the *Phospho1*$^{-/-}$ mouse, in spite of the restored PP_i levels (Yadav et al., 2011). In contrast, a significant improvement in the skeletal phenotype of *Phospho1*$^{-/-}$ mice is achieved through simultaneous ablation of *Spp1* (which encodes OPN) (Yadav et al., 2014).

Intriguingly, the double ablation of *Phospho1* and *Alpl* in mice completely abolishes skeletal mineralisation in embryonic mice highlighting the critical role and

cooperativity of both phosphatases in the control of biomineralisation (Yadav et al., 2011). From this work, the authors of this study proposed that MVs initiate mineralization by a dual mechanism: PHOSPHO1-mediated intravesicular generation of P_i and phosphate transporter-mediated influx of P_i via the Na/P_i co-transporter, P_it1. Mice that were double deficient in *Phospho1* and *P_iT1* showed extensive hyperosteoidosis and displayed significantly decreases in BV/TV, trabecular number and bone mineral density, as well as decreased stiffness and strength (Yadav et al., 2016)

Fascinatingly, atomic force microscopy studies revealed reduced numbers of MV from *Phospho1*$^{-/-}$ chondrocytes. Alongside its role in provision of intravesicular P_i, PHOSPHO1 activity may also act, by a yet undefined mechanism, to regulate MV formation and/or release (Yadav et al., 2016).

Despite our understanding of the non-redundant role of PHOSPHO1 in the initiation of MV mineralisation, data surrounding the regulation of its expression are limited. Microarray analysis of murine embryonic limb bud cultures transfected with Runx2-adenovirus, identified *Phospho1* as one of the major upregulated genes (Nishimura et al., 2012). A more striking upregulation of *Phospho1* was observed with the overexpression of Smad3 in MC3T3 cell cultures (Hisa et al., 2011).

1.5.2.4. Ankylosis protein

The multipass transmembrane protein, ANK (progressive ankyloses, *ank*), facilitates the intracellular to extracellular transport of the mineralisation inhibitor PP_i (Ho et al., 2000). Mice homozygous for the progressive ankyloses trait (*ank/ank*), develop debilitating ossification of the synovial joints and tendons (Hakim et al., 1984). The

trait is the result of a spontaneous recessive mutation, specifically, a nonsense mutation which results in the truncation of the *ank* gene), with homozygotic animals rarely surviving beyond 5 months of age and exhibiting reduced body size (Krug et al., 1989). Interestingly, despite its expression amongst many of the soft tissues, ectopic mineralisation within these tissues has yet to be extensively characterised. The hypomineralisation and high serum PP_i levels exhibited by the *Alpl*$^{-/-}$ mouse are corrected in the *Alpl*$^{-/-}$:*ank/ank* double deficient mouse, thus providing confirmatory evidence of the role of ANK in regulating extracellular PP_i levels (Harmey et al., 2004). Decreased extracellular PP_i levels in the *ank/ank* mouse also similarly decrease the expression of OPN, a well-known inhibitor of HA nucleation (Wang et al., 2005). Interestingly, although both NPP1 and ANK activity results in increased extracellular PP_i levels, the simultaneous genetic ablation results in an additive effect with regard to the hypermineralisation phenotype. Protein localisation studies confirmed the presence of NPP1 and ANK in osteoblast protein lysates, but only NPP1 was found to be present in protein lysates from MV derived from osteoblasts (Harmey et al., 2004). These differences in subcellular localisation may go some way to explain the differences in the pathologies of the *Enpp1*$^{-/-}$ and *ank/ank* mice.

1.5.2.5. Sodium dependent P_i cotransporters

MV lacking the intravesicular phosphatase, PHOSPHO1, still possess HA mineral within their sheltered interior, as observed by electron and atomic force microscopy studies (Yadav et al., 2011, Yadav et al., 2016). The concomitant ablation of the primary extravesicular phosphatase, TNAP, results in MV devoid of any mineral and a complete lack of bone mineralisation in general (Yadav et al., 2011). P_i transporters

have therefore been implicated in the extra to intra-vesicular transport of P_i during skeletal mineralisation. The type III sodium/P_i cotransporters, P_it1 and P_it2 are expressed by osteoblasts and chondrocytes, with P_it1 identified as the major mediator of P_i transport within these cell types (Millán, 2012). The induction of P_it1 mRNA has been observed *in vitro* in response to established osteogenic factors such as PTH, BMP-2 and Ca^{2+} (Suzuki et al., 2006). Injection of foscarnet (a competitive inhibitor of sodium/P_i cotransporters) over the calvaria of neonatal rats inhibits the progression of mineralisation of the calvaria (Yoshiko et al., 2007). On the contrary, the chondrocyte-specific ablation of P_it1, or the hypomorphic expression of P_it1 *in vivo*, does not induce any abnormal skeletal phenotype (Bourgine et al., 2013, Yadav et al., 2016). The authors noted that the expression of P_it2 was upregulated 2-fold in response to the reduced P_{it}1 expression (Bourgine et al., 2013). MVs derived from the $P_it1^{col1/col1}$ mice are devoid of mineralisation, underscoring a non-redundant role for P_it1 in transporting extravesicularly generated P_i to MVs (Yadav et al., 2016). Unlike P_it1, where the global ablation is embryonic lethal (Beck et al., 2010), $P_i t2^{-/-}$ mice exhibit around a 50% survival rate. Although limited to a conference abstract, the characterisation of the skeletal phenotype of these mice revealed a marked impairment of growth plate mineralisation and bone formation (Beck-Cormier et al., 2015). The temporal-spatial expression of these P_i transporters requires further investigation to fully understand their role(s) in skeletal mineralisation.

1.5.3. Lipid metabolism in MVs: A new player linked to P_i generation and bone mineralisation?

1.5.3.1. Sphingomyelin phosphodiesterase 3

Sphingolipids are an extremely diverse and bioactive class of lipid compounds. Although historically, sphingolipids were believed to be inert structural molecules, they are now well recognised as potent signalling molecules regulating numerous cellular events for example; differentiation, proliferation, growth, apoptosis, membrane trafficking, autophagy and cell-cell and cell-matrix interactions (Merrill et al., 2005, Merrill, 2011). Importantly, there is a mounting body of evidence implicating sphingolipid metabolites (in particular, ceramide and sphingosine-1-phosphate) as regulators of osteoblast, osteoclast and chondrocyte survival and function (Oldknow et al., 2015). Exhibiting strong expression within bone, cartilage and neuronal tissues, the membrane bound neutral sphingomyelinase 2 (nSMase2, encoded by the *Smpd3* gene) hydrolyses SM to generate ceramide and PCho (Khavandgar and Murshed, 2015). The vector targeted or mutagenic ablation of nSMase2 activity, as observed in the *Smpd3*$^{-/-}$ and *fro/fro* (*fragilitas ossium)* mouse strains respectively highlighted the essential role for this enzyme in skeletogenesis and mineralisation (Muriel et al., 1991, Stoffel et al., 2005).

The phenotypic characterisation of the *fro/fro* mouse in particular, revealed marked hypomineralisation of the skeleton and dentition and deformed and retarded growth of the long bones. *In vitro*, osteoblasts from the *fro/fro* mouse display reduced ECM mineralisation. Correction of the bone and dentin mineralisation defects is achieved in the *fro/fro* mouse through a *Col1a1* promoter driven expression of *Smpd3* (Khavandgar et al., 2011, Khavandgar et al., 2013). Local and cell-autonomous roles

of nSMase2 are further evident by the fact that *frofro*;*Col1a1*-*Smpd3* mice still exhibit chondrocyte mineralisation defects. *Smpd3*$^{-/-}$ and *fro/fro* mice present with an increased zone of hypertrophic chondrocytes and poorly mineralised chondrocyte ECM (Stoffel et al., 2007, Khavandgar et al., 2011). Ceramide is known to induce the apoptosis of terminally differentiated chondrocytes (MacRae et al., 2006, Kakoi et al., 2014). Although the mechanisms of hypertrophic chondrocyte mineralisation are debated, apoptosis is implicated and as such, the reduced ceramide levels in *fro/fro* mouse may explain the impairment of chondrocyte mineralisation (Khavandgar et al., 2011). Recent studies were able to recapitulate the chondrocyte defects of the *fro/fro* mouse through the targeted deletion of *Smpd3* in chondrocyte using the *Col2a1*-Cre (Li et al., 2016). Interestingly however, inactivation of the alternative *de novo* pathway of ceramide synthesis in dihydroceramide desaturase 1 -deficient (*Des1*$^{-/-}$) mice does not produce any bone mineralisation defects (personal communication with Prof. Murshed, McGill University, Montreal). This observation raises the possibility that the other nSMase2 metabolite, PCho, might play a role in bone mineralisation.

Importantly for the studies of this thesis, nSMase2 has been identified in proteomic studies of MV isolations (Thouverey et al., 2009, Thouverey et al., 2011). Furthermore, nSMase2 is implicated in mediating exosome release during the calcification of vascular smooth muscle cell cultures (Kapustin et al., 2015). It is evident therefore that the effects of nSMase2 during mineralisation are likely to be multifactorial. The generation of PCho through the hydrolysis of SM is of primary interest, as it provides a mechanism in combination with the activity of PHOSPHO1 for the generation of P_i within MV.

1.5.3.2. Choline kinase enzymes

The *de novo* synthesis of the major constituent of mammalian lipid bilayers, PC, occurs through two pathways: i) the methylation of PE by the PE-N-methyltransferase enzymes and ii) The CDP-choline (or Kennedy) pathway (Aoyama et al., 2004). The first reaction in the Kennedy pathway is the ATP-dependent conversion of choline to PCho, catalysed by the choline kinase (CK) enzymes. Cloning of cDNAs derived from rat liver lysates identified three isoforms of CK; CKα1 and CKα2 (obtained through alternative splicing of the *Chkα* gene) and CKβ (a product of the *Chkβ* gene) (Uchida, 1994). The importance of PC as a structural and functional component of lipid membranes ensures the CK genes are ubiquitously expressed in mammalian tissues (Gibellini and Smith, 2010). The earliest investigations of CK in bone revealed the lack of induction of these enzymes in response to Vitamin D and calcitonin (Stern and Vance, 1987). However, it wasn't until 2006, that the characterisation of a mouse possessing an intragenic deletion within the *Chkβ* gene, resulting in the ablation of CKβ protein, highlighted a role for CK enzymes in bone formation. The *rmd/rmd* mouse exhibits marked growth retardation and bowing of the forelimb bones alongside its pathological feature of severe muscular dystrophy (contrastingly, only affecting the hindlimbs) (Sher et al., 2006). This cranial-caudal anomaly was later explained by a differential expression of CK isoforms between the forelimbs and the hindlimbs (Wu et al., 2010). The *flp/flp* mouse (possessing an ENU-induced mutation of *Chkβ* gene) presents with reduced BMD and the disrupted activity of both osteoclasts and osteoblasts. *Flp/flp* osteoclasts are present in higher numbers and display increased Cathepsin K activity than their WT counterparts. On the contrary, osteoblasts from the *flp/flp* mice poorly mineralise their ECM *in vitro (Kular et al., 2015)*. The genetic

ablation of *Chkα* is embryonic lethal (Wu et al., 2008). Small molecule inhibition of CKα activity *in vitro* however, results in reduced ECM mineralisation and TNAP activity (Li et al., 2014b). Silencing of *Chkα* expression in MG-63 cells reduces PCho levels by 80% (Li et al., 2014b). PCho is readily hydrolysed by PHOSPHO1 and as such these data surrounding CK enzymes provide further connection between lipid metabolism and mineralisation which are worthy of exploration.

1.6. Aims

The extensive characterisation of the skeletal phenotype of the *Phospho1*$^{-/-}$ mouse has confirmed the importance of this intravesicular enzyme during the initiation of mineralisation. Furthermore, emerging evidence, especially that gained from analysis of the *fro/fro* mouse, implicates MV lipid metabolism in the mineralisation process. In particular, it is hypothesised that nSMase2 and CK, work in tandem with PHOSPHO1 during the initiation of skeletal mineralisation through the generation and processing of PCho respectively (Figure 1.5.). Unfortunately, currently used *in vitro* models of mineralisation in which to investigate these relationships rely on the use of β-glycerophosphate (βGP), a substrate for TNAP. As the production of P_i from TNAP-mediated βGP catalysis may interfere with the endogenous mechanisms of P_i generation, new model systems are needed to study the relationship between PHOSPHO1 and nSMase2. Therefore, the aims of Chapter 3 are to:

I. Establish phosphatase-substrate free conditions for the *in vitro* mineralisation of osteoblast-like cell cultures, primary calvarial osteoblast cell cultures and and embryonic metatarsal cultures.

II. Investigate the temporal mRNA and protein expression of key mineralisation dependent enzymes within these models.

The development and characterisation of these model system will assist in studies seeking to understand the regulation of the key mineralisation genes. Indeed, it is apparent from the literature that there is a paucity of information surrounding the regulation of, in particular, *Phospho1* and *Smpd3*. Interestingly, *Phospho1* was recently identified as one of a number of genes regulated by PTH in osteocyte-like cells (St John et al., 2015)). As PTH can exert both anabolic and catabolic effects on the skeleton, I hypothesised that the regulation of *Phospho1* by PTH could provide a novel mechanism to explain these effects. Therefore, the aims of Chapters 4 and 5 are to:

III. Characterise the effects of PTH on osteoblasts *in vitro*.

IV. Examine the skeletal expression of key mineralisation genes in response to intermittent PTH and continuous PTH exposure *in vivo*.

V. Determine the role of *Phospho1* in the osteoanabolic and osteocatabolic effects of intermittent PTH and continuous PTH respectively.

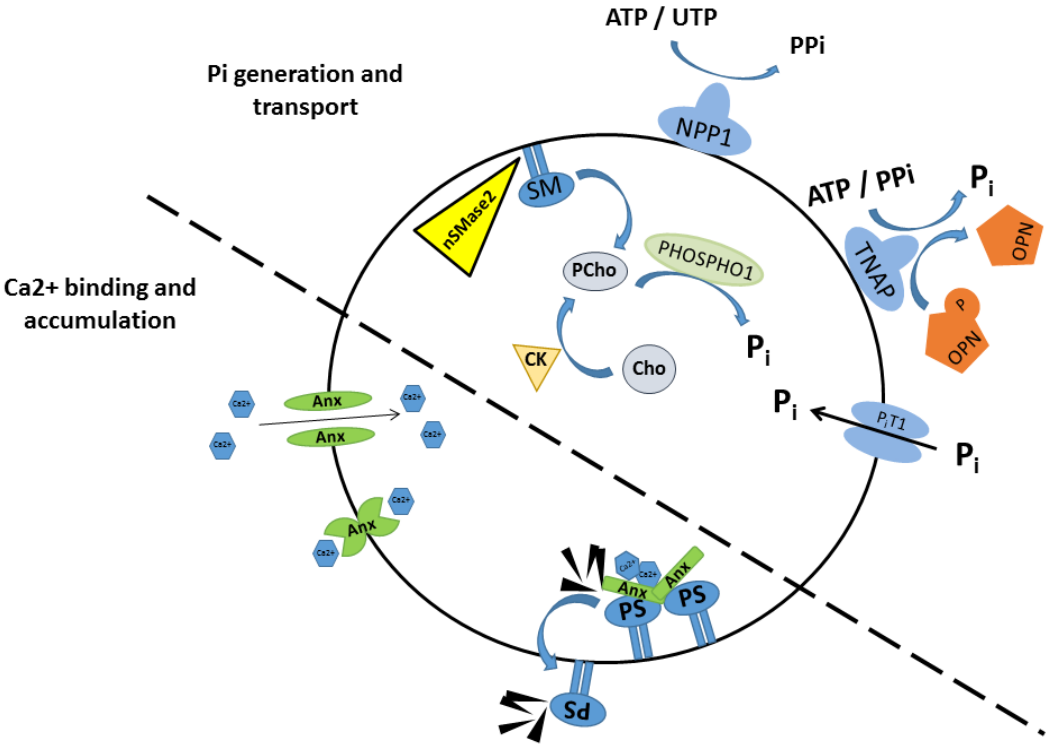

Figure 1.5. Hypothetical P_i and Ca^{2+} accumulation within MVs.

P_i generation within MVs is primarily carried out through the hydrolysis of PCho (or PEth) by PHOSPHO1. PCho may be derived from the breakdown of membrane sphingomyelin by nSMAse2 or through the *de novo* synthesis from choline by the action of the CK (choline kinase) enzymes. NPP1 and TNAP are the major extravesicular regulators of PP_i and P_i. Extravesicular P_i, may be transported to the interior of MVs through the actions of P_it1. Calcium accumulation is primarily carried out by the actions of Annexins (Anx) and the acidic phospholipid, phosphatidylserine (PS). Anx and PS are also involved in the nucleation of ACP.

Chapter 2

Materials & Methods

2.1. Reagents and solutions

All chemicals were purchased from Sigma Aldrich (Poole, UK) unless otherwise stated. Tissue culture media, reagents and plastic ware were purchased from Thermo Fisher Scientific (Northumberland, UK) unless otherwise stated. The composition of media and buffers used are detailed in Appendix I.

2.2. Cell culture

2.2.1. Thawing frozen cell stocks

Cryovials of frozen cell stocks were initially thawed in a beaker of 37°C water. The cryovial contents were next transferred to a universal and 5 mL of pre-warmed (37°C) maintenance media (Appendix I) was added dropwise. The cell suspension was gently agitated and spun at 1000 x g for 5 min. The supernatant was discarded and the resultant cell pellet was resuspended in the cell-type specific media and transferred to a T175 tissue culture flask and incubated in a humidified atmosphere (37°C, 5% CO_2).

2.2.2. Freezing cell stocks

To maintain stocks of cell-lines, cultured cells in the log-phase of growth (i.e. sub-confluent) were initially detached from the culture flask through the use of trypsin-ethylenediaminetetraacetic acid (EDTA). In brief, cell monolayers were rinsed in serum-free α-minimum essential medium (MEM) prior to incubation with trypsin-EDTA for 5 min at 37°C to detach the cells. Maintenance media, which contains foetal bovine serum to inactivate the trypsin, was then added to the flasks and cells were harvested by centrifugation at 1000 x g for 5 min. Cells were resuspended in a 1:1 mix of maintenance media and freezing mix (Appendix I) to give a cell concentration of 2-3 x 10^6 cells/mL. Cryovials containing 1 mL of cell suspension were stored at -70°C

in a polystyrene box lined with cotton wool for up to one week prior to their transfer to -150°C for long-term storage.

2.2.3. MC3T3 cells

The pre-osteoblast like cell-lines MC3T3-clone 14 and MC3T3-clone 24 (Wang et al., 1999) (ATCC, Teddington, UK) were cultured in maintenance media at 37°C, 5% CO_2. For experimentation, cells were trypsinised (as described in 2.2.2.), counted using a haemocytometer and then plated in multi-well plates at a density of 1 x 10^4 cells/cm^2. Upon confluency, maintenance media was replaced with MC3T3 mineralisation media (Appendix I) to induce the differentiation and support ECM mineralisation of MC3T3 cell cultures. Cell cultures were maintained for up to 14 days and media was replaced every 2-3 days.

2.2.4. IDG-SW3 cells

IDG-SW3 cells (a kind gift from Prof. Bonewald, University of Missouri) were initially expanded through culture in IDG-SW3 proliferation media (containing recombinant mouse Interferon-γ which is required to induce expression of the SV40 large tumor antigen and maintain proliferation of this cell line, Appendix I) at 33°C (Woo et al., 2011). For experimentation, cells were trypsinised (as described in 2.2.2.), counted using a haemocytometer and then plated in multi-well plates at a density of 4 x 10^4 cells/cm^2. Upon confluency, proliferation media was replaced with IDG-SW3 mineralisation media (Appendix I) to induce the differentiation and support ECM mineralisation of IDG-SW3 cell cultures. Cell cultures were transferred to 37°C and maintained for up to 28 days with media changes every 2-3 days. The culture of IDG-SW3 cells was carried out on type I collagen coated plasticware.

2.2.5. Murine calvarial osteoblast isolation and culture.

The calvariae from 3-4 day old new born WT and *Phospho1*$^{-/-}$ mice were dissected under sterile conditions as previously described (Jonason and O'Keefe, 2014). Isolated calvariae were washed in Hank's balanced salt solution (HBSS) and subjected to serial enzymatic and chemical digestions at 37°C with constant agitation. In brief, calvariae were initially subjected to a type II collagenase (10 mg/ml, Worthington, New Jersey, USA) digestion for 10 min after which the supernatant was discarded. Next, calvariae were again exposed to type II collagenase for 30 min, with the supernatant and subsequent phosphate buffered saline (PBS) wash were retained (fraction 1). Following this, calvariae were incubated with 4 mM EDTA for 10 min with the supernatant and subsequent HBSS wash were retained (fraction 2). A final 30 min, type II collagenase digestion was carried out and the supernatant was retained (fraction 3). Primary osteoblasts were harvested, by combining all fractions and centrifuging them at 1000 x g for 5 min. The resultant cell pellet was resuspended in maintenance media and transferred to tissue culture flasks, where they were maintained in a humidified atmosphere (37°C, 5% CO_2) until 70-80% confluent. For experimentation, cells were trypsinised (as described in 2.2.2.), counted using a haemocytometer and then plated in multi-well plates at a density of 1 x 10^4 cells/cm^2. Upon confluency, maintenance media was replaced with primary osteoblast mineralisation media to induce the differentiation and support ECM mineralisation of primary osteoblast cell cultures. Cell cultures were maintained for up to 28 days and media was replaced every 2-3 days.

2.2.6. Human subchondral bone osteoblast isolation and culture

Human samples were obtained following ethical guidelines (Tissue Governance, NHS Lothian) and consent from patients undergoing total knee replacement for osteoarthritis in collaboration with Mr. Anish Amin (Orthopaedic surgeon, NHS Lothian). Upon advice from Mr. Amin, the non-osteoarthritic condyle of the tibia was subjected to the following protocol to isolate the subchondral osteoblasts.

Articular cartilage was removed from the tibial condyle and the underlying bone cut into small fragments (2-3 mm^3) using bone clippers. These fragments were washed briefly six times in PBS containing 10% v/v penicillin streptomycin (PenStrep solution). Bone fragments were then incubated for 10 min at 37°C in trypsin-EDTA. The bone fragments were subsequently washed in PBS and then incubated for 30 min at 37°C in 10 mg/mL type II collagenase. Next, the bone fragments were washed 3 x 5 min in PenStrep solution. The processed bone fragments were then used to establish explant cultures in T75 flasks with human osteoblast culture media (Appendix I). Media was changed every three days and at 70-80% confluency, cells were trypsinised (as described in 2.2.2.), counted using a haemocytometer and then plated in multi-well plates at a density 3 x 10^4 cells/well. Experiments utilising human subchondral osteoblast cell cultures were carried out upon confluency.

2.3. *Ex-vivo* organ culture

2.3.1. Murine embryonic metatarsal dissection and culture

WT and *Phospho1*$^{-/-}$ embryos were culled by decapitation on embryonic day 15. The hind limbs of each embryo were dissected and placed into pre-warmed preparation media (Appendix I) under sterile conditions. Using a dissecting microscope the central three metatarsals from each hind limb were carefully isolated and maintained in

preparation media (Houston et al., 2016a). Metatarsals were cultured in 24-well tissue culture plates; each well contained one bone and 300 µL metatarsal media (Appendix I). Metatarsals were cultured in a humidified atmosphere (37°C, 5% CO_2) for up to 7 days. The culture media was not changed during the culture (Haaijman et al., 1997). The total length of the metatarsal and the length of the mineralisation zone were measured along the centre line using image analysis software (DS Camera Control Unit DS-L1, Nikon, Surrey, UK).

2.3.2. Murine calvariae dissection and culture

The calvariae from 4-day old, new born WT mice were dissected aseptically and transferred to pre-warmed calvariae culture media (Appendix I). Next, calvariae were halved along the sagittal suture, and hemi-calvariae were cultured in 24-well tissue culture plates with 350 µL of calvariae culture media for 24 hours (h) prior to experimentation. After 24 h, culture media was replaced with fresh media and supplemented with experimental reagents for up to 24 h.

2.4. RNA Methods

2.4.1. Isolation of RNA from cell cultures

Cultured cells were scraped from individual wells in 1 mL of ice cold PBS, pelleted at 12000 x g for 1 min and stored at -70°C. Total RNA was extracted using the RNeasy mini kit (Qiagen, West Sussex, UK) according to the manufacturer's instructions. It is essential that cell pellets are fully homogenised in RLT buffer with 1% v/v β-mecaptoethanol by vortexing before progressing with the remainder of the protocol. The concentration and quality (as assessed by the 260:280 nm wavelength absorbance ratio) was determined using a nanodrop spectrophotometer (ND-1000, Thermo Fisher Scientific).

2.4.2. Isolation of RNA from murine tissues

Murine tissues obtained from animal dissection or *ex vivo* culture were snap frozen in liquid nitrogen and stored at -70°C. Total RNA was extracted using the RNeasy lipid tissue mini kit (Qiagen) as described herein. In brief, murine tissues were homogenised in 1 mL of Qiazol (Qiagen) using a T10 basic ULTRA-TURRAX homogeniser (IKA, Staufen, Germany). The homogenised samples were incubated for 5 min at room temperature prior to the addition of 200 µL of chloroform. Samples were shaken vigorously for 15 s and centrifuged at 12000 x g for 15 min at 4°C. Centrifugation of the sample induces a phase separation, consisting of an organic lower phase, an interphase and an aqueous upper phase; the aqueous phase was transferred to a 2 mL safelock Eppendorf (Sigma Aldrich) and care was taken not to transfer any of the interphase or organic phase. To the aqueous upper phase, 600 µL of 70% v/v ethanol was added to precipitate the RNA. The RNA was captured, processed and eluted in nuclease-free water (NFW) according to the manufacturer's instructions. The concentration and quality (as assessed by the 260:280 nm wavelength absorbance ratio) was determined using a nanodrop spectrophotometer.

2.4.3. Reverse transcription of RNA

The reverse transcription of RNA to cDNA was carried out utilising the DNA polymerase, Superscript II. In brief, 2 µL of random hexamers (random hexamer diluted 1:60, Thermo Fisher Scientific) was added to 10 µL of diluted RNA from sections 2.4.1. and 2.4.2. and incubated at 70°C for 10 min in a Hybaid polymerase chain reaction (PCR) express thermal cycler (Thermo Fisher Scientific). The samples were immediately cooled on ice. A mastermix comprising, 4 µL 5X first-strand buffer, 2 µL dithiothreitol (DTT, 0.1 M), 1 µL deoxyribonucleotide triphosphate mix (10 mM)

and 1 µL Superscript II enzyme (all Thermo Fisher Scientific) was prepared and 8 µL of the mastermix was added to each sample. The samples were run on the following programme in the Hybaid PCR machine: 25°C for 10 min, 42ºC for 50 min, 70°C for 15 min and held at 4°C. The resulting cDNA samples were diluted to 5 ng/µL with NFW and stored at -20°C.

2.4.4. Real-time quantitative polymerase chain reaction (RT-qPCR) and quantification of gene expression

RT-qPCR reactions were carried out in a 96-well PCR plates and cycled in a Stratagene Mx3000P PCR cycler (Agilent Technologies, Santa Clara, USA). Each qPCR reaction was performed with 5 µL (25 ng) of diluted cDNA from section 2.4.3. and 15 µL of qPCR mastermix which comprised: 1µL primers (10µM, forward and reverse primer), 10 µL 2X PrecisionPlus SYBR green mastermix (PrimerDesign, Southampton, UK) and 4µL NFW. The following program was used to perform the qPCR reaction: Initial hotstart enzyme activation (2 min at 95°C) followed by 40 cycles of denaturation (15 s at 95°C) and annealing (1 min at 60°C). A post-PCR melt curve analysis was carried out to ensure only one PCR product was formed during the qPCR reaction. Three technical replicates were performed for each sample and reactions analysing the expression of suitable housekeeping genes were similarly performed. The relative expression of the target genes was calculated using the $2^{-\Delta\Delta Ct}$ method (Livak and Schmittgen, 2001).

2.4.5. Primer validation

Primers were tested for amplification efficiency by performing the qPCR reaction on serial dilutions of cDNA (known to express the target gene) and producing a standard curve from the amplification (Ct) results (Fig 2.1.A). Primers were considered

acceptable if the amplification efficiency was within the range of 90-110%, with an R^2 value between 0.90 and 1.00, and amplification curves were regularly spaced along the dilution series. Primer specificity was demonstrated both by the generation of a single peak in the melt curve (Fig 2.1.B) and by Sanger sequencing of the qPCR product. In brief, qPCR products were cleaned of salts and impurities using a QIAquick PCR purification kit (Qiagen). Purified PCR products were sent for Sanger sequencing at Edinburgh Genomics. The National Centre for Biotechnology Information (NCBI) Basic local Alignment Search Tool (BLAST) was used to compare the resulting sequences to the mouse genome (Fig 2.1.C).

2.5. Protein methods

2.5.1. Protein extraction from cell cultures

Cultured cells were rinsed in ice cold PBS and scraped in 200 µL of radio-immunoprecipitation assay (RIPA, Thermo Fisher Scientific) buffer containing 15% v/v complete protease inhibitor cocktail (Roche, West Sussex, UK) and 1% v/v phosphatase inhibitor cocktail 2. Samples were vortexed and stored at -20°C until further use.

2.5.2. Protein extraction from murine tissues

Murine tissues obtained from animal dissection or *ex vivo* culture were snap frozen in liquid nitrogen and stored at -70°C. Murine tissues were homogenised in 500 µL of RIPA buffer containing 15% v/v complete protease inhibitor cocktail and 1% v/v phosphatase inhibitor cocktail 2 using a T10 basic ULTRA-TURRAX homogeniser. Homogenised samples were stored at -20°C until further use.

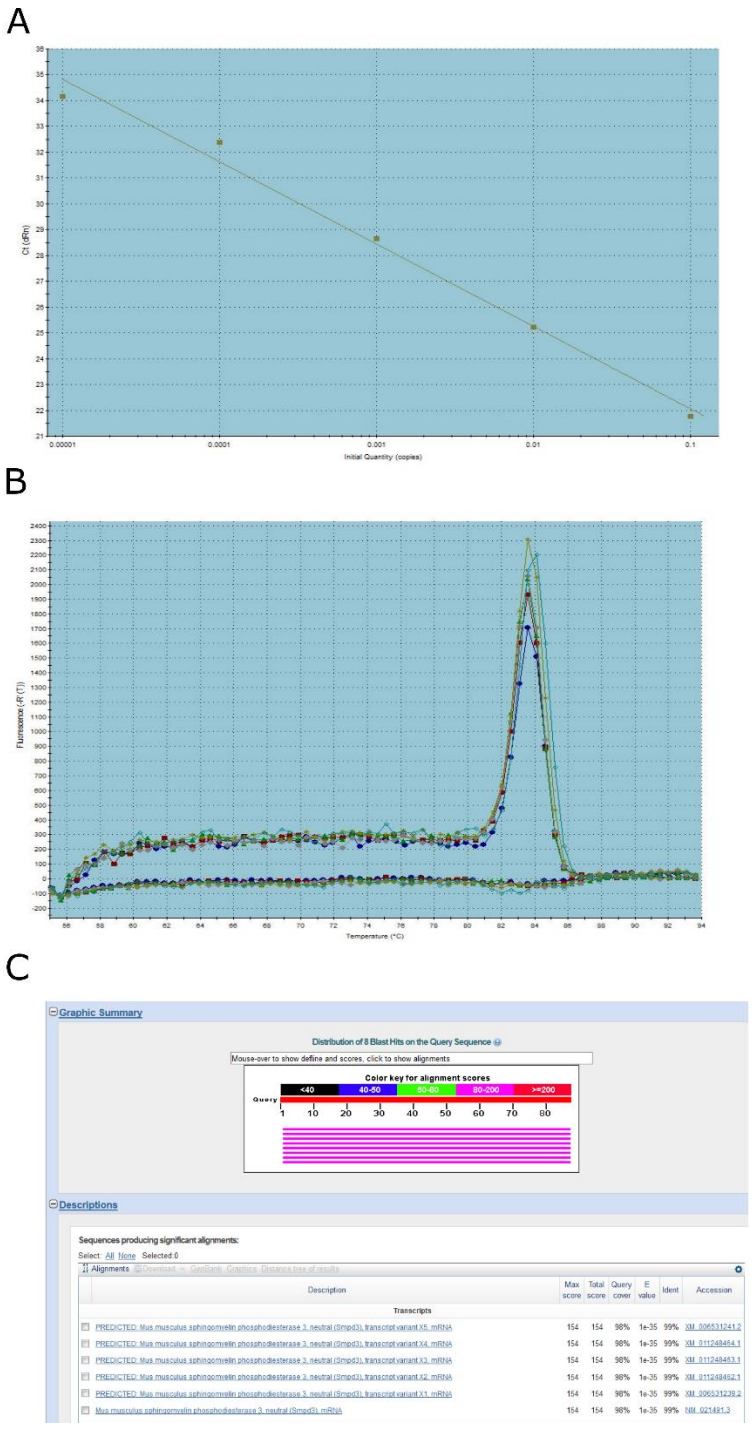

Figure 2.1. Validation of qPCR primer efficiency and specificity.

Representative image of **(A)** standard curve, **(B)** melt curve and **(C)** NCBI BLAST results confirming the identity of sequenced qPCR product.

2.5.3. Determination of protein concentration

The Bio-Rad Detergent Compatible (DC) protein assay (Bio-Rad, Hertfordshire, UK) was used to determine the protein concentration of extractions from sections 2.5.1. and 2.5.2. Serial dilutions of bovine γ-globulin (2 mg/mL, protein standard, Bio-Rad) were initially prepared to generate a standard curve. Next, 5 µL of protein standard or samples were pipetted in duplicate into a 96-well plate followed by 25 µL alkaline copper tartrate (reagent A') and 200 µL Folin's reagent (reagent B). The plate was shaken briefly and incubated for 15 min at room temperature. The absorbance at 750 nm was assessed in each well using a Multiskan Ascent microplate reader (Thermo Fisher Scientific). The protein concentration of the samples was determined through extrapolation from the generated standard curve.

2.5.4. Western blotting

Following protein concentration determination (section 2.5.3.) the appropriate volume of protein lysate to provide between 10-20 µg was calculated and combined with 4X lithium dodecyl sulphate sample buffer (Thermo Fisher Scientific) and DTT reducing agent (Thermo Fisher Scientific) prior to denaturation at 70°C for 10 min. Denatured protein samples and a pre-stained molecular weight marker (All Blue, Bio-Rad) were chilled on ice prior to being loaded into 10% Bis-Tris polyacrylamide gels (Thermo Fisher Scientific). Proteins were separated by electrophoresis at 200 V for 50 min in a Novex gel tank (Thermo Fisher Scientific) containing 1X MOPS (3-(N-morpholino) propanesulfonic acid) running buffer (Appendix I). Antioxidant (2.5 µL/mL, Thermo Fisher Scientific) was added to the centre compartment of the tank to preserve reduced proteins. After separation, proteins within the polyacrylamide gels were transferred onto Hybond-enhanced chemoluminesence nitrocellulose membrane (GE Healthcare,

Buckinghamshire, UK). In brief, the nitrocellulose membrane was placed onto the polyacrylamide gel and sandwiched between transfer buffer (Appendix I) soaked filter paper and sponges within a transfer module (Thermo Fisher Scientific). The transfer of proteins was carried out on ice for 90 min at 30 V.

Following transfer, nitrocellulose membranes were washed 5 x 5 min in PBS. Membranes were subsequently blocked in Odyssey blocking buffer (LI-COR Biosciences, Nebraska, USA) for 1 h at room temperature. The membranes were probed with primary antibodies diluted at the appropriate concentrations in Odyssey blocking buffer overnight at 4°C with constant agitation. Nitrocellulose membranes were next washed 3 x 5 min in PBS prior to incubation with the appropriate secondary antibodies (Appendix II) for 50 min at room temperature and protection from light. After extensive washing in PBS, antibodies were detected using the Odyssey CLx infrared scanner (LI-COR Biosciences) (Eaton et al., 2013). Scans were performed in either the 700 nm or 800 nm channels as appropriate with a scan resolution of 169 µm. In some experiments, quantification of the western blots was performed with Image Studio Lite (LI-COR Biosciences).

To allow the probing of multiple protein targets on the same nitrocellulose membrane, antibodies were stripped from membranes using restore plus stripping buffer (Thermo Fisher Scientific) for 40 min at room temperature and with constant agitation. After extensive washing with PBS, membranes were re-probed with the appropriate secondary antibodies and visualised using the Odyssey CLx infrared scanner to confirm successful stripping.

2.6. Lipid methods

2.6.1. Lipid extraction and quantification

Cultured embryonic metatarsals from section 2.3.1. were snap frozen in liquid nitrogen and stored at -70°C until further processing. Next, metatarsals (20 bones per sample) were incubated with 200 µL type II collagenase (10 mg/ml) at 37°C for 4 h with constant agitation. After this incubation, the samples were again snap frozen in liquid nitrogen and stored at -70°C. Lipids were extracted from collagenase digested samples according to the method of Folch et al., 1957. Samples were transferred to borosilicate glass tubes with PFTE lined caps (13 mm diameter, Thermo Fisher Scientific) and 4 mL of chloroform/methanol (2:1, v/v) was added. Samples were vortexed extensively and incubated for 1 h in a sonicating water bath at room temperature. The mixture was partitioned through the addition of 1.25 mL of potassium chloride (0.1 M), vortexed briefly, and centrifuged at 1500 x g for 10 min to induce phase separation. The organic, lower phase was transferred to a new borosilicate glass tube using a glass Pasteur pipette and subsequently dried under a stream of nitrogen gas. The dried lipid extract was reconstituted in 200 µL methanol containing 5 mM ammonium formate. Glycophospholipid analysis and quantification was performed by Professor Phillip Whitfield at the Lipidomics Research Facility, Inverness, UK using liquid chromatography (hydrophilic interaction chromatography column) mass spectrometry (Exactive Orbitrap mass spectrometer, Thermo Fisher Scientific).

2.7. *In vivo* methods

2.7.1. Animal welfare and generation

All animal experiments were approved by the Roslin Institute's Animal Users Committee and the animals were maintained in accordance with Home Office

guidelines for the care and use of laboratory animals. Animals were maintained under conventional housing conditions with a 12 h light/dark cycle and free access to food and water. *Phospho1*$^{-/-}$ mice, which possess a cytosine to thymidine mutation in codon 74 of exon 2 (introducing a stop codon) of the *Phospho1* gene, were generated as previously described (Ciancaglini et al., 2010). Separate colonies of WT (C57BL/6J) and *Phospho1*$^{-/-}$ mice were maintained and genotyping of offspring was performed as described in section 2.7.2.

2.7.2. DNA extraction and genotyping

Ear snips from WT and *Phospho1*$^{-/-}$ mice were collected and the DNA was extracted using DNA extraction solutions I and II (Appendix IV). In brief, 75 μL of solution I was added to each ear snip and samples were incubated at 95°C for 30 min. The reaction was stopped by the addition of 75 μL of solution II. PCR was performed on extracted DNA using PCR primers targeted toward exon 3 of the murine *Phospho1* gene (Appendix IV). The resulting amplified DNA was subjected to restriction digest with BsrDI restriction enzyme (New England Biolabs, Massachusetts, USA) through the addition of 5 μL of restriction digest master mix (Appendix IV) to the DNA and incubation at 65°C for 1 h. Digested samples were electrophoresed on a 1.5% w/v agarose: Tris-borate-EDTA gel containing 0.01% v/v SYBRsafe (Thermo Fisher Scientific) and the gels were visualised using a Gel Doc XR+ System (Bio-Rad). HyperLadder 1kb (Bioline, London, UK) was used as a molecular weight marker.

2.7.3 Parathyroid hormone administration

Recombinant human parathyroid hormone 1-34 (rhPTH 1-34, BACHEM, Bubendorf, Switzerland) was reconstituted in sterile PBS and stored in aliquots at -70°C. Prior to

in vivo administration, rhPTH 1-34 was diluted to the appropriate concentration with 0.9% w/v saline containing 0.2% w/v bovine serum albumin (vehicle solution). For single dose and intermittent studies, animals were weighed on the day of injection and 50 µL injections containing 80 µg/kg rhPTH 1-34 or vehicle solution were administered subcutaneously. The continuous administration of rhPTH 1-34 was carried out using a subcutaneously implanted Alzet micro-osmotic pump (Model 1004, Durect Corp., California, USA). In brief, micro-osmotic pumps were filled with 100 µL of rhPTH 1-34 (0.308 mg/ml) or vehicle solution and submerged in sterile 0.9% w/v saline and incubated at 37°C for 48 h prior to surgical implantation. This priming step ensured the pumps released their contents at the defined rate immediately upon implantation. Pumps were implanted subcutaneously, posterior to the scapula in accordance with manufacturer's guidelines.

2.7.4. Processing of tissue to paraffin

Murine tissues destined for histology or immunohistochemistry were dissected, and in the case of bone samples, freed from any soft tissues immediately following sacrifice of the animal. Dissected tissues were fixed in 4% w/v paraformaldehyde (PFA) for 24 h. Soft tissues (kidney and thyroid) were then stored in 70% v/v ethanol until further processing. After 24 h in fixative, bone samples were transferred to 10% w/v EDTA (pH 7.4) and maintained at 4°C with constant agitation for up to four weeks. EDTA was changed every 2-3 days. Tissues were next dehydrated and processed to paraffin wax using a Leica ASP300S tissue processor (Leica Microsystems, Milton Keynes, UK) with the following steps applied: two 1 h incubations in 70% v/v ethanol, two 1 h incubations in 95% v/v ethanol, two 1 h incubations in absolute ethanol, two 1 h incubations in xylene, three 1 h incubations in paraffin wax (at 60°C and under

vacuum). Processed tissues were embedded in paraffin wax using plastic moulds and allowed to set at 4°C prior to storing at room temperature. Using a Leica RM2235 microtome (Leica) equipped with MX35 Premier plus Microtome Blades (Thermo Fisher Scientific), wax blocks were trimmed to expose the sample surface. The paraffin embedded samples were then cooled and tissues were sectioned at 5 μm thickness. Sections were floated into a water bath at 40°C, before being transferred to poly-L-lysine coated microscope slides (VWR International Ltd., Lutterworth, UK). Slides were stored at room temperature until required.

2.7.5. Immunohistochemistry

The spatial localisation of TNAP within paraffin embedded bone sections was assessed by immunohistochemistry. First, sections of paraffin embedded bone (section 2.7.4.) were de-waxed in xylene and rehydrated through a series of alcohols to dH_2O. Next, an antigen retrieval process was carried to out to expose the antigenic site on proteins which are readily cross-linked by methylene bridges during PFA fixation. Antigen retrieval was carried out by immersing slides in either citrate buffer (Appendix I) for 90 min at 70°C. Slides were next washed in PBS (3 x 5 min) before inactivation of endogenous tissue peroxidases by incubating the slides in 0.3% v/v hydrogen peroxide in methanol for 30 min at room temperature. Slides were washed in dH_2O (5 min) and PBS (3 x 5 min). Being careful not to disturb the tissue sections, slides were blotted dry and a wax pen (Daido Sangyo Co. Ltd., Tokyo, Japan) was used to create a boundary around the section. Sections were incubated in a blocking solution (normal goat serum diluted 1:5 in 5% v/v foetal bovine serum in PBS) for 30 min at room temperature. The blocking solution was tipped off and again the sections were blotted dry before being incubated with the primary antibody (TNAP, diluted 1:200 in 5% v/v

foetal bovine serum in PBS) or control rat IgG overnight at 4°C in a humidity chamber so as to prevent evaporation. The following day, slides were washed in PBS (3 x 5 min) and incubated with the goat anti-rat horseradish peroxidase-conjugated secondary antibody (diluted 1:100 in 5% v/v foetal bovine serum in PBS) for 1 h at room temperature. Slides were again washed in PBS (3 x 5 min) and subsequently incubated with 3,3'-diaminobenzidine for 15 s and washed thoroughly in dH_2O. Slides were dehydrated through a series of alcohols and xylene and counterstained with haematoxylin using the Leica ST5010 Autostainer XL. Slides were mounted with DePeX (VWR International Ltd.) and visualised using a Nikon E600 microscope with a digital camera attachment. Images were obtained using Image Tool Version 3.00.

2.7.6. Micro-computed tomography imaging

Micro-computed tomography (μCT) imaging was used to assess trabecular and cortical bone architecture in the tibiae of experimental mice. Tibiae were dissected, freed from any surrounding soft tissues and stored in dH_2O at -20°C prior to scanning. High resolution scans were performed by Dr Katherine Staines or Mr Mark Hopkinson, using a Skyscan 1172 (Skyscan, Kontich, Belgium) μCT system, with the X-ray tube operated at 50 kV and 200 μA, 1600 ms exposure time with a 0.5 mm aluminium filter and a voxel size of 5 μm. Scans were then reconstructed using NRecon 1.6.9.4 (Skyscan, Kontich, Belgium). All downstream processes were performed by myself. CTAn 1.13.5.1 + version software (Skyscan, Kontich, Belgium) was used to perform 2D/3D analysis of reconstructed scans including tibial length. Metaphyseal trabecular bone of the proximal tibia was assessed in a 250 slice stack, 5% of the total bone length below the first appearance of a trabecular 'bridge' connecting the two primary spongiosa bone islands (Fig 2.2.A, (Javaheri et al., 2015))

Cortical bone was assessed in 100 slice stacks at 37% and 50% of the total bone length (proximal-middle, Fig 2.2.B) from the reference starting slice (first appearance of the medial tibial condyles) (Sugiyama et al., 2008). To assess bone mineral density (BMD), BMD phantoms were used to calibrate the CTAn software. BMD phantoms of known calcium hydroxyapatite mineral densities of 0.25 and 0.75 g/cm^3 were scanned and reconstructed using the same parameters as used for bone samples.

2.7.7. Three point bending analysis

Mechanical testing was performed on tibiae from the defined groups of male mice using an LXR material testing machine (Lloyd Instruments, West Sussex, UK) fitted with an 100 N load cell. The span was fixed at 10 mm, and the cross-head was lowered at 1 mm/min. Data were recorded after every 0.2 mm change in deflection. Each bone was tested to failure, with failure points being identified as the point of maximum load from the load–extension curve. The maximum stiffness was defined as the maximum gradient of the rising portion of this curve (Aspden, 2003).

2.8. In vitro assays

2.8.1. Alizarin red staining and quantification

The calcium deposition within cell cultures was assessed by alizarin red staining. Cells were washed with PBS prior to fixing for 5 min in 4% w/v PFA. Alizarin red stain (2% w/v, pH 4.2) was used to stain the cell monolayers for 5 min at room temperature. Unbound stain was removed by repeated washing of the cell monolayers with dH_2O. Stained monolayers were imaged with a digital camera by Mr Norrie Russell of The Roslin Institute. Quantification of the bound alizarin red stain was carried out by initially leaching the dye through the addition of 10% w/v cetylpyridinium chloride for 1 h. The absorbance of the resultant solution was determined at a wavelength of

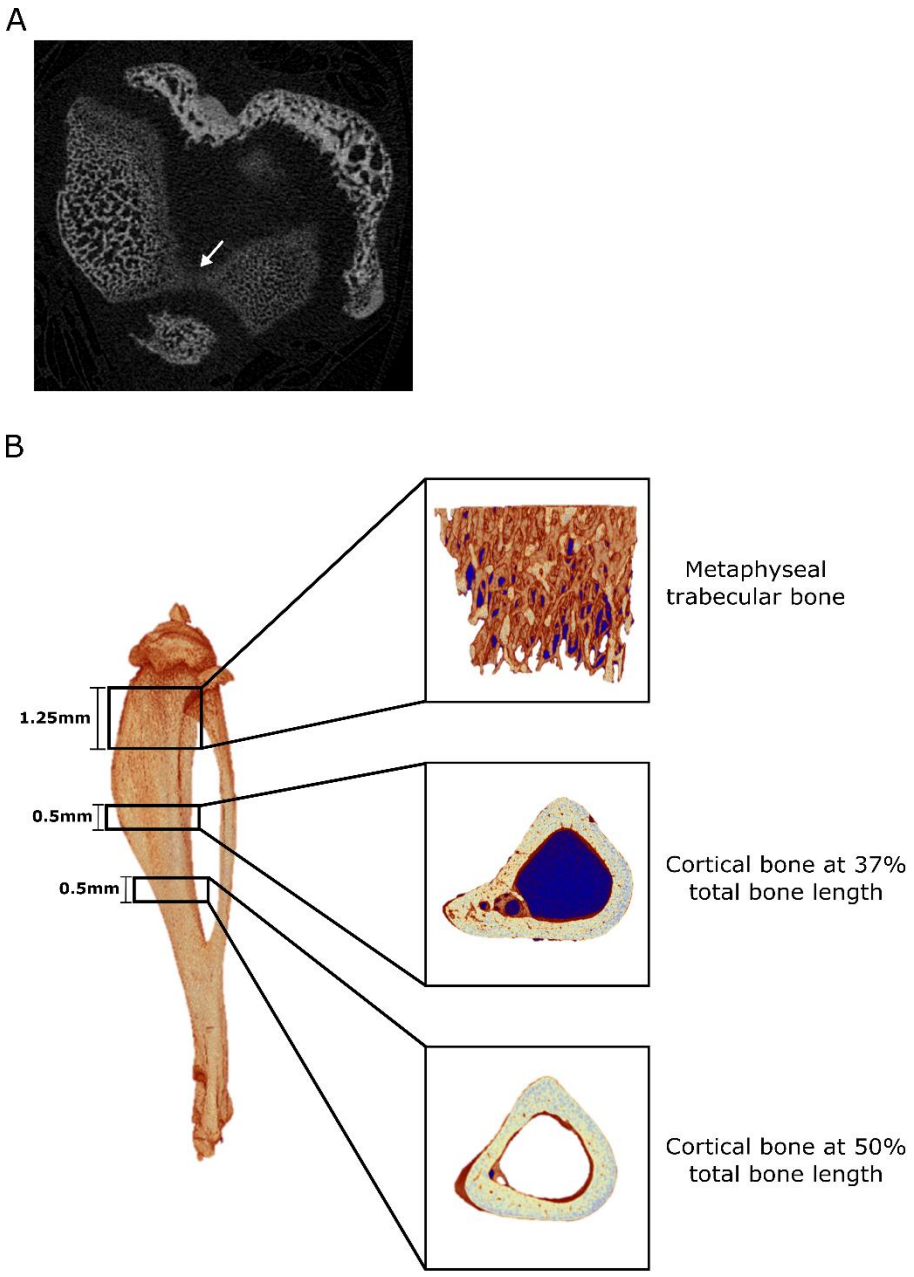

Figure 2.2. Analysis of bone microarchitecture by µCT.

(A) Representative image showing the trabecular 'bridge' connecting the two primary spongiosa bone islands. Metaphyseal trabecular bone was assessed in a 1.25 mm section, beginning 5% below this reference point **(B)** Representative images of metaphyseal trabecular bone and cortical bone at 37% and 50% of the total bone length.

570 nm using a Multiskan Ascent microplate reader. Each biological replicate was tested in duplicate, and 10% w/v cetylpyridinium chloride was used as a blank.

2.8.2. Calcium assay

To assess serum calcium, serum from experimental mice was prepared from a terminal blood sample. Whole blood was allowed to clot on ice for 30 min prior to centrifugation at 1000 x g for 10 min. The resultant supernatant (serum) was aliquoted and stored at -70°C. Serum calcium was assessed by a colorimetric assay (Randox calcium assay, Randox Laboratories Ltd., County Antrim, UK). In brief, 6.25 µL of calcium standard and serum samples were pipetted in duplicate into a 96-well plate. Equal volumes of buffer R1 and buffer R2 (containing O-Cresophthalein, which forms a violet complex with calcium ions under alkaline conditions) were combined and 250 µL of the buffer mixture was pipetted into wells containing standard and samples. The plate was gently vortexed and the absorbance of each well was determined at a wavelength of 570 nm using a Multiskan Ascent microplate reader.

2.8.3. Bone formation and resorption marker assays

The concentrations of P1NP and CTX-1 were assessed in the serum of experimental mice using a rat/mouse P1NP or rat/mouse CTX-1 enzyme immunoassay (Immunodiagnostic Systems, Newcastle, UK) respectively. The assays were performed by Ms Elaine Seawright. Quantification of serum concentration was achieved through extrapolation from the generated standard curves.

2.9. Statistical methods

Data were analysed with appropriate statistical tests using Graphpad Prism 6 (Graphpad Software, California, USA). All data were initially assessed for normality

and equal variance to determine whether parametric or non-parametric tests should be used. Student's t-test, one-way analysis of variance (ANOVA) and two-way ANOVA (with *post hoc* Holm-Sidak pairwise multiple comparison tests between individual groups) were applied where appropriate on parametric data sets. The Kruskal-Wallis test (with *post hoc* Dunn's tests between individual groups) was used when comparing multiple data sets which were not normally distributed. Data are presented as mean ± standard error of the mean (S.E.M.) and 'N' refers to the number of individual samples assessed in the study.

Chapter 3

Development and characterisation of novel *in vitro* models of ECM mineralisation

3.1. Introduction

Biomineralisation of vertebrate tissues, *i.e*. the deposition and propagation of HA within the ECM is an essential prerequisite in the provision of functional bone, dentin and growth plate cartilage (Anderson, 1995). This complex process depends on the coordination of both biochemical and physicochemical processes, mediated, in part, through a tightly controlled balance of promoters and inhibitors of mineralisation (Millán, 2012, Giachelli, 2005). During the initiation of skeletal mineralisation, amorphous calcium phosphate nucleates within the sheltered interior of MVs (Anderson, 2003, Cui et al., 2016). Believed to bud from the apical membrane of osteoblasts and hypertrophic chondrocytes in bone and growth plate cartilage respectively (Thouverey et al., 2009, Wuthier and Lipscomb, 2011), MV composition is directly related to their function. In particular, the inner leaflet of the MV membrane shows selective enrichment in PS, which alongside Anx, serve to accumulate calcium and aid the nucleation of calcium-phosphate complexes (Cotmore et al., 1971, Wu et al., 2002). Phosphatases too are essential regulators of ECM mineralisation, modifying local levels of P_i, PP_i and indeed, the phosphorylation status of OPN, a key regulator of ECM mineralisation (Narisawa et al., 2013).

The glycosylphosphatidylinositol anchored ectozyme, TNAP, is perhaps the most well established promoter of ECM mineralisation, catalysing the breakdown of PP_i to P_i in the extra-vesicular environment to generate a P_i/PP_i ratio conducive to HA propagation within the ECM (Register et al., 1986, Millan, 2006). Defective TNAP activity resulting from missense mutations in the *ALPL* gene, as observed in the human condition HPP (Henthorn and Whyte, 1992), or the complete genetic ablation of the *Alpl* gene in mice, results in severe hypomineralisation of the skeleton and teeth

ensuing after birth (Harmey et al., 2004, Yadav et al., 2012). Contrastingly, NPP1, is a plasma membrane glycoprotein generating PP_i in the extra-vesicular environment from nucleoside triphosphates (Mackenzie et al., 2012b). Concomitant ablation of *Enpp1* on a *Alpl*$^{-/-}$ genetic background partially restores the serum PP_i levels and normalises skeletal mineralisation (Harmey et al., 2004), highlighting the antagonistic roles of these two MV enzymes. Intriguingly however, pioneering studies utilising electron microscopy revealed that MVs from patients with hypophosphatasia and *Alpl*$^{-/-}$ mice possess crystals of HA within their interiors (Anderson et al., 1997, Anderson et al., 2004). These findings highlight alternative mechanisms of generating a PP_i:P_i ratio conducive to mineral formation within the interior of MV.

Active within chondrocyte- and osteoblast- derived MV (Roberts et al., 2004, Stewart et al., 2006) and expressed exclusively in mineralising bone, cartilage and dentin (Houston et al., 2004, Roberts et al., 2007, McKee et al., 2013), PHOSPHO1, is essential for the initiation of MV mediated mineralisation. Small molecule inhibition of PHOSPHO1 in MV's derived from *Alpl*$^{-/-}$ mice significantly affects their ability to calcify *in vitro* (Roberts et al., 2007). The genetic ablation of *Phospho1* results in severely hypomineralised skeletal and dental tissues with resulting bowing of the long bones, spontaneous fractures and scoliosis (Huesa et al., 2011, Yadav et al., 2011, McKee et al., 2013, Rodriguez-Florez et al., 2015). This phenotype may be underpinned by the recent observation that MV-mediated initiation of mineralization was impaired in chondrocytes from *Phospho1* deficient mice (Yadav et al., 2016). Complete ablation of skeletal mineralisation is observed in *Phospho1*$^{-/-}$;*Alpl*$^{-/-}$ double knockout embryos and in metatarsals cultured in the presence of both PHOSPHO1 and TNAP inhibitors (Yadav et al., 2011, Huesa et al., 2015). *In vitro*, PHOSPHO1 shows

high phosphohydrolase activity towards PCho and PEth, two metabolites derived from lipid metabolism (Roberts et al., 2004).

More recently, hypomineralisation of skeletal and dental tissues was observed in the *fro/fro* mouse, a mouse containing a major deletion in the sphingomyelinase phosphodiesterase 3 (*Smpd3)* gene (Khavandgar et al., 2011, Khavandgar et al., 2013). *Smpd3* encodes for neutral sphingomyelinase 2 (nSMase2) which catalyses the breakdown of the membrane lipid SM to ceramide and PCho. Through their role in the generation and processing of PCho, nSMase2 and PHOSPHO1 respectively, may function together to liberate P_i for skeletal mineralisation (Khavandgar and Murshed, 2015). The links between lipid metabolism and skeletal mineralisation have been bolstered through investigation CK enzymes, which phosphorylate choline to produce PCho. *Flp/flp* mice, which possess a mutation in exon 1 of the choline kinase β (*Chkβ*) gene, exhibit low bone mass and reduced osteoblast ECM mineralisation *in vitro* (Kular et al., 2015). Similarly, the pharmacological inhibition of choline kinase alpha (*Chkα*) in human osteosarcoma MG-63 cells leads to a diminished mineralisation capacity and a reduction in TNAP activity (Li et al., 2014b). The essential role of phosphate manipulation in the initiation of skeletal mineralisation, has, as highlighted above, been confirmed through the use of transgenic mouse models and *in vitro* models of mineralisation. To date however, these enzymes have been studied in isolation. To investigate whether any interplay exists between these enzymes, they must be studied simultaneously. Despite this, the examination of this potential interplay is hampered by the currently accepted *in vitro* models of mineralisation.

ECM mineralisation has been studied *in vitro* in a number of clonal cell lines, primary cell cultures and organ culture model systems. Well-established methodologies for inducing ECM mineralisation in these models requires the addition of phosphate sources with βGP the most common choice amongst most researchers. The use of βGP to induce ECM mineralisation however, has a number of limitations, particularly when seeking to investigate the regulation and control of enzymes essential for ECM mineralisation. For example, *Alpl* expression and activity is enhanced in the presence of βGP (Orimo and Shimada, 2006). Furthermore, the presence of matrix mineralisation in βGP supplemented cultures is considered by many, to merely indicate the presence of alkaline phosphatase activity, as was observed by Khouja et al. (1990), in which human trabecular osteoblasts mineralised their ECM to the same extent as human skin fibroblasts. The authors of this latter study additionally observed significant amounts of calcium and phosphate deposits in cell-free cultures (Khouja et al., 1990). This stimulation of alkaline phosphatase activity is a hindrance to the study of additional mineralisation regulators as it may modulate the requirement of underlying physiological processes in the production of P_i for HA formation. It is therefore crucial that exogenous phosphatase-substrate free models of ECM mineralisation are developed to allow the investigation of the expression and regulation of essential regulators of MV-mediated ECM mineralisation.

3.2. Hypothesis

ECM mineralisation can be achieved *in vitro* without the use of exogenous phosphatase substrates. ECM mineralisation involves the co-ordinated expression of key regulators of P_i generation.

3.3. Aims

I) Identify suitable phosphatase-substrate free conditions for the *in vitro* mineralisation of MC3T3 osteoblast-like cell lines, primary calvarial osteoblasts and cultured embryonic metatarsals.

II) Examine the temporal mineralisation of these *in vitro* models under phosphatase-substrate free conditions.

III) Determine the temporal expression patterns of PHOSPHO1, TNAP and nSMase2 during mineralisation in the *in vitro* models developed in Aim I.

3.4. Materials and methods

3.4.1. MC3T3 cell culture

The MC3T3-C24 control empty-vector transfected (EV) and MC3T3-C24 FLAG-tagged PHOSPHO1 transfected (FP1) cells were previously generated by Dr Carmen Huesa (Huesa et al., 2015). MC3T3-C14, MC3T3-C24, MC3T3-C24 EV and MC3T3-C24 FP1 cell lines were seeded in multi-well plates at 1 x 10^4 cells/cm^2 in maintenance medium and cultured as described in section 2.2.3 (see Table 1 for review of the characteristics of these and other cell lines used in this thesis). To investigate the mineralisation of MC3T3-C24 EV and MC3T3-C24 FP1 cell cultures in exogenous phosphatase-substrate free conditions (section 3.5.1.), cells were cultured for 14 days in maintenance media containing either: 50 µg/mL ascorbic acid (AA), 50 µg/mL AA and 1.5 mM calcium chloride, 50 µg/mL AA and 3.0 mM calcium chloride or 50 µg/mL AA and 6 mM calcium chloride. To provide a comparison, MC3T-C24 EV and MC3T3-C24 FP1 cell cultures were cultured with maintenance media containing: 50 µg/mL AA plus 5 mM βGP or 50 µg/mL AA plus 3 mM PCho (i.e. phosphatase-substrate containing media). MC3T3-

Table 1. Characteristics of cell lines used.

Cell line		Original Source material	Model	Characteristics	Reference
MC3T3-E1	MC3T3-C24 EV	Postnatal calvaria (C57BL/6)	Pre-osteoblast → mature osteoblast transition	↓ *Phospho1* expression ↓ mineralisation	Huesa et al., 2015
	MC3T3-C24 FP1			↑ *Phospho1* expression ↑ mineralisation	Huesa et al., 2015
	MC3T3-C24			↓ *Phospho1* expression ↓ mineralisation	Wang et al., 1999
	MC3T3-C14			↑ *Phospho1* expression ↑ mineralisation	Wang et al., 1999
IDG-SW3		Long bone chips (*Immortomouse/ Dmp1-GFP*$^{+/-}$ mouse)	Late osteoblast → late osteocyte transition	Characteristic temporal expression of osteocyte markers (e.g. *E11*, *Dmp1* and *Sost*)	Woo et al., 2011

C14 and MC3T3-C24 cultures were supplemented with MC3T3 mineralisation media from day 0 for up to 10 days.

3.4.2. Primary calvarial osteoblast cell culture

Primary osteoblasts from the calvaria of new born wild-type (WT) and *Phospho1*$^{-/-}$ mice were extracted and seeded in multi-well plates at 1 x 10^4 cells/cm^2 with maintenance medium as described in section 2.2.5. To investigate the mineralisation of primary osteoblast cultures in exogenous phosphatase-substrate free conditions (section 3.5.2.), cells were cultured for 28 days in maintenance media containing either: 50 µg/mL AA, 50 µg/mL AA and 1.5 mM calcium chloride, 50 µg/mL AA and 3.0 mM calcium chloride or 50 µg/mL AA and 6 mM calcium chloride. To provide a comparison, WT and *Phospho1*$^{-/-}$ cell cultures were cultured with maintenance media containing: 50 µg/mL AA plus 5 mM βGP or 50 µg/mL AA plus 3 mM PCho. For the

assessment of temporal mineralisation and gene expression, primary osteoblast cultures from WT and *Phospho1*$^{-/-}$ mice were supplemented with primary osteoblast mineralisation media from day 0 for up to 28 days.

3.4.3. Metatarsal organ culture

The middle three metatarsals from WT and *Phospho1*$^{-/-}$ E15 mice were isolated aseptically as detailed in section 2.3.1. To investigate the validity of pooling the middle three metatarsals, the anatomical location of the dissected metatarsal was recorded and metatarsals were described as either the 2nd (medial of the three metatarsals), 3rd or 4th (lateral of the three metatarsals). Metatarsals were cultured for 7 days in metatarsal medium supplemented with 1 mM βGP.

To investigate the mineralisation of cultured E15 metatarsals in exogenous phosphatase-substrate free conditions (section 3.5.4.), groups of between 5-10 metatarsals were cultured in 300 µL of the following media for up to 7 days: metatarsal medium (*i.e.* AA only) alone, or metatarsal medium supplemented with 1.5 mM calcium chloride, 3 mM calcium chloride or 6 mM calcium chloride. The total length, and length of the mineralised zone were measured daily as described in section 2.3.1. To provide a comparison, metatarsals were similarly cultured in metatarsal media supplemented with either 1 mM βGP or 3 mM PCho.

3.4.4. Assessment of ECM mineralisation

The ECM mineralisation of MC3T3 and primary osteoblast cell cultures was assessed by alizarin red staining. Cell monolayers were fixed in 4% PFA on the specified day of culture and alizarin red staining and quantification was carried out as described in section 2.8.1.

3.4.5. Gene expression analysis

MC3T3 and primary osteoblast cell cultures were scraped from the culture plastic-ware on the specified day of culture and RNA was extracted as described in 2.4.1. E15 metatarsals were snap frozen in liquid nitrogen (LN_2) at the relevant time point in culture and RNA was extracted according to section 2.4.2. Five metatarsals were pooled for each sample to provide sufficient RNA. RNA from cell and organ cultures was reverse transcribed according to 2.4.3. RT-qPCR was performed on three technical replicates per sample and the results for each gene of interest were normalised to the housekeeping gene *Atp5b.* Relative gene expression was calculated using the ΔΔCt method (section 2.4.4.) and expressed as a fold change against control cultures.

3.4.6. Protein analysis

Protein was extracted from cells and cultured E15 metatarsal samples (5 bones per sample) at the specified day of culture as described in sections 2.5.1. and 2.5.2. respectively. The concentration of the protein lysate was determined by DC assay as described in section 2.5.3. Fifteen micrograms of protein was loaded and the resultant nitrocellulose were probed by western blotting for PHOSPHO1, nSMase2, TNAP and β-actin as described in section 2.5.4.

3.5. Results

3.5.1. Establishing suitable exogenous phosphatase-substrate free conditions for the mineralisation of MC3T3-C24 EV and MC3T3-C24 FP1 cell cultures.

The expression of *Phospho1* and *Alpl* mRNA in MC3T3-C24 EV and MC3T3-C24 FP1 cell cultures was assessed at day 0 (*i.e.* upon confluency) by RT-qPCR. *Phospho1* expression was significantly increased in MC3T3-C24 FP1 cell cultures compared to

MC3T3-C24 EV cell cultures ($P<0.01$, Fig. 3.1.A). There was no difference in *Alpl* expression observed between the two cell lines (Fig. 3.1.B).

The ECM mineralisation of MC3T3-C24 EV and MC3T3-C24 FP1 cell cultures, cultured in the presence of various mineralisation promoting supplements was assessed on day 14 of culture by alizarin red staining and subsequent spectrophotometric quantification of the leached stain. Cultures supplemented with ascorbic acid only displayed no signs of mineral deposition by day 14 (Fig. 3.1. C & D). MC3T3-C24 FP1 cells cultured in the presence of 5 mM βGP displayed extensive ECM mineralisation which was significantly greater ($P<0.001$) than in βGP supplemented MC3T3-C24 EV cultures. Comparable, pronounced ECM mineralisation was observed in MC3T3-C24 FP1 cultures supplemented with 3 mM PCho, which was, again, significantly greater ($P<0.001$) than in 3 mM PCho supplemented MC3T3-C24 EV cultures. The ECM mineralisation of cell cultures was next determined in the presence of varying concentrations of calcium chloride; a molecule which is not cleaved by phosphatases. The addition of 1.5 mM calcium chloride to MC3T3-C24 FP1 cultures induced ECM mineralisation to around 70% of that seen in 5 mM βGP treated cultures. The ECM mineralisation of MC3T3-C24 FP1 cultures treated with 1.5 mM calcium chloride was also significantly greater than similarly treated MC3T3-C24 EV cultures ($P<0.01$). Furthermore, ECM mineralisation was completely absent in MC3T3-C24 EV cultures treated with 3 mM and 6 mM calcium chloride. In MC3T3-C24 FP1 cultures, 3 mM calcium chloride induced very low levels of ECM mineralisation, whilst in the presence of 6mM calcium chloride, there was a complete absence of ECM mineralisation (Fig. 3.1.C & D).

3.5.2. Establishing suitable exogenous phosphatase-substrate free conditions for the mineralisation of WT and *Phospho1*$^{-/-}$ primary calvarial osteoblast cell cultures.

In a similar experiment, ECM mineralisation was assessed in WT and *Phospho1*$^{-/-}$ primary osteoblast cultures, cultured in the presence of differing mineralisation media. After 28 days in cultures, ascorbic acid only treated cultures (both WT and *Phospho1*$^{-/-}$) displayed no evidence of ECM mineralisation as assessed by alizarin red staining (Fig. 3.2.). The addition of 5 mM βGP induced ECM mineralisation of primary osteoblast cultures with WT cultures showing a significantly greater extent of mineralisation compared to *Phospho1*$^{-/-}$ cultures ($P<0.001$). Extensive ECM mineralisation was likewise observed with the addition of 3mM PCho to WT and *Phospho1*$^{-/-}$ primary osteoblast cell cultures. WT primary osteoblast cultures treated with calcium chloride displayed ECM mineralisation in a dose dependent manner. ECM mineralisation was completely absent in the presence of 1.5 mM calcium chloride whereas mineralisation in the presence of 6 mM calcium chloride was comparable to that observed with 5 mM βGP treated cultures. In *Phospho1*$^{-/-}$ primary osteoblast cultures the trend was similar, although ECM mineralisation in the presence of 1.5, 3.0 and 6 mM calcium chloride was significantly less than that observed in corresponding WT cultures ($P<0.01$, Fig. 3.2.).

3.5.3. Comparison of the *in vitro* growth and mineralisation capacity of anatomically distinct E15 metatarsals

The growth and mineralisation capacity of the 2nd, 3rd and 4th metatarsals from E15 mice was assessed to confirm the validity of the practice of pooling these metatarsals

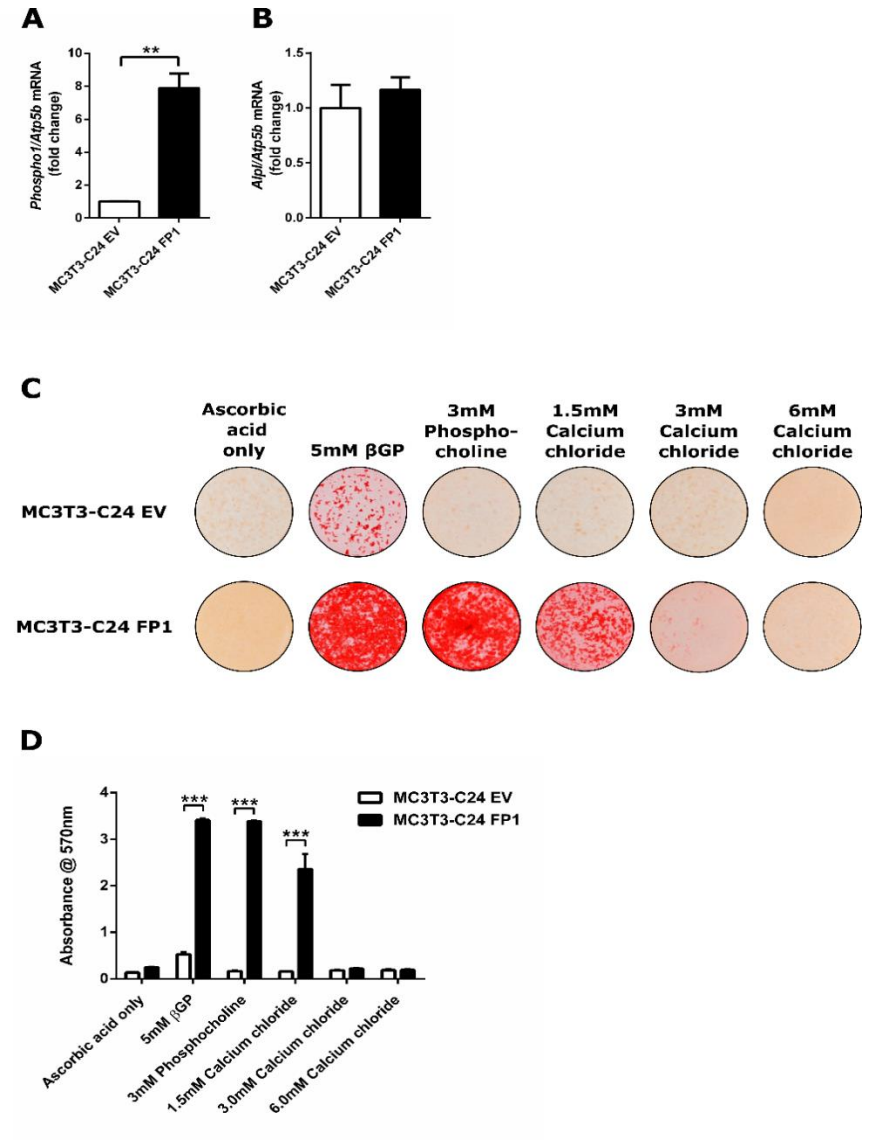

Figure 3.1. Establishing suitable exogenous phosphatase-substrate free conditions for the mineralisation of MC3T3-C24 EV and MC3T3-C24 FP1 cell cultures.

RT-qPCR analysis of **(A)** *Phospho1* **(B)** *Alpl* mRNA expression in MC3T3-C24 EV and MC3T3-C24 FP1 cell cultures upon confluency. **(C)** Representative images of alizarin red staining and **(D)** relative quantification of cetylpyridinium chloride leached bound dye from MC3T3-C24 EV and MC3T3-C24 FP1 cell cultures at day 14. Data are represented as mean ± S.E.M. (N=3 replicates). ** P<0.01 and *** P<0.001 in comparison to MC3T3-C24 EV cell cultures.

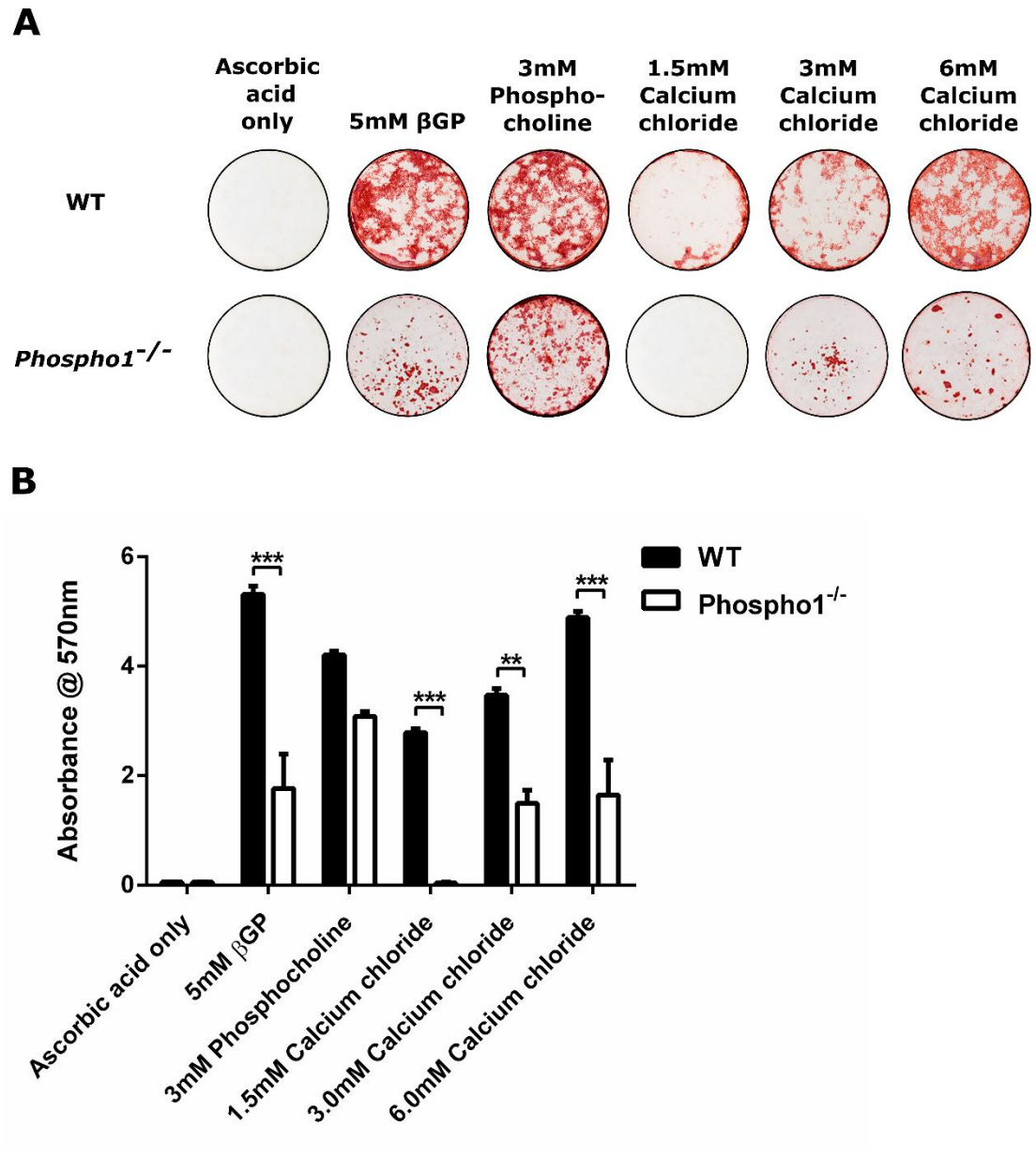

Figure 3.2. Establishing suitable exogenous phosphatase-substrate free conditions for the mineralisation of WT and *Phospho1*$^{-/-}$ primary calvarial osteoblast cell cultures.

(A) Representative images of alizarin red staining and **(B)** relative quantification of cetylpyridinium chloride leached bound dye from WT and *Phospho1*$^{-/-}$ primary calvarial osteoblast cell cultures at day 28. Data are represented as mean ± S.E.M. (N=3 replicates). ** P<0.01 and *** P<0.001 in comparison to WT cultures.

in experiments utilising this model. Metatarsals where cultured in metatarsal medium containing 1 mM βGP for 7 days, and the growth and appearance of mineral was monitored. E15 metatarsals displayed no evidence of diaphyseal mineral upon dissection (day 0). Metatarsals from all groups exhibited increased linear growth through the course of the 7 day culture. No statistical differences in growth between the 2nd, 3rd and 4th metatarsals were observed at any point in the culture period. By day 7 in culture the length of the 2nd, 3rd and 4th metatarsals had increased 93.6±2.84%, 73.5±3.09% and 81.3±7.13% from day 0 respectively. Mineralisation of E15 metatarsals was first observed on day 2 of culture and the length of mineralised region increased daily in all groups. At day 6 of culture the mineralised zone of cartilage was 28.14±2.10%, 28.40±1.62%, and 25.36±1.19% of the total length of the metatarsal respectively. No significant differences in the extent of mineral were observed between metatarsals at any of the time points. The central three metatarsals from WT E15 embryos were cultured in metatarsal media containing various additives for 7 days with the length of the rudiment and any diaphyseal mineral recorded each day. As no differences were observed in the growth or mineralisation capacity of the central three metatarsals (Fig. 3.3.), metatarsals were pooled upon dissection. E15 metatarsals did not possess mineralisation upon dissection (day 0).

3.5.4. Mineralisation of E15 metatarsals in exogenous phosphatase-substrate free conditions

In all of the conditions tested, metatarsals exhibited increased linear growth during the culture period. There were no significant differences in the percentage increase in length from day 0 between the different media additives. Metatarsals supplemented with 1 mM βGP displayed evidence of diaphyseal mineral by day 2 in culture. There

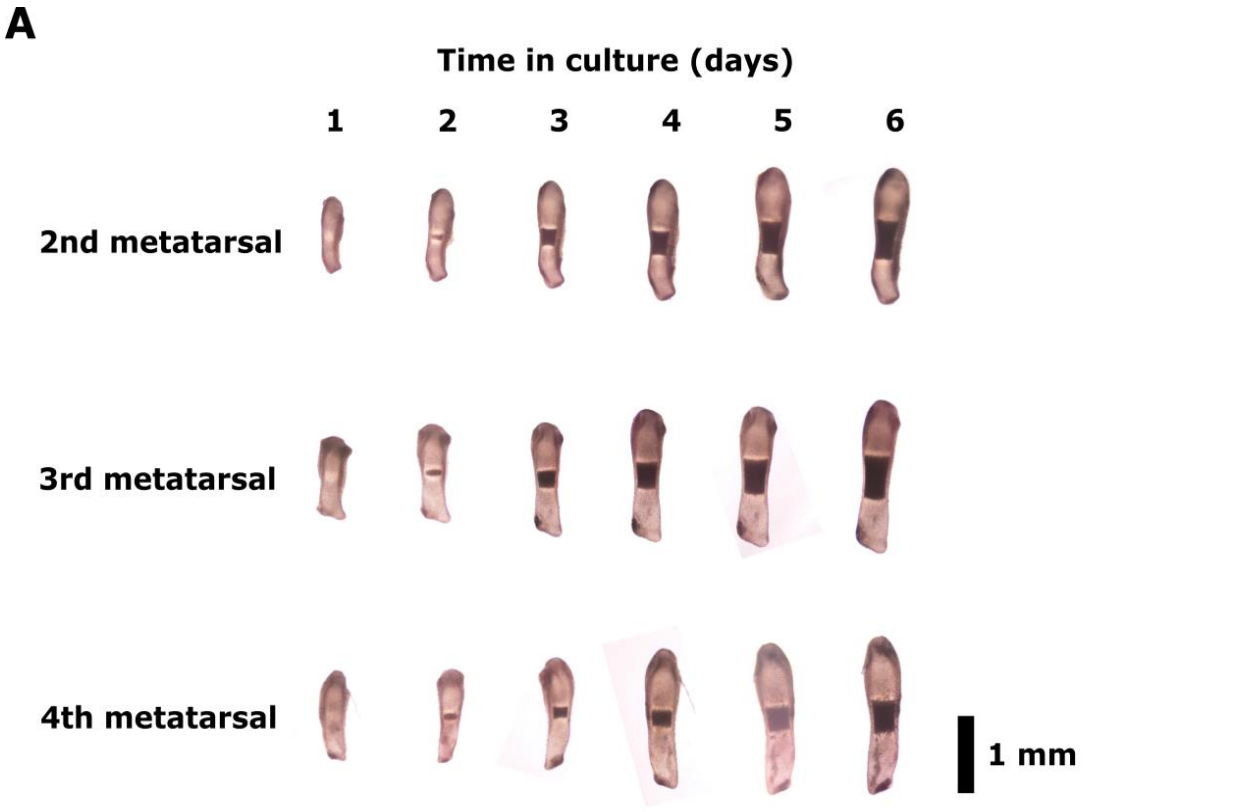
A
Time in culture (days)
1
2
3
4
5
6
2nd metatarsal
3rd metatarsal
4th metatarsal
1 mm

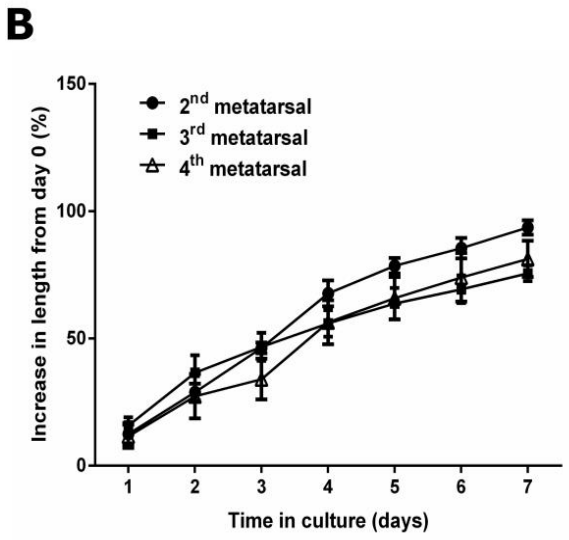
B
Increase in length from day 0 (%)
150
100
50
0
2nd metatarsal
3rd metatarsal
4th metatarsal
1
2
3
4
5
6
7
Time in culture (days)

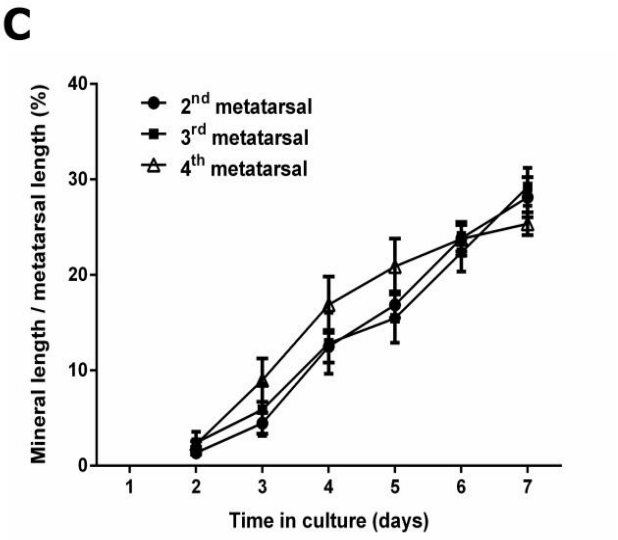
C
Mineral length / metatarsal length (%)
40
30
20
10
0
2nd metatarsal
3rd metatarsal
4th metatarsal
1
2
3
4
5
6
7
Time in culture (days)

(Previous page) Figure 3.3. Comparison of the growth and mineralisation capacity of anatomically distinct WT E15 metatarsals in culture.

(A) Representative images of the 2nd, 3rd and 4th metatarsals during culture. **(B)** Analysis of the growth rate and **(C)** percentage mineral of the 2nd, 3rd and 4th WT E15 metatarsals cultured for 7 days. Data are represented as mean ± S.E.M. (N=6 replicates).

was a complete absence of mineralisation observed in metatarsals supplemented with 3 mM calcium chloride. Metatarsals cultured with 1.5 mM calcium chloride mineralised their ECM from day 3 onwards, but the extent of ECM mineralisation was noticeably less than that of non-calcium chloride treated rudiments. Metatarsals cultured with ascorbic acid only and 3 mM PCho supplemented media showed evidence of diaphyseal mineral at day 3, which increased daily. By day 7 in culture, metatarsals cultured in ascorbic acid only media and 1 mM βGP supplemented media displayed significantly increased percentage mineral compared to 3 mM PCho and 1.5 mM calcium chloride supplemented metatarsals ($P<0.01$, Fig. 3.4.C).

3.5.5. Assessment of the temporal ECM mineralisation of MC3T3-C14 and MC3T3-C24 cultures.

Based on the data shown in Fig. 3.1.C & D, MC3T3-C14 and MC3T3-C24 cells were cultured in 1.5 mM calcium chloride supplemented mineralisation media (MC3T3 mineralisation media) and matrix mineralisation was assessed by alizarin red staining and quantified as described in section 3.4.4. MC3T3-C14 cells mineralised their matrix by day 10 in culture ($P<0.001$ compared to day 0, Fig.3.5.). Alizarin red staining was not observed in MC3T3-C24 cultures. Quantification of the alizarin red staining confirmed the enhanced ECM mineralisation in MC3T3-C14 cell cultures compared to MC3T3-C24 cell cultures ($P<0.001$) which is in agreement with previously published data.

3.5.6. Analysis of the temporal gene and protein expression during MC3T3-C14 and MC3T3-C24 matrix mineralisation

The temporal expression of key mineralisation-dependent enzymes was investigated in MC3T3-C14 and MC3T3-C24 cell cultures by RT-qPCR and western blotting.

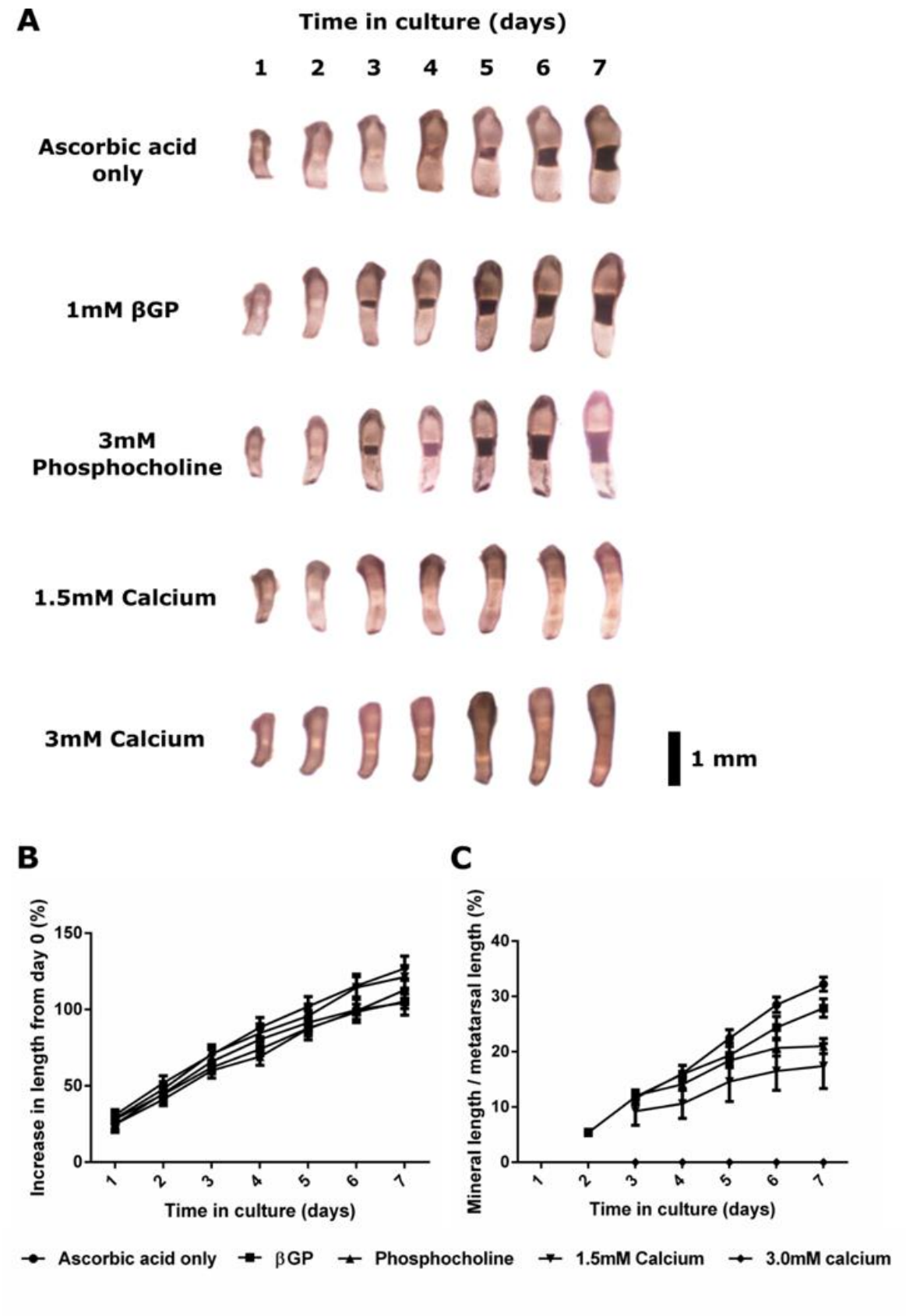
A
Time in culture (days)
1 2 3 4 5 6 7
Ascorbic acid only
1mM βGP
3mM Phosphocholine
1.5mM Calcium
3mM Calcium
1 mm
B
Increase in length from day 0 (%)
150
100
50
0
1 2 3 4 5 6 7
Time in culture (days)
C
Mineral length / metatarsal length (%)
40
30
20
10
0
1 2 3 4 5 6 7
Time in culture (days)
Ascorbic acid only
βGP
Phosphocholine
1.5mM Calcium
3.0mM calcium

(Previous page) Figure 3.4. Establishing suitable exogenous phosphatase-substrate free conditions for the mineralisation of cultured WT E15 metatarsals.

(A) Representative images during culture. **(B)** Comparison of the growth rate of WT E15 metatarsals cultured with the various additives for 7 days. **(C)** Comparison of the percentage mineral of WT E15 metatarsals cultured with the various additive for 7 days. Data are represented as mean ± S.E.M. (N=6 replicates).

Phospho1 mRNA expression markedly increased in a temporal manner in MC3T3-C14 cell cultures and by day 10, mRNA levels were ~150-fold higher ($P<0.001$) compared to day 0 (Fig. 3.6.A). Furthermore *Phospho1* mRNA expression was significantly higher in MC3T3-C14 cultures compared to MC3T3-C24 cultures at day 3, 5, 7 and 10 in culture. A similar temporal increase in *Alpl* and *Smpd3* was also noted and by day 10 in culture the expression of both genes in MC3T3-C14 cell cultures was increased by >60-fold ($P<0.001$) compared to day 0 (Fig. 3.6.B & C). *Smpd3* mRNA expression was significantly higher in MC3T3-C14 cultures compared to MC3T3-C24 cultures at day 3, 5, 7 and 10 in culture. *Alpl* mRNA expression, on the other hand, was similarly expressed throughout the culture period by both cell lines. *Enpp1* mRNA displayed a steady state expression between days 0 and 7 in culture which was comparable in MC3T3-C14 and MC3T3-C24 cultures. By day 10 of culture, *Enpp1* mRNA expression was markedly increased in MC3T3-C14 cell cultures ($P<0.001$ compared to day 0, $P<0.001$ compared to MC3T3-C24 cell cultures). The mRNA expression of *Chkβ* was comparable between MC3T3-C14 and MC3T3-C24 cell cultures until day 10 of culture when its expression was enhanced in MC3T3-C14 cultures ($P<0.001$, Fig. 3.6.F). The mRNA expression of Chkα on the other hand, was significantly greater in MC3T3-C24 cell cultures at days 5, 7 and 10 of culture ($P<0.01$). The changes in *Phospho1*, *Alpl* and *Smpd3* gene expression were similarly noted at the protein level by western blotting (Fig. 3.6.G & H).

3.5.7. Assessment of the temporal mineralisation of WT and *Phospho1*$^{-/-}$ primary calvarial osteoblast cell cultures.

Based on the data presented in Fig. 3.2.A & B, WT and *Phospho1*$^{-/-}$ primary calvarial osteoblasts were cultured in 6 mM calcium chloride supplemented mineralisation

media (primary osteoblast mineralisation media) for 28 days. Matrix mineralisation was assessed at days 0 (confluency), 7, 14, 21 and 28 of culture by alizarin red staining and quantification as described in 3.4.4. The first evidence of ECM mineralisation was observed at day 21 of culture in both WT and *Phospho1*$^{-/-}$ cultures (P<0.001 for both genotypes compared to day 0). By day 28 in culture, WT osteoblast cultures displayed extensive ECM mineralisation which was significantly greater than that of *Phospho1*$^{-/-}$ osteoblast cultures (P<0.001, Fig. 3.7.).

3.5.8. Analysis of the temporal gene and protein expression during WT and *Phospho1*$^{-/-}$ primary calvarial osteoblast matrix mineralisation.

RT-qPCR and western blotting were used to investigate the mineralisation-dependent gene and protein expression respectively throughout the culture of WT and *Phospho1* $^{-/-}$ primary calvarial osteoblast matrix mineralisation. In WT osteoblast cultures, *Phospho1* mRNA expression showed a marked and temporal up-regulation, peaking at day 21 of culture (P<0.001 compared to day 0, Fig. 3.8.A) prior to returning to basal levels at day 28 of culture. *Smpd3* mRNA expression in WT osteoblast cultures displayed similar increases to day 21 (P<0.001 compared to day 0, Fig. 3.8.C). Furthermore, *Smpd3* mRNA expression was significantly greater in WT cell cultures compared to *Phospho1*$^{-/-}$ osteoblast cultures at days 14 and 21 of culture (P<0.001). By day 28, *Phospho1*$^{-/-}$ cultures displayed comparable expression of *Smpd3* to WT cultures. *Alpl* mRNA expression was found to temporally increase during the ECM mineralisation of WT and *Phospho1*$^{-/-}$ osteoblast cultures. In WT osteoblast cultures, *Alpl* mRNA expression peaked at day 21 of culture (P<0.001 compared to day 0, Fig. 3.8.B) where it was likewise significantly greater than *Phospho1*$^{-/-}$ cultures. By day 28 of culture, the expression of *Alpl* mRNA had fallen from day 21 levels and was

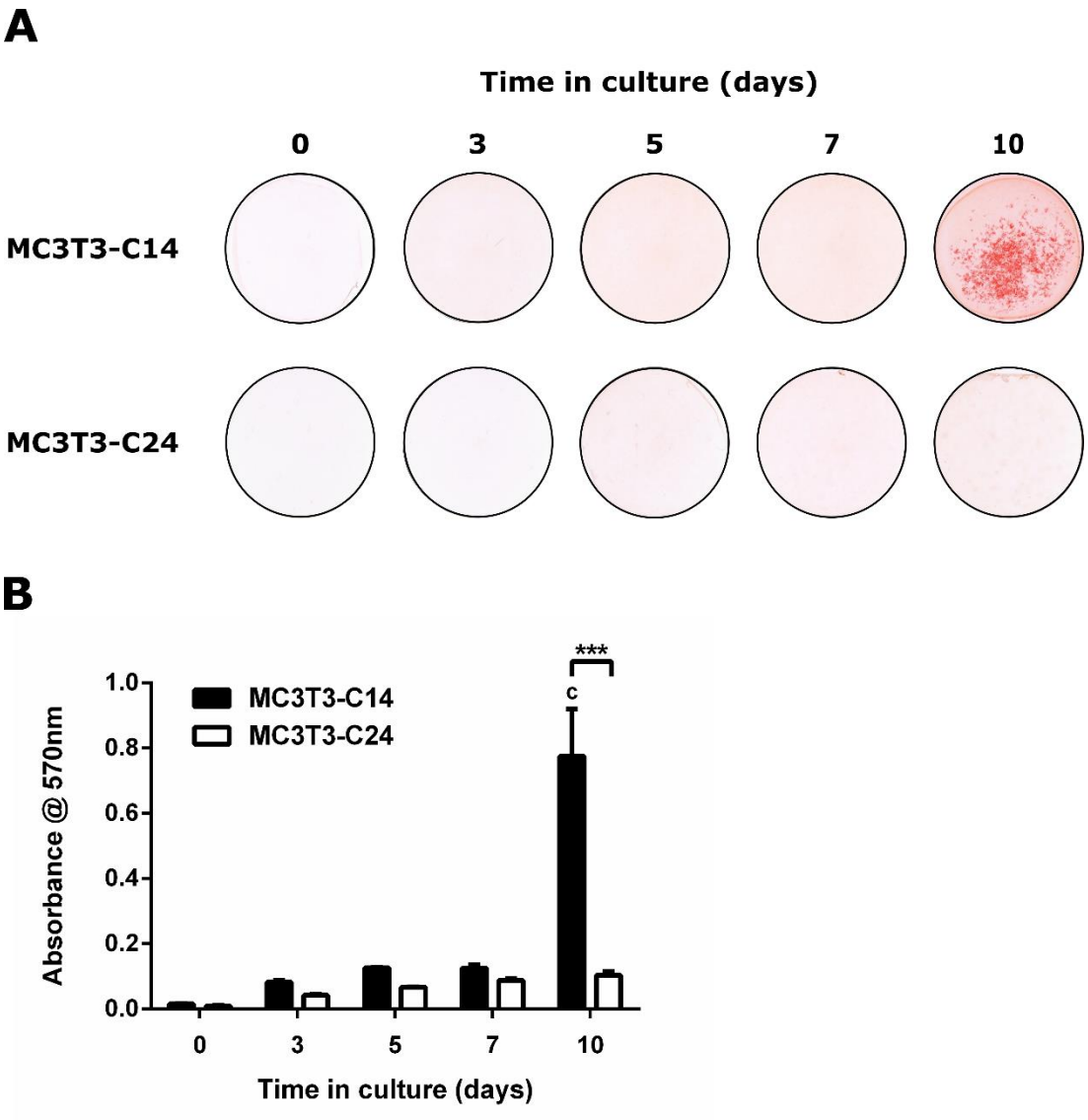

Figure 3.5. Temporal mineralisation of MC3T3-C14 and MC3T3-C24 cell cultures in 1.5 mM calcium chloride supplemented media.

(A) Representative images of alizarin red staining of cell monolayers at day 0 (confluency), 3, 5, 7 and 10 of culture. **(B)** Relative quantification of cetylpyridinium chloride leached bound dye from MC3T3-C14 and MC3T3-C24 cell cultures at each time point in culture. Data are represented as mean ± S.E.M. (N=3 replicates), Two-way ANOVA, $^{C}P<0.001$ in comparison to day 0, *** $P<0.001$ in comparison to MC3T3-C24 cultures.

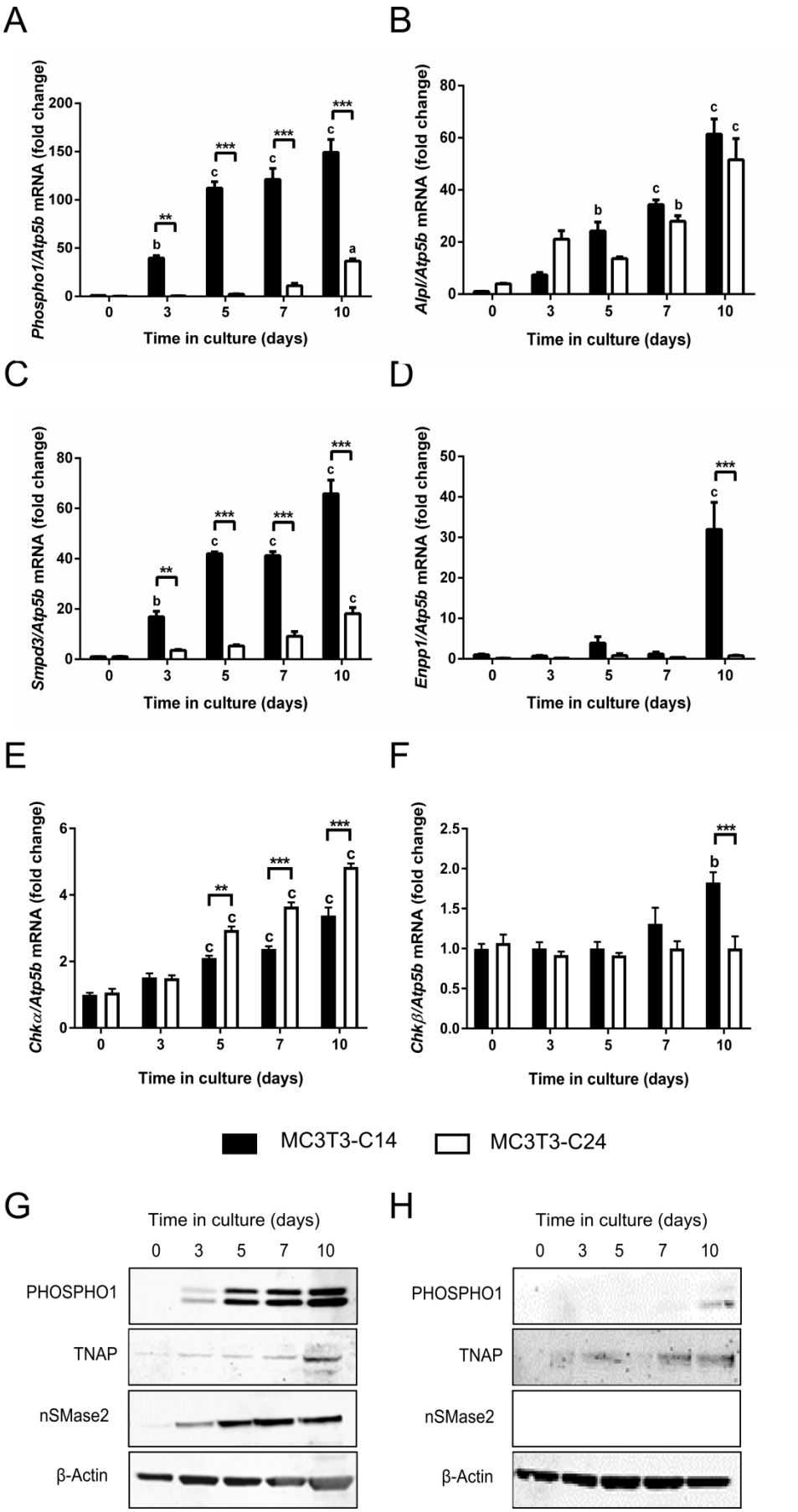
A
B
C
D
E
F
Phospho1/Atp5b mRNA (fold change)
Alpl/Atp5b mRNA (fold change)
Smpd3/Atp5b mRNA (fold change)
Enpp1/Atp5b mRNA (fold change)
Chkα/Atp5b mRNA (fold change)
Chkβ/Atp5b mRNA (fold change)
Time in culture (days)
MC3T3-C14
MC3T3-C24
G
H
Time in culture (days)
PHOSPHO1
TNAP
nSMase2
β-Actin

(Previous page) Figure 3.6. Analysis of the temporal gene and protein expression during MC3T3-C14 and MC3T3-C24 matrix mineralisation.

RT-qPCR analysis of **(A)** *Phospho1*, **(B)** *Alpl*, **(C)** *Smpd3*, **(D)** *Enpp1*, **(E)** *Chkα* and **(F)** *Chkβ* mRNA expression in MC3T3-C14 and MC3T3-C24 cell cultures at day 0 (confluency), 3, 5, 7 and 10 of culture. **(G)** Western blotting of PHOSPHO1, TNAP, nSMase2 and the loading control, β-actin, at day 0, 3, 5, 7 and 10 of MC3T3-C14 cell culture. **(H)** Western blotting of PHOSPHO1, TNAP, nSMase2 and the loading control, β-actin, at day 0, 3, 5, 7 and 10 of MC3T3-C24 cell culture. Data are represented as mean ± S.E.M. (N=3 replicates), Two-way ANOVA, $^{a}P<0.05$, $^{b}P<0.01$ and $^{c}P<0.001$ in comparison to day 0, **P<0.01 and *** P<0.001 in comparison to MC3T3-C24 cultures at each time point in culture.

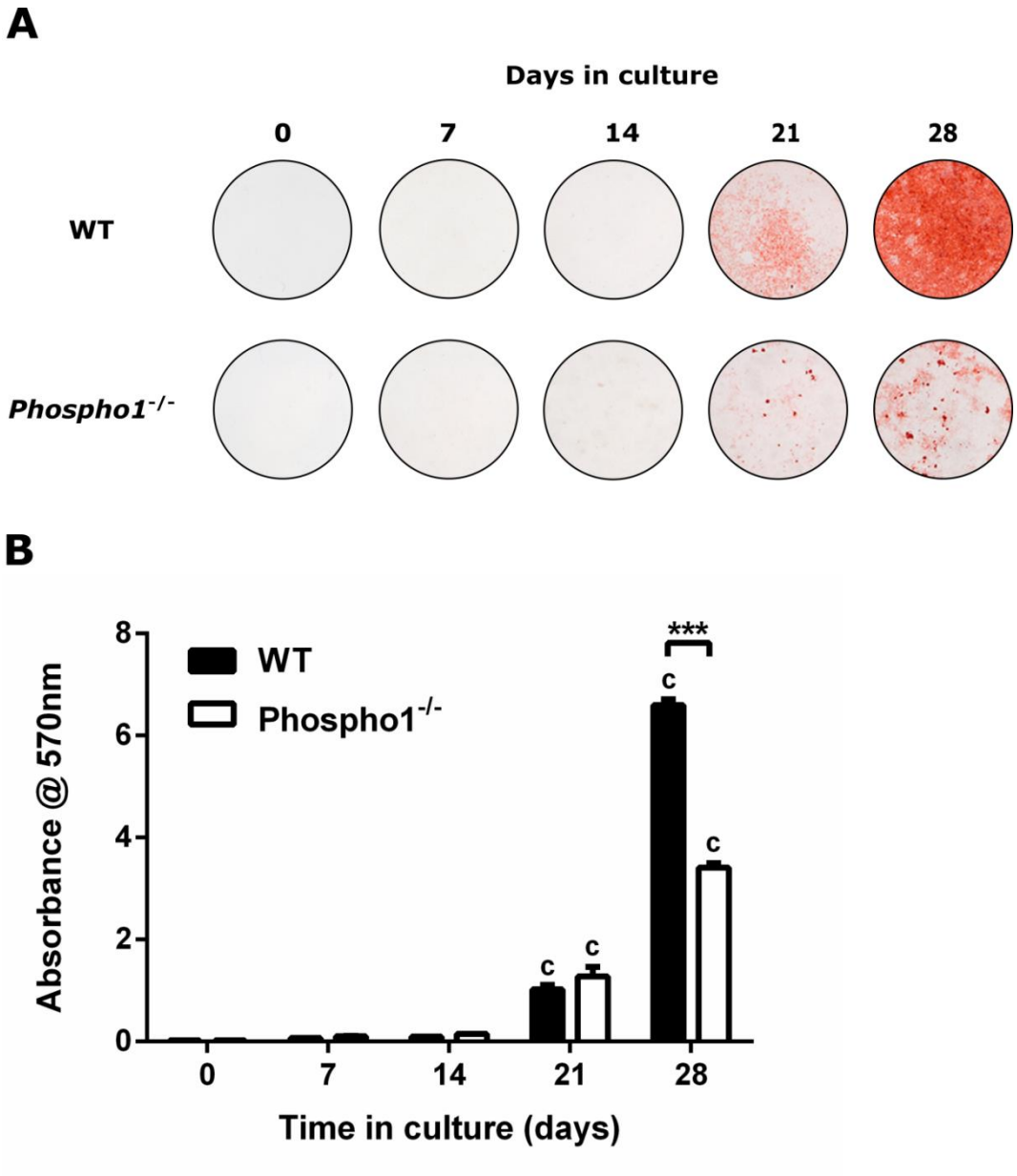

Figure 3.7. Temporal mineralisation of WT and *Phospho1*$^{-/-}$ primary calvarial osteoblast cell cultures in 1.5 mM calcium chloride supplemented media.

(A) Representative images of alizarin red staining of cell monolayers at day 0 (confluency), 7, 14, 21 and 28 of culture. **(B)** Relative quantification of cetylpyridinium chloride leached bound dye from WT and *Phospho1*$^{-/-}$ primary calvarial osteoblast cell cultures at each time point in culture. Data are represented as mean ± S.E.M. (N=3 replicates), Two-way ANOVA, $^{C}P<0.001$ in comparison to day 0, *** $P<0.001$ in comparison to *Phospho1*$^{-/-}$ cultures.

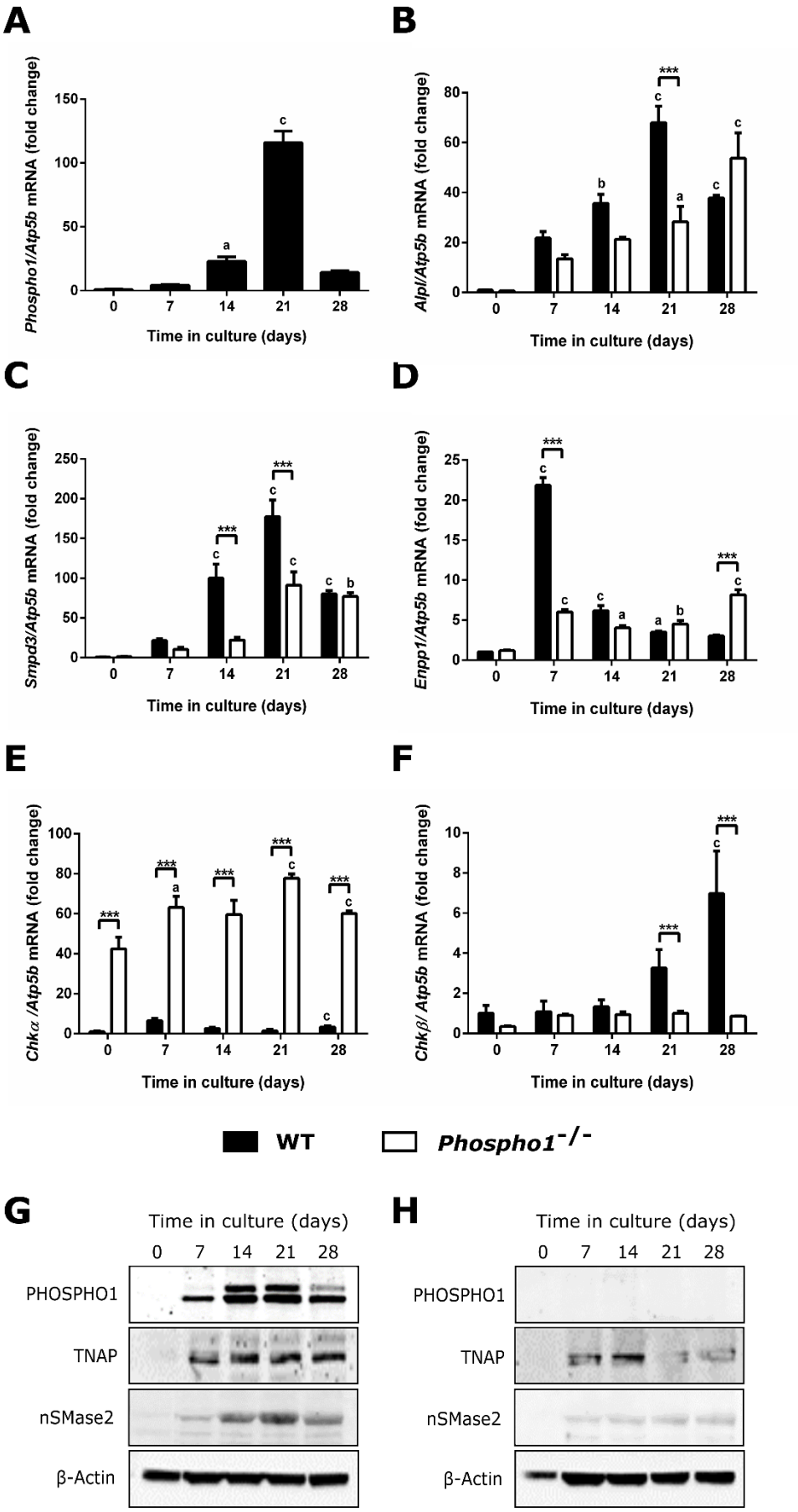
A
Phospho1/Atp5b mRNA (fold change)
Time in culture (days)
B
Alpl/Atp5b mRNA (fold change)
Time in culture (days)
C
Smpd3/Atp5b mRNA (fold change)
Time in culture (days)
D
Enpp1/Atp5b mRNA (fold change)
Time in culture (days)
E
Chkα /Atp5b mRNA (fold change)
Time in culture (days)
F
Chkβ/ Atp5b mRNA (fold change)
Time in culture (days)
WT
Phospho1-/-
G
Time in culture (days)
0 7 14 21 28
PHOSPHO1
TNAP
nSMase2
β-Actin
H
Time in culture (days)
0 7 14 21 28
PHOSPHO1
TNAP
nSMase2
β-Actin

(Previous page) Figure 3.8. Analysis of the temporal gene and protein expression during WT and *Phospho1*$^{-/-}$ primary calvarial osteoblast matrix mineralisation.

RT-qPCR analysis of **(A)** *Phospho1*, **(B)** *Alpl*, **(C)** *Smpd3*, **(D)** *Enpp1*, **(E)** *Chkα* and **(F)** *Chkβ* mRNA expression in WT and Phospho1$^{-/-}$ primary osteoblast cell cultures at day 0 (confluency), 7, 14, 21 and 28 of culture. **(G)** Western blotting of PHOSPHO1, TNAP, nSMase2 and the loading control, β-actin, at day 0, 7, 14, 21 and 28 of WT primary osteoblast cell cultures. **(H)** Western blotting of PHOSPHO1, TNAP, nSMase2 and the loading control, β-actin, at day 0, 7, 14, 21 and 28 of *Phospho1*$^{-/-}$ primary osteoblast cell cultures. Data are represented as mean ± S.E.M. (N=3 replicates), Two-way ANOVA, $^{a}P<0.05$, $^{b}P<0.01$ and $^{c}P<0.001$ in comparison to day 0, *** $P<0.001$ in comparison to *Phospho1*$^{-/-}$ cultures at each time point in culture.

comparable to the expression level of *Phospho1*$^{-/-}$ cultures. The changes in *Phospho1*, *Alpl* and *Smpd3* gene expression were similarly noted at the protein level by western blotting (Fig. 3.8.G & H). *Enpp1* expression levels were increased from day 7 onwards in both WT and *Phospho1*$^{-/-}$ osteoblast cultures ($P<0.05$ compared to day 0, Fig. 3.8.D). *Phospho1*$^{-/-}$ osteoblast cultures showed significantly enhanced *Chkα* mRNA expression at all time points in culture compared to WT cultures ($P<0.001$, Fig. 3.8.E). *Chkβ* mRNA expression in *Phospho1*$^{-/-}$ osteoblasts did not change throughout the 28-day culture. In WT cultures, *Chkβ* showed strong up-regulation at day 28 ($P<0.001$ compared to day 0) and indeed it expression was enhanced compared to *Phospho1*$^{-/-}$ cultures at days 21 and 28 of culture ($P<0.001$, Fig. 3.8.F).

3.5.9. Comparison of the growth and mineralisation capacity of WT and *Phospho1*$^{-/-}$ E15 metatarsals in culture

Based on the data described in section 3.5.4. the metatarsals from WT and Phospho1$^{-/-}$ E15 embryos were dissected and cultured for five days in AA only supplemented metatarsal media. Metatarsals from both genotypes progressively increased their length during the five day culture. WT metatarsals displayed increased longitudinal growth compared to *Phospho1*$^{-/-}$ counterparts from day three in culture onwards ($P<0.001$ compared to *Phospho1*$^{-/-}$ counterparts, Fig. 3.9.B). Cultured WT metatarsals displayed clear evidence of diaphyseal mineralisation initiating at day three, and increasing as previously shown in section 3.5.4. up to day five in culture (Fig. 3.9.C). Compared to WT metatarsals, cultured *Phospho1*$^{-/-}$ metatarsals displayed reduced mineralisation at both days four and five of culture ($P<0.001$). Qualitative assessment of the mineralisation zone during the culture period revealed a reduced

capacity of the mineralisation zone in *Phospho1*$^{-/-}$ metatarsals at all time points assessed.

3.5.10. Analysis of the temporal gene and protein expression during WT and *Phospho1*$^{-/-}$ E15 metatarsal mineralisation *in vitro.*

RT-qPCR and western blotting were used to investigate the mineralisation-dependent gene and protein expression respectively at days 1, 3 and 5 of the culture of WT and *Phospho1*$^{-/-}$ E15 metatarsals. In WT metatarsals, *Phospho1* mRNA expression and PHOSPHO1 protein was found to be strongly up-regulated at days 3 and 5 of culture compared to day 1 ($P<0.001$, Fig. 3.10.A,G & H). Quantification of TNAP protein revealed a temporal increase during the culture period in both WT and *Phospho1*$^{-/-}$ metatarsals (Fig. 3.10.I). This was similarly shown through assessment of *Alpl* mRNA expression (Fig. 3.10.B). In contrast, the levels of nSMase2 protein were found to be significantly higher in WT compared to *Phospho1*$^{-/-}$ metatarsals at both days 3 and 5 (Fig. 3.10.J). Indeed there was also a temporal rise in the expression of *Smpd3* mRNA in WT metatarsals peaking at day 5 ($P<0.001$, Fig.3.10.C), where its expression was likewise significantly higher than in *Phospho1*$^{-/-}$ metatarsals ($P<0.001$). There were no significant differences in the mRNA expression of *Enpp1* or *Chkβ* during the culture period or between genotypes. *Chkα* on the other hand, showed a strong enhancement of expression in *Phospho1*$^{-/-}$ metatarsals compared to WT metatarsals at all time points in culture ($P<0.001$, Fig. 3.10.E).

3.6. Discussion

ECM mineralisation has to date been studied extensively *in vitro* through the use of

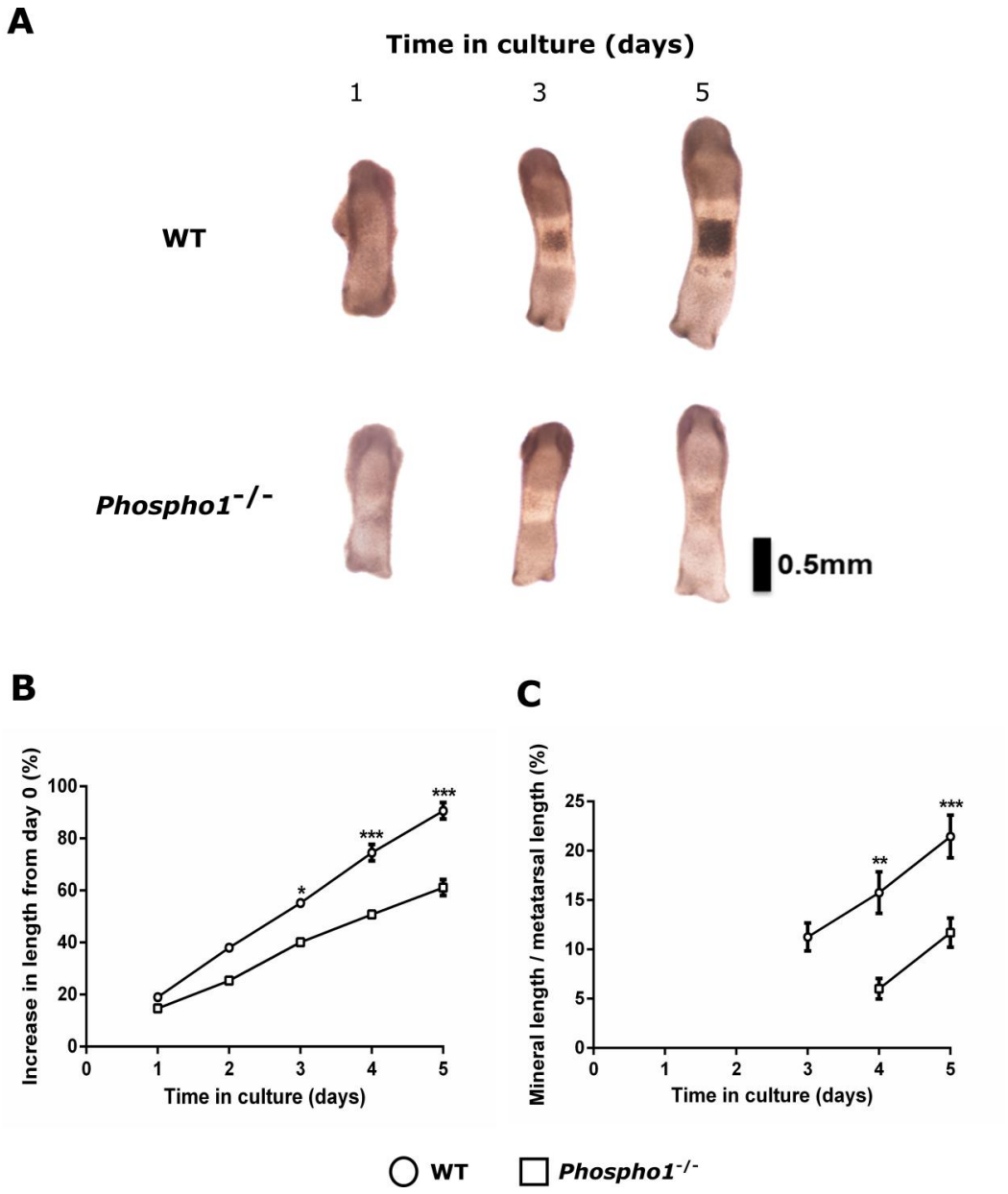

Figure 3.9. Comparison of the growth and mineralisation capacity of WT and *Phospho1*$^{-/-}$ E15 metatarsals in culture.

(A) Representative images WT and Phospho1$^{-/-}$ E15 metatarsals during culture. **(B)** Comparison of the growth rate of WT and *Phospho1*$^{-/-}$ E15 metatarsals cultured in ascorbic acid only media for 5 days. **(C)** Comparison of the percentage mineral of WT and *Phospho1*$^{-/-}$ E15 metatarsals cultured in ascorbic acid only media for 5 days. Data are represented as mean ± S.E.M. (N=6 replicates), Two-way ANOVA, *P<0.05, **P<0.01 and ***P<0.001 compared to *Phospho1*$^{-/-}$ metatarsals at each time point in culture.

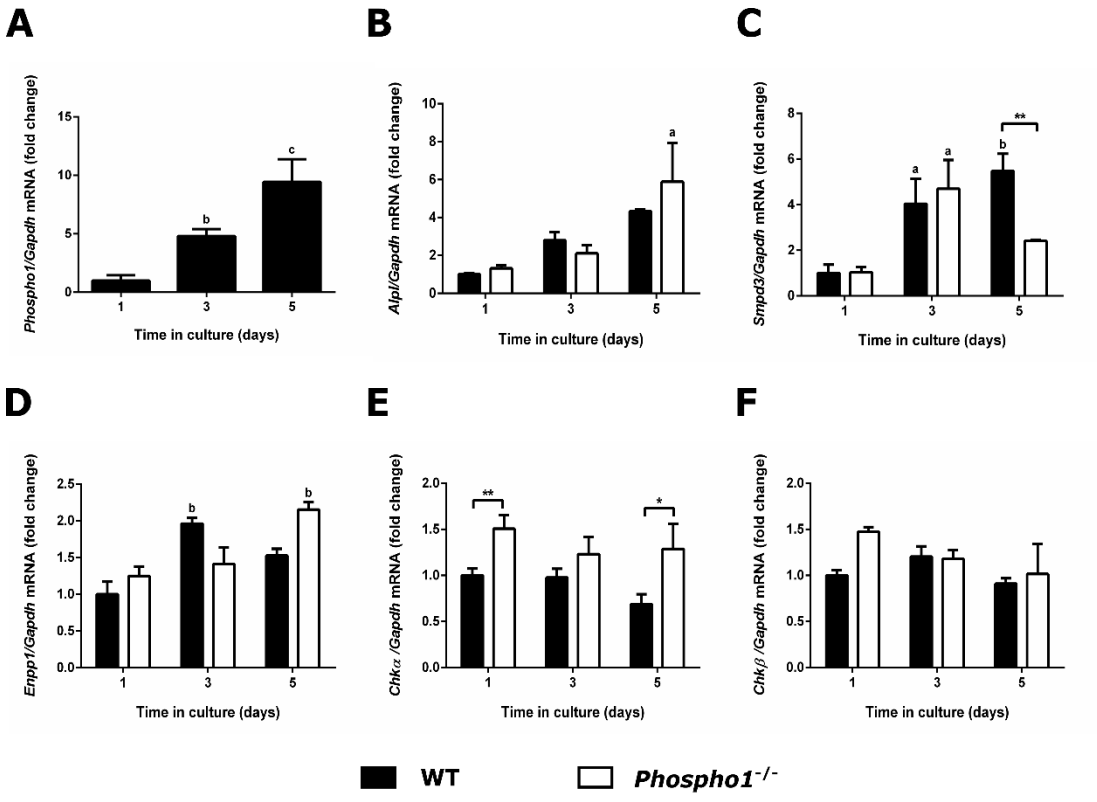
A
B
C
Phospho1/Gapdh mRNA (fold change)
Alpl/Gapdh mRNA (fold change)
Smpd3/Gapdh mRNA (fold change)
Time in culture (days)
D
E
F
Enpp1/Gapdh mRNA (fold change)
Chkα /Gapdh mRNA (fold change)
Chkβ /Gapdh mRNA (fold change)
WT
Phospho1-/-

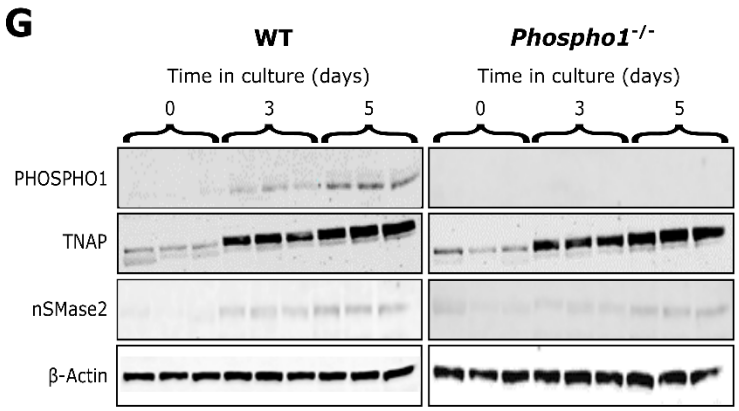
G
WT
Phospho1-/-
Time in culture (days)
0
3
5
PHOSPHO1
TNAP
nSMase2
β-Actin

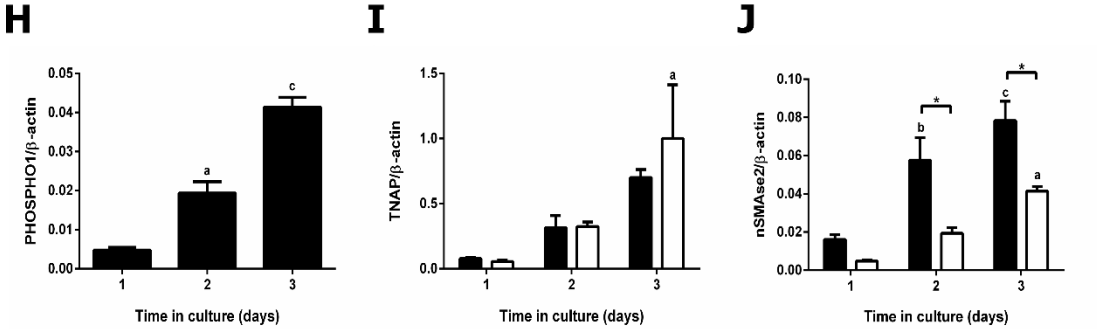
H
I
J
PHOSPHO1/β-actin
TNAP/β-actin
nSMAse2/β-actin
Time in culture (days)

(Previous page) Figure 3.10. Analysis of the temporal gene and protein expression during WT and *Phospho1*$^{-/-}$ E15 metatarsal mineralisation *in vitro*.

RT-qPCR analysis of **(A)** *Phospho1*, **(B)** *Alpl*, **(C)** *Smpd3*, **(D)** *Enpp1*, **(E)** *Chkα* and **(F)** *Chkβ* mRNA expression in WT and *Phospho1*$^{-/-}$ E15 metatarsals at day 1, 3 and 5 of culture. **(G)** Western blotting of PHOSPHO1, TNAP, nSMase2 and the loading control, β-actin, at day 0, 7, 14, 21 and 28 of WT and *Phospho1*$^{-/-}$ E15 metatarsals at day 1, 3 and 5 of culture. Relative quantification of **(H)** PHOSPHO1, **(I)** TNAP and **(J)** nSMase2 protein levels during the culture of WT and *Phospho1*$^{-/-}$ E15 metatarsals. Data are represented as mean ± S.E.M. (n=3 replicates, with 5 metatarsals per replicate), Two-way ANOVA, $^{a}P<0.05$, $^{b}P<0.01$ and $^{c}P<0.001$ in comparison to day 0, *P<0.05 and ** P<0.001 in comparison to *Phospho1*$^{-/-}$ metatarsals at each time point in culture.

immortalised cell lines, primary cell cultures and organ cultures. Despite this, the use of βGP in these cultures as an inducer of mineralisation has limited the ability to understand the physiological mechanisms surrounding the initiation of mineralisation. The data presented in this Chapter has led to the establishment of phosphatase-substrate free conditions for the culture of three distinct models of *in vitro* ECM mineralisation. Furthermore, these models systems have been employed to begin to understand the temporal expression of key regulators of ECM mineralisation.

This study initially utilised the murine osteoblast-like cell line, MC3T3-E1, originally isolated by (Sudo et al., 1983). In particular, sub-clones 14 and 24 of the MC3T3-E1 cell lines, characterised previously as having respectively low and high basal expression levels of *Alpl* (Wang et al., 1999) were used. Clone 14 cells express high levels of *Runx2*, *Bglap* (osteocalcin) and *Ibsp* (bone sialoprotein) compared with clone 24 cells (Wang et al., 1999). My observation here that clone 14 cells express significantly higher levels of *Phospho1* than clone 24 cells may explain the inability of clone 24 cells to induce *in vivo* osteogenesis or *in vitro* ECM mineralisation despite high levels of TNAP (Wang et al., 1999, Huesa et al., 2015). The presence of PHOSPHO1 may be essential to drive the initiation of MV mineralisation, a process that is not thought to involve TNAP (Millán, 2012, Yadav et al., 2016). The suitability of MC3T3 cell cultures as models of *in vivo* mineralisation have been further strengthened through the identification that the organisation, orientation and composition of the mineral phase formed within these cultures is remarkably similar to that of bone (Addison et al., 2015). The observation that MC3T3-C14 cells show evidence of ECM mineralisation within 10 days highlights their use as a rapid and reproducible model of ECM mineralisation. The mineralisation of the cartilaginous

ECM of hypertrophic chondrocytes is an essential precursor for subsequent functional bone formation (Heilig et al., 2016). The study of isolated chondrocytes *in vitro* however, has limitations, for example, the dedifferentiation and loss of key markers such as *Col2a1* (Ma et al., 2013). The mouse metatarsal explant culture provides a highly physiological *ex vivo* model for studying endochondral ossification (Haaijman et al., 1999, Marino et al., 2016). In particular, the absence of HA mineral in E15 metatarsal bones means that they provide an unrivalled model to investigate the initiation of skeletal mineralisation. The maintenance of the discrete chondrocyte zones, cell-cell and cell-matrix interaction offers conditions closer to the *in vivo* situation than cells in culture (Scheven and Hamilton, 1991, Coxam et al., 1996, Andrade et al., 2011). Furthermore, the absence of foetal calf serum from these cultures allows for a more defined media and eliminates the variability in ECM mineralisation which is often associated with the use of animal sera (Boskey and Roy, 2008).

Unfortunately, with the purpose of the current study in mind, *i.e.* to understand the temporal expression of key regulators of MV phosphate generation, the currently accepted methods of inducing ECM mineralisation in the models described, limit their use. It is vital that the ECM mineralisation observed in these models is cell mediated. The addition of βGP to the aforementioned model systems, a substrate of TNAP (Roberts et al., 2004), was a major concern for the current study. In the presence of recombinant TNAP, mineral deposition has been observed in human fibroblast cultures and cell-free, media only cultures supplemented with 10 mM βGP (Khouja et al., 1990, Chung et al., 1992). Greater than 80% hydrolysis of βGP occurs in the presence of TNAP (Bellows et al., 1992). The generation of supra-physiological levels

of P_i alongside calcium (~1 mM in most basal media) results in the precipitation of amorphous calcium phosphate (Boskey and Roy, 2008). Gronowicz et al. (1989) showed this non-physiological mineralisation, characterised by ectopic mineralisation (i.e. out-with the collagenous matrix), in rat parietal bone cultures in the presence of 1-10 mM βGP. The effects of other exogenous phosphate sources on the induction of TNAP and other essential phosphate generating enzymes has not been studied as thoroughly. Regardless, this study sought to understand the expression of enzymes involved in the endogenous production of P_i, and as such it was the aim of this study to eliminate the use of βGP from *in vitro* models of ECM mineralisation.

Experimentation carried out in this Chapter identified calcium chloride supplementation as a suitable inducer of ECM mineralisation in cell culture experiments. ECM mineralisation of around 70% of that observed in βGP treated cultures, was achieved in the presence of calcium chloride in both MC3T3 and primary calvarial osteoblasts cultures. This study expands on previous studies which observed ECM mineralisation in the presence of calcium chloride, albeit with concomitant P_i supplementation, in rat osteoblast-like cell cultures and vascular smooth muscle cell calcification studies (Chang et al., 2000, Kapustin et al., 2011). Chang et al. (2008) achieved osteoblast ECM mineralisation with 14 mM calcium chloride supplemented media. Previous reports however, highlight that TNAP activity may be enhanced in osteoblastic ROS17/2.8 cells cultured with calcium chloride concentration exceeding 6 mM (Rashid et al., 2003), hence in this study only calcium chloride concentrations of less than 6 mM were assessed. The present study would have benefited from analysis of cell-free cultures in the presence of the calcium containing media assessed, so as to rule out any non-cell mediated precipitation of calcium phosphate.

Intriguingly, E15 metatarsals failed to initiate diaphyseal mineralisation when cultured in 3 mM calcium chloride supplemented media despite exhibiting typical longitudinal growth. The presence of sodium bicarbonate in the culture medium (a standard buffering agent in αMEM) alongside calcium chloride may lead to the formation of calcium carbonate, and thus reduction of free calcium levels (Amin et al., 2009). This may provide some explanation to the observed inhibition of mineral formation. The mineralisation of cultured metatarsals was however achieved in ascorbic acid only supplemented metatarsal media. The addition of ascorbic acid only, provides the optimum conditions to investigate the role of phosphatases in the initiation of mineralisation.

Having established suitable, phosphatase-substrate free conditions for the culture of osteoblasts and embryonic metatarsals, the temporal expression of key regulators of ECM mineralisation was assessed in these *in vitro* models. In all of the models assessed in this study, PHOSPHO1, nSMase2 and TNAP displayed coordinated and significant increases in the levels of transcript and protein prior to the onset of ECM mineralisation. In particular, the similarities in the temporal rise of PHOSPHO1 and nSMase2 protein bolsters the idea that these phosphatases work in tandem to generate P_i within MV during the initiation of mineralisation. Furthermore, PHOSPHO1 has recently been implicated in the biogenesis of MV (Yadav et al., 2016) and as such its expression prior to the onset of mineralisation may be crucial for the formation of MV that ultimately contain a precipitated carbonate-substituted hydroxyapatitic mineral phase (Anderson, 1969, Register et al., 1986). Perhaps unsurprising, the function of nSMase2 has similarly been linked with MV biogenesis, whereby siRNA and pharmacological inhibition of nSMase2 activity results in reduced MV production,

albeit in macrophages and vascular smooth muscle cell cultures (Kapustin et al., 2015, Chen et al., 2016, Thouverey et al., 2011). The higher expression of TNAP late on (day 10) in MC3T3-C14 cell cultures is indicative of its role in the later stages of mineralisation where it allows the propagation of HA within the ECM beyond the confines of the MV membrane (Huesa et al., 2011, Millán, 2012). In contrast, TNAP was strongly expressed early on (day 7) in WT primary osteoblast cultures and in E15 metatarsals, suggesting that it may be necessary to modulate the ECM P_i/PP_i ratio in advance of the mineral propagation stage. Alternatively, recent studies have highlighted the importance of extravesicular to intravesicular P_i transport through the type III Na/P_i co-transporter, P_it1 (Yadav et al., 2016). The production of P_i through TNAP hydrolysis of PP_i in the extravesicular environment and its transport into MV may provide an additional and necessary source of P_i for the nucleation of calcium phosphate within MV and may explain why MV mineralisation is not completely absent in *Phospho1* deficient mice (Yadav et al. 2016). These findings also highlight the similar expression patterns of PHOSPHO1 and nSMase2 during osteoblast and hypertrophic chondrocyte ECM mineralisation. However, it is essential to take into account that this study did not assess the activity of the proteins investigated. Changes in mRNA or protein abundance are not directly related to enzyme activity or the concentrations of the generated or utilised intravesicular metabolites (Glanemann et al., 2003).

Alpl expression and TNAP activity have previously been shown to be reduced in the *Phospho1*$^{-/-}$ mouse (Yadav et al., 2011). In the current study, *Alpl* expression was similarly decreased in mineralising osteoblast cultures with either diminished or absent *Phospho1* expression. Expanding on this, nSMase2 expression was markedly reduced

in MC3T3-C24 cell cultures and *Phospho1*$^{-/-}$ calvarial osteoblast and metatarsal cultures. One might hypothesise, that in the absence of PCho utilisation by PHOSPHO1, there is a reduced requirement to generate PCho through the hydrolysis of sphingomyelin by nSMase2. In *Chkβ*$^{-/-}$ chondrocyte cultures, the reduced substrate (PCho) generation, results in an enhancement of PHOSPHO1 expression, perhaps as a compensatory rescue mechanism to ensure sufficient P_i generation for calcium phosphate precipitation (Li et al., 2014a). In this study, *Chkα* expression was notably higher in *Phospho1*$^{-/-}$ osteoblast and metatarsal cultures. These data are in disagreement with the hypothesis that in the absence of PHOSPHO1 there would a reduced demand for PCho generation. Importantly, despite both isoforms (*Chkα* and *Chkβ*) being involved in the generation of PCho and PEth, recent studies have shown that these enzymes have divergent roles in cancer pathogenesis (Gallego-Ortega et al., 2009). It is possible therefore, that these enzymes also play differential roles in skeletal mineralisation.

The expression of *Enpp1* which generates extravesicular PP_i through its phosphodiesterase and pyrophosphatase activity (Mackenzie et al., 2012b, Kato et al., 2012), was the only negative regulator of mineralisation examined in this study. *Enpp1* expression was moderately upregulated during the mineralisation of primary calvarial osteoblast and embryonic metatarsals cultures. In MC3T3-C14 cell cultures, *Enpp1* expression displayed a marked upregulation at day 10 of culture, when mineral could first be observed by alizarin red staining. It is plausible that the expression of *Enpp1* is suppressed during the initiation of mineralisation and induced by the presence of HA so as to provide some form of negative regulation to the extravesicular propagation of mineral. In future experiments, it would be worthwhile examining the expression of

other proteins know to modulate local PP_i levels, for example ANK and ABCC6 an ATP-binding cassette, which, by an as yet unidentified mechanism, raises extracellular levels of PP_i (Jansen et al., 2013).

Data from this Chapter provides a comprehensive understanding of the temporal expression of phosphate manipulating enzymes during ECM mineralisation. Indeed, it is the first *in vitro* evidence which bolsters the hypothesis that nSMase2 and PHOSPHO1 function in tandem for the generation and processing of PCho respectively, during the initiation of MV-mediated mineralisation. Furthermore, the reduced expression of nSMase2 in the absence of PHOSPHO1, highlights a potential negative feedback mechanism. In addition, the exogenous phosphatase-substrate free culture conditions developed in this Chapter will allow the further investigation of the interplay and regulation of these enzymes to be carried out.

Chapter 4

Investigating the effects of parathyroid hormone on PHOSPHO1 *in vitro*

4.1. Introduction

In the previous Chapter, the paucity of information surrounding the expression patterns and regulation of the key regulators of MV mediated mineralisation, PHOSPHO1 and nSMase2 was emphasised. Chapter 3 addressed this in part, by providing data on the temporal expression of these enzymes during ECM mineralisation *in vitro*. With such an essential role in the initiation of mineralisation, targeting the regulation of PHOSPHO1 and nSMase2 could provide a novel target for therapeutic interventions seeking to modulate the mineralisation process. This Chapter sought to uncover if these mineralisation-dependent enzymes were under endocrine regulation.

Shortly after the original identification of *Phospho1* as a novel phosphatase, expressed exclusively in mineralising bone and cartilage (Houston et al., 1999), researchers sought to uncover the regulation of the enzyme *in vitro*. These original studies, focussed their attention to the human osteosarcoma cell line SaOS-2, where they showed that neither dexamethasone, estradiol, Vitamin D_3, PTH nor parathyroid hormone related peptide (PTHrP) elicited any effect on the expression of *Phospho1* (Houston et al., 2004). Although limited in the extent of data provided, there exists additional data regarding the regulation of *Phospho1* (described as 4G8 by the authors) expression by TGFβ, however this work only appeared in a meeting abstract (Aukhil et al., 2000). Knowledge surrounding the regulation of *Smpd3* expression is more comprehensive. To date, tumour necrosis factor α, BMP-2, PTHrP and the master regulator of chondrogenesis, SOX9, have all been shown to modulate the expression of *Smpd3 in vitro* (Chae et al., 2009, Clarke et al., 2011, Kakoi et al., 2014, Li et al., 2016).

A recent RNA-seq analysis by St John et al., 2015, revealed that *Phospho1* and *Smpd3* expression are negatively regulated by PTH treatment in IDG-SW3 cells (an osteocyte-like cell line). This study extends a growing body of evidence revealing that PTH can regulate a plethora of genes involved in bone formation and osteoblast function (Silva and Bilezikian, 2015). Indeed, a microarray study of PTH treated UMR-106-01 cells, a rat osteosarcoma cell line, revealed >100 differentially regulated genes, with the gene expression profile closely mimicking the gene expression pattern observed during osteoblast differentiation (Qin et al., 2003). The transcription and post-translational modification (phosphorylation) of Runx2, the transcription factor and master regulator of osteoblast differentiation, are also strongly enhanced by PTH (Krishnan et al., 2003). Interestingly, the overexpression of *Runx2* in mouse limb bud cultures simultaneously enhances the expression of both *Phospho1* and *Smpd3* (Nishimura et al., 2012). These alterations in osteoblast gene expression may underscore the ability of PTH to elicit both anabolic and catabolic effects on the skeleton depending on the duration of the exposure. For example daily injections of low dose PTH are anabolic to the skeleton whereas continuous exposure to PTH, the likes observed in hyperparathyroidism, results in bone loss and increased porosity especially in the cortical compartment (Locklin et al., 2003). Indeed, despite an overall increase in bone remodelling (Eriksen, 2002), the enhancement of RANKL expression and thus osteoclastogenesis, and the suppression of OPG (Ma et al., 2001), ensures that any increases in bone formation are outweighed by a prevailing bone resorption response. Furthermore, the bone formation response that occurs is predominated by osteoid production rather than a true mineralised bone matrix (Dempster et al., 1999). The

reduction in bone mineral density (BMD) associated with hyperparathyroidism (Iida-Klein et al., 2005) may be a direct effect of PTH on key regulators of mineralisation.

This study therefore, sought to examine the effect of PTH exposure on PHOSPHO1, TNAP and nSMase2 expression in osteoblast-like cells and calvariae explants as well as to identify the PTH signal transduction pathways involved.

4.2. Hypothesis

Phospho1 is potently regulated by PTH in osteoblasts in a cAMP/PKA dependent manner.

4.3. Aims

I) Confirm the down-regulation of *Phospho1* expression in IDG-SW3 cells

II) Detail the temporal PTH regulation of *Phospho1*, *Smdp3* and *Alpl* in osteoblasts.

III) Determine whether the regulation of these genes by PTH is dependent on protein synthesis

IV) Investigate the PTH signalling pathways in osteoblasts that mediate the changes in *Phospho1*, *Alpl* and *Smpd3* gene expression

4.4. Materials and Methods

4.4.1. IDG-SW3 cell culture

IDG-SW3 cells were seeded in 6-well plates at 4 x 10^4 cells/cm^2 with IDG-SW3 proliferation medium as described in section 2.2.4. Upon confluency, proliferation media was replaced with differentiation media and cultures were maintained for up to 28 days with media changes every 2-3 days. IDG-SW3 cultures were exposed to PTH (50 nM) for 24 h prior to each of the time points investigated.

4.4.2. MC3T3-C14 cell culture

MC3T3-C14 cells were plated at 1 x 10^4 cells/cm^2 in 6-well plates and cultured in maintenance medium as described in section 2.2.3. Upon confluency, maintenance media was replaced with MC3T3 mineralisation media and cultures were maintained for up to 14 days with media changes every 2-3 days.

To examine the effects of continuous PTH on MC3T3-C14 gene and protein expression, the culture media was replaced with fresh mineralisation media containing either bPTH (1-34) (Sigma-Aldrich) (referred to as PTH) at various concentrations (0.5 -50 nM) or vehicle (PBS) and for various lengths of time (15 min - 72 h). Unless otherwise stated, cells were cultured for six days (from confluency) under osteogenic conditions prior to the addition of PTH in order to avoid suppression of osteoblast differentiation (Bellows et al., 1990, Isogai et al., 1996). To investigate the signalling pathways mediating the effects of PTH, cells were also treated with forskolin (25 µM, Sigma-Aldrich), phorbol 12-myristate 13-acetate (PMA, 100 nM, Sigma-Aldrich), PKI (5-24) (100 nM, Santa Cruz Biotechnology, Texas, USA) and napthol-AS E-phosphate (20 µM, Sigma-Aldrich) or appropriate vehicle controls for the time indicated. To assess the requirement of protein synthesis in the PTH regulation of *Phospho1*, *Alpl* and *Smpd3*, cells were pre-incubated for 2 h with cycloheximide (25 µM, Sigma-Aldrich) or DMSO control prior to stimulation with either 50 nM PTH or PBS for 6 h.

To examine the effects of intermittent PTH, MC3T3-C14 cell cultures were exposed to 50 nM PTH for either 1 h or 6 h in every 24 h period. After the PTH exposure period

was finished, cell monolayers were rinsed in MC3T3 mineralisation media, before culturing cells in this media for the remainder of the 24 h.

4.4.3. Murine calvariae culture

Calvariae from 4-5 day old wild-type (WT) pups were dissected under sterile conditions. Hemi-calvariae were cultured in 24-well plates in 350 μL of calvaria culture medium as described in section 2.3.2. After 24 h hemi-calvariae were treated with 50 nM PTH, forskolin (25 μM), PMA (100 nM), and PKI (5-24) (100 nM) or appropriate vehicle controls for the times indicated.

4.4.4. Murine primary calvarial osteoblast culture

Primary osteoblasts from the calvaria of new born WT and *Phospho1*$^{-/-}$ mice were extracted and seeded in 6-well plates at 1 x 10^4 cells/cm^2 with maintenance medium as described in section 2.2.5. Upon confluency, maintenance media was replaced with primary osteoblast mineralisation media and cultures were maintained for up to 28 days with media changes every 2-3 days. Primary osteoblast cultures were exposed to PTH (50 nM) for 24 h prior to each of the time points investigated.

4.4.5. Human subchondral bone osteoblast culture

Subchondral bone osteoblasts were extracted from excised human knee replacement samples as described in section 2.2.6. Osteoblasts were seeded in 6-well plates at 3 x 10^4 cells/cm^2 in human osteoblast maintenance media. Upon confluency, cell cultures were exposed to PTH (50 nM) for 24 h.

4.5.6. Embryonic metatarsal culture

The central three metatarsals from WT embryonic day 15 (E15) mice were dissected under sterile conditions and cultured in 24-well plates containing 350 μL metatarsal

medium as described in section 2.3.1. Metatarsals were cultured for 4 days, at which point they were exposed to PTH (50 nM) for 24 h.

4.4.7. Gene expression analysis

Cell monolayers and tissue from organ cultures were harvested at the specific time point in culture. RNA was extracted and reverse transcribed as described in sections 2.4.1. 2.4.2. and 2.4.3. respectively. RT-qPCR was performed on three technical replicates per sample and the results for each gene of interest were normalised to the appropriate housekeeping gene for the sample: *Atp5b* was used for MC3T3-C14; murine primary osteoblasts and murine calvarial organ cultures; *Gapdh* was used for IDG-SW3 and murine E15 metatarsal cultures; *GAPDH* was used for human subchondral bone osteoblast cultures. Relative gene expression was calculated using the ΔΔCt method (section 2.4.4.) and expressed as a fold change against control cultures.

4.4.8. Protein analysis

Protein was extracted from MC3T3-C14 cell monolayers at the specified time point of culture as described in section 2.5.1. The concentration of the protein lysate was determined by DC assay as described in section 2.5.3. and protein (15 μg) was electrophoresed in 10% Bis-Tris polyacrylamide gels. The resultant nitrocellulose membrane was probed by western blotting for PHOSPHO1, nSMase2, TNAP and β-actin as described in section 2.5.4.

4.4.9. Assessment of ECM mineralisation

The ECM mineralisation of MC3T3-C14 cell cultures continuously exposed to PTH for 10 days was assessed by alizarin red staining. Cell monolayers were fixed in 4%

PFA on the specified day of culture and alizarin red staining and quantification was carried out as described in section 2.8.1.

4.5. Results

4.5.1 The effects of PTH on the expression of Phospho1 in IDG-SW3 cells.

To validate and expand on the findings of St John et al., 2015, IDG-SW3 cells were treated with 50 nM PTH for 24 h at different time points during the 28 day culture period. A downregulation of *Phospho1* expression was noted at all time points assessed ($P<0.05$, Fig. 4.1.).

4.5.2. The effects of PTH on gene and protein expression in MC3T3 cells

Initial experiments assessed the ability of varying concentrations of PTH to regulate *Phospho1*, *Alpl* and *Smpd3* expression in MC3T3-C14 cells. MC3T3-C14 cells were treated with 0.05 – 50 nM PTH for 24 h on day 6 of culture, when initial mineral formation could be observed with light microscopy. At concentrations of 0.5 nM and above, PTH significantly down-regulated *Phospho1* mRNA expression ($P<0.001$, Fig. 4.2.A). PTH increased *Alpl* expression at the two highest concentrations examined, 25 nM ($P<0.05$) and 50 nM ($P<0.001$), whereas it down regulated *Smpd3* expression at all concentrations examined ($P<0.001$, Fig. 4.2.B & C). Western blotting confirmed that the changes in gene expression were replicated at the protein level (Fig. 4.2.J).

The temporal effects of PTH on *Phospho1*, *Alpl* and *Smpd3* expression at day 7 of culture (matching the end point in experiments described in Fig. 4.2.A-C) were next examined. PTH rapidly down-regulated *Phospho1* after 15 min which was further exacerbated after 1 h and 6 h exposures ($P<0.001$, Fig. 4.2.D). By 24 h, the down-

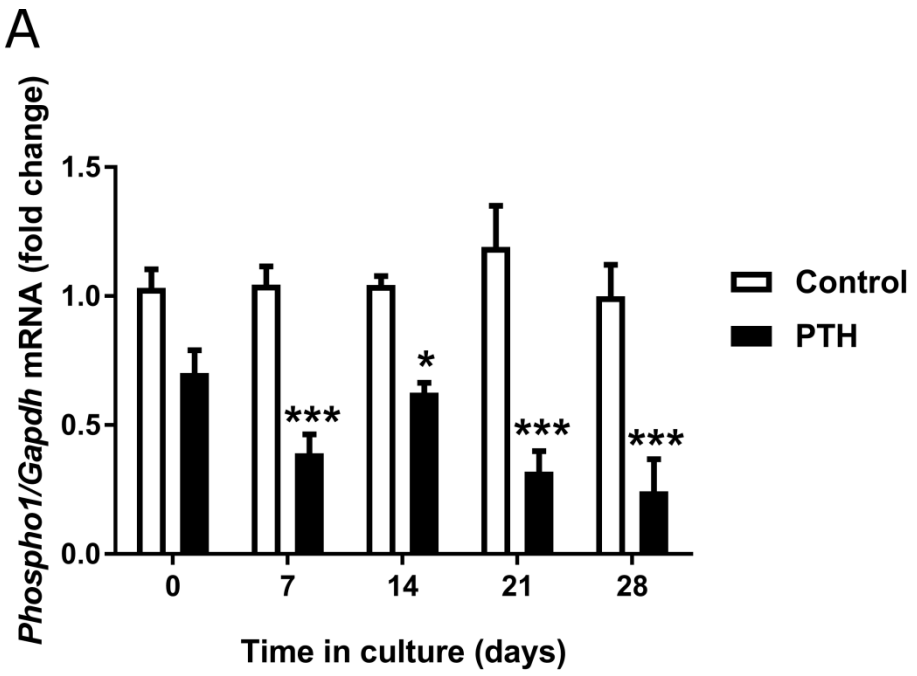

Figure 4.1. The effects of PTH on *Phospho1* expression in IDG-SW3 cells.

(A) *Phospho1* mRNA expression in response to 24 h bPTH (1-34) (50 nM) exposure in IDG-SW3 cells at different stages of differentiation (confluency (day 0), days 7, 14, 21 and 28 post confluency). N=3, P<0.05* and P<0.001*** in comparison to control treated cultures.

regulation of *Phospho1* by PTH was lessened ($P<0.05$) and after 48 h and 72 h exposures *Phospho1* expression had returned to basal levels. Enhancement of *Alpl* expression by PTH was noted after 1 h ($P<0.05$), peaking at 6 h ($P<0.001$) before returning to control levels after 24 h and longer exposures (Fig. 4.2.E). The expression pattern of *Smpd3* in response to PTH was similar to that of *Phospho1* however the speed of reduced expression and its normalisation were slower (Fig. 4.2.F). Changes in protein levels of PHOSPHO1, TNAP and nSMase2 reflected their respective changes in gene expression (Fig. 4.2.K). Notably, the expression levels of PHOSPHO1 and nSMase2 were less and TNAP was greater after 24 h and 48 h PTH exposure. After a 72 h exposure all proteins were expressed at a comparable level to the control treated cultures.

Finally, the effect of PTH (50 nM, 24 h) on the expression of *Phospho1*, *Alp1* and *Smpd3* was assessed in MC3T3-C14 cells at different stages of differentiation. *Phospho1* and *Smpd3* regulation by PTH was not dependent on the differentiation status of the cell cultures, with both genes being significantly down-regulated ($P<0.001$) at 0, 7 and 10 days in culture (Fig. 4.2.G & I). In contrast, PTH induced expression of *Alpl* was more restricted and only reached significance at day 0 ($P<0.01$, Fig. 4.2.H). Little or no PHOSPHO1, nSMase2 or TNAP protein was expressed at day 0 in culture and this was not obviously altered by PTH treatment (Fig. 4.2.L). At days 7 and 10 however, PTH decreased PHOSPHO1 and nSMase2 expression whilst increasing TNAP expression, consistent with the gene expression data.

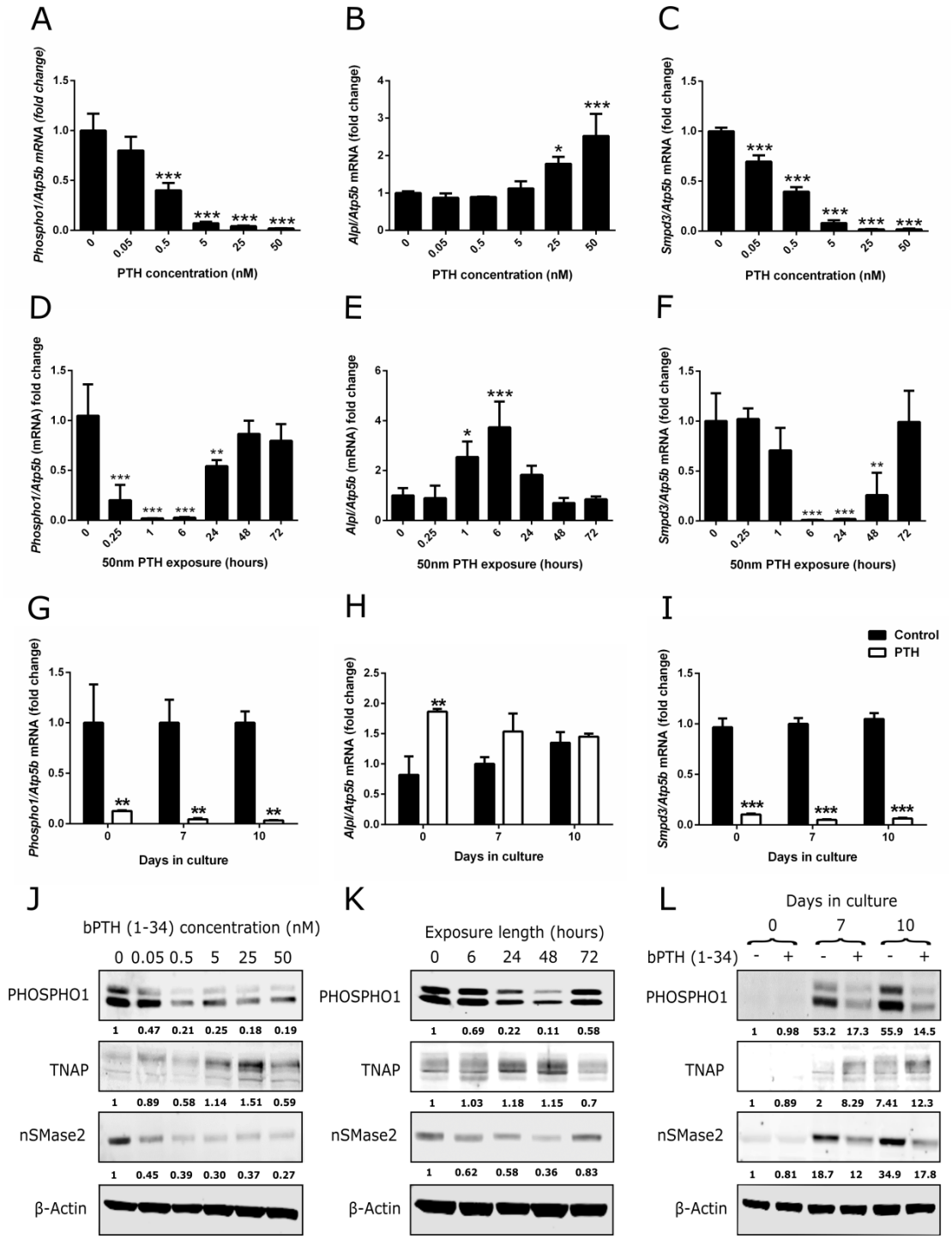
A
Phospho1/Atp5b mRNA (fold change)
PTH concentration (nM)
B
Alpl/Atp5b mRNA (fold change)
PTH concentration (nM)
C
Smpd3/Atp5b mRNA (fold change)
PTH concentration (nM)
D
Phospho1/Atp5b (mRNA) fold change
50nm PTH exposure (hours)
E
Alpl/Atp5b (mRNA) fold change
50nm PTH exposure (hours)
F
Smpd3/Atp5b mRNA (fold change)
50nm PTH exposure (hours)
G
Phospho1/Atp5b mRNA (fold change)
Days in culture
H
Alpl/Atp5b mRNA (fold change)
Days in culture
I
Control
PTH
Smpd3/Atp5b mRNA (fold change)
Days in culture
J
bPTH (1-34) concentration (nM)
0 0.05 0.5 5 25 50
PHOSPHO1
1 0.47 0.21 0.25 0.18 0.19
TNAP
1 0.89 0.58 1.14 1.51 0.59
nSMase2
1 0.45 0.39 0.30 0.37 0.27
β-Actin
K
Exposure length (hours)
0 6 24 48 72
PHOSPHO1
1 0.69 0.22 0.11 0.58
TNAP
1 1.03 1.18 1.15 0.7
nSMase2
1 0.62 0.58 0.36 0.83
β-Actin
L
Days in culture
0 7 10
bPTH (1-34) - + - + - +
PHOSPHO1
1 0.98 53.2 17.3 55.9 14.5
TNAP
1 0.89 2 8.29 7.41 12.3
nSMase2
1 0.81 18.7 12 34.9 17.8
β-Actin

(Previous page) Figure 4.2. Regulation of key mineralisation genes by PTH in MC3T3-C14 cells.

RT-qPCR analysis of **(A)** *Phospho1*, **(B)** *Alpl* and **(C)** *Smpd3* mRNA expression in response to a 24 h exposure of various doses of bPTH (1-34) on day 6 of culture. RT-qPCR analysis of **(D)** *Phospho1*, **(E)** *Alpl* and **(F)** *Smpd3* mRNA expression in response to various exposure times of bPTH (1-34) (50 nM). The timing of PTH addition was adjusted to ensure all experiments finished on day 7 of culture. RT-qPCR analysis of **(G)** *Phospho1*, **(H)** *Alpl* and **(I)** *Smpd3* mRNA expression in response to 24 h exposure PTH (50 nM) in MC3T3-C14 cells at different stages of differentiation (confluency (day 0), days 7 and 10 post confluency). **(J)** Western blotting analysis of PHOSPHO1, TNAP, nSMase2 in response to a 24 h exposure of various doses of PTH. The fold change in fluorescence intensity against control treated cultures (normalised against beta-actin) is shown below each protein of interest. **(K)** Western blotting analysis of PHOSPHO1, TNAP, nSMase2 in response to various exposure times of PTH (50 nM). The fold change in fluorescence intensity against control treated cultures (normalised against beta-actin) is shown below each protein of interest. **(L)** Western blotting analysis of PHOSPHO1, TNAP, nSMase2 in response a 24 h PTH (50 nM) exposure in MC3T3-C14 cells at different stages of differentiation. The fold change in fluorescence intensity against day 0 control treated cultures (normalised against beta-actin) is shown below each protein of interest. N=3, $P<0.05$*, $P<0.01$** and $P<0.001$*** in comparison to controls.

4.5.3. The effects of continuous PTH on the ECM mineralisation of MC3T3-C14 cell cultures

The addition of 50 nM PTH every 48 h to MC3T3-C14 cell cultures for 10 days caused a reduction in the extent of matrix mineralisation compared to control cultures as assessed by the quantitative alizarin red assay (0.141±0.005 vs. 0.083±0.018, $P< 0.05$, data no shown).

4.5.4. The effects of PTH on gene expression in murine calvariae.

Murine hemi-calvariae were treated with 50 nM PTH for 2, 6 and 24 h. A significant downregulation of both *Phospho1* and *Smpd3* expression in response to PTH was observed at 2 h ($P<0.05$), 6 h and 24 h ($P<0.001$, Fig. 4.3.A & C). Likewise, PTH exposure induced a down-regulation of *Alpl* expression, albeit only with 24 h exposure ($P<0.01$, Fig. 4.3.B).

4.5.5. The effects of cycloheximide on *Phospho1*, *Alpl* and *Smpd3* gene regulation by PTH.

To determine whether PTH directly regulates *Phospho1*, *Alpl* and *Smpd3* gene expression, MC3T3-C14 cells were pre-treated for 1 h with the protein synthesis inhibitor cycloheximide (25 µM), followed by treatment with 50 nM PTH for 6 h. Cycloheximide treatment alone did not affect basal levels of *Phospho1*, *Alpl* or *Smpd3*. In the presence of cycloheximide, PTH reduced the expression of *Phospho1* (44.1%, $P<0.01$) but this was not to the same extent observed in the absence of cycloheximide (93.9%, $P<0.001$, Fig. 4.4.A). Cycloheximide treatment did not affect the potent regulation of *Alpl* and *Smpd3* expression by PTH (Fig. 4.4.B & C).

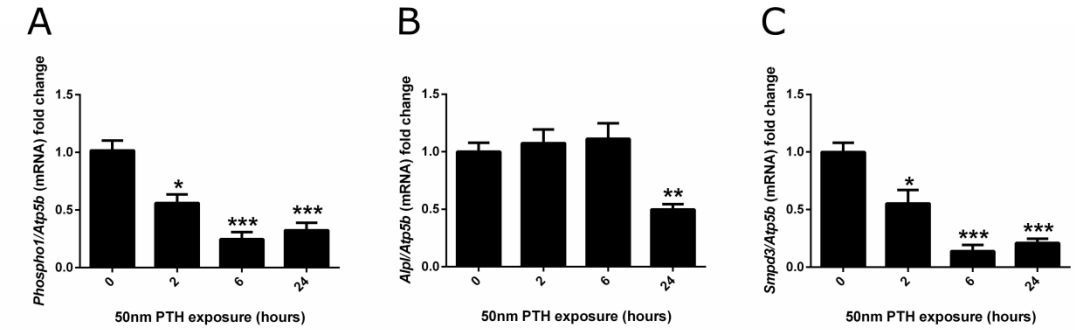

Figure 4.3. Regulation of key mineralisation genes by PTH in cultured calvariae.

RT-qPCR analysis of **(A)** *Phospho1*, **(B)** *Alpl* and **(C)** *Smpd3* mRNA expression in response to various exposure times of PTH (50 nM). N>3 per time point, P<0.05* and P<0.001*** in comparison to control.

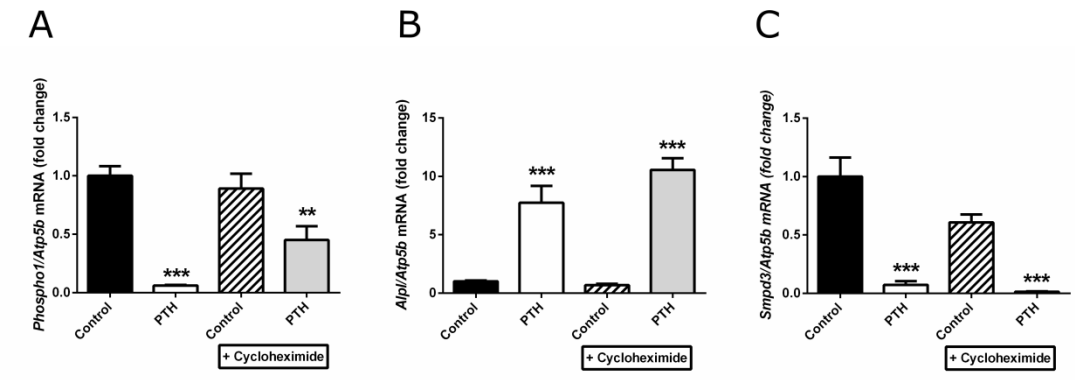

Figure 4.4. The effects of bPTH (1-34) on *Phospho1*, *Alpl* and *Smpd3* in MC3T3-C14 cells does not require protein synthesis.

MC3T3-C14 cells were treated for 6 h with 50 nM PTH or vehicle control after a 2 h pre-treatment with 25 μM cycloheximide (CHX) or solvent control on day 7 in culture. **(A)** *Phospho1*, **(B)** *Alpl* and **(C)** *Smpd3* mRNA expression was assessed by RT-qPCR. N=3, P<0.05*, P<0.01** and P<0.001*** in comparison vehicle control.

4.5.6. Identification of the intracellular signalling pathways responsible for PTH regulation of *Phospho1*, *Alpl* and *Smpd3* expression.

Binding of PTH to the G-protein coupled receptor parathyroid hormone 1 receptor (PTH1R) primarily activates cAMP/PKA and PKC signalling pathways (Qin et al., 2004). To determine which of these pathways was utilised by PTH to regulate *Phospho1*, *Alpl* and *Smpd3* expression, MC3T3-C14 cells and murine hemi-calvariae were treated with the cAMP inducer forskolin (10 µM) or the PKC activator, PMA (100 nM) for 24 h. In MC3T3-C14 cells, forskolin replicated the effects of 50 nM PTH by inducing significant decreases in *Phospho1* ($P<0.001$) and *Smpd3* expression ($P<0.001$) whilst significantly increasing the expression of *Alpl* ($P<0.001$). PMA treated cells displayed no differences in *Phospho1*, *Alpl* or *Smpd3* expression compared to control cultures (Fig. 4.5.A-C). The gene expression results in MC3T3-C14 cells were confirmed at the protein level by western blotting (Fig. 4.5.D). In hemi-calvariae, forskolin similarly replicated the effects of 50 nM PTH by inducing a significant decrease in *Phospho1* ($P<0.05$), *Smpd3* ($P<0.001$) and *Alpl* ($P<0.001$) expression (Fig. 4.5.E-G). PMA treated hemi-calvariae displayed no differences in *Phospho1* expression, however the expression of *Alpl* and *Smpd3* was strongly down-regulated by exposure to PMA ($P<0.001$) (Fig. 4.5.E-G). To confirm the role of the cAMP/PKA signalling pathway as the mediator of the effects of PTH in MC3T3-C14 cells, cell cultures were treated with the PKA inhibitor PKI (5-24) (100 nM) alone or in the presence of PTH for 6 h. The addition of PKI (5-24) alone did not alter the basal expression of *Phospho1*, *Alpl* or *Smpd3*. The addition of the PKA inhibitor reduced the ability of 50 nM PTH to significantly inhibit the expression of *Phospho1* and

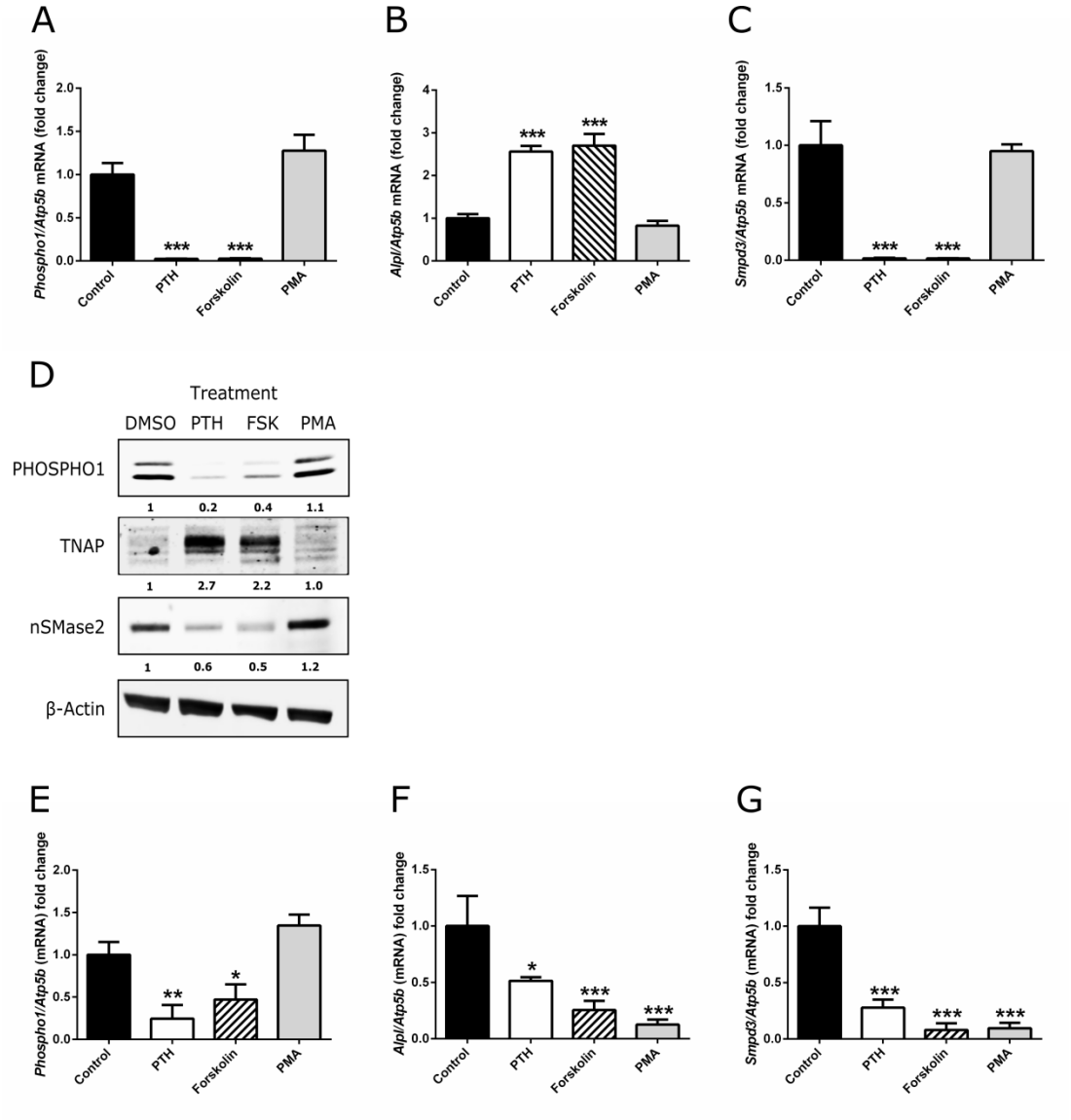

Figure 4.5. Investigation of signalling pathways regulating the effects of PTH.

MC3T3-C14 cells were treated with 50 nM PTH, 25 μM forskolin, 100 nM PMA or vehicle control for 24 h on day 6 in culture. **(A)** *Phospho1*, **(B)** *Alpl* and **(C)** *Smpd3* mRNA expression was assessed by RT-qPCR. **(D)** Western Blotting analysis of MC3T3-C14 cells treated as described above. Hemi-calvariae were treated with 50 nM PTH, 25 μM forskolin, 100 nM PMA or vehicle control for 24 h. **(E)** *Phospho1*, **(F)** *Alpl* and **(G)** *Smpd3* mRNA expression was assessed by RT-qPCR. N=3, P<0.05*, P<0.01** and P<0.001*** in comparison vehicle control.

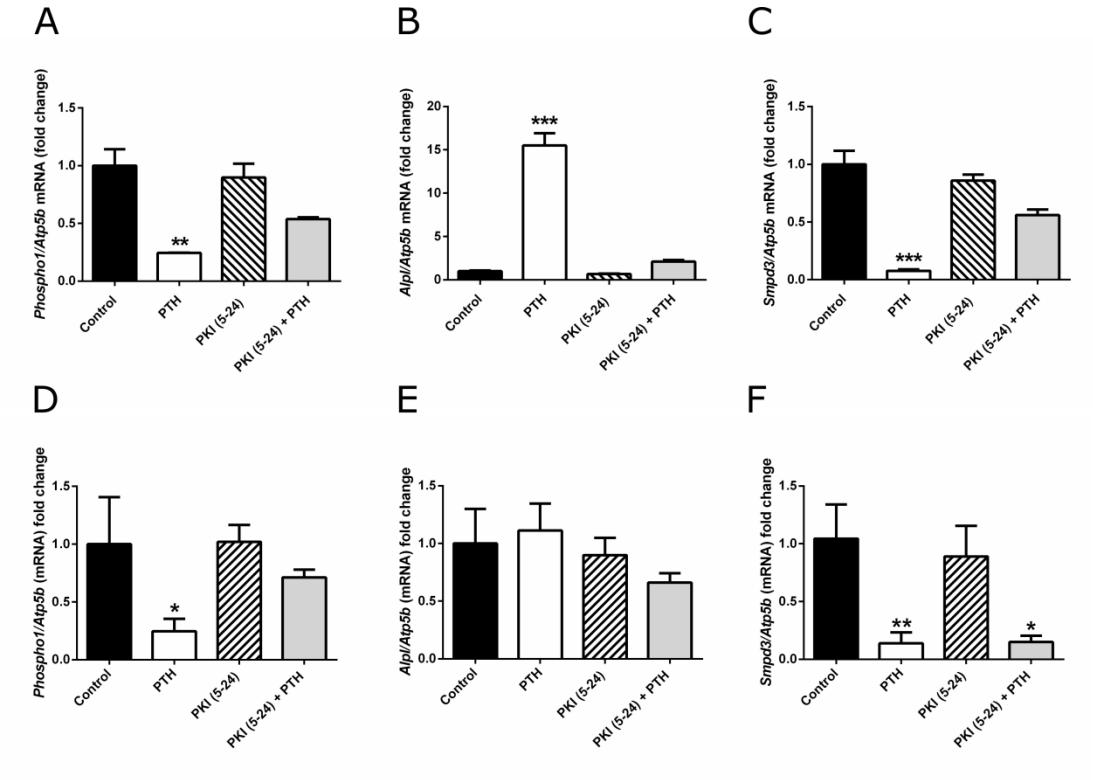

Figure 4.6. Inhibition of PKA signalling pathway abolishes the effects of PTH.

MC3T3-C14 cells and hemi-calvariae were treated with 50 nM PTH or vehicle control for 6 h following a 1 h pre-treatment with 100 nM PKI (5-24) on day 6 of culture. **(A)** *Phospho1*, **(B)** *Alpl* and **(C)** *Smpd3* mRNA expression in MC3T3-C14 and **(D)** *Phospho1*, **(E)** *Alpl* and **(F)** *Smpd3* mRNA expression in hemi-calvariae, all assessed by RT-qPCR. N=3, P<0.05*, P<0.01** and P<0.001*** in comparison to vehicle control.

*Smpd3 (*Fig. 4.6.A & C*)*. Similarly, the induction of *Alpl* expression by PTH was abrogated by the co-incubation of PKI (5-24) (Fig. 4.6.B). In cultured hemi-calvariae, PKI (5-24) inhibited the down regulation of *Phospho1* by PTH (Fig 4.6.D), whereas the down-regulation of *Smpd3* by PTH was not affected by PKI (5-24) ($P<0.001$, Fig. 4.6.F). In light of the previous data (Fig. 4.3.B) where PTH did not alter *Alpl* expression after 6 h (*cf.* 24 h) it was not surprising that PTH or the co-incubation of PKI and PTH had no effect on *Alpl* expression (Fig. 4.6.E).

4.5.7. Investigation of transcription factors which may mediate the effects of PTH in cultured MC3T3 cells and murine calvariae.

To investigate the role of the transcription factor CREB (cAMP response element-binding protein) in mediating the effects of PTH on *Phospho1* expression, napthol AS-E phosphate (20 µM, a CREB, CREB binding protein (CBP) interaction inhibitor) was pre-incubated with MC3T3-C14 cells for 1 h prior to the addition of PTH (50 nM) for 6 h. Napthol AS-E phosphate exposure did not modulate the downregulation of *Phospho1* observed in the presence of PTH (Fig. 4.7.A). To understand the expression profile of other known osteoblast regulating transcription factors, MC3T3-C14 cells and murine calvariae were exposed to PTH for up to 6 h and the expression of the transcription factors *Runx2, Sp7, Atf4 and Trps1* was assessed by RT-qPCR. The effects on expression were modest, in brief, the expression of *Runx2* and *Trps1* did not change in response to PTH exposure (Fig. 4.7.B & E) where as *Sp7* expression was reduced after a 6 h PTH exposure ($P<0.01$, Fig. 4.7.C) and *Atf4* was enhanced after 15 min PTH exposure ($P<0.01$, Fig. 4.7.D). In cultured murine calvariae, the expression of *Runx2*, *Atf4* and *Trps1* was not altered in response to PTH (Fig. 4.7.F, H & I). In contrast, Sp7 expression was significantly down regulated ($P<0.05$, Fig. 4.7.G).

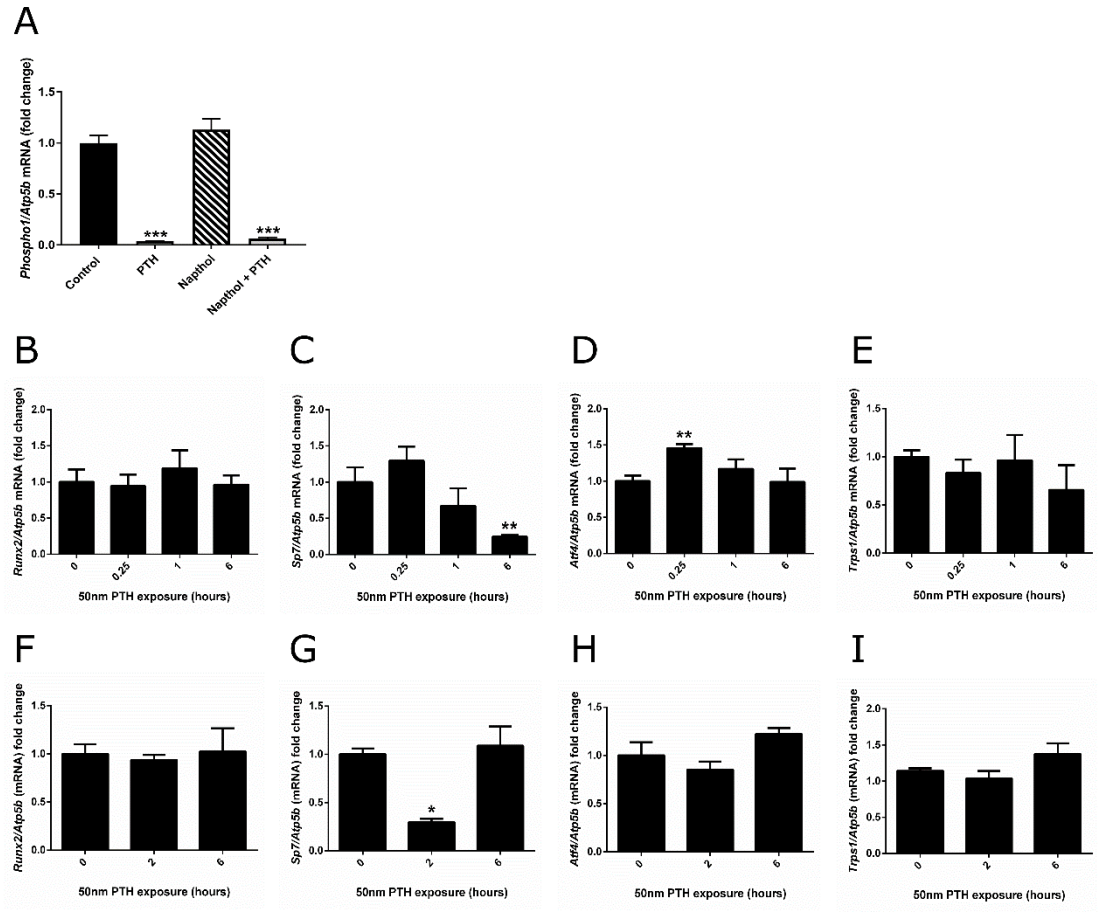

Figure 4.7. Understanding the involvement of transcription factors in mediating the effects of PTH.

MC3T3-C14 cells were treated with 50 nM PTH or vehicle control for 6 h following a 1 h pre-treatment with 20 µM napthol AS-E phosphate on day 6 of culture. **(A)** *Phospho1* mRNA expression was assessed by RT-qPCR. **(B)** *Runx2,* **(C)** *Sp7,* **(D)** *Atf4* and **(E)** *Trps1* mRNA expression was assessed by RT-qPCR in MC3T3-C14 cell cultures in response to a short-term exposure to 50 nM PTH on day 7 of culture. **(F)** *Runx2,* **(G)** *Sp7,* **(H)** *Atf4* and **(I)** *Trps1* mRNA expression was assessed by RT-qPCR in cultured murine calvariae in response to a short-term exposure to 50 nM PTH. N=3, P<0.05*, p<0.01** in comparison to control treated cultures.

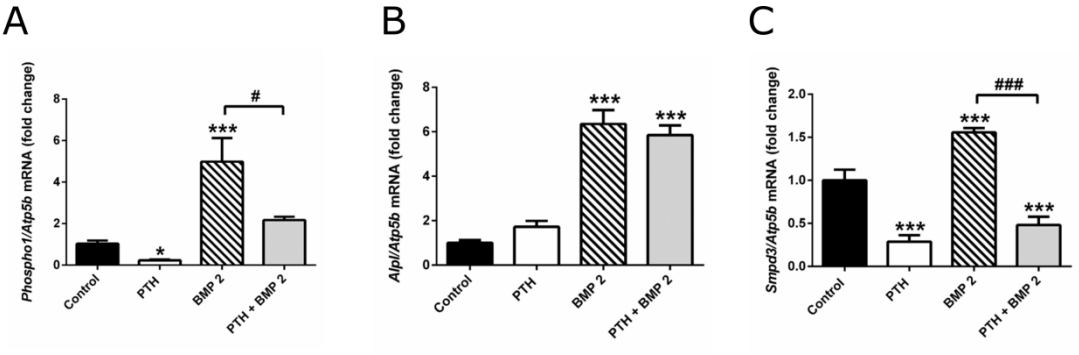

Figure 4.8. Combined effects of continuous PTH and BMP-2 exposure on *Phospho1*, *Alpl* and *Smpd3* expression in MC3T3-C14 cells.

(A) *Phospho1*, **(B)** *Alpl and* **(C)** *Smpd3* mRNA expression was assessed by RT-qPCR in MC3T3-C14 cell cultures in response to a 24 h exposure to 50 nM PTH, 300 ng/mL BMP-2 or both on day 6 of culture. N = 3, *P<0.05, ***P<0.001 in comparison to control treated cultures, $^{###}$P<0.001 in comparison with BMP-2-treated cultures

4.5.8. Investigating the combined effects of continuous PTH and BMP-2 exposure on gene expression in MC3T3 cells

To investigate the effects of PTH exposure in MC3T3 cells treated with BMP-2, cells were cultured with either 50 nM PTH, 300 ng/mL BMP-2 or both for 24 h on day 6 of culture, and the expression of *Phospho1*, *Alpl* and *Smpd3* was assessed by RT-qPCR. BMP-2 exposure significantly induced the expression of *Phospho1*, *Alpl* and *Smpd3* ($P<0.001$, Fig. 4.8.A–C). The stimulatory effect of BMP-2 on *Phospho1* expression was nullified by the dual exposure of PTH, which caused *Phospho1* expression to return to unstimulated control levels (Fig. 4.8.A). In contrast, the *Smpd3* expression in cells treated with PTH or PTH and BMP-2 was similar ($P<0.001$, Fig. 4.8.C), suggesting that *Smpd3* expression was highly sensitive to PTH exposure. The increased expression of *Alpl* by BMP-2 was not affected by the co-incubation of PTH.

4.5.9. Alternate regulation of *Phospho1* by PTH in primary osteoblast and embryonic metatarsal cultures.

The effects of PTH on the regulation of *Phospho1* expression was further assessed in murine primary calvarial osteoblasts, human subchondral bone osteoblasts and murine E15 metatarsals. Surprisingly, *Phospho1* expression was enhanced in response to 24 h exposure to PTH in all three model systems. In murine primary calvarial osteoblasts, PTH enhancement of *Phospho1* expression was observed at day 0, 7, 14, 21 and 28 of culture ($P<0.001$, Fig. 4.9.A). In human subchondral bone osteoblasts (derived from three different patients), 24 h PTH exposure resulted in a 5.7-fold increase compared to control cultures ($P<0.001$, Fig. 4.9.B). Finally, murine E15 metatarsals cultured for 4 days in mineralising conditions, exhibited an upregulation of *Phospho1* expression in response to 24 h PTH treatment ($P<0.001$, Fig. 4.9.C).

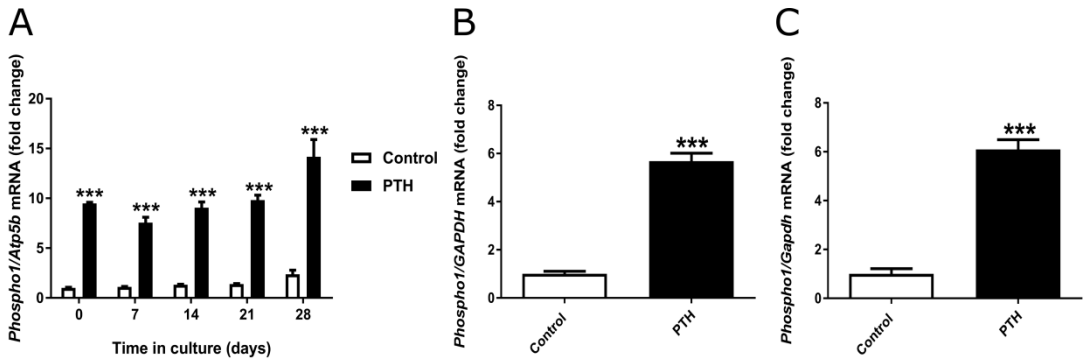

Figure 4.9. Alternate regulation of *Phospho1* by PTH in primary osteoblast and embryonic metatarsal cultures.

(A) *Phospho1* mRNA expression in response to 24 h bPTH (1-34) (50 nM) exposure in murine primary osteoblast cells at different stages of differentiation (confluency (day 0), days 7, 14, 21 and 28 post confluency) (N=3). **(B)** *Phospho1* mRNA expression in response to 24 h bPTH (1-34) (50 nM) exposure in human subchondral bone osteoblast cells. (N=3) **(C)** *Phospho1* mRNA expression in response to 24 h bPTH (1-34) (50 nM) exposure on day 4 of culture in murine E15 metatarsals. N=3, 5 bones per replicate, P<0.001*** in comparison to control treated cultures.

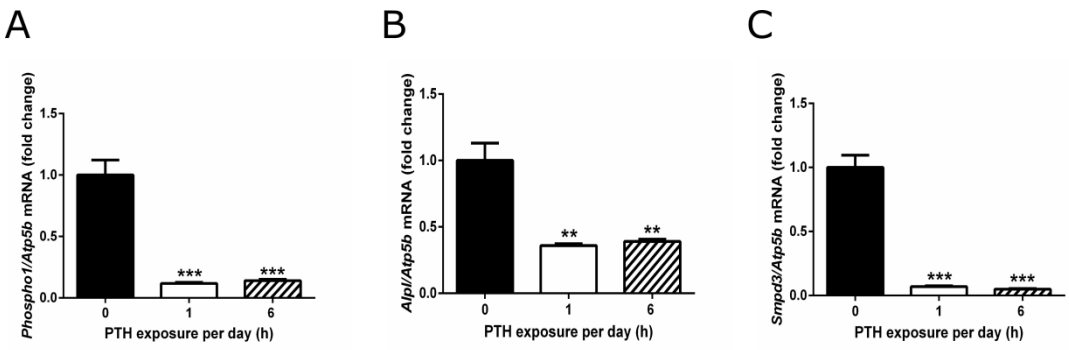

Figure 4.10. The effects of intermittent PTH exposure on the expression of *Phospho1*, *Alpl* and *Smpd3* in MC3T3-C14 cells.

MC3T3-C14 cells were cultured in mineralising conditions for 10 days. For either 1h or 6 h every day, cells were exposed to PTH before returning to standard mineralisation media. The mRNA expression of **(A)** *Phospho1*, **(B)** *Alpl and* **(C)** *Smpd3* was assessed by RT-qPCR on day 10 of culture. N = 3, **P<0.05, ***P<0.001 in comparison to control treated cultures.

4.5.10. The effects of intermittent PTH on the expression of *Phospho1, Alpl* and *Smpd3 in vitro*.

To assess the effect of intermittent PTH on mineralisation gene expression in MC3T3-C14 cell cultures, cells were exposed to 50nM PTH for either 1 h or 6 h in every 24 h period for 10 days. Surprisingly, the expression of *Phospho1*, *Alpl* and *Smpd3* were all significantly downregulated with both 1 h and 6 h intermittent PTH exposure ($P<0.001$, Fig. 4.10.A-C).

4.6. Discussion

The crucial role of both *Phospho1* and *Smpd3* in the mineralisation of the skeleton and dentition are well established (Yadav et al., 2011, Khavandgar et al., 2011, McKee et al., 2013, Khavandgar et al., 2013). Despite this understanding of their function, there exists a hiatus in the knowledge surrounding their regulation. A recent transcriptome sequencing investigation however, has revealed that *Phospho1* is regulated by PTH in osteocytes (St John et al., 2015). This study provided the impetus for this research, which sought to determine the effects of PTH on the regulation of PHOSPHO1, nSMase2 and TNAP expression in osteoblasts.

This study initially expanded the analysis of St John et al. (2015) (who had treated IDG-SW3 cells after 35 days in culture with PTH) by assessing the effects of PTH at different differentiation stages of these cells. Confirming and extending the results of this study, *Phospho1* downregulation by PTH was observed at every time point investigated. IDG-SW3 cells recapitulate the late osteoblast to late osteocyte progression, initially expressing high levels of *Alpl* before showing significant increases in *Sost* expression by day 21 of culture (Woo et al., 2011). These initial

results suggest that the PTH regulation of *Phospho1* is not limited to osteocytes as originally suggested by St John et al. (2015). The effect of PTH on osteoblasts was therefore investigated more thoroughly in the experiments described herein. This study provides the first evidence for the potent regulation of *Phospho1* and *Smpd3* by PTH in osteoblast-like cells and cultured calvariae. Data presented here builds on previous investigations that sought to uncover the regulation of mineralisation-dependent genes by growth factors and hormones. The enhancement of nSMase2 expression by BMP signalling was recently elucidated in chondrocytes and C2C12 cells (Kakoi et al., 2014, Chae et al., 2009). These findings have been confirmed and expanded, by revealing that PTH exposure is able to significantly down-regulate *Smpd3* expression even in the presence of BMP-2. *Phospho1* expression was similarly enhanced by BMP-2 exposure, with concomitant PTH exposure restoring expression levels to those of control cultures. The effects of BMP signalling on PHOSPHO1 regulation and the interaction between BMP and PTH signalling are intriguing and worthy of further investigation. Whilst no interaction between PTH and BMP- 2 in the regulation of *Alpl* expression was found, the effects of PTH alone on *Alpl* expression have been well documented. For example, intermittent exposure to PTH has been shown to stimulate ALP activity and bone nodule formation (Terakado et al., 1995). However, it should be noted that the inhibition of osteoblast differentiation by PTH has been reported in other studies (Zerega et al., 1999, van der Horst et al., 2005) and this variation in response may be explained by differences in osteoblast differentiation stage and PTH exposure time and dosage.

PTH can exert entirely opposing effects on bone, which depend upon the length of exposure. Intermittent exposure to PTH is anabolic to the skeleton, with reactivation

of bone lining cells (Dobnig and Turner, 1995), inhibition of osteoblast apoptosis (Jilka et al., 1999), and down-regulation of sclerostin, the potent negative regulator of Wnt signalling and bone formation (Kramer et al., 2010). Currently, rhPTH (1-34) (Teriparatide) is the only anabolic therapy for osteoporosis aimed at preventing both vertebral and non-vertebral fractures in post-menopausal women (Poole and Reeve, 2005). Contrastingly, continuous exposure to PTH, as observed in hyperparathyroidism, is catabolic to bone, increasing osteoclastogenesis through upregulation of RANKL and inhibition of OPG expression (Ma et al., 2001). Knowledge of the effects of continuous exposure to PTH are however limited with regards to the regulation of mineralisation promoting enzymes despite an overall increase in the remodelling rate observed in hyperparathyroidism (Eriksen, 2002).

The nature of the PTH administration described in this study, whereby PTH is added to the culture medium and the medium is not changed before the experiments are stopped for collection of RNA/protein, most closely resembles a continuous exposure to PTH. Indeed a number of investigations to date have demonstrated this method of PTH exposure to better model the catabolic effects of PTH (Ishizuya et al., 1997, Liu et al., 2012). With bovine PTH (1-34) having a reported half-life of 10-12 h *in vitro* a biologically effective dose of ~3 nM should have remained in the cultures after 48 h. However, as the time exposure studies show (Fig. 4.2.D-E), *Phospho1* and *Alpl* gene expression levels were normalised by 48 h. This suggests the lack of a biologically effective dose of PTH at this time point. In contrast, *Smpd3* expression remained significantly down regulated at 48 h possibly reflecting the increased sensitivity of this gene to PTH challenge (Fig. 4.2.F). These data bring into question the levels of

biologically active PTH remaining in the experimental cultures and highlight the limitations of this approach. However, this method of PTH exposure is in contrast to *in vitro* studies which seek to model the effects of intermittent PTH, whereby PTH is added to cell cultures for 1-6 h per 24 or 48 h incubation cycle (Ishizuya et al., 1997, Lotinun et al., 2002). These *in vitro* intermittent exposure methods were replicated in this study and showed comparable inhibition of *Phospho1* and *Smpd3* expression as achieved with continuous exposure. The findings presented here therefore, show for the first time that PTH administration to MC3T3-C14 cell cultures inhibits the expression of *Phospho1* and *Smpd3.*

The reduction of PHOSPHO1 and nSMase2 may provide a novel mechanism by which continuous PTH exposure results in decreased bone mineral density. Continuous exposure to PTH reduced the extent of matrix mineralisation in MC3T3-C14, which has similarly been observed in rat calvarial osteoblast cultures (Ishizuya et al., 1997). Intriguingly, recent studies have also provided data which highlight a role for PHOSPHO1 and nSMase2 in the biogenesis of matrix vesicles (Thouverey et al., 2011, Kapustin et al., 2015, Yadav et al., 2016). It is possible therefore, that the reduced mineralisation of MC3T3-C14 cell cultures observed in response to continuous exposure to PTH is due to both a decreased number of MVs being released and a decrease in their ability to initiate amorphous hydroxyapatite formation. Despite this, *Alpl* expression was induced in response to PTH in MC3T3-C14 cell cultures. An enhancement of *Alpl* expression and TNAP activity in response to a continuous exposure to PTH has previously been shown in periodontal ligament cells (Wolf et al., 2013) and in the UMR-106 cell line (Kano et al., 1994) respectively. Even with this

body of evidence in mind, the differential regulation of *Phospho1* and *Alpl* by PTH is perhaps surprising. The genetic ablation of *Phospho1* in the mouse, leads to reduced serum TNAP activity and reduced *Alpl* expression in cultured chondrocytes derived from these mice (Yadav et al., 2011). Importantly, cultured hemi-calvariae exposed to continuous PTH exposure for 24 h displayed a downregulation of *Alpl* expression (Fig. 4.3.B). The *ex vivo* culture of calvariae may provide a more physiologically relevant model of osteoblast behaviour due to the maintenance of both cell-cell and cell-matrix interactions in three-dimensional space.

To enact its effects, PTH binds to the PTH1R , a G-protein coupled receptor, through a receptor binding domain between amino acids 15-24 (Mannstadt et al., 1999). Both PKA and PKC signal transduction pathways may be activated by binding of PTH to PTH1R. The effects of PTH are primarily elicited through the PKA pathway whereby, stimulatory $G\alpha_s$ proteins activate adenylyl cyclase, with subsequent production of cAMP and phosphorylation of PKA (Silva and Bilezikian, 2015). A limited number of genes, for example those encoding the insulin like growth factor binding protein 5 and TGF-β1, have been found to be regulated by $G\alpha_q$ activation which results in PKC activation, 1,4,5-inositol triphosphate production and a rise in intracellular Ca^{2+} (Qin et al., 2004). A critical role for the cAMP-PKA pathway in mediating the effects of PTH on PHOSPHO1, nSMase2 and TNAP expression in osteoblast cell culture models has been revealed in this study. Firstly, the adenylyl cyclase agonist, forskolin, replicated the effects of PTH whereas exposure to the PKC agonist, PMA, caused no effects. Furthermore, specific inhibition of the cAMP activation of PKA by the synthetic peptide PKI (5-24) abrogated the effects of PTH on *Phospho1*, *Alpl* and

Smpd3 expression (these results of these investigatory experiments are summarised in Table 2). In support of a role for PKA signalling in the downregulation of the mineralisation-dependent enzymes, PHOSPHO1 and nSMase2, studies to date have shown the inhibition of both MC3T3-E1 matrix mineralisation and bone nodule formation by cultured rat calvarial cells with long term exposure to forskolin (Kaneki et al., 1999, Tintut et al., 1999). Experiments utilising cycloheximide, revealed that this genetic regulation did not appear to be solely dependent on protein synthesis. It was noted that cycloheximide appeared to partially affect the downregulation of *Phospho1* by PTH exposure (inducing a 49.5% decrease as opposed to a 93.9% decrease by PTH alone). Despite this, it is well accepted that cycloheximide can exert off-target effects (McMahon, 1975) and these may account for this difference.

As the archetypal target of the cAMP/PKA signalling pathway, the role of the transcription factor CREB was investigated as a potential facilitator of the effects of PTH on *Phospho1* mRNA expression. Napthol AS-E phosphate has previously been shown to inhibit the interaction between phosphorylated CREB and the histone acetyltransferase, CBP, thus mitigating the gene expression modulating potential of this interaction (Best et al., 2004). Napthol AS-E phosphate did not affect the PTH mediated downregulation of *Phospho1* in MC3T3-C14 cells. A more comprehensive investigation of the transcription factor binding sites of the *Phospho1* promoter will be required to identify other potential PKA targets. The expression of the osteogenic transcription factors *Runx2*, *Sp7* and *Atf4* and *Trps1*, of which the latter has recently been implicated in the regulation of *Phospho1* in a preodontoblastic cell line (Kuzynski et al., 2014), were additionally assessed. In both cultured murine calvariae and MC3T3-C14 cells, *Sp7* expression was reduced in response to PTH. This suggests that

osterix (encoded by the *Sp7* gene), one of the master transcription factors regulating osteogenic differentiation, may be an important transcription factor in the regulation of both *Phospho1* and/or *Smpd3* expression (Nishimura et al., 2012). Again, the transcriptional and epigenetic regulation of these mineralisation-dependent genes requires further study.

These data are novel for the PTH control of *Phospho1* and *Smpd3* expression but previous reports have demonstrated the involvement of the cAMP-PKA pathway in the regulation (both positive and negative) of TNAP activity in a variety of cell culture models of mineralisation (Ishizuya et al., 1997, Wolf et al., 2013, Kano et al., 1994, Terakado et al., 1995). The PTH-dependent enhancement of TNAP activity has been shown to be enacted through cAMP-PKA mediated activation of p38 MAP kinase (Rey et al., 2007). In the cultured calvariae experiments, cAMP stimulation by forskolin simulated the effects of PTH by inducing a downregulation of *Phospho1, Alpl and Smpd3*. In contrast to MC3T3-C14 cell cultures however, PMA similarly induced the downregulation of *Alpl* and *Smpd3* and blockade of PKA activation by PKI (5-24) did not affect the PTH induced downregulation of *Smpd3.* To date, *Phospho1* has been shown to be exclusively expressed by osteoblasts, hypertrophic chondrocytes, odontoblasts and calcifying vascular smooth muscle cells (Houston et al., 2004, McKee et al., 2013, Kiffer-Moreira et al., 2013). *Smpd3* and *Alpl* on the other hand are more broadly expressed amongst different tissues and cell types. Although providing a more physiological environment, the presence of osteocytes, osteoclasts and stromal cells, as well as osteoblasts at differing stages of development in the

Table 2. Summary of the effects of the activator and inhibitor experiments performed in MC3T3-C14 cell cultures.

Activator / Inhibitor	**Action**	**Rationale**	**Effects on Phospho1 expression**
Cycloheximide	Protein synthesis inhibitor	Assess the role of protein synthesis in the PTH regulation of *Phospho1*	No effect
Forskolin	Adenylyl cyclase activator	Assess the role of the PKA signalling pathway in mediating the effects of PTH on *Phospho1*	Replicated the effects of PTH (i.e. inhibition of *Phospho1* expression)
PMA	PKC activator	Assess the role of the PKC signalling pathway in mediating the effects of PTH on *Phospho1*	No effect
PKI (5-24)	Competitive PKA inhibitor	Confirm the role of PKA in mediating the effects of PTH on *Phospho1*	No reduction in *Phospho1* expression in the presence of PTH
Napthol AS-E phosphate	Inhibits the interaction between CREB and CREB binding protein	Assess the role of the transcription factor CREB in mediating the effects of PTH on *Phospho1*	No effect

ex vivo calvariae model, may be confounding our investigation of the signalling pathways in this model.

Further complexity regarding the PTH-mediated regulation of *Phospho1* arose through experimentation in additional *in vitro* models. In contrast to MC3T3-C14 and calvarial

organ cultures, E15 metatarsal cultures alongside primary osteoblasts derived from both murine calvaria and human subchondral bone, all displayed increased *Phospho1* expression in response to 24 h PTH treatment (see Table 3 for summary of the effects of PTH on the different cell/organ culture models assessed). Of course, one must be cautious when interpreting the results from clonal cell lines, such as MC3T3-C14, whose responsiveness to PTH may be distinct from heterogeneous cell populations observed in primary cell cultures or indeed *in vivo*. More stringent analysis of the effects of continuous and intermittent PTH exposure *in vivo* will be needed to assess the endocrine regulation of *Phospho1* expression within bone.

In summary, the data presented here provide evidence for a potent negative regulation of *Phospho1* and *Smpd3* by continuous exposure to PTH in MC3T3-C14 and calvarial organ cultures. This downregulation of essential mediators of skeletal mineralisation may provide a novel mechanism which explains the poor bone quality observed in response to sustained and elevated exposures to PTH. Additional studies *in vivo* will be indispensable to confirm the regulation of *Phospho1* and *Smpd3* in bone.

Table 3. Summary of the effects of PTH on various cell/organ culture models.

Model System	Effect of PTH (50 nM; 24 h)		
	Phospho1	*Smpd3*	*Alpl*
IDG-SW3	↓	n/a	n/a
MC3T3-C14	↓	↓	↑
Primary murine calvarial osteoblast	↑	n/a	n/a
Murine calvarial culture	↓	↓	↓
Embryonic metatarsals	↑	n/a	n/a
Primary human subchondral osteoblasts	↑	n/a	n/a

Chapter 5

Examining the *in vivo* regulation of *Phospho1* by parathyroid hormone

5.1. Introduction

The potent regulation of *Phospho1* and *Smpd3* by PTH, as observed in Chapter 4, may provide an additional mechanism which goes some way to explain the disparate effects of intermittent and continuous PTH exposure. The previous Chapter highlighted, through examination of the literature surrounding TNAP's regulation by PTH, that understanding the effects of PTH *in vitro* is challenging and has produced conflicting results (Yee, 1985, Kato et al., 1990). This is at least in part due to the variety of cell lines and culture model systems utilised, the difficulty in replicating intermittent and continuous exposure *in vitro* and the complexity of PTH's role *in vivo*. With this in mind, and to get a more physiological comprehension of the biological effects of PTH on mineralisation-dependent gene expression, the overarching aim of this Chapter was to investigate the effects of PTH on these genes *in vivo*.

PTH has long been known as one of the major regulators of calcium, and to a lesser extent, phosphate homeostasis in mammals. Binding of PTH to the PTH1R within the primary target tissues of the kidney and bone elicits a range of molecular and cellular events which ultimately results in an increase in serum calcium concentration (Schluter, 1999, Hewison et al., 2000, Silva and Bilezikian, 2015). This present study however, is primarily concerned with the anabolic effects of exogenously administered PTH on bone. These anabolic effects have similarly been known for some time. Indeed, pioneering studies by Reeve and colleagues in the seventies revealed an increased bone formation rate in osteoporotic women in response to daily exposure to low dose PTH 1-34 (Reeve et al., 1976a, Reeve et al., 1976b). The large, multicentre trial of Neer et al. (2001) highlighted the efficacy of daily injection of PTH 1-34 in reducing vertebral and non-vertebral fractures, alongside increasing BMD in post-

menopausal osteoporotic women. As the only approved osteoanabolic agent (although PTH 1-34 is likely to lose this exclusivity with the impending approval of anti-sclerostin antibodies in 2017 (MacNabb et al., 2016)), the molecular events underpinning this anabolism are beginning to be more thoroughly understood.

Cells of the osteoblast lineage are the primary effectors of the osteoanabolic effects of PTH. Indeed, intermittent PTH (iPTH) exposure significantly increases osteoblast number (Silva and Bilezikian, 2015). Through the induction of *Runx2, Sp7* and *c-Fos* transcription, PTH promotes the commitment and differentiation of mesenchymal cells and osteoblast precursors to progress through the osteoblast lineage (Aslan et al., 2012). In addition, PTH modulates the expression and post-transcriptional regulation of apoptotic signalling molecules to reduce osteoblast apoptosis (Jilka et al., 1999, Bellido et al., 2003). Interestingly, osteoblast number increases, whilst the pool of quiescent bone lining cells shrinks in response to PTH exposure (Dobnig and Turner, 1995). Lineage tracing experiments confirmed that PTH exposure induces the reactivation of bone lining cells to functional osteoblasts (Kim et al., 2012). More recently, utilising the same lineage tracing technique, Jang et al. (2015) revealed that PTH also delays the transition of mature osteoblasts to bone lining cells. Osteocytes (terminally differentiated osteoblasts) express the PTH1R and are therefore also targets of PTH. The secreted glycoprotein, and potent negative regulator of the osteogenic WNT/β-catenin signalling pathway, SOST, is an important target of PTH signalling. PTH strongly inhibits *Sost* mRNA expression (Keller and Kneissel, 2005, Kramer et al., 2010), thereby offering an explanation for the bone anabolic actions of PTH. *In vitro* studies identified the cAMP/PKA signalling pathway as the mediator of the effect and more recent *in vivo* studies have highlighted the importance of the LRP

5/6 in mediating bone mass accrual in the absence of SOST (Li et al., 2005, Wan et al., 2008). As PHOSPHO1 activity is essential for successful ECM mineralisation, and is potently regulated by PTH (Houston et al., 2016), I hypothesised that its modulation *in vivo* could provide a novel unrecognised mechanism explaining the anabolic effects of PTH on bone.

In the discussion of Chapter 4, the effects of continuous PTH (cPTH) exposure, in terms of the upregulation of the RANKL/OPG ratio and unrestrained osteoclastogenesis, were described. It is probable however, that these effects represent only a small portion of the mechanisms contributing to the catabolic effects of cPTH. Indeed, Onyia et al. (2005) revealed 173 genes uniquely regulated by cPTH in the distal femur of rats. The negative regulation of PHOSPHO1 and nSMase2 expression in MC3T3-C14 cell cultures in response to cPTH exposure (Houston et al., 2016), draws attention to the modulation of key mineralisation-effector proteins as a means of explaining the osteocatabolic effects of cPTH *in vivo*.

This thesis has previously highlighted the importance of PHOSPHO1 in the initiation of skeletal mineralisation. This Chapter sought to investigate the regulation of *Phospho1* and other key regulators of skeletal mineralisation by iPTH and cPTH exposure in mouse bone. Additionally, the availability of the *Phospho1*$^{-/-}$ mouse allowed me to investigate the hypothesis that PHOSPHO1 is required for the full repertoire of osteoanabolic effects of iPTH *in vivo*.

5.2. Hypothesis

The anabolic effects of iPTH on bone are mediated, in part, through the upregulation of *Phospho1* and *Smpd3*. Conversely, the poor bone quality observed with continuous

exposure to PTH is mediated, in part, through the downregulation of *Phospho1* and *Smpd3*. The genetic ablation of *Phospho1* will diminish the anabolic and catabolic effects of iPTH and cPTH respectively.

5.3. Aims

I) Investigate the effects of a short-term PTH exposure on the expression of key mineralisation-dependent genes *in vivo*.

II) Determine the effects of long term iPTH on mineralisation-dependent gene expression and bone microarchitecture in both WT and *Phospho1*$^{-/-}$ mice.

III) Examine the effects of a 28-day continuous infusion of PTH on mineralisation-dependent gene expression and bone microarchitecture in both WT and *Phospho1*$^{-/-}$ mice.

IV) Investigate the PTH target genes within the kidney of iPTH treated mice as a possible mechanism to explain the differences between the WT and *Phospho1*$^{-/-}$ response to this therapy.

5.4. Materials and methods

5.4.1. PTH preparation

Recombinant human parathyroid fragment 1-34 (from here on referred to as PTH) was reconstituted in PBS, aliquoted and stored at -20°C. Prior to injection or filling of micro osmotic pumps, PTH was diluted to the appropriate concentration in 0.9% saline containing 0.2% w/v BSA.

5.4.2. PTH administration

5.4.2.1. Single dose PTH administration

Male, WT mice at 28-days of age received a single subcutaneous injection of PTH (80 μg/kg) or vehicle control (0.9% w/v saline containing 0.2% w/v BSA) before culling by cardiac puncture under terminal anaesthesia 6 h later. The left femur was dissected, the epiphyses removed and marrow eliminated by centrifugation prior to snap freezing in LN_2 and storage at -70°C for subsequent gene expression analyses.

5.4.2.2. Intermittent administration of PTH

Male, WT and *Phospho1*$^{-/-}$ mice at 28-days of age received a subcutaneous injection of PTH (80 μg/kg) or vehicle control once daily for 14 or 28 days. Mice were weighed each day prior to the injection. Mice were culled 24 h after the final injection of PTH by cardiac puncture under terminal anaesthaesia. The left femur was dissected, the epiphyses removed and marrow eliminated by centrifugation prior to snap freezing in LN_2 and storage at -80°C. The left kidney was dissected and freed from any surrounding adipose before snap freezing in LN_2 and storage at -80°C. The distal half of the femur and the left kidneywas used to extract mRNA for gene expression analysis as described in section 5.4.3.

5.4.2.3. Continuous delivery of PTH

The continuous administration of PTH was carried out using subcutaneously implanted micro-osmotic pumps. Male, WT and *Phospho1*$^{-/-}$ mice underwent surgical implantation of the mini-osmotic pumps at 28-days of age. Mice were deemed suitable for the surgery if they were greater than 20 g in weight on the day of surgery. Micro-osmotic pumps were filled with 100 μL of PTH (0.308 mg/mL) or vehicle control and

submerged in sterile 0.9% w/v saline and incubated at 37°C for 48 h prior to surgical implantation. This priming step ensured the pumps began releasing their contents at the indicated rate immediately upon implantation. Pumps were implanted subcutaneously, posterior to the scapula in accordance with manufacturer's guidelines and released 0.11 μL/h for 28 days. This strategy delivered PTH up to a maximum of 80 μg/day. Mice were culled on day 29 post-surgery by cardiac puncture under terminal anaesthesia.

5.4.3. Gene expression analysis

The distal femora and left kidney of all mice were homogenised in Qiazol reagent and total RNA was extracted using an RNeasy lipid mini kit as described in section 2.4.2. RT-qPCR was performed in triplicate on between 4-6 biological replicates and the results for each gene of interest were normalised to the appropriate housekeeping gene (*Atp5b* for bone samples and *Gapdh* for kidney samples). Relative gene expression was calculated using the ΔΔCt method (section 2.4.4.) and expressed as a fold change against the WT vehicle control treated samples.

5.4.4. Immunohistochemistry

The left tibiae from experimental mice were processed to paraffin wax and sectioned at a thickness of 5μm as described in section 2.7.4. Immunolocalisation of TNAP was carried out as described in section 2.7.6. TNAP antibody was diluted 1:200 in FBS/PBS, with HRP-conjugated Goat anti-Rat secondary antibodies (1:100) used to detect TNAP antibody binding. Incubation of tissues sections with DAB for 15 s allowed visualisation of antibody binding and TNAP localisation. Rat IgG control

experiments were similarly carried out to ensure there was no non-specific binding of the secondary antibodies.

5.4.5. Micro computed topography

The right tibiae from experimental mice was dissected immediately upon death, freed from any surrounding soft tissues and stored in dH_2O at -20°C prior to µCT scanning. MicroCT scanning and reconstruction was carried out as described in section 2.7.7. Metaphyseal trabecular bone of the proximal tibia was assessed in a 250 slice stack, 5% of the total bone length below the first appearance of a trabecular 'bridge' connecting the two primary spongiosa bone islands as described in section 2.2.7. Cortical bone was assessed in 100 slice stacks at 37% and 50% of the total bone length (proximal-middle) from the reference starting slice (first appearance of the medial tibial condyles). To assess BMD, BMD phantoms were used to calibrate the CTAn software. BMD phantoms of known calcium hydroxyapatite mineral densities of 0.25 and 0.75 g/cm3 were scanned and reconstructed using the same parameters as used for bone samples.

5.4.6. Biomechanical testing

Biomechanical testing of the right tibiae from experimental mice was carried out by three-point bending using an LXR material testing machine as described in section 2.7.8.

5.4.7. Analysis of serum calcium

Serum was prepared from the terminal blood sample of experimental mice as described in section 2.8.2. Total serum calcium was assessed by a colorimetric assay (Randox calcium assay) as described in section 2.8.2.

5.4.8. Analysis of bone turnover markers

Serum was prepared from the terminal blood sample of experimental mice as described in section 2.8.2. Serum P1NP and CTX-1 were assay by enzyme immunoassay as described in section 2.8.3.

5.5. Results

5.5.1. PTH exerts rapid effects on mineralisation gene expression *in vivo*

Gene expression within the femora of 4 week old, male WT mice was assessed after a 6 h exposure to a single subcutaneous injection of PTH (80 µg/kg). Animals exposed to PTH displayed around a 60% increase in the mRNA expression of *Phospho1* compared with vehicle treated animals ($P<0.01$, Fig. 5.1.A). *Alpl* and *Smpd3* mRNA expression were similarly increased in response to PTH treatment (29%, $P<0.01$ and 45%, $P<0.001$ respectively, Fig. 5.1.B & C). *Chkα* and *Chkβ* expression was not affected by PTH. The expression of the PP_i generating, *Enpp1*, was enhanced with PTH exposure ($P<0.05$). *Sost* expression displayed a trend towards inhibition by PTH exposure, but this did not reach statistical significance (Fig. 5.1.G). The osteoblast transcription factor, *Runx2*, showed a 50% increase in expression ($P<0.05$, Fig. 5.1.I) with PTH administration. *Trps1* was similarly increased in PTH treated femora (51%, $P<0.05$, Fig. 5.1.J).

5.5.2. The effects of 14-day iPTH exposure on mineralisation gene expression within the femora of WT and *Phospho1*$^{-/-}$ mice.

Gene expression was investigated by RT-qPCR within the distal femur of WT and *Phospho1*$^{-/-}$ mice receiving daily injection of PTH (80 µg/kg/day) or vehicle control for 14-days. In WT animals, exposure to PTH induced a 3.1-fold increase in

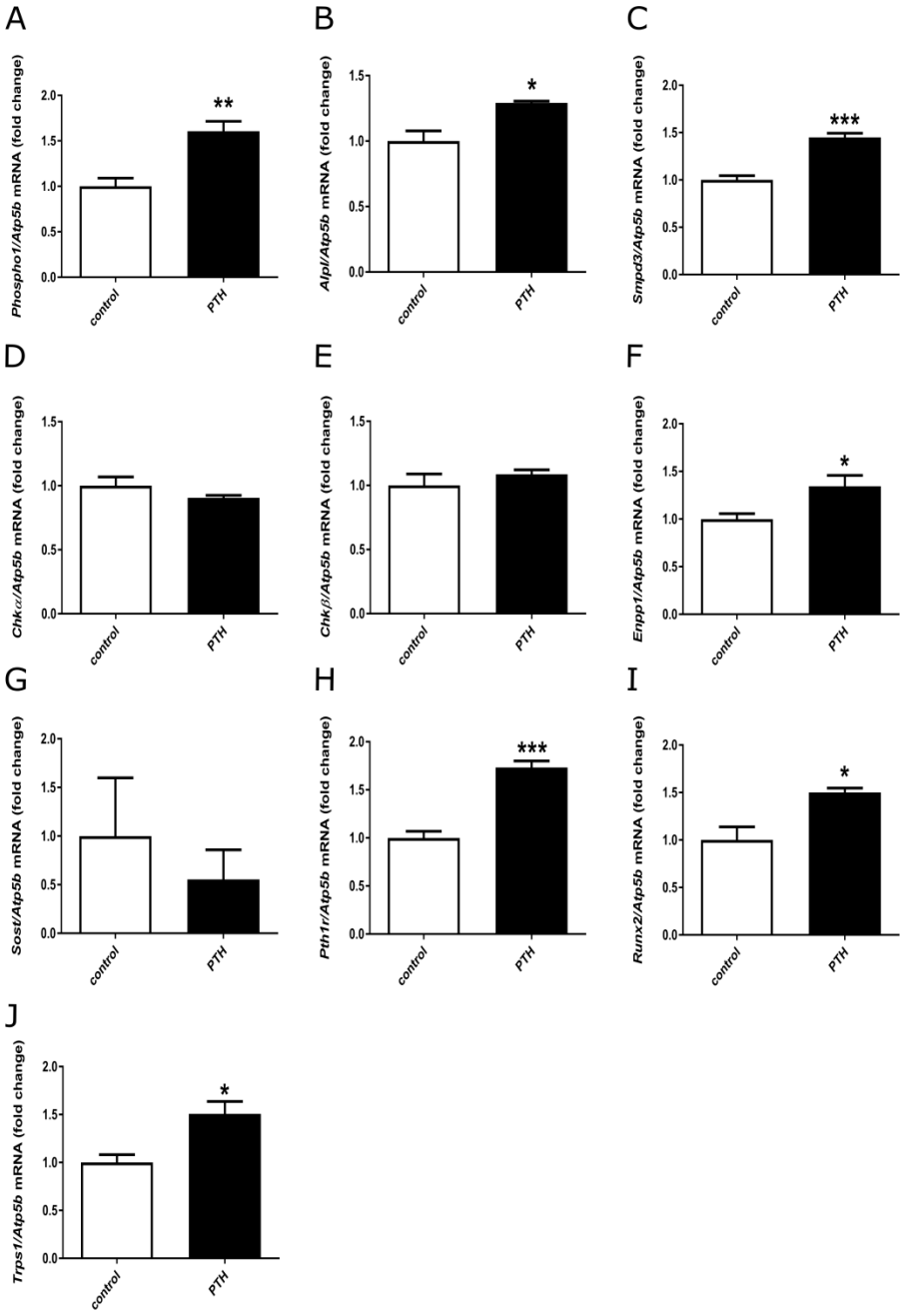

Figure 5.1. The effects of a single dose of PTH on gene expression within the femora of WT mice.

RT-qPCR analysis of the mRNA expression within the femora of WT mice, 6 h following a single dose of PTH (80 µg/kg). **(A)** *Phospho1* **(B)** *Alpl* **(C)** *Smpd3* **(D)** *Chkα* **(E)** *Chkβ* **(F)** *Enpp1* **(G)** *Sost* **(H)** *Pth1r* **(I)** *Runx2* and **(J)** *Trps1*. Data are represented as mean ± S.E.M. N=4, *P<0.05, **P<0.01, ***P<0.001 compared to control.

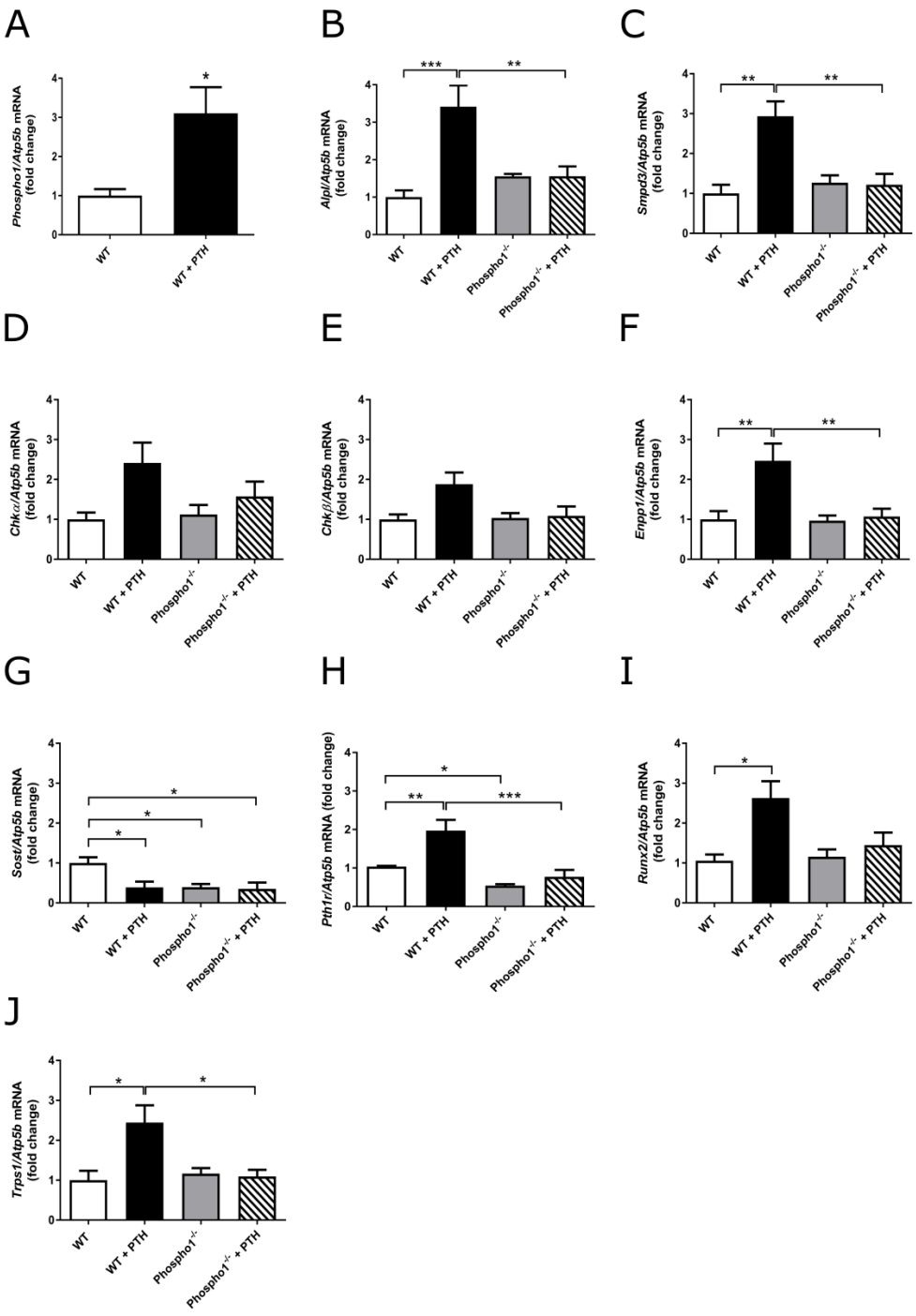

Figure 5.2. The differential effects of 14-days iPTH on gene expression within the femora of WT and *Phospho1*$^{-/-}$ mice.

RT-qPCR analysis of the mRNA expression within the distal femora of WT and *Phospho1*$^{-/-}$ mice receiving iPTH (80 µg/kg/day) for 14-days. **(A)** *Phospho1* **(B)** *Alpl* **(C)** *Smpd3* **(D)** *Chkα* **(E)** *Chkβ* **(F)** *Enpp1* **(G)** *Sost* **(H)** *Pth1r* **(I)** *Runx2* and **(J)** *Trps1*. Data are represented as mean ± S.E.M. N=4, *P<0.05, **P<0.01, ***P<0.001.

Phospho1 expression compared to vehicle treated control animals ($P<0.05$, Fig. 5.2.A). Similarly *Smpd3* and *Alpl* displayed increases in their expression in response to this experimental regimen in WT mice ($P<0.01$ and $P<0.001$ respectively compared to vehicle treated WT animals, Fig. 5.2.C & D). In contrast, *Phospho1*$^{-/-}$ mice displayed no increases in either *Smpd3* or *Alpl* compared to non-treated (control) *Phospho1*$^{-/-}$ mice. In WT animals receiving PTH, *Chka* and *Chkb* showed a 2.4 and 1.9-fold increase in expression respectively compared to control animals, although this was not significant (Fig. 5.2.D & E). As expected, WT mice receiving PTH injections exhibited a reduction in *Sost* expression compared to vehicle control counterparts ($P<0.05$). The basal expression of *Sost* mRNA in *Phospho1*$^{-/-}$ was significantly reduced compared to WT mice ($P<0.05$, Fig. 5.2.G). Despite this, *Phospho1*$^{-/-}$ mice treated with PTH showed no further decrease in *Sost*. *Pth1r* was induced with iPTH administration in WT animals ($P<0.01$ compared to vehicle control animals) but not in *Phospho1*$^{-/-}$ animals. The effects of PTH on *Runx2* and *Trps1* expression in WT mice observed in the single dose study were accentuated with 14 days intermittent treatment. *Runx2* and *Trps1* expression showed a 2.6 and 2.4-fold increase respectively ($P<0.05$, Fig. 5.2.I & J) in WT mice receiving iPTH. *Phospho1*$^{-/-}$ mice showed no change in the expression of these transcription factors in response to PTH.

5.5.3. The effects of 14-day iPTH exposure on the bone microarchitecture and biomechanical properties in WT and *Phospho1*$^{-/-}$ mice.

The effects of the 14-day iPTH exposure on bone microarchitecture within both WT and *Phospho1*$^{-/-}$ tibiae was determined by μCT scanning. Metaphyseal trabecular

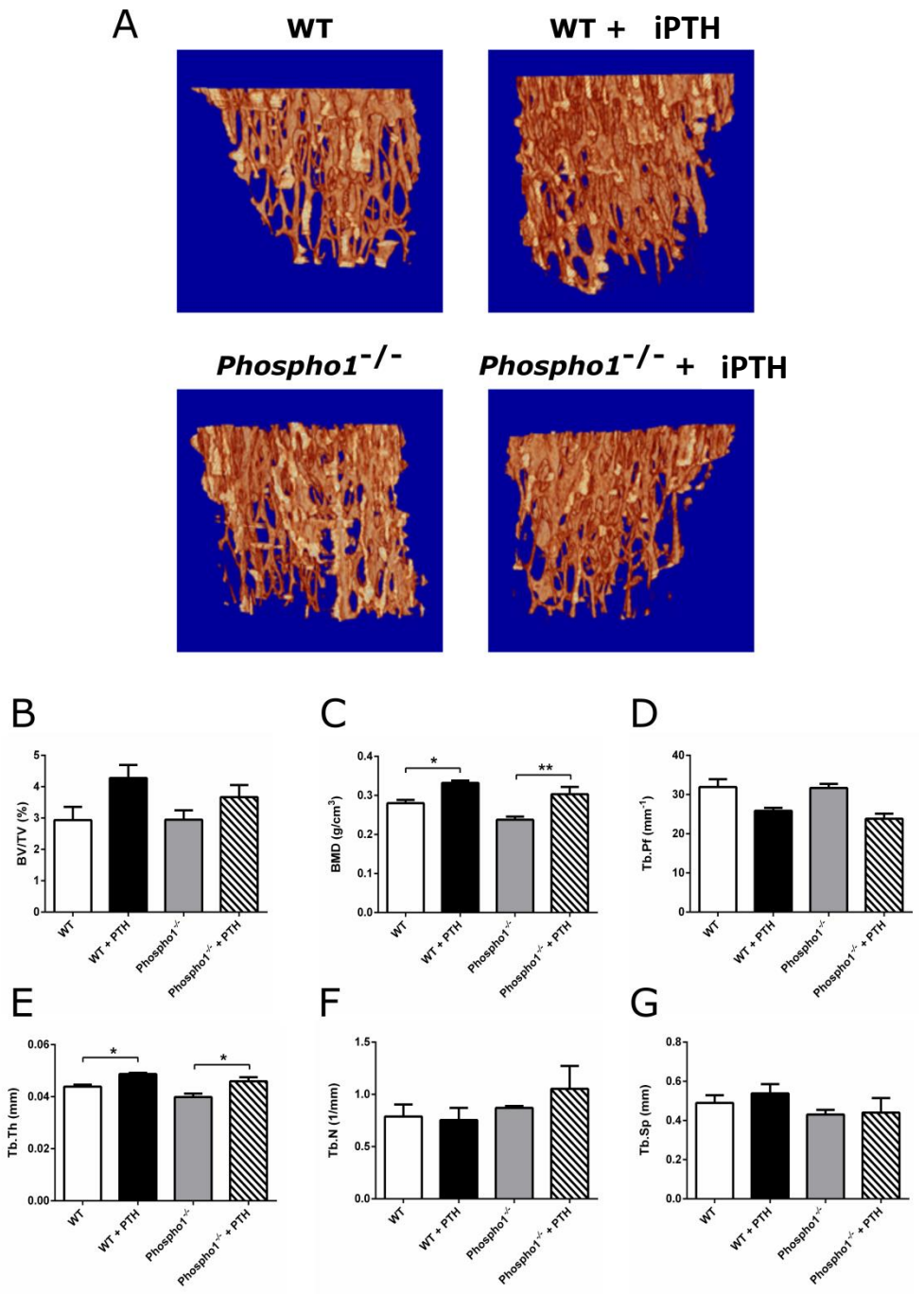

Figure 5.3. Metaphyseal trabecular bone parameters in WT and *Phospho1*$^{-/-}$ mice receiving iPTH or vehicle control for 14-days.

(A) Representative 3D µCT images of metaphyseal trabecular bone in WT and *Phospho1*$^{-/-}$ mice receiving iPTH (80 µg/kg/day) or vehicle control for 14-days. Analysis of the trabecular bone parameters **(B)** trabecular bone volume/ total volume (BV/TV) **(C)** trabecular bone mineral density (BMD) **(D)** trabecular pattern factor (Tb.Pf) **(E)** trabecular thickness (Tb.Th.) **(F)** trabecular number (Tb.N.) and **(G)** trabecular separation (Tb.Sp.). Data are represented as mean ± S.E.M. N=4, *P<0.05, **P<0.01.

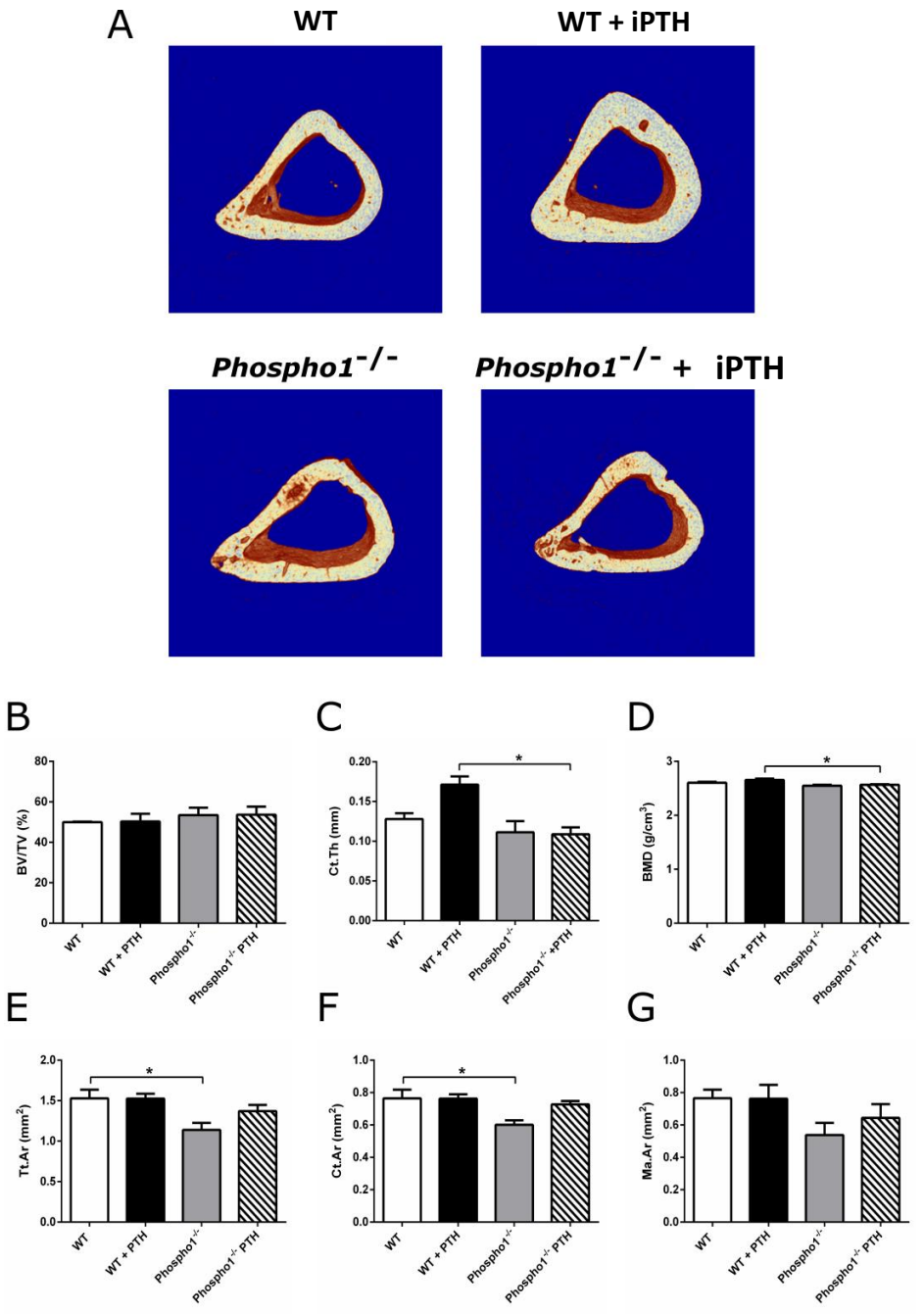

Figure 5.4. Cortical bone parameters at 37% tibial length in WT and *Phospho1*$^{-/-}$ mice receiving iPTH or vehicle control for 14-days.

(A) Representative 3D micro-CT images of tibial cortical bone at 37% tibial length (Proximal to middle) in WT and *Phospho1*$^{-/-}$ mice receiving iPTH (80 µg/kg/day) or vehicle control for 14-days. Analysis of the cortical bone parameters **(B)** cortical bone volume/ total volume (BV/TV) **(C)** cortical cross-sectional thickness (Ct.Th.) **(D)** cortical bone mineral density (BMD) **(E)** cortical tissue area (Tt.Ar.) **(F)** cortical bone area (Ct.Ar.) and **(G)** medullary area (Ma.Ar.). Data are represented as mean ± S.E.M. N≥4, *P<0.05.

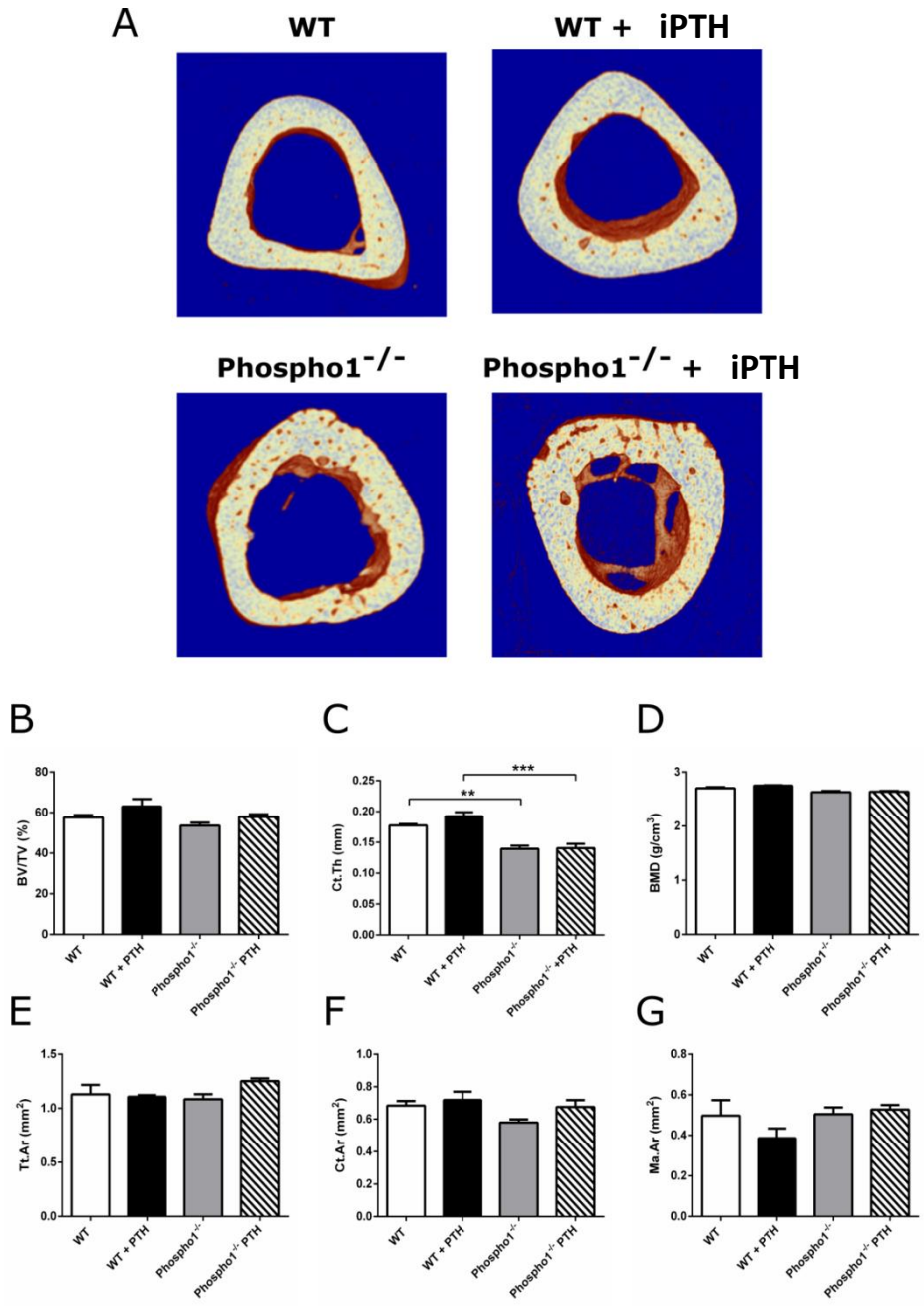

Figure 5.5. Cortical bone parameters at 50% tibial length in WT and *Phospho1*$^{-/-}$ mice receiving iPTH or vehicle control for 14-days.

(A) Representative 3D micro-CT images of tibial cortical bone at 50% tibial length in WT and *Phospho1*$^{-/-}$ mice receiving iPTH (80 µg/kg/day) or vehicle control for 14-days. Analysis of the cortical bone parameters; **(B)** cortical bone volume/ total volume (BV/TV) **(C)** cortical cross-sectional thickness (Ct.Th.) **(D)** cortical bone mineral density (BMD) **(E)** cortical tissue area (Tt.Ar.) **(F)** cortical bone area (Ct.Ar.) and **(G)** medullary area (Ma.Ar.). Data are represented as mean ± S.E.M. N≥4, **P<0.01, ***P<0.001.

bone was assessed in a 1.25 mm volume of interest beginning at 5% below the reference point as described in section 5.4.4. Modest increases in trabecular thickness and BMD were noted in response to PTH exposure in both genotypes ($P<0.05$, Fig. 5.3.). There were no further changes detected in response to PTH in the trabecular compartment. Cortical bone was assessed in 500 μm regions at 37% (proximal to middle) and 50% of the total tibia length as described in section 5.4.4. No differences at either location were observed in response to 14-days iPTH exposure in both WT and *Phospho1*$^{-/-}$ tibiae (Figs. 5.4. & 5.5.). Perhaps unsurprisingly, no differences were noted in the biomechanical properties of the tibia as assessed by 3-point bending in response to the 14-day intermittent PTH exposure (Fig. 5.6.)

5.5.4. Body weight, serum calcium and bone formation and resorption markers of WT and *Phospho1*$^{-/-}$ mice exposed to iPTH for 28-days.

PTH injections were well tolerated and there were no adverse effects during the experiment. Assessment of the body weights during the experiment revealed no differences between control mice and mice receiving iPTH. There was however a trend towards increased weight in WT mice receiving iPTH compared to control mice, although this was not significant (Fig. 5.7.A). There were no differences in serum calcium between genotypes or treatments as assessed by colorimetric assay (Fig. 5.7.B). Serum P1NP appeared increased in response to iPTH exposure in both genotypes but this was not significant (Fig. 5.7.C). The serum concentration of CTX-1 was not affected by iPTH in either genotype (Fig. 5.7.D).

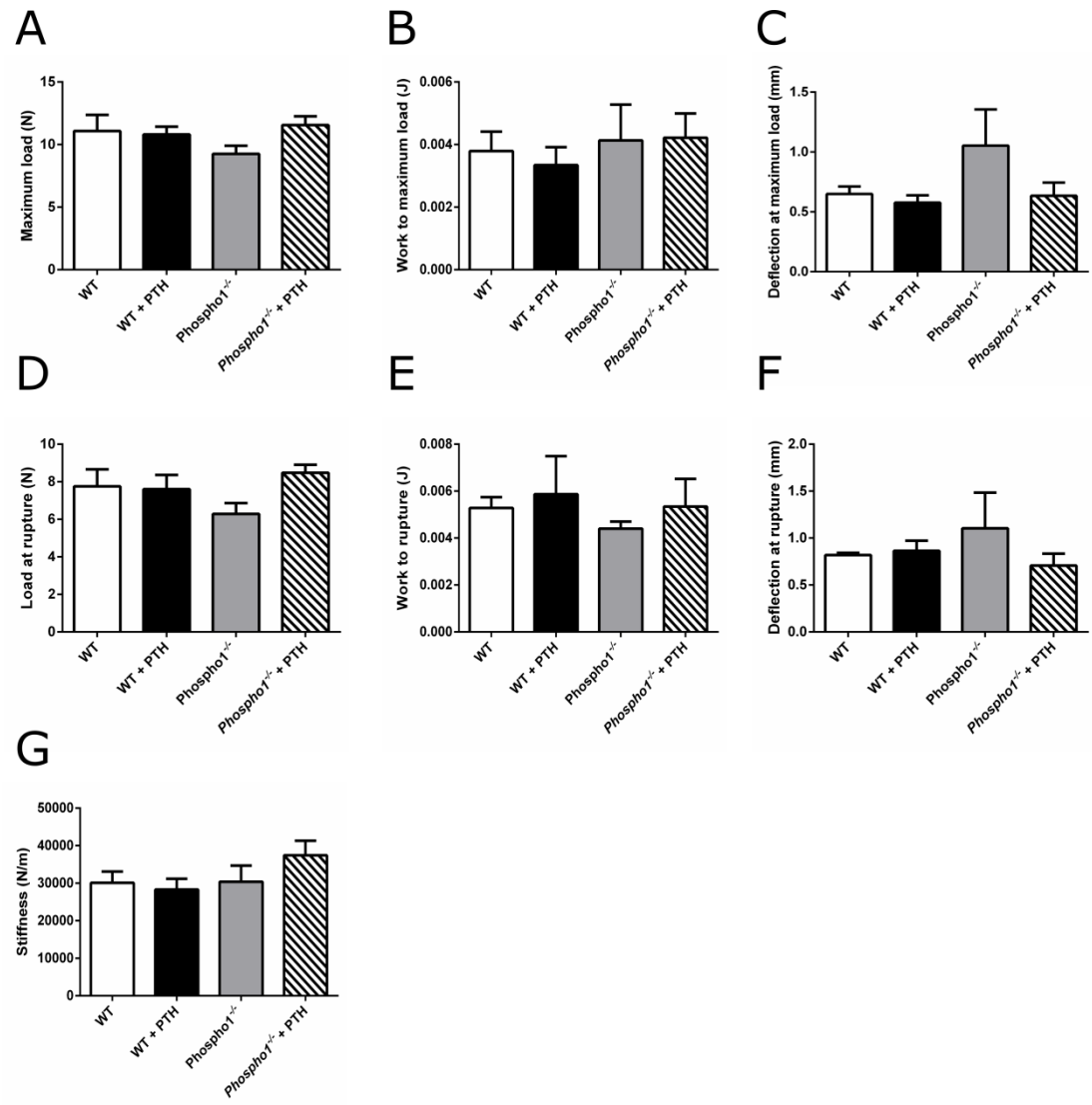

Figure 5.6. Three-point bending analysis of the tibia from WT and *Phospho1*$^{-/-}$ mice receiving iPTH or vehicle control for 14-days.

Analysis of the biomechanical parameters **(A)** maximum load **(B)** work to maximum load **(C)** deflection at maximum load **(D)** load at rupture **(E)** work to rupture **(F)** deflection at rupture and **(G)** stiffness in the tibiae of WT and *Phospho1*$^{-/-}$ mice receiving iPTH (80 µg/kg/day) or vehicle control for 14-days. Data are represented as mean ± S.E.M. N=4.

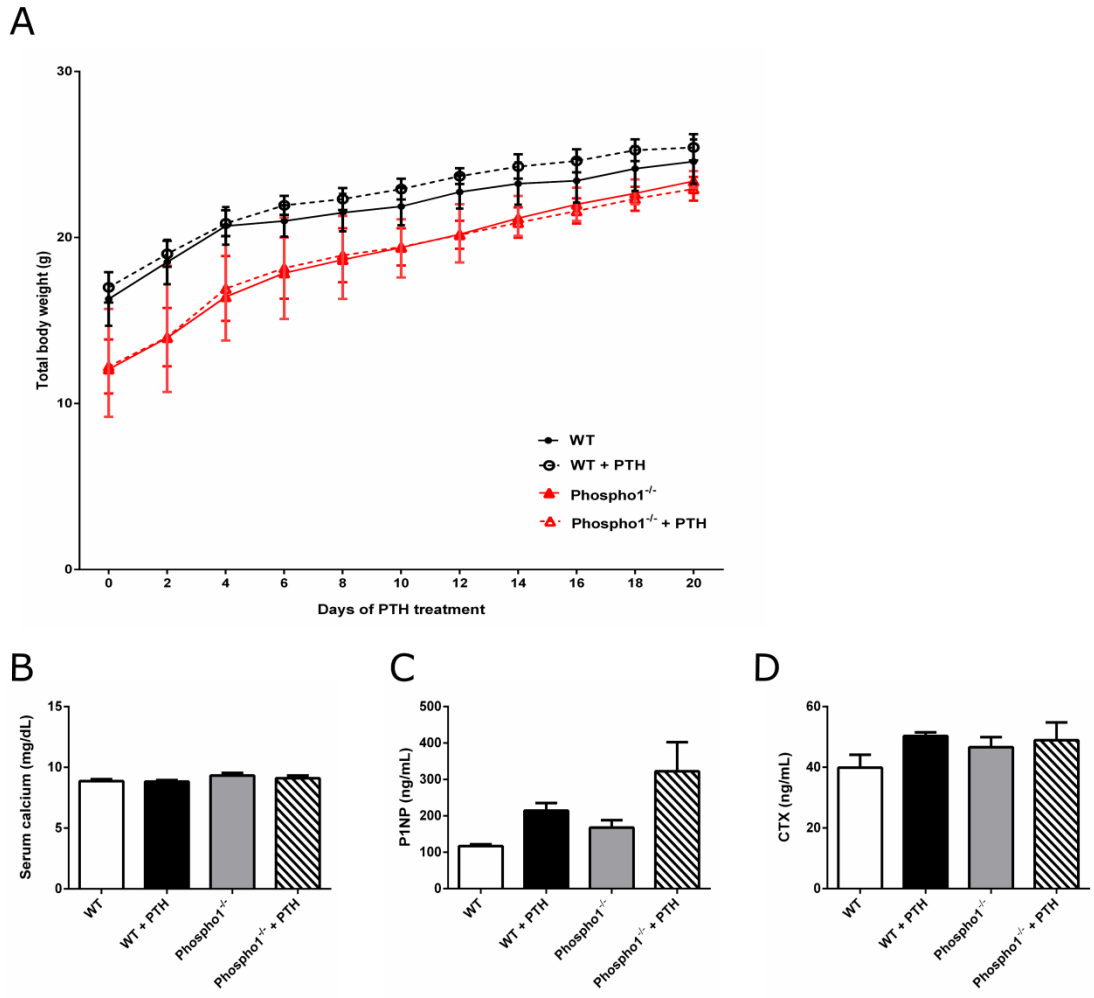

Figure 5.7. Body weight, serum calcium and bone formation and resorption markers of WT and *Phospho1*$^{-/-}$ mice exposed to iPTH for 28-days.

(A) Body weights (up to day 20) of WT and *Phospho1*$^{-/-}$ mice receiving iPTH or vehicle control. **(B)** Total calcium, **(C)** P1NP and **(D)** CTX-1 were assessed in the serum obtained from the terminal blood sample of WT and *Phospho1*$^{-/-}$ mice receiving iPTH or vehicle control for 28-days. Data are represented as mean ± S.E.M. (N>5).

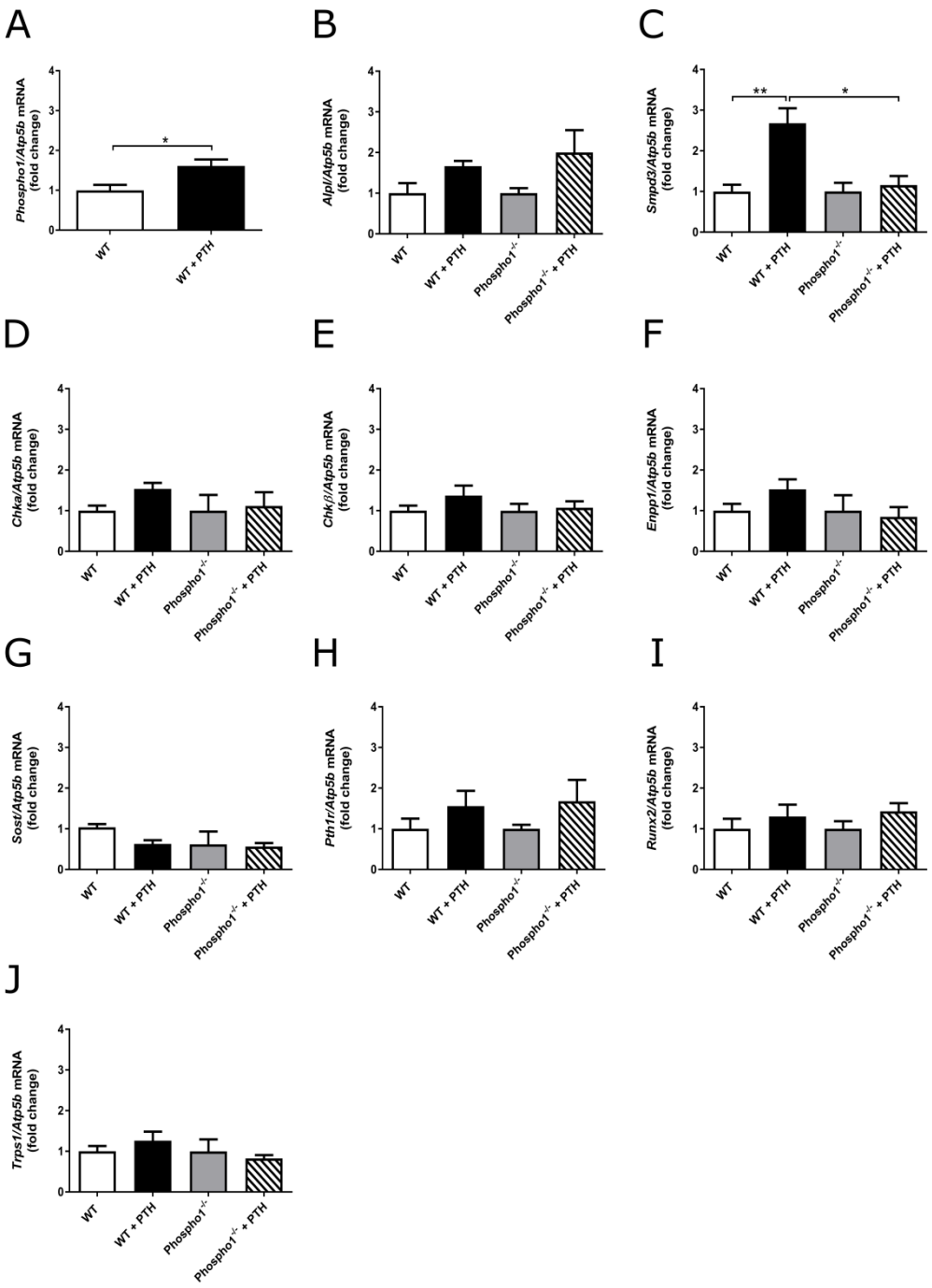

Figure 5.8. The differential effects of 28-days iPTH on gene expression within the femora of WT and *Phospho1*$^{-/-}$ mice.

RT-qPCR analysis of the mRNA expression within the distal femora of WT and *Phospho1*$^{-/-}$ mice receiving iPTH (80 µg/kg/day) for 28-days. **(A)** *Phospho1* **(B)** *Alpl* **(C)** *Smpd3* **(D)** *Chkα* **(E)** *Chkβ* **(F)** *Enpp1* **(G)** *Sost* **(H)** *Pth1r* **(I)** *Runx2* and **(J)** *Trps1*. Data are represented as mean ± S.E.M. N=4, *P<0.05, **P<0.01.

5.5.5. The effects of 28-day iPTH exposure on mineralisation gene expression within the femora of WT and *Phospho1*$^{-/-}$ mice.

With 28-day iPTH, *Phospho1* mRNA expression remained enhanced in the distal femur compared to vehicle control treated animals (P<0.05, Fig.5.8.A). *Smpd3* expression was similarly enhanced in response to iPTH in WT mice but this was not observed in *Phospho1*$^{-/-}$ treated mice (P<0.01, Fig.5.8.C). There was no significant enhancement of *Alpl Chkα, Chkβ* or *Enpp1* mRNA expression in either genotype in response to 28-day iPTH. *Sost* expression was marginally down-regulated by 28-day iPTH exposure in WT femora (although this was found not to be statistically significant). The transcription factors, *Trps1* and *Runx2* no longer exhibited any enhancement in response to 28-day iPTH exposure in WT or indeed, in *Phospho1*$^{-/-}$ femora.

5.5.6. The effects of 28-day iPTH exposure on the bone microarchitecture and biomechanical properties in WT and *Phospho1*$^{-/-}$ mice.

Assessment of the trabecular compartment in 28-day intermittent PTH exposed WT and *Phospho1*$^{-/-}$ mouse tibiae, revealed increased trabecular thickness (P<0.05) and BMD (P<.0.01, Fig. 5.9.). These parameters were likewise enhanced in WT mice treated with PTH compared to PTH treated *Phospho1*$^{-/-}$ mice (P<.0.01 in both cases). The percentage bone volume (BV/TV) was enhanced in PTH treated WT mice (P<0.01 compared to WT control), but not in *Phospho1*$^{-/-}$ animals. Trabecular pattern factor (Tb.Pf, a measurement of trabecular connectivity (Hahn et al., 1992)) was reduced in response to 28-day iPTH exposure in both genotypes (P<0.05, Fig. 5.9.D).

With 28 daily injections of PTH, the anabolic response in cortical parameters was now evident in WT mice. Cortical BV/TV was increased in both 37% and 50%

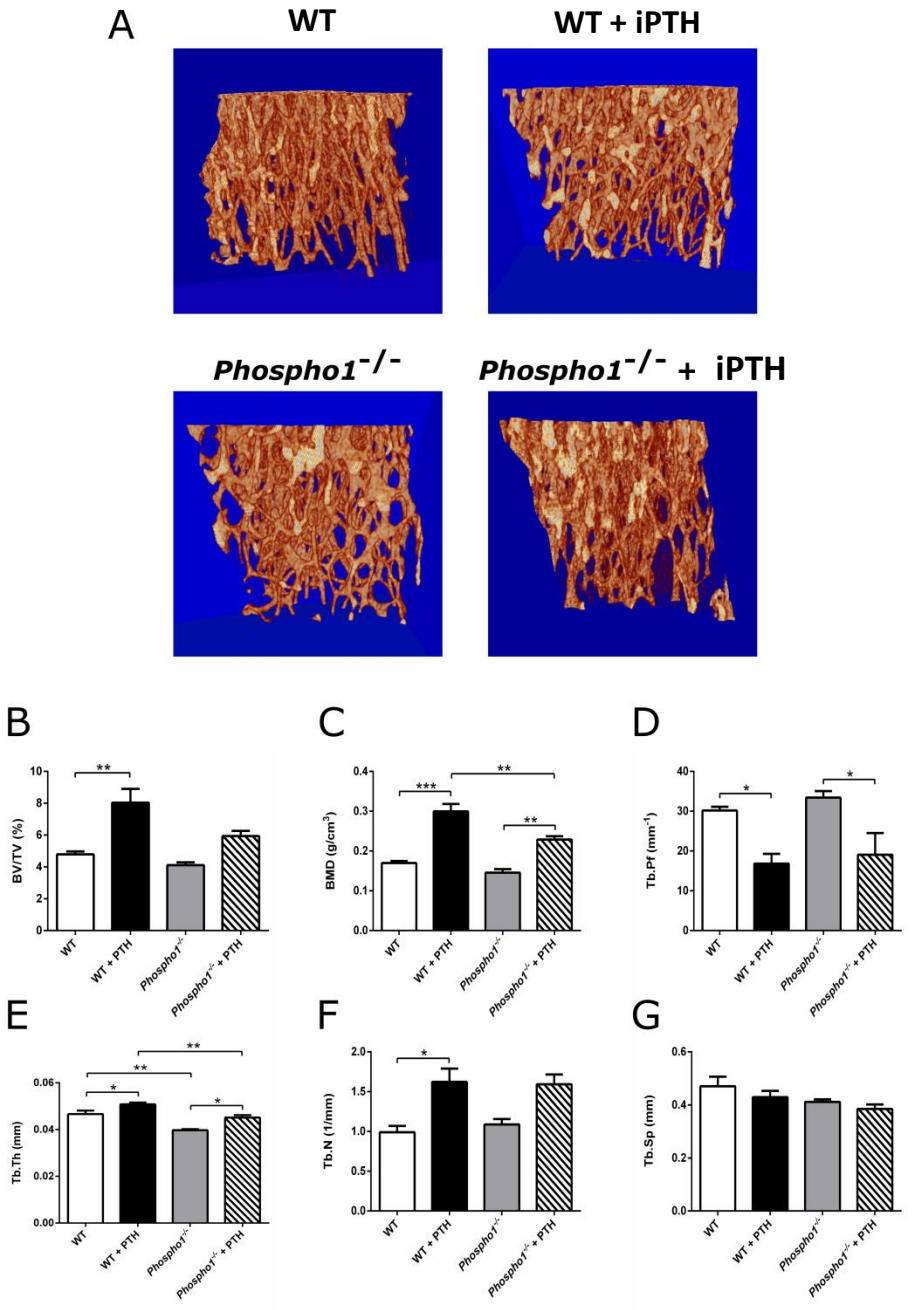

Figure 5.9. Metaphyseal trabecular bone parameters in WT and *Phospho1*$^{-/-}$ mice receiving iPTH or vehicle control for 28-days.

(A) Representative 3D µCT images of metaphyseal trabecular bone in WT and *Phospho1*$^{-/-}$ mice receiving iPTH (80µg/kg/day) or vehicle control for 28-days. Analysis of the trabecular bone parameters **(B)** trabecular bone volume/ total volume (BV/TV) **(C)** trabecular bone mineral density (BMD) **(D)** trabecular pattern factor (Tb.Pf) **(E)** trabecular thickness (Tb.Th.) **(F)** trabecular number (Tb.N.) and **(G)** trabecular separation (Tb.Sp.). Data are represented as mean ± S.E.M. N>4, *P<0.05, **P<0.01, ***P<0.001.

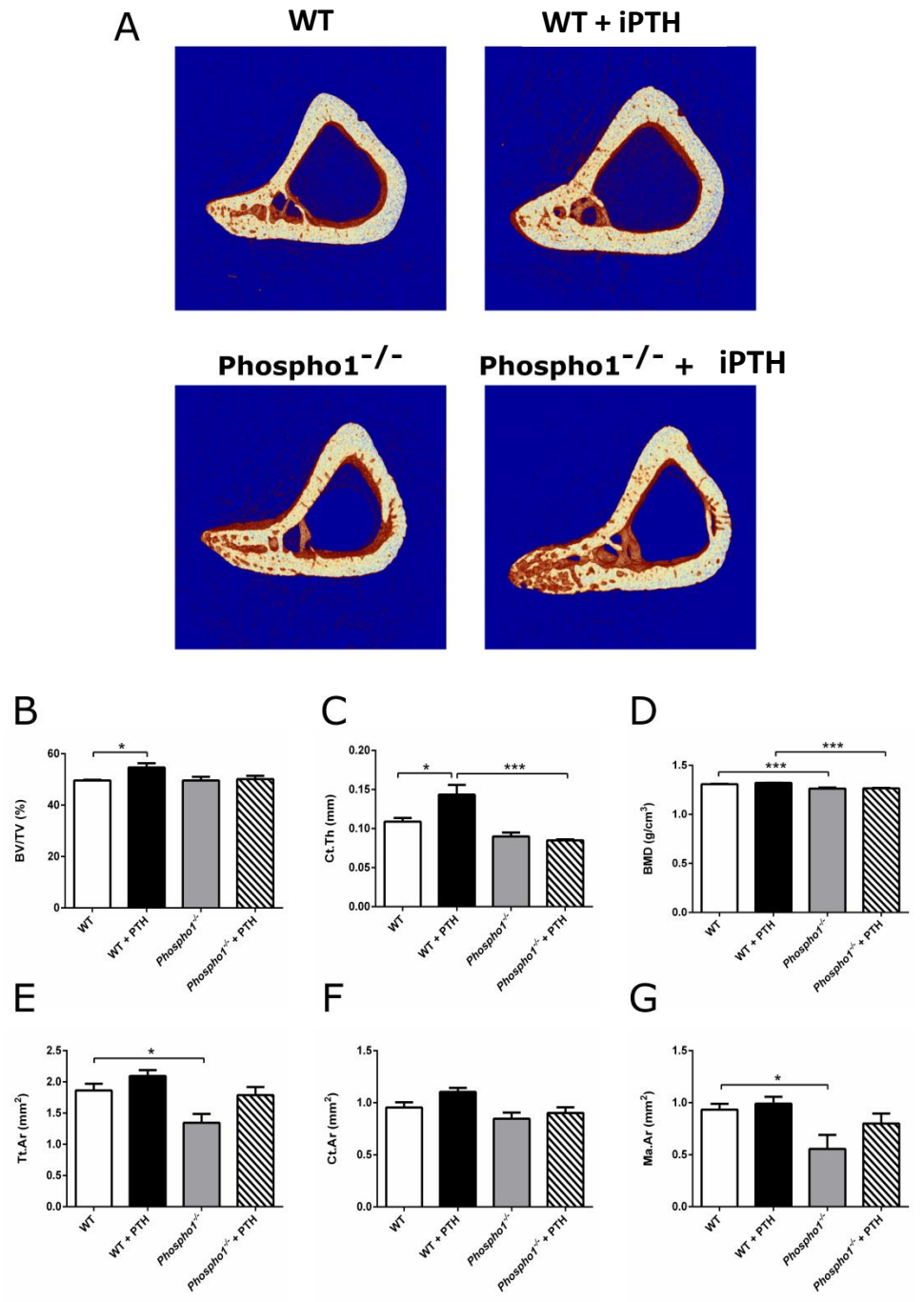

Figure 5.10. Cortical bone parameters at 37% tibial length in WT and *Phospho1*$^{-/-}$ mice receiving iPTH or vehicle control for 28-days.

(A) Representative 3D micro-CT images of tibial cortical bone at 37% tibial length (Proximal to middle) in WT and *Phospho1*$^{-/-}$ mice receiving iPTH (80 µg/kg/day) or vehicle control for 28-days. Analysis of the cortical bone parameters **(B)** cortical bone volume/ total volume (BV/TV) **(C)** cortical cross-sectional thickness (Ct.Th.) **(D)** cortical bone mineral density (BMD) **(E)** cortical tissue area (Tt.Ar.) **(F)** cortical bone area (Ct.Ar.) and **(G)** medullary area (Ma.Ar.). Data are represented as mean ± S.E.M. N≥4, *P<0.05, ***P<0.001.

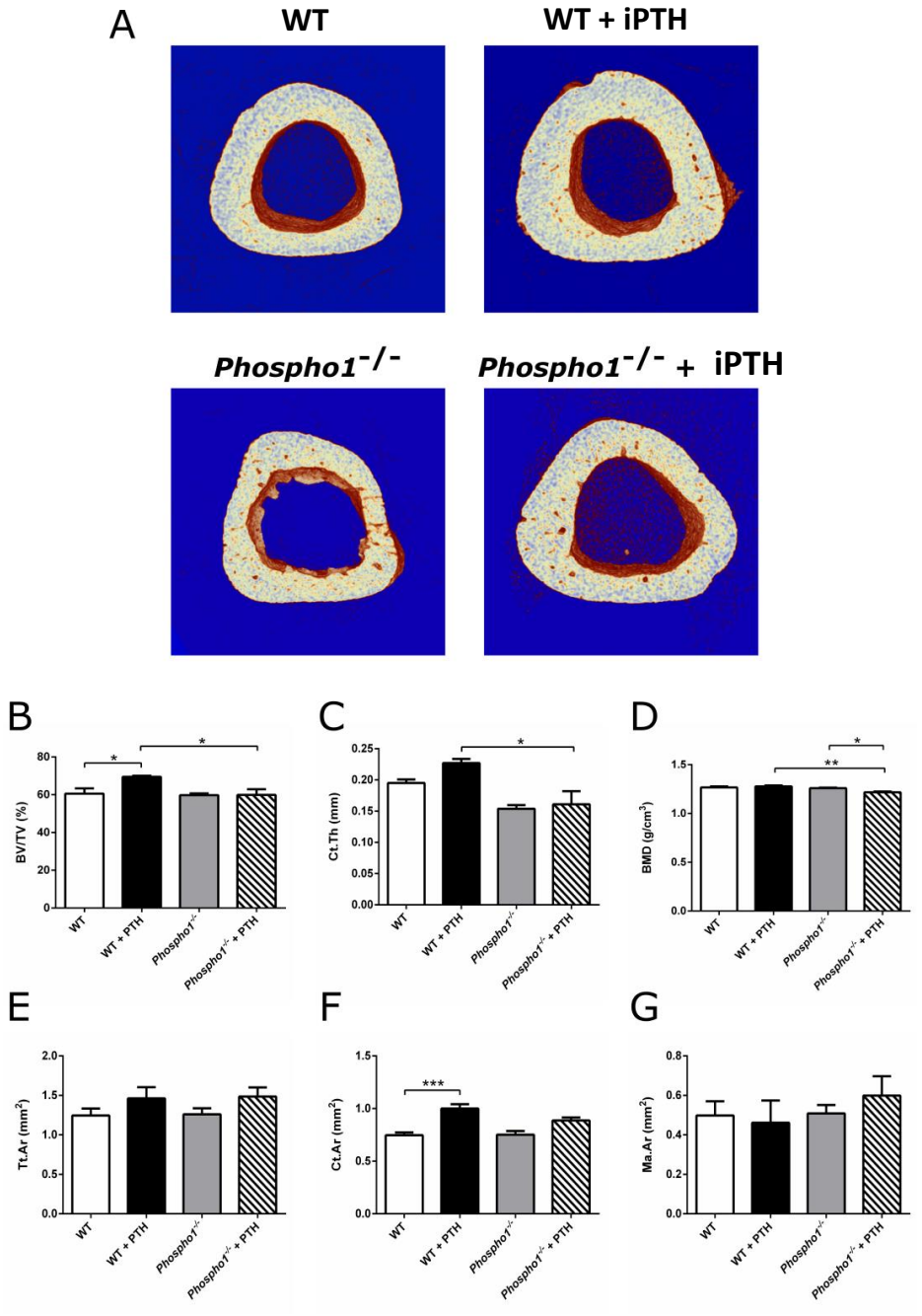

Figure 5.11. Cortical bone parameters at 50% tibial length in WT and *Phospho1*$^{-/-}$ mice receiving iPTH or vehicle control for 28-days.

(A) Representative 3D micro-CT images of tibial cortical bone at 50% tibial length in WT and *Phospho1*$^{-/-}$ mice receiving iPTH (80 µg/kg/day) or vehicle control for 28-days. Analysis of the cortical bone parameters, **(B)** cortical bone volume/ total volume (BV/TV) **(C)** cortical cross-sectional thickness (Ct.Th.) **(D)** cortical bone mineral density (BMD) **(E)** cortical tissue area (Tt.Ar.) **(F)** cortical bone area (Ct.Ar.) and **(G)** medullary area (Ma.Ar.). Data are represented as mean ± S.E.M. N≥4, *P<0.05, **P<0.01, ***P<0.001.

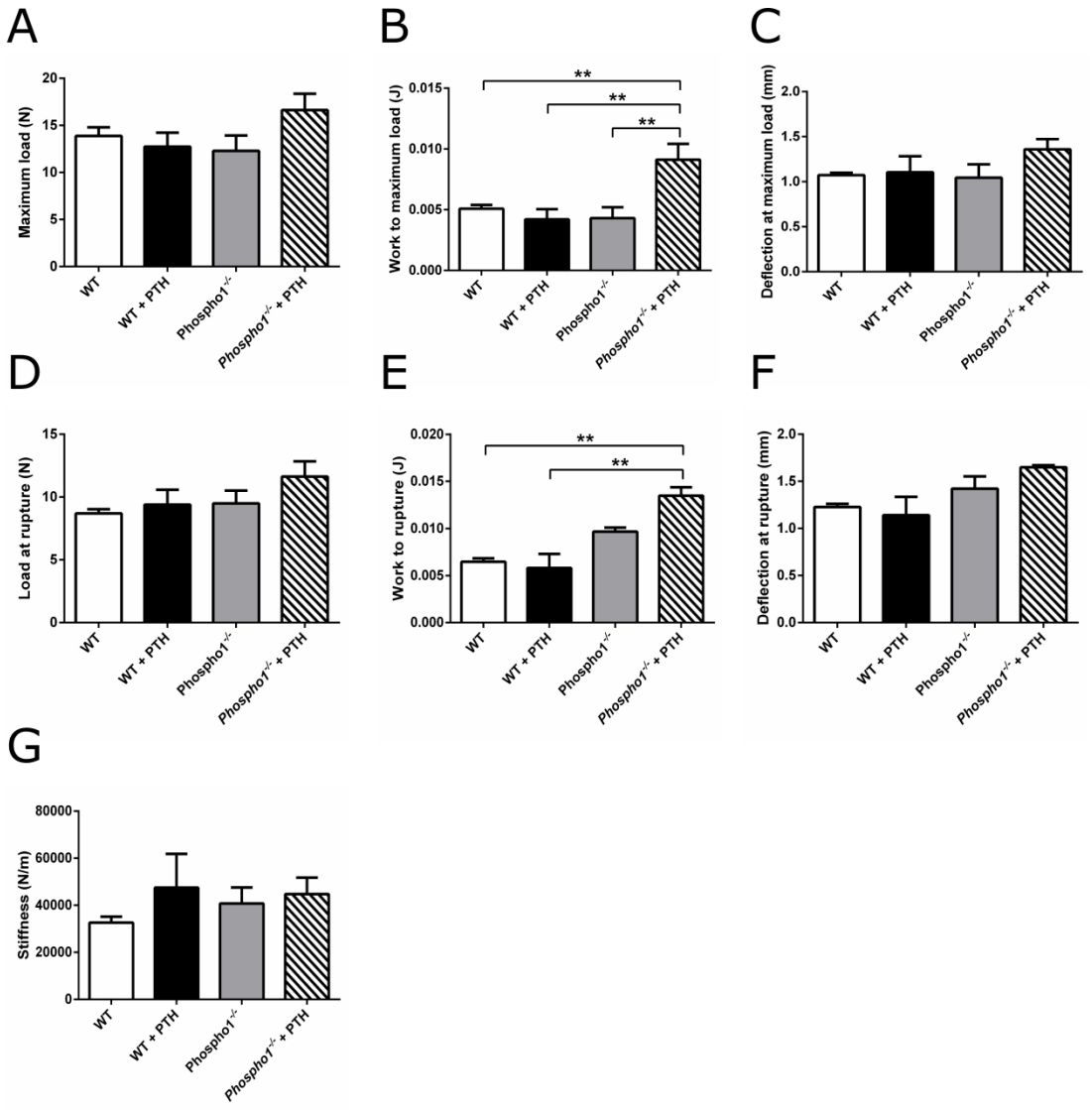

Figure 5.12. Three-point bending analysis of the tibia from WT and *Phospho1*$^{-/-}$ mice receiving iPTH or vehicle control for 28-days.

Analysis of the biomechanical parameters **(A)** maximum load **(B)** work to maximum load **(C)** deflection at maximum load **(D)** load at rupture **(E)** work to rupture **(F)** deflection at rupture and **(G)** stiffness in the tibiae of WT and *Phospho1*$^{-/-}$ mice receiving iPTH (80 µg/kg/day) or vehicle control for 28-days. Data are represented as mean ± S.E.M. N=4, **P<0.01.

compartments in PTH treated WT mice ($P<0.05$, Figs. 5.10. & 5.11. respectively). This was not observed in *Phospho1*$^{-/-}$ animals. In WT mice exposed to iPTH, cortical thickness and BMD were significantly greater than *Phospho1*$^{-/-}$ treated animals ($P<0.01$). No differences were observed in cortical bone area, medullary area or total cortical area in response to iPTH in either genoptype at either site (Figs. 5.10. & 5.11.). Biomechanical testing did not reveal any obvious effects of 28-day iPTH on the strength of the tibia from WT or *Phospho1*$^{-/-}$ mice (Fig. 5.12).

5.5.7. TNAP immunohistochemistry within the tibiae of WT and *Phospho1*$^{-/-}$ mice exposed to iPTH for 28-days.

TNAP was localised within the hypertrophic chondrocyte zone and bone forming surfaces of trabeculae. Additionally, TNAP staining was observed in the osteoblasts residing on the endosteum and periosteum. In iPTH treated WT tibiae, there appeared to be more TNAP staining in the trabecular region compared to vehicle treated WT tibiae (Fig. 5.13.A). Furthermore, there appeared to be a larger zone of TNAP immunoreactivity within the growth plate of iPTH treated WT mice compared to vehicle treated WT tibiae. Similar observations were noted in *Phospho1*$^{-/-}$ mice receiving iPTH. TNAP staining of cortical bone did not appear to be affected by iPTH treatment in either genotype (Fig. 5.13.B).

5.5.8. The effects of 28-day cPTH exposure on mineralisation gene expression within the femora of WT and *Phospho1*$^{-/-}$ mice.

The continuous exposure of WT and *Phospho1*$^{-/-}$ mice to PTH had profoundly contrasting effects on mineralisation gene expression compared to the iPTH exposure. *Phospho1* mRNA expression was not changed in the distal femur in response to this exposure regime in WT mice (Fig. 5.14.A). The expression of both *Alpl* and *Smpd3*

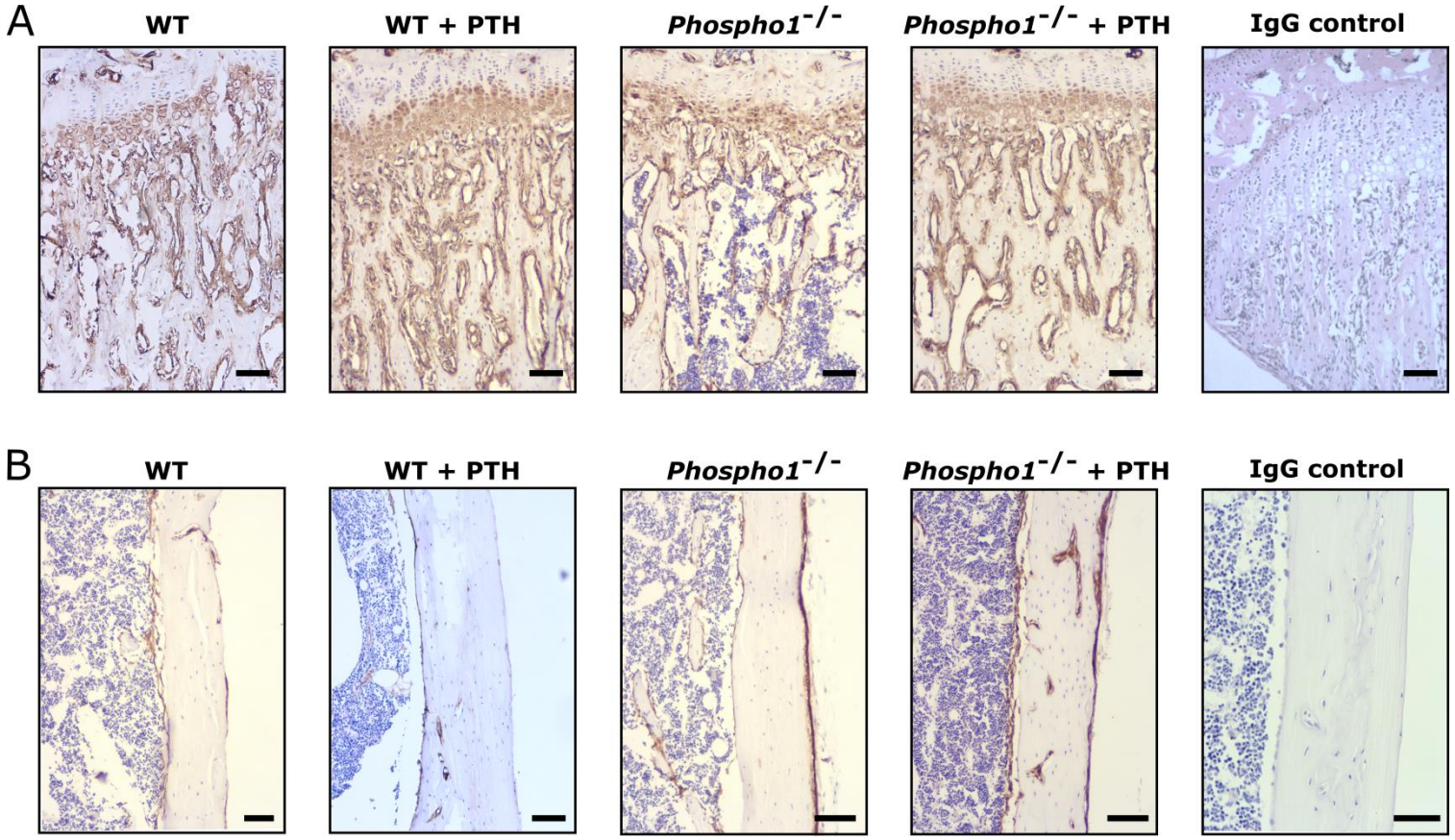

Figure 5.13. Localisation of TNAP by immunohistochemistry

Representative images of TNAP Localisation on **(A)** trabecular and **(B)** cortical bone surfaces. Images acquired at x10 magnification. Black bars equal to 50µm.

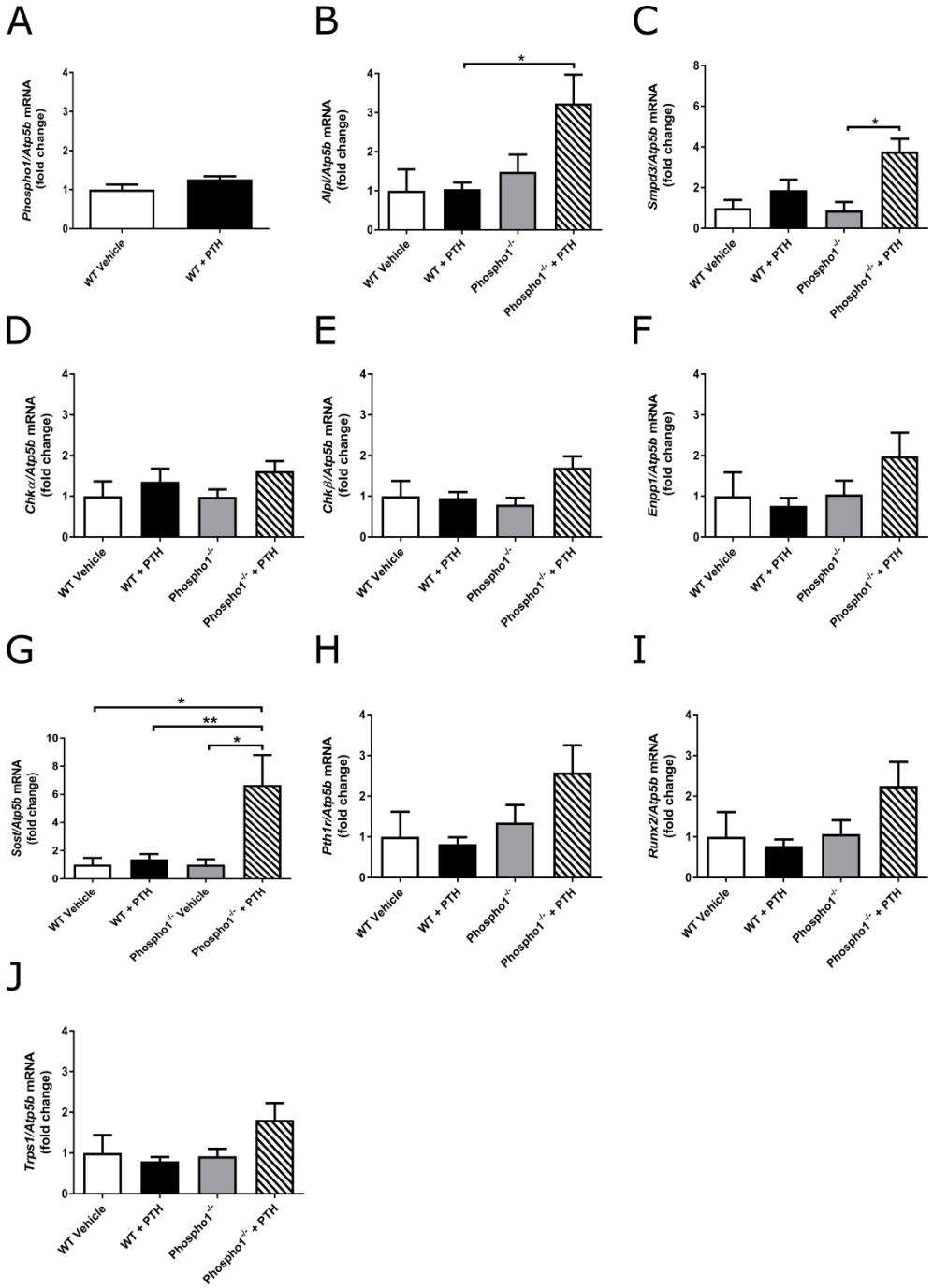

Figure 5.14. The effects of 28-day continuous PTH on gene expression within the femora of WT and *Phospho1*$^{-/-}$ mice.

RT-qPCR analysis of the mRNA expression within the distal femora of WT and *Phospho1*$^{-/-}$ mice receiving continuous PTH for 28-days. **(A)** *Phospho1* **(B)** *Alpl* **(C)** *Smpd3* **(D)** *Chkα* **(E)** *Chkβ* **(F)** *Enpp1* **(G)** *Sost* **(H)** *Pth1r* **(I)** *Runx2* and **(J)** *Trps1*. Data are represented as mean ± S.E.M. N>5, *P<0.05, **P<0.01.

was significantly upregulated in *Phospho1*$^{-/-}$ mice but not in WT mice exposed to cPTH ($P<0.05$ Fig. 5.14.B & C). The continuous exposure to PTH did not affect the expression of *Chkα*, *Chkβ*, *Enpp1*, *Pth1r*, *Runx2* or *Trps1* in the distal femora of either genotype of mice. Surprisingly, *Sost* expression in WT femora was not affected by continuous PTH exposure. However, in *Phospho1*$^{-/-}$ mice continuously exposed to PTH, *Sost* expression within the distal femora was markedly enhanced ($P<0.01$, Fig. 5.14.G).

5.5.9. The effects of 28-day cPTH exposure on the bone microarchitecture and biomechanical properties in WT and *Phospho1*$^{-/-}$ mice.

Male WT and *Phospho1*$^{-/-}$ mice exposed to 28-day cPTH displayed no changes in trabecular or cortical bone architecture within the tibia compared to vehicle treated control animals (Figs. 5.15., 5.16. & 5.17.). Not unsurprisingly, there were no differences observed in the biomechanical properties of the tibia in either genotype in response to this PTH exposure (Fig. 5.18.).

5.5.10. Understanding the expression of components of systemic phosphate regulation within the bone and kidney.

In an attempt to further investigate the potential mechanism regulating the altered response to iPTH in *Phospho1*$^{-/-}$ mice, the expression of known regulators of systemic phosphate homeostasis were assessed within the bone and kidney (i.e. the primary target organs of PTH). Within the kidney, the expression of *Pth1r* in *Phospho1*$^{-/-}$ mice was around 46% of that seen in WT kidneys ($P<0.01$, Fig. 5.19.A). The well-established upregulation of *Cyp27b1* (25-hydroxyvitamin D_3 1α-hydroxylase) in response to PTH exposure was not observed in this 14-day intermittent model. Despite

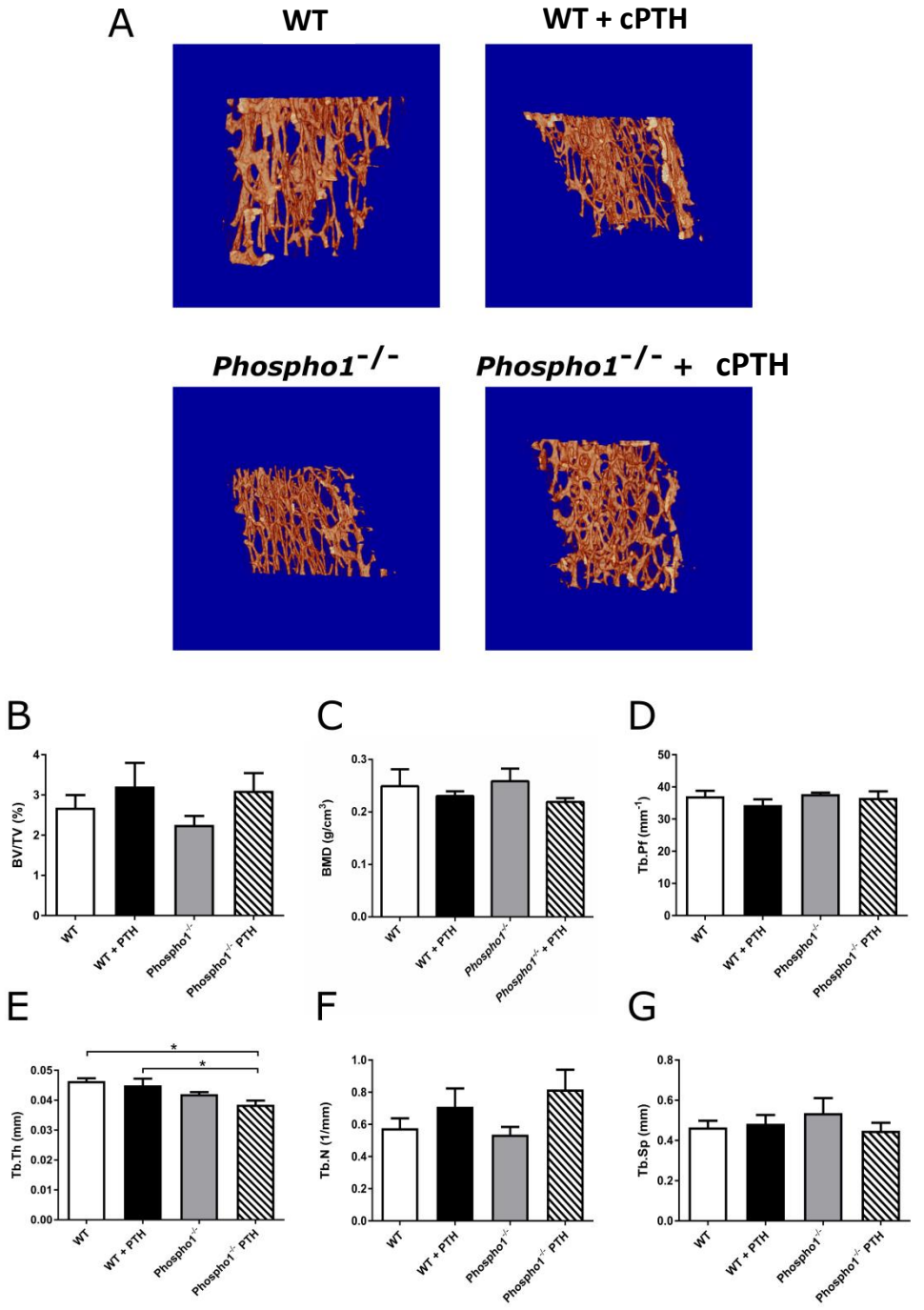

Figure 5.15. Metaphyseal trabecular bone parameters in WT and *Phospho1*$^{-/-}$ mice receiving continuous PTH or vehicle control for 28-days.

(A) Representative 3D µCT images of metaphyseal trabecular bone in WT and *Phospho1*$^{-/-}$ mice receiving continuous PTH or vehicle control for 28-days. Analysis of the trabecular bone parameters **(B)** trabecular bone volume/ total volume (BV/TV) **(C)** trabecular bone mineral density (BMD) **(D)** trabecular pattern factor (Tb.Pf) **(E)** trabecular thickness (Tb.Th.) **(F)** trabecular number (Tb.N.) and **(G)** trabecular separation (Tb.Sp.). Data are represented as mean ± S.E.M. N>5, *P<0.05.

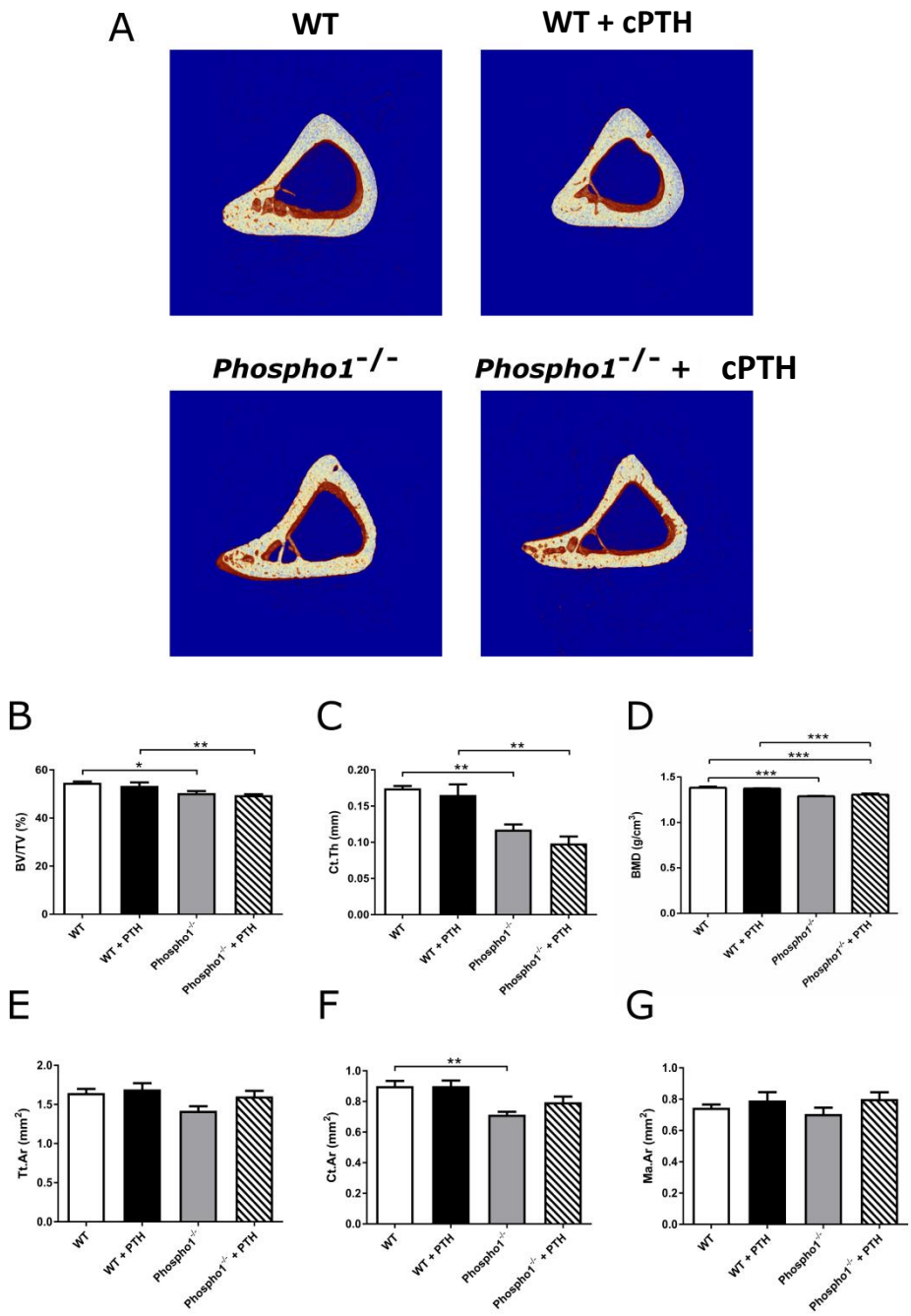

Figure 5.16. Cortical bone parameters at 37% tibial length in WT and *Phospho1*$^{-/-}$ mice receiving continuous PTH or vehicle control for 28-days.

(A) Representative 3D micro-CT images of tibial cortical bone at 37% tibial length (Proximal to middle) in WT and *Phospho1*$^{-/-}$ mice receiving continuous PTH or vehicle control for 28-days. Analysis of the cortical bone parameters **(B)** cortical bone volume/ total volume (BV/TV) **(C)** cortical cross-sectional thickness (Ct.Th.) **(D)** cortical bone mineral density (BMD) **(E)** cortical tissue area (Tt.Ar.) **(F)** cortical bone area (Ct.Ar.) and **(G)** medullary area (Ma.Ar.). Data are represented as mean ± S.E.M. N>5, *P<0.05, **P<0.01.

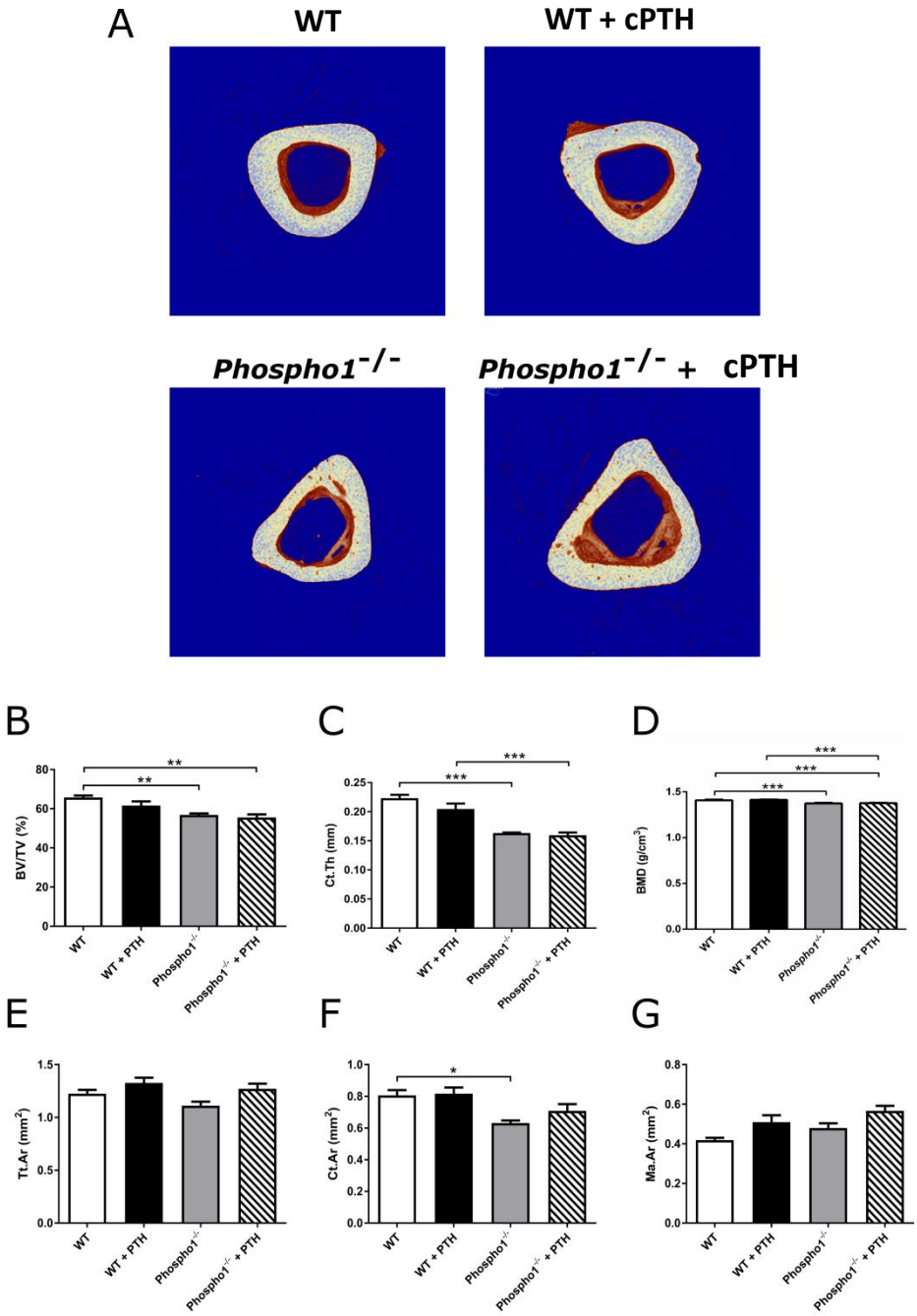

Figure 5.17. Cortical bone parameters at 50% tibial length in WT and *Phospho1*$^{-/-}$ mice receiving continuous PTH or vehicle control for 28-days.

(A) Representative 3D micro-CT images of tibial cortical bone at 50% tibial length in WT and *Phospho1*$^{-/-}$ mice receiving continuous PTH or vehicle control for 28-days. Analysis of the cortical bone parameters **(B)** cortical bone volume/ total volume (BV/TV) **(C)** cortical cross-sectional thickness (Ct.Th.) **(D)** cortical bone mineral density (BMD) **(E)** cortical tissue area (Tt.Ar.) **(F)** cortical bone area (Ct.Ar.) and **(G)** medullary area (Ma.Ar.). Data are represented as mean ± S.E.M. N>5, *P<0.05, **P<0.01, ***P<0.001.

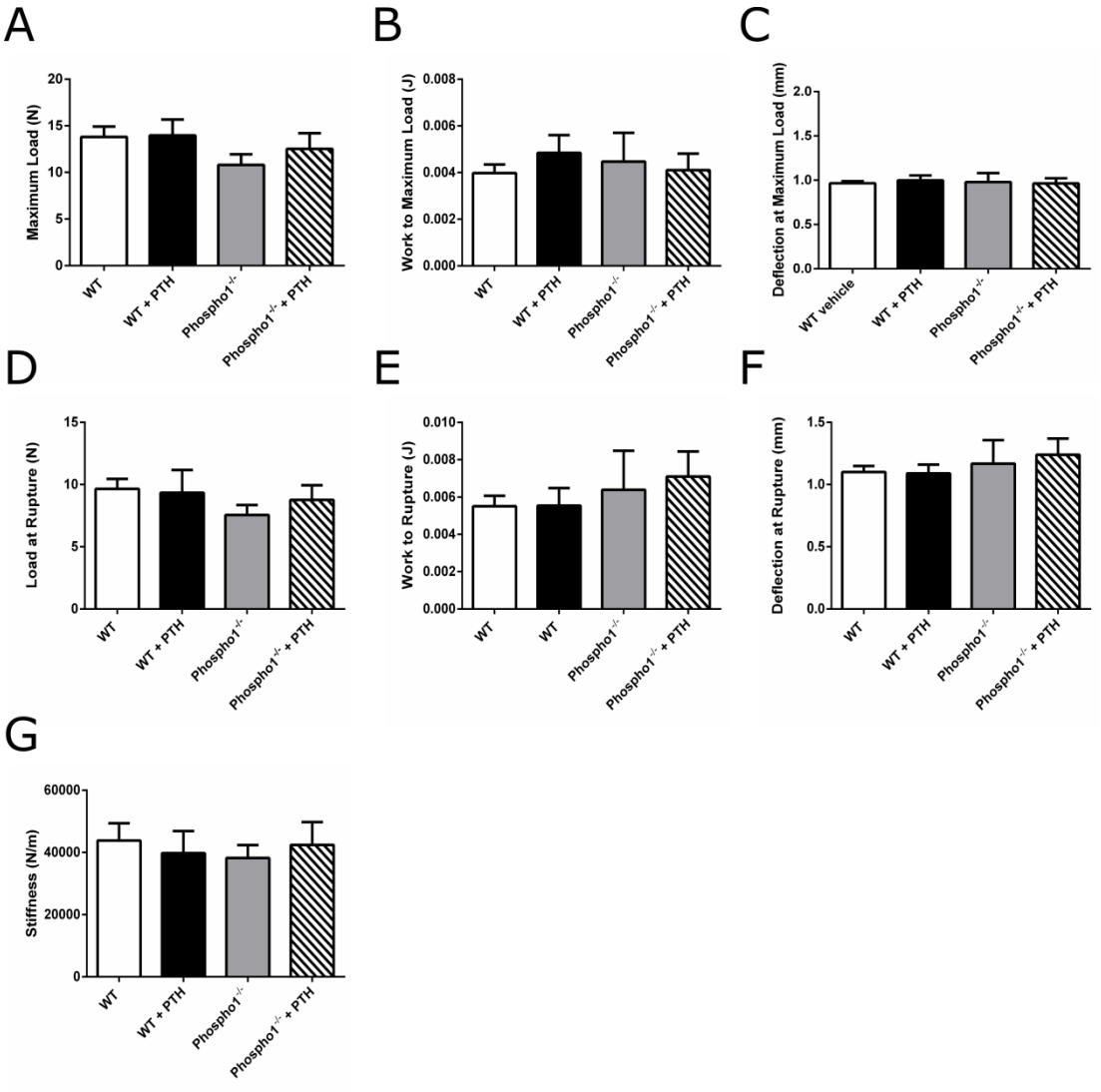

Figure 5.18. Three-point bending analysis of the tibia from WT and *Phospho1*$^{-/-}$ mice receiving cPTH or vehicle control for 28-days.

Analysis of the biomechanical parameters **(A)** maximum load **(B)** work to maximum load **(C)** deflection at maximum load **(D)** load at rupture **(E)** work to rupture **(F)** deflection at rupture and **(G)** stiffness in the tibiae of WT and *Phospho1*$^{-/-}$ mice receiving cPTH or vehicle control for 28-days. Data are represented as mean ± S.E.M. N>5.

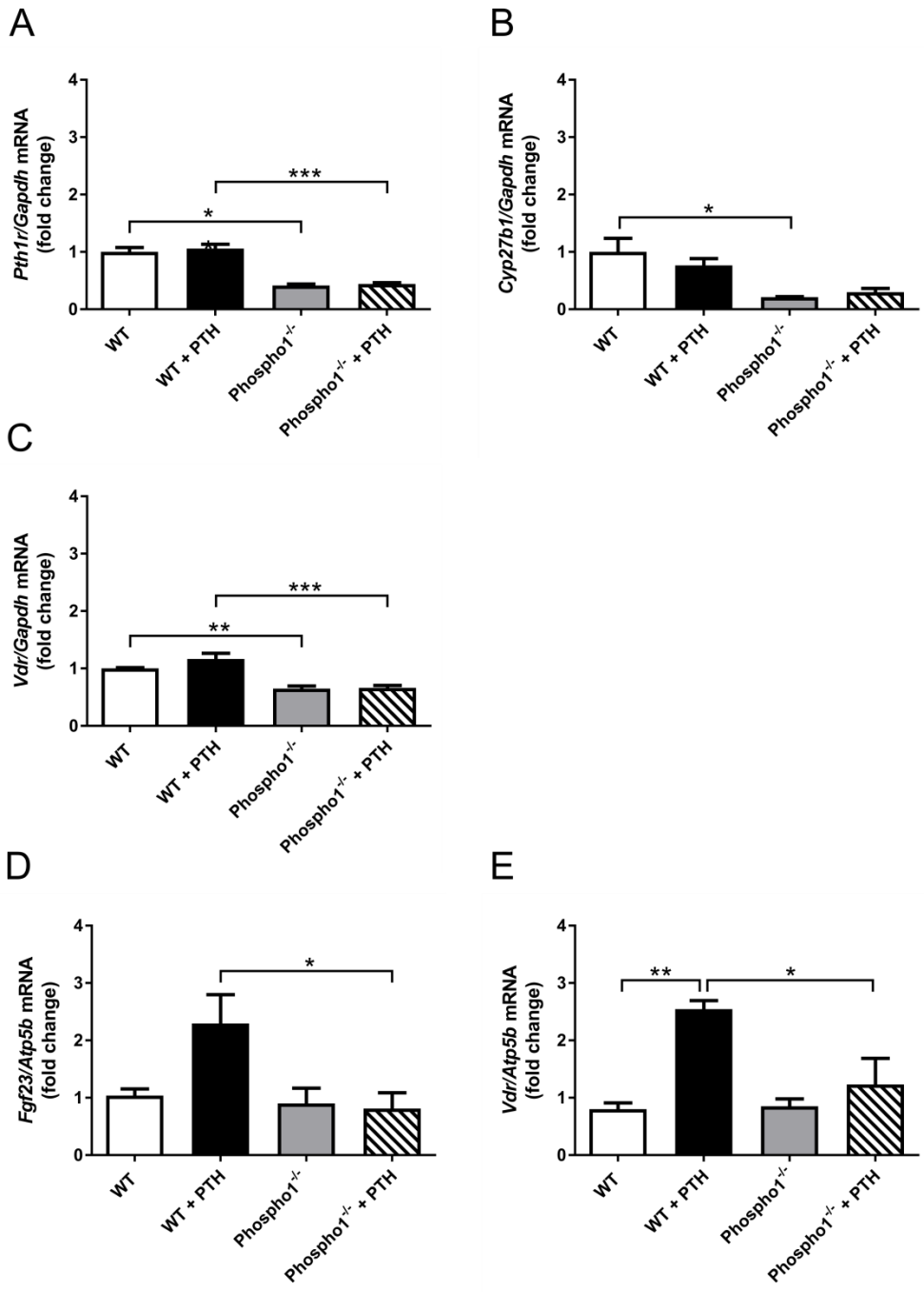

Figure 5.19. Disturbed expression of components of phosphate regulation within the femora and kidney of *Phospho1*$^{-/-}$ mice.

RT-qPCR analysis of the mRNA expression within the kidney of WT and *Phospho1*$^{-/-}$ mice receiving iPTH (80 µg/kg/day) for 14-days. **(A)** *Pth1r* **(B)** *Cyp27b1* and **(C)** *Vdr*. RT-qPCR analysis of the mRNA expression within the distal femora of WT and *Phospho1*$^{-/-}$ mice receiving iPTH (80 µg/kg/day) for 14-days. **(D)** *Fgf23* and **(E)** *Vdr*. Data are represented as mean ± S.E.M. N>4, *P<0.05, **P<0.01, ***P<0.001.

this, the basal levels of *Cyp27b1* expression was decreased in *Phospho1*$^{-/-}$ kidneys compared to WT ($P<0.05$). The basal expression of the vitamin D receptor (*Vdr)* was similarly found to exhibit reduced expression levels in *Phospho1*$^{-/-}$ kidney ($P<0.05$) but not in bone (Fig. 5.19.C & E). In the distal femora, PTH induced the upregulation of *Fgf23* and *Vdr* expression in WT animals but not in *Phospho1*$^{-/-}$ mice.

5.6. Discussion

The pleiotropic effects of PTH on bone, which are dictated by the frequency of the exposure, have been progressively uncovered, aiding our understanding of the osteoanabolic effects of iPTH therapy and pathological bone loss associated with hyperparathyroidism. The mineralisation of osteoid, during both the initial formation of the skeleton and modelling and remodelling events, provides mechanical integrity to bone. The intravesicular phosphatase, PHOSPHO1 is essential for the initiation of MV-mediated HA formation, through the generation of P_i from the hydrolysis of phospholipid metabolites PCho and PEth (Roberts et al., 2004, Yadav et al., 2011). This Chapter sought to uncover the regulation of *Phospho1* expression by PTH *in vivo*.

In this study, I investigated several iPTH challenge models in order to assess the effects of acute (6 h) and chronic exposure (14 and 28 days) of PTH to provide a comprehensive analysis of the temporal effects of iPTH on *Phospho1* expression and other gene markers of bone mineralisation. *Phospho1* expression in the distal femur was enhanced in response to both a single, 6 h exposure to PTH and long term (14 day and 28 day) iPTH exposure in male WT mice. The genetic ablation of *Phospho1* results in a disproportionate osteoid:bone volume ratio, greenstick fractures and bowing of long bones due to severe hypomineralisation (Yadav et al., 2011, Huesa et al., 2011,

Rodriguez-Florez et al., 2015). In addition, the biogenesis of MV is impaired in the absence of *Phospho1* (Yadav et al., 2016). Despite this, the knowledge surrounding the effects of enhanced *Phospho1* expression during ECM mineralisation are scant. In fact, the findings I presented in Chapter 3, in which the overexpression of *Phospho1* in MC3T3-C24 osteoblast-like cells enhanced ECM mineralisation compared to non-transfected cell cultures (Huesa et al., 2015) appears to be the only available information on this subject. With this, albeit limited knowledge in mind, it is reasonable to propose that the iPTH-mediated enhancement of *Phospho1* expression will lead to the enhancement of skeletal mineralisation. This hypothesis is bolstered by the fact that MVs (and thus potentially PHOSPHO1) have been shown to participate in the mineralisation of mature rat bone during the remodelling process (Hoshi and Ozawa, 2000). Furthermore, *Phospho1* expression has been observed in the medullary bone of adult chickens. Medullary bone (a source of calcium for egg shell formation) is continually remodelled in 24 h cycles and as such, the presence of *Phospho1* could indicate a potential involvement in the mineralisation of osteoid during bone remodelling (Stewart et al., 2006). Furthermore, immunohistochemical localisation studies on the chicken have shown that PHOSPHO1 expression is also associated with osteons in cortical bone that were actively mineralising their osteoid. No immunoreactivity was observed in closed osteons (Stewart et al., 2006). These findings point towards a role for PHOSPHO1 throughout the lifespan of the skeleton. As nSMase2 is similarly implicated in the biogenesis of MV and indeed, more directly in the mineralisation process (through the generation of PCho as a substrate for PHOSPHO1) (Thouverey et al., 2011, Khavandgar et al., 2011, Khavandgar and

Murshed, 2015), the upregulation of *Smpd3* observed in this study in response to iPTH is likely to have facilitated the anabolic effects of iPTH.

This present study additionally assessed the expression of the transcription factors *Runx2* and *Trps1* in the distal femur of male mice treated with PTH. *Runx2* and *Trps1* mRNA expression was enhanced in WT mice in response to both a 6 h PTH exposure and a 14-day iPTH exposure but not in 28-day iPTH or continuously exposed mice. *Trps1*, a GATA transcription factor which primarily acts to repress the transcription of genes has recently been shown to be connected with the mineralisation process (Napierala et al., 2008, Kuzynski et al., 2014). Mutations in the *Trps1* gene lead to the human condition tricho-rhino-phalangeal syndrome which is characterised by craniofacial and skeletal dysplasias (Momeni et al., 2000). The siRNA mediated knockdown of *Trps1* in a pre-odontoblastic cell line leads to the suppression of *Phospho1* and *Smpd3* expression (Kuzynski et al., 2014). It is perhaps somewhat counterintuitive then that the same researchers found that the overexpression of *Trps1* results in decreased ECM mineralisation of these cell cultures (Kuzynski et al., 2014). Further studies will need to be performed to investigate the role of *Trps1* in mediating *Phospho1* expression. Although scarce, the research on *Runx2* regulation of *Phospho1* is more convincing. The overexpression of *Runx2* in mouse limb bud cultures leads to a 4-fold increase in *Phospho1* expression (Nishimura et al., 2012). *Runx2* directs mesenchymal precursors to the osteoblast lineage (Komori, 2010) and as such its expression precedes that of *Phospho1*. It is well stablished that *Runx2* may be phosphorylated by PTH-directed activation of PKA (Franceschi and Xiao, 2003). Immunoprecipitation studies will be required to unequivocally confirm the ability of *Runx2* to bind to the *Phospho1* promoter. However, the data presented here alongside

that of Nishimura et al. (2012) certainly suggests a role for *Runx2* in positively regulating *Phospho1* expression.

Despite the differential effects of iPTH observed between WT and *Phospho1*$^{-/-}$ mice, with respect to the expression of key mineralisation genes, there were only modest differences noted in their anabolic response to 28-day iPTH. In particular the osteoanabolic response to 28-day iPTH in trabecular bone was only moderately diminished in the absence of *Phospho1*. Interestingly however, there was an anabolic response noted in the cortical compartments of WT mice receiving 28-day iPTH but not in *Phospho1*$^{-/-}$. In fact, *Phospho1*$^{-/-}$ mice actually displayed decreased cortical BMD with iPTH exposure. It is well established that the osteoanabolic effects of iPTH are more rapidly observed in cancellous as opposed to cortical bone (Rubin et al., 2002). Moreover, reported BMD decreases during spaceflight are greater in the trabecular compartment (2.2-2.7%/ month) as opposed to the cortical compartment (0.4-0.5%/ month) (Lang et al., 2004). Of course, trabecular bone is more metabolically active than cortical bone due to its greater surface area (Clarke, 2008). The lack of induction of *Runx2* in *Phospho1*$^{-/-}$ mice in response to iPTH, and therefore the potential reduced recruitment of osteoblasts from mesenchymal precursors, may have further slowed the remodelling rate of bone. It is therefore possible, that given an extended period of iPTH, *Phospho1*$^{-/-}$ mice would display anabolic features in the cortical compartment. Unfortunately this laboratory has struggled to successfully develop a method for detecting PHOSPHO1 in the mouse by immunohistochemistry. Personal communication with Dr Brian Foster (Ohio State University) has indicated that this current problem is not specific to our own laboratory despite their previous successful immunolocalisation of PHOSPHO1 in teeth (Zweifler et al., 2016). This

suggests a batch difference in the commercial production of the PHOSPHO1 antibody and this has hampered efforts to investigate any potential differences between trabecular and cortical bone PHOSPHO1 localisation. There were no obvious differences in the localisation or staining levels of TNAP within the cortical bone WT and *Phospho1*$^{-/-}$ mice exposed to 28-day iPTH (Fig. 5.13.).

In this study, the continuous infusion of PTH over 28-days in male mice (from 4 weeks of age) did not induce any catabolic effects on bone microarchitecture as assessed by µCT. This was surprising as many previous studies have reported a catabolic effect on the skeleton of cPTH infusion (Hock and Gera, 1992, Uzawa et al., 1995, Iida-Klein et al., 2005). Investigations into the lack of effect observed uncovered a recent study which similarly noted this lack of catabolism. Babey et al. (2015) infused PTH 1-34 (60µg/kg/day) for 28-days into 12-week old male and female mice (similar to the protocol used in my studies) and detected decreased trabecular thickness, BMD and BV/TV in the distal femur of female mice only. This study additionally observed that osteoclast precursors derived from female mice were significantly more responsive to RANKL and macrophage colony stimulating factor compared to male mice. In contrast, bone marrow stromal cell cultures from male mice continuously exposed to PTH mineralised their ECM to a greater extent than cultures derived from female mice (Babey et al., 2015). This is not an isolated observation; trabecular bone preservation in male mice receiving cPTH infusion being noted previously (Cheng et al., 2013). Additional hints of gender specific differences in the response to chronic, high doses of PTH are available from the literature surrounding the human condition of hyperparathyroidism. Small scale studies from sample populations in Spain and India, revealed a more severe disease in women compared to men, with women exhibiting a

reduction in bone mass throughout the skeleton whereas men appear to have a bone sparing phenotype (Rico et al., 1994, Shah et al., 2012). Intriguingly, the results of my studies imply that the skeleton of male mice is responsive to the anabolic effects of iPTH but not to the catabolic effects of cPTH (the effects of iPTH and cPTH are summarised in Table 4). This to the best of my knowledge is a novel finding. Overall, the findings of my current work, alongside the research described herein, provide sufficient evidence to doubt the currently accepted dogma that cPTH exposure leads to bone loss under all conditions. Specifically, it highlights the importance of considering sex differences and the influence of the gonadal steroids in future endocrine experiments.

Table 4. Summary of the effects of iPTH and cPTH in WT and *Phospho1*$^{-/-}$ mice.

Exposure regimen	WT			*Phospho1*$^{-/-}$		
	Phospho1 expression (femur)	Trabecular thickness	Cortical thickness (at 37% total bone length)	*Phospho1* expression (femur)	Trabecular thickness	Cortical thickness (at 37% total bone length)
14-day intermittent (80 µg/kg/day)	↑↑	↑	no change	n/a	↑	no change
28-day intermittent (80 µg/kg/day)	↑	↑	↑	n/a	↑	no change
28-day continuous (80 µg/kg/day)	no change	no change	no change	n/a	no change	no change

The expression of genes which regulate the PTH-Vitamin D-FGF-23 axis within the kidney and bone were assessed after PTH exposure in both WT and *Phospho1*$^{-/-}$ mice. This was done in an attempt to explain the different response to PTH between WT and *Phospho1* deficient mice. The characterisation of the *Phospho1*$^{-/-}$ mouse by Yadav et

al. (2011) did not report details on these key systemic regulators of phosphate despite observing severe hypomineralisation in the skeletons of the *Phospho1*$^{-/-}$ mice. It might be expected that *Phospho1*$^{-/-}$ mice would exhibit some sort of P_i sparing phenotype. Reduced *Pth1r* expression was observed in the bone of *Phospho1*$^{-/-}$ animals (6 week old male) compared to WT. However, the receptor exhibited similar reduced expression in the kidney of *Phospho1*$^{-/-}$ animals. These data point towards reduced bone resorption (through reduced remodelling) and reduced reabsorption of P_i at the proximal tubule of the kidney. These data on the expression of the *Pth1r* are in disagreement with previously published data which revealed that *Phospho1*$^{-/-}$ mice have high levels of the bone formation and resorption serum markers, N-terminal propeptide (P1NP) and C-terminal telopeptide of type I collagen (CTX), indicative of an increased remodelling rate (Huesa et al., 2011). Increased remodelling in the *Phospho1*$^{-/-}$ mouse is proposed to be a response to the pathological incidence of greenstick fractures exhibited in the bones of these mice (Huesa et al., 2011). Of course, PTH is not the only regulator of bone remodelling and the effects of other hormones (e.g. Insulin, Vitamin D) and growth factors (e.g. Insulin like growth factor 1, BMPs) must be investigated in the *Phospho1*$^{-/-}$ mouse. For example, although the data concerning the effects of PTH on FGF-23 regulation are disparate (Franceschi and Xiao, 2003), I observed differences in the response of *Fgf23* mRNA expression to PTH exposure between WT and *Phospho1*$^{-/-}$ mice. A comprehensive metabolomics study may be necessary to explain the differences between WT and *Phospho1*$^{-/-}$ mice in their skeletal response to PTH exposure.

This Chapter has unequivocally confirmed the potent regulation of *Phospho1* and *Smpd3* by PTH *in vivo*. Stimulation of the expression of the genes by PTH, points

towards a role for these enzymes during bone modelling and remodelling. Additionally, these data highlight a role for *Phospho1* in mediating the anabolic effects of iPTH, in particular in cortical bone. Studies modelling the continuous exposure to PTH add to the emerging body of evidence revealing that the osteocatabolic effects of this exposure may be limited to female mice. As a whole these data expand our knowledge of the regulation of key mineralisation genes which will be taken forward to benefit the pursuit of therapeutic agents to regulate biomineralisation.

Chapter 6

Final discussion and future work

Mineralisation of the ECM of bone and cartilage is an essential prerequisite to a functional skeleton. On the other hand, in soft tissues, mineralisation is typically pathologic, disrupting the normal physiology of the affected tissue. As such, this process is tightly regulated, both locally and systemically. The compartmentalisation of the initiation of mineralisation within specialised extracellular vesicles (MVs) provides an additionally regulatory element. The composition and function of the protein constituents are steadily being uncovered. PHOSPHO1, discovered in 1999 within chick growth plate chondrocytes (Houston et al., 1999), is now known to be essential for the initiation of mineralisation within MV. The genetic ablation of *Phospho1* results in severely hypomineralised and ductile bones (Yadav et al., 2011, Huesa et al., 2011, Rodriguez-Florez et al., 2015), reduced MV biogenesis and function (Yadav et al., 2016) and altered osteocytogenesis and lacunae morphology (Javaheri et al., 2015). Despite this knowledge of the skeletal phenotype associated with the absence of *Phospho1*, little is known about its genetic and molecular regulation, nor its interaction with other MV components. The work reported in this thesis aimed to provide an understanding of these unknowns through both *in vitro* and *in vivo* experimentation.

The *in vitro* study of the essential phosphatases and phosphate transporters of MV mineralisation has to date been limited by the use of βGP to induce ECM mineralisation, a substrate for TNAP, the major MV phosphatase. The work presented in Chapter 3, highlighted that ECM mineralisation in the absence of βGP is achievable. Osteoblast cell cultures exposed to Ca^{2+} exhibited ECM mineralisation comparable to that observed in βGP treated cultures. Of course, this approach is not without limitations as Ca^{2+} is capable of inducing a number of cellular functions such as

differentiation, proliferation, adhesion and endo- and exo-cytosis amongst others. With further characterisation however, these phosphatase-substrate free mineralisation conditions will allow investigators to successfully investigate the mechanisms of endogenous P_i generation during mineralisation. Embryonic metatarsals displayed diaphyseal mineralisation when cultured in serum free conditions supplemented with ascorbic acid only. This represents the optimum conditions for analysis of phosphatase function (and endogenous Pi production). However, this model is limited to the study of chondrocyte directed cartilage mineralisation. Both these culture models were utilised to examine the temporal expression of key mineralisation enzymes during osteoblast and chondrocyte mineralisation. Of particular interest was the finding that PHOSPHO1 and nSMase2 appear to be simultaneously upregulated prior to the appearance of mineralisation. Furthermore, in the absence of PHOSPHO1, nSMase2 expression is downregulated. These findings bolster the hypothesis that these enzymes work in tandem for the generation and processing of PCho during ECM mineralisation. However, the expression pattern of these enzymes alone is not confirmatory of cooperative function. Substrate and enzymatic product analysis should be performed by mass spectrometry within these models. Furthermore, the expression analysis experiments detailed in Chapter 3 should be performed with *fro/fro* calvarial osteoblasts and embryonic metatarsals. Although *fro/fro* skeletal tissues exhibit reduced ceramide levels (due to the lack of sphingomyelinase activity) the PCho levels have not been investigated. One might hypothesise that these would similarly be reduced, and as such PHOSPHO1 activity might be correspondingly reduced. It would be informative to generate and analyse the skeleton of *fro/fro;Phospho1*$^{-/-}$ compound homozygotes. If the osteomalacia of the double knock-out mouse was greater than

observed in either the *Smpd3* or *Phospho1* deficient mouse then it is likely that both gene products influence ECM mineralisation via independent mechanisms. However as hypothesised in this work, if the osteomalacia of the double knock-out mouse was similar this would suggest that nSMase2 and PHOSPHO1 might act in the same pathway e.g. nSMase2 acts upstream of PHOSPHO1.

As the skeleton of the *fro/fro* mice are severely hypomineralised, it is unlikely that other PCho generating enzymes (e.g. CK) are upregulated to provide PCho for P_i generation by PHOSPHO1. Perinatal lethality of the *fro/fro* mouse has limited its use as it is difficult (and expensive) to breed and accrue enough experimental animals. However, Alebrahim et al. (2014) recently generated a *fro/fro* mouse with tetracycline inducible-*Smpd3* expression. The early embryonic expression of *Smpd3* improves the survivability of the *fro/fro* mouse.

The characterisation of the *fro/fro* (Khavandgar et al., 2011) and *Chkβ*$^{-/-}$ mice (Sher et al., 2006) and the striking skeletal mineralisation defects observed provided the impetus for the work of this thesis, which in part, sought to investigate the interplay between these enzymes (which both generate PCho) and PHOSPHO1. Of course, nSMase2 and CK activity are not the only mechanisms of PCho generation and furthermore, recombinant human PHOSPHO1 exhibits activity towards PCho and PEth (Roberts et al., 2004). Studies on the lipid composition of MV have shown that the PE, PC and SM content of MVs is reduced rapidly during mineralisation. MV mineralisation is also associated with a rise in diacylglycerols and monoacylglycerols indicative of phospholipase C and lysophospholipase C activity respectively (Mebarek et al., 2013). Interestingly, MV membranes are enriched in lysophosphospholipids

(LP) which contain only one fatty acid moiety (Wu et al., 2002). The generation of PCho from LPC is classically viewed as a three step process in vertebrates (Cole et al., 2012). Recently, NPP6 was characterised as possessing choline-specific glycerophosphodiester phosphodiesterase activity, showing specificity towards LPC in *in vitro* assays (Sakagami et al., 2005). The direct generation of PCho from LPC by NPP6 could provide an alternative mechanism to provide PHOSPHO1 substrate within MVs. The data surrounding NPP6 is however limited, and to date its presence within MVs has not been established although data from this laboratory has confirmed it expression within bone by immunoblotting and immunohistochemistry (unpublished observations). Phospholipase C activity is often generically assumed to mean phosphatidylinositol-PLC activity which results in the generation of the established signalling molecule inositol 1,4,5, triphosphate. PC specific PLC isoforms have not been reported in vertebrates, but if identified the production of PCho and DAG from PC could, hypothetically, be yet another source of PCho within MVs.

As alluded to earlier, to truly investigate the role of lipid metabolism in ECM mineralisation, analysis of lipid precursors and metabolites will be necessary. Moreover this analysis should be performed in transgenic mouse models. The analysis of MV lipid composition and fluctuation during biomineralisation by thin layer chromatography (carried out by Wu et al. (2002)) are limited by current standards. The advances in mass spectrometry techniques now allows for the extensive characterisation and quantification of lipids in biological samples. Despite this, MS still remains challenging in mineralised samples, with phosphate salts being particular problematic by affecting the ionisation of analytes and introducing significant noise into generated spectra. Despite this, MS-approaches to lipid analysis are being reported

in the literature (Gotliv et al., 2006, Dambach et al., 2004, Zhu et al., 2016). It was originally an aim of this studentship to characterise the 'lipodomes' of the *in vitro* model systems developed in Chapter 3 during ECM mineralisation but prohibitive costs of this approach made it impossible to make major progress towards this aim. Despite this, with the assistance and expertise of Prof. Phillip Whitfield of the Lipidomics research facility, University of the Highlands and Islands, Inverness, I have been able to obtain some preliminary lipidomic data from cultured embryonic metatarsal samples. Lipids were extracted from metatarsal samples (20 bones) after collagenase digestion using established methods (Folch et al., 1957) and described in section 2.6.1. The resultant lipid extracts underwent liquid chromatography-mass spectrometry as described in section 2.6.1. and performed by Prof. Whitfield. These preliminary experiments generated data about eight classes of phospholipids (Fig. 6.1.). These results are yet to be normalised to a yet to be determined variable, however they demonstrate the ability to obtain quantitative lipidomic data from embryonic metatarsal samples. Furthermore samples were spiked with non-physiologic lipid species prior to analysis and acted as an internal standard from which to quantify the picomolar quantities of the lipids within the samples (Fig. 6.1.). As I and others have recently written about (Marino et al., 2016), embryonic metatarsals are a highly physiological model of endochondral ossification, in particular, the E15 stage provides a means of investigating the initiation of mineralisation. In our lipidomic experiments, the final volume infused in the mass spectrometer was the equivalent of four metatarsals further emphasising the practicality of this approach for future studies.

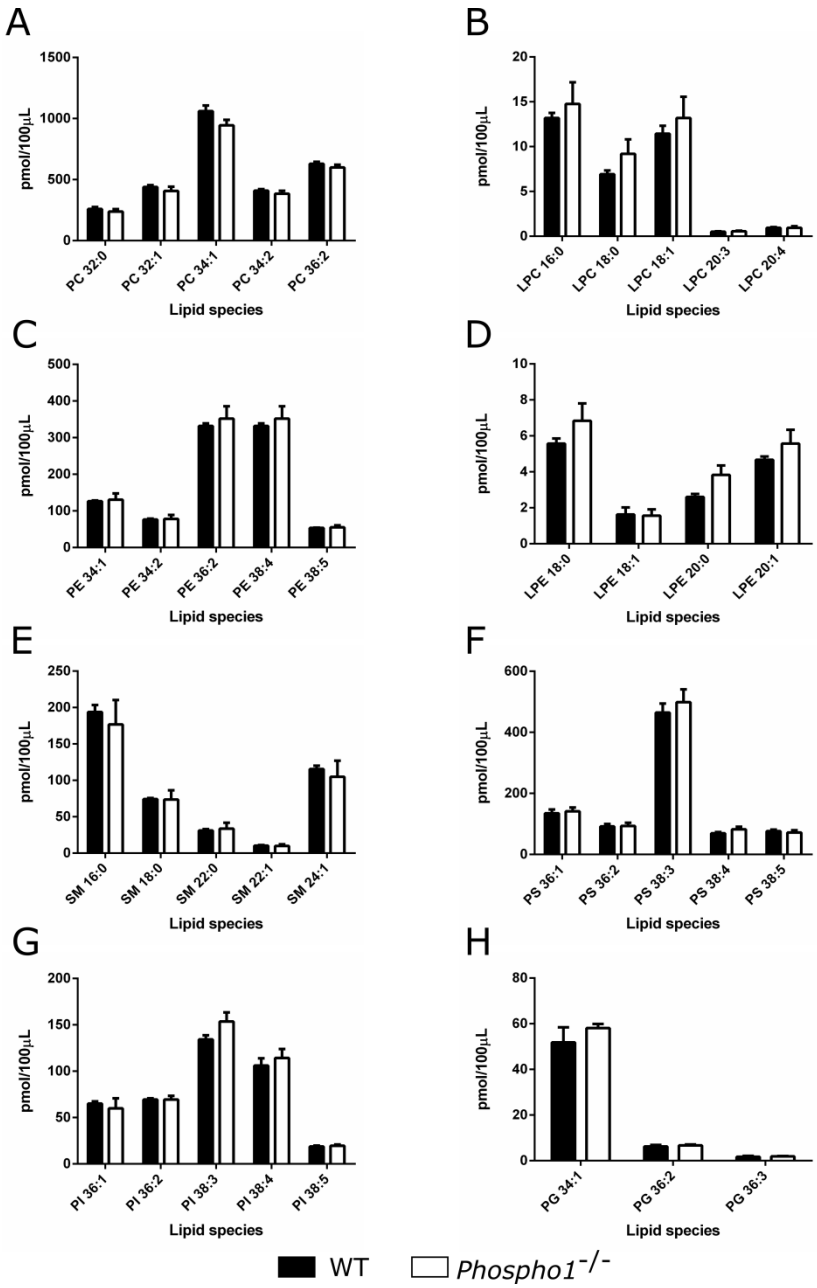

Figure 6.1. Quantification of lipids extracted from cultured embryonic metatarsals.

Total lipids were extracted from WT and Phospho1$^{-/-}$ E15 metatarsals cultured for 5 days. Separation and quantification of lipid species was performed by HPLC-MS. **(A)** Phosphatidylcholine (PC) species **(B)** Lysophosphatidylcholine (LPC) species **(C)** Phosphatidylethanolamine (PE) species **(D)** Lysophosphatidylethanolamine (LPE) species **(E)** Sphingomyelin (SM) species **(F)** Phosphatidylserine (PS) species **(G)** Phosphatidylinositol (PI) species **(H)** Phosphatidylglycerol (PG) species. Data are presented as mean ± S.E.M for N=3 samples per genotype.

Primarily through the modulation of osteoblast recruitment, proliferation and apoptosis, iPTH exposure increases bone formation on periosteal, endocortical and trabecular bone surfaces (Kousteni and Bilezikian, 2008). Furthermore, PTH suppresses the expression of the Wnt antagonist, SOST from osteocytes. This thesis presents data revealing that PTH potently modulates the expression of *Phospho1* and *Smpd3*, and that iPTH enhances the expression of these genes *in vivo*. The role of these two enzymes in skeletal mineralisation has been discussed in detail in this thesis. A schematic model of the actions of iPTH on the expression of *Phospho1* and *Smpd3*, and the downstream effects of this on MVs are presented in Fig. 6.2. The genetic ablation or pharmacological inhibition of PHOSPHO1 or nSMase2 results in profound mineralisation defects and reduced MV release. The work of this thesis additionally found, that in the absence of *Phospho1*, *Smpd3* expression was not induced by iPTH, and neither were there any anabolic effects of iPTH within cortical bone. Whilst this is preliminary data, it is tempting to propose that the enhancement of *Phospho1* and *Smpd3* expression provides an additional means of explaining the osteoanabolic effects of iPTH on the skeleton. To add weight to this hypothesis it must be first confirmed that upregulation of *Phospho1* expression in adult bone results in an increase in BMD. C57Bl/6J mice overexpressing *Phospho1* under the influence of the *col1a1* promoter (i.e. bone specific) have been developed and are awaiting characterisation by this laboratory. These mice will be useful to investigate the effects of *Phospho1* upregulation, however a mouse with inducible *Phospho1* expression (perhaps through a tetracycline-dependent transcriptional control system) will be required to answer the aforementioned question, i.e. does the upregulation of *Phospho1* in adult bone increase BMD. These mice may also be important to

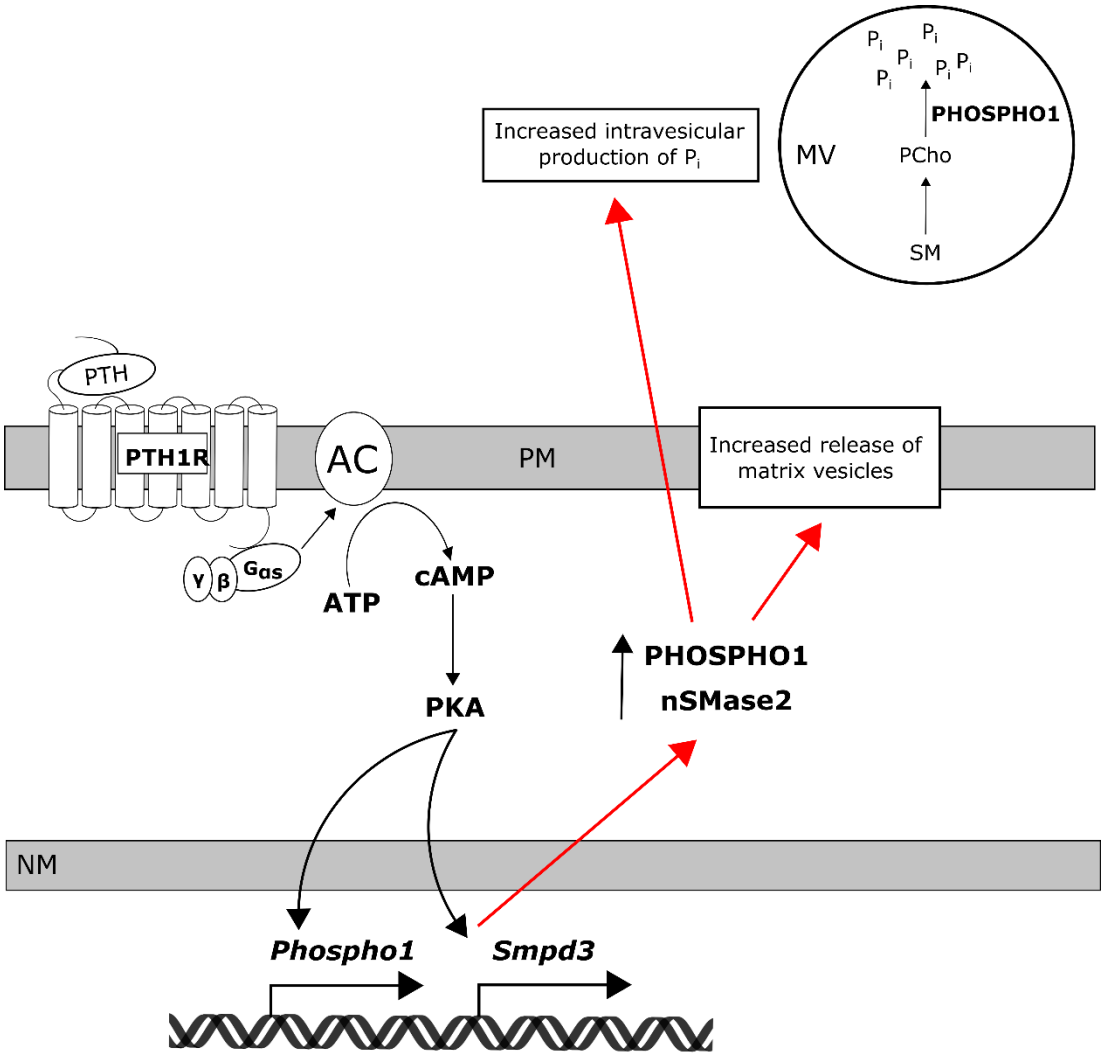

Figure 6.2. Schematic model of the effects of PTH on *Phospho1* and *Smpd3*.

Results from this thesis have identified the cAMP/PKA signalling pathway as the key intracellular pathway regulating *Phospho1* and *Smpd3* expression. Furthermore, iPTH upregulates the expression of *Phospho1* and *Smpd3* in WT mouse femur. Based on current knowledge of the roles of PHOSPHO1 and nSMase2, this upregulation is proposed to have multifaceted roles on MVs including the increase in MV release and the upregulation of Pi generation within MVs. These roles are hypothesised to increases local mineralisation of the ECM. Adenylyl cylclase (AC), Adenosine triphosphate(ATP), cyclic adenosine monophosphate (cAMP), Protein kinase A (PKA), parathyroid hormone (PTH), parathyroid hormone 1 receptor (PTH1R), matrix vesicle (MV), plasma membrane (PM), nuclear membrane (NM), sphingomyelin (SM), phosphocholine (PCho), inorganic phosphate (P_i).

investigate the influence of PHOSPHO1 on fracture repair. A recent abstract at the ASBMR in 2015 from the laboratory of Monzur Murshed (McGill University, Montreal) indicated that long bones from *Phospho1* deficient mice repaired their bones poorly after rod immobilised fracture surgery. This work suggests that PHOSPHO1 plays an integral role during bone fracture repair and may be a therapeutic target to improve the fracture healing process.

From the *in vitro* observation that cPTH exposure inhibited the expression of *Phospho1* (Chapter 4 and (Houston et al., 2016)), in an osteoblast cell line it was hypothesised that the bone loss observed in hyperparathyroidism may be a result of reduced mineralisation gene expression by osteoblasts coupled with the enhanced osteoclastogenesis classically reported. Indeed hyperparathyroidism appears to affect bone mass in the cortical compartment whilst sparing cancellous bone mass and increasing osteoblast number (Dempster et al., 2007, Jilka et al., 2010). Intermittent PTH experiments have underscored a more important role for PHOSPHO1 in cortical bone. Unfortunately, the experiments performed in Chapter 5 to investigate the effects of cPTH on WT and *Phospho1* deficient mice were performed in male mice which, I discovered after the completion of my studies, have been reported not to exhibit the well-established osteocatabolic effects of cPTH (Babey et al., 2015). These studies should be repeated in female mice to test the involvement, if any, of PHOSPHO1 during cPTH induced bone loss. On first appearances, the observation that PTH positively and negatively regulates *Phospho1* expression depending on the length of exposure, may seem inconsistent with the high bone mass phenotype of hypoparathyroidism. However, hypoparathyroidism is characterised by low bone turnover (parathyroidectomised rats exhibit reduced RANKL expression (Ueno et al.,

2003)), and not excessive osteoblast activity. Indeed, OCN positive osteoblasts (*i.e.* mature osteoblasts) are reduced in hypoparathyroidism and SOST levels are high (Rubin et al., 2011), implying bone formation is slowed. Additionally, the regulation of *Phospho1* by other endocrine and paracrine factors in the absence of PTH cannot be ruled out, for example, this study also identified BMP-2 as a positive regulator of *Phospho1* expression (Chapter 4, Fig. 4.8.).

The positive regulation of *Phospho1* and *Smpd3* by BMP-2 is certainly worthy of further investigation. BMP-2 is powerfully osteogenic and is used clinically to improve the repair of non-union fractures. BMP-2 upregulates the expression of the osteogenic transcription factor, *Runx2*, through the activation of Dlx5, a transcriptional activator of *Runx2* (Lee et al., 2003, Samee et al., 2008). Induction of Runx2 expression has been shown to enhance *Phospho1* expression in mouse limb bud cultures (Nishimura et al., 2012). Thus it is possible that BMP-2 upregulates *Phospho1* expression through activation of Runx2. As a starting point, cycloheximide studies would be useful to determine if the action of BMP-2 on *Phospho1* is a direct effect or one that requires a protein intermediary. With this in mind, a recent microarray study of Smad3 overexpressing MC3T3-E1 osteoblast like cells, revealed a 157-fold increase in *Phospho1* transcript level (Hisa et al., 2011). Evidence is emerging that BMP-2 can activate the non-canonical BMP signalling pathways involving Smad2/3, albeit in murine gonadotrope-like cells (Wang et al., 2014).

A variety of human conditions, characterised by disrupted mineralisation, have been shown to be the result of mutations within known and discrete genetic loci. For example, the pathogenesis of sclerosteosis, fibrodysplasia ossificans progressiva, HPP

and pseudoxanthoma elasticum has been linked to mutations within the *SOST, ACVR1, ALPL* and *ABCC6* genes respectively (Balemans et al., 2001, Shore et al., 2006, Henthorn and Whyte, 1992, Nitschke et al., 2012). These conditions are typically severe albeit rare. In contrast, the aetiology of osteoporosis is multifactorial and may secondarily arise as a result of other complications. To date, no disorders of mineralisation have been linked to mutations in the *PHOSPHO1* locus. However it is tantalising to speculate that inhibition of PHOSPHO1 function may be implicated in the high incidence of bone fractures amongst people taking acid-suppressive medications such as proton pump inhibitors (PPI). Three recent large epidemiologic studies completed in Denmark, UK and Canada have reported an increased risk of osteoporosis related fractures including fractures of the hip with chronic PPI therapy (Yang et al., 2006, Vestergaard et al., 2006, Targownik et al., 2008). PPIs such as omeprazole, esomeprazole, pantoprazole and lansoprazole are commonly prescribed to control and prevent symptoms of chronic unrelenting conditions such as gastroesophageal reflux disease, ulcers and dyspepsia and patients are prescribed PPIs for protracted periods of time (Jacobson et al., 2003). The commonly accepted explanation for the casual relationship between PPI use and bone fractures is the impairment of calcium absorption leading to secondary hyperparathyroidism and increased osteoclastic bone resorption (Vestergaard et al., 2006). This calcium malabsorption maybe a consequence of PPI induced reduction in acid production (hypochlorhydria) in the stomach and proximal duodenum leading to the retention of calcium in its food matrix and defective calcium absorption. However, studies on the effects of hypochlorhydria on calcium absorption have been equivocal, suggesting a limited role of reduced acid secretion in the development of fractures (Bo-Linn et al.,

1984, Marcinowska-Suchowierska et al., 1995). These, and other conflicting data, suggest that PPI use may increase fracture incidence by a mechanism that is in addition to, or independent of, its effect of calcium malabsorption and secondary hyperparathyroidism. Previous studies in this laboratory have identified lansoprazole as a potent PHOSPHO1 inhibitor, which when tested *in vivo* can inhibit bone mineralisation (Roberts et al., 2007, MacRae et al., 2010). Further studies are required to evaluate if PHOSPHO1 mediates the bones response to PPI administration.

Furthermore, methylation of the PHOSPHO1 locus has been associated with future risk of developing type II diabetes (Chambers et al., 2015, Dayeh et al., 2016) and consistent with this observation, work from this laboratory has shown that *Phospho1*$^{-/-}$ mice exhibit improved glucose and insulin tolerance and resist high-fat-diet induced obesity and diabetes. Surprisingly, this protective phenotype was manifested in the absence of altered levels of undercarboxylated osteocalcin, the principal bone endocrine hormone (Oldknow *et al*. unpublished)

The results of Chapter 5 of this thesis has provided preliminary evidence for a role of PHOSPHO1 in eliciting the anabolic effects of PTH in bone, which are worthy of further investigation. To explore a potential role for PHOSPHO1 in human bone mineralisation, it would be beneficial to first investigate its role in a large animal model. Despite the advantages of rodents in the study of protein function and disease pathogenesis, the morphological, anatomical and mechanical properties of rodent bone do not accurately model the human situation (Aerssens et al., 1998). Pigs, like humans exhibit Haversian remodelling and growth plate fusion and have similar femoral cross

sectional diameters, making them an attractive candidate to more appropriately study the regulation of bone mineralisation (Bagi et al., 2011, Li et al., 2015).

The recent sequencing and annotation of the *Sus scrofa* (domestic pig) genome improves the practicality of the pig as a model species (Groenen et al., 2012). This, in combination with the emergence of engineered nuclease technologies such as the clustered, regularly interspaced, short palindromic repeats (CRISPR)/Cas9 systems, allows the rapid, and relatively easy, generation of genome edited pigs. In brief, CRISPR associated protein 9 (Cas9) is a double stranded nuclease derived from Streptococcus pyogenes which may be targeted to cut the genome via an RNA-guide molecule. Double strand cleavage through the activity of Cas9 stimulated non-homologous end joining, a DNA repair mechanisms which is particularly prone to the introduction of insertion and deletion mutations (Sander and Joung, 2014). During my PhD, three pairs of CRISPR guides were designed against the pig PHOSPHO1 gene. The guides were designed to target a region within pig *PHOSPHO1*, homologous to exon 3 of the murine *Phospho1* gene. This is the same region containing an adenine to thymine substitution which generates the stop codon and thus loss of functional PHOSPHO1 within the *Phospho1*$^{-/-}$ mouse. To date these guides have been cloned into Cas9 containing, mammalian expression vectors and transfected into a pig fibroblast cell line. Due to time constraints the ability of these constructs to cleave at the target site has yet to be tested. If successful, these constructs may be used to generate genome edited founder pigs through the method of Lillico et al. (2013). Characterisation of the skeleton of *PHOSPHO1*$^{-/-}$ pigs will provide a more reliable insight into its potential role in humans.

Reference list

Addison, W. N., Azari, F., Sørensen, E. S., Kaartinen, M. T. & Mckee, M. D. 2007. Pyrophosphate inhibits mineralization of osteoblast cultures by binding to mineral, up-regulating osteopontin, and inhibiting alkaline phosphatase activity. *Journal of Biological Chemistry,* 282**,** 15872-15883.

Addison, W. N., Nakano, Y., Loisel, T., Crine, P. & Mckee, M. D. 2008. MEPE-ASARM peptides control extracellular matrix mineralization by binding to hydroxyapatite: An inhibition regulated by PHEX cleavage of ASARM. *Journal of Bone and Mineral Research,* 23**,** 1638-1649.

Addison, W. N., Masica, D. L., Gray, J. J. & Mckee, M. D. 2010. Phosphorylation-dependent inhibition of mineralization by osteopontin ASARM peptides is regulated by PHEX cleavage. *Journal of Bone and Mineral Research,* 25**,** 695-705.

Addison, W. N., Nelea, V., Chicatun, F., Chien, Y. C., Tran-Khanh, N., Buschmann, M. D., Nazhat, S. N., Kaartinen, M. T., Vali, H., Tecklenburg, M. M., Franceschi, R. T. & Mckee, M. D. 2015. Extracellular matrix mineralization in murine MC3T3-E1 osteoblast cultures: An ultrastructural, compositional and comparative analysis with mouse bone. *Bone,* 71**,** 244-256.

Aerssens, J., Boonen, S., Lowet, G. & Dequeker, J. 1998. Interspecies Differences in Bone Composition, Density, and Quality: Potential Implications for in Vivo Bone Research. *Endocrinology,* 139**,** 663-670.

Agarwal, R. & Garcia, A. J. 2015. Biomaterial strategies for engineering implants for enhanced osseointegration and bone repair. *Advanced Drug Delivery Reviews,* 94**,** 53-62.

Alebrahim, S., Khavandgar, Z., Marulanda, J. & Murshed, M. 2014. Inducible transient expression of Smpd3 prevents early lethality in fro/fro mice. *Genesis,* 52**,** 408-16.

Ali, S. Y., Sajdera, S. W. & Anderson, H. C. 1970. Isolation and Characterization of Calcifying Matrix Vesicles from Epiphyseal Cartilage. *Proceedings of the National Academy of Sciences,* 67**,** 1513-1520.

Amin, A. K., Huntley, J. S., Bush, P. G., Simpson, H. R. W. & Hall, A. C. 2009. Chondrocyte Death in Mechanically Injured Articular Cartilage-The Influence of Extracellular Calcium. *Journal of Orthopaedic Research,* 27**,** 778-784.

Anderson, H. C. 1967. Electron microscopic studies of induced cartilage development and calcification. *Journal of Cellular Biology,* 35**,** 81-101.

Anderson, H. C. 1969. Vesicles Associated with Calcification in Matrix of Epiphyseal Cartilage. *Journal of Cell Biology,* 41**,** 59-&.

Anderson, H. C. 1995. Molecular biology of matrix vesicles. *Clin Orthop Relat Res***,** 266-280.

Anderson, H. C., Hsu, H. H., Morris, D. C., Fedde, K. N. & Whyte, M. P. 1997. Matrix vesicles in osteomalacic hypophosphatasia bone contain apatite-like mineral crystals. *American Journal of Pathology,* 151**,** 1555-1561.

Anderson, H. C. 2003. Matrix vesicles and calcification. *Current Rheumatology Reports,* 5**,** 222-6.

Anderson, H. C., Sipe, J. B., Hessle, L., Dhamyamraju, R., Atti, E., Camacho, N. P. & Millan, J. L. 2004. Impaired calcification around matrix vesicles of growth plate and bone in alkaline phosphatase-deficient mice. *American Journal of Pathology,* 164**,** 841-847.

Anderson, H. C., Garimella, R. & Tague, S. E. 2005a. The role of matrix vesicles in growth plate development and biomineralization. *Frontiers in Bioscience,* 10**,** 822-37.

Anderson, H. C., Harmey, D., Camacho, N. P., Garimella, R., Sipe, J. B., Tague, S., Bi, X., Johnson, K., Terkeltaub, R. & Millán, J. L. 2005b. Sustained osteomalacia of long bones despite major improvement in other hypophosphatasia-related mineral deficits in tissue nonspecific alkaline phosphatase/nucleotide pyrophosphatase phosphodiesterase 1 double-deficient mice. *American Journal of Pathology,* 166**,** 1711-1720.

Andrade, A. C., Chrysis, D., Audi, L. & Nilsson, O. 2011. Methods to study cartilage and bone development. *Endocrinology and Development,* 21**,** 52-66.

Aoyama, C., Liao, H. & Ishidate, K. 2004. Structure and function of choline kinase isoforms in mammalian cells. *Progress in Lipid Research,* 43**,** 266-281.

Aslan, D., Andersen, M. D., Gede, L. B., De Franca, T. K., Jørgensen, S. R., Schwarz, P. & Jørgensen, N. R. 2012. Mechanisms for the bone anabolic effect of parathyroid hormone treatment in humans. *Scandinavian Journal of Clinical and Laboratory Investigation,* 72**,** 14-22.

Aspden, R. M. 2003. Mechanical testing of bone ex vivo. *Bone Research Protocols,* 80**,** 369-379.

Aukhil, I., Cui, C., Yunhong, B. & Cooper, L. F. 2000. Identification and characterization of a novel gene in developing bone, cartilage and cardiac muscle. *Molecular Biology of the Cell,* 11**,** 163A.

Babey, M., Wang, Y., Kubota, T., Fong, C., Menendez, A., Elalieh, H. Z. & Bikle, D. D. 2015. Gender-Specific Differences in the Skeletal Response to Continuous PTH in Mice Lacking the IGF1 Receptor in Mature Osteoblasts. *Journal of Bone and Mineral Research,* 30**,** 1064-1076.

Bagi, C. M., Berryman, E. & Moalli, M. R. 2011. Comparative Bone Anatomy of Commonly Used Laboratory Animals: Implications for Drug Discovery. *Comparative Medicine,* 61**,** 76-85.

Balcerzak, M., Hamade, E., Zhang, L., Pikula, S., Azzar, G., Radisson, J., Bandorowicz-Pikula, J. & Buchet, R. 2003. The roles of annexins and alkaline phosphatase in mineralization process. *Acta Biochimica Polonica,* 50**,** 1019-1038.

Balemans, W., Ebeling, M., Patel, N., Van Hul, E., Olson, P., Dioszegi, M., Lacza, C., Wuyts, W., Van Den Ende, J., Willems, P., Paes-Alves, A. F., Hill, S., Bueno, M., Ramos, F. J., Tacconi, P., Dikkers, F. G., Stratakis, C., Lindpaintner, K., Vickery, B., Foernzler, D. & Van Hul, W. 2001. Increased bone density in sclerosteosis is due to the deficiency of a novel secreted protein (SOST). *Human Molecular Genetics,* 10**,** 537-543.

Baron, R. & Hesse, E. 2012. Update on bone anabolics in osteoporosis treatment: rationale, current status, and perspectives. *Journal of Clinical Endocrinology and Metabolism,* 97**,** 311-25.

Beck, L., Leroy, C., Beck-Cormier, S., Forand, A., Salaun, C., Paris, N., Bernier, A., Urena-Torres, P., Prie, D., Ollero, M., Coulombel, L. & Friedlander, G. 2010. The Phosphate Transporter PiT1 (Slc20a1) Revealed As a New Essential Gene for Mouse Liver Development. *Plos One,* 5.

Bellido, T., Ali, A. A., Plotkin, L. I., Fu, Q., Gubrij, I., Roberson, P. K., Weinstein, R. S., O'brien, C. A., Manolagas, S. C. & Jilka, R. L. 2003. Proteasomal degradation of Runx2 shortens parathyroid hormone-induced anti-apoptotic signaling in osteoblasts - A putative explanation for why intermittent administration is needed for bone anabolism. *Journal of Biological Chemistry,* 278**,** 50259-50272.

Bellows, C. G., Heersche, J. N. M. & Aubin, J. E. 1992. Inorganic-phosphate added Exogenously or released from Beta-glycerophosphate Initiates Mineralization of Osteoid Nodules in vitro. *Bone and Mineral,* 17**,** 15-29.

Bellows, C. G., Ishida, H., Aubin, J. E. & Heersche, J. N. M. 1990. Parathyroid Hormone Reversibly Suppresses the Differentiation of Osteoprogenitor Cells into Functional Osteoblasts. *Endocrinology,* 127**,** 3111-3116.

Bernard, G. W. & Pease, D. C. 1969. An electron microscopic study of initial intramembranous osteogenesis. *American Journal of Anatomy,* 125**,** 271-90.

Best, J. L., Amezcua, C. A., Mayr, B., Flechner, L., Murawsky, C. M., Emerson, B., Zor, T., Gardner, K. H. & Montminy, M. 2004. Identification of small-molecule antagonists that inhibit an activator:coactivator interaction. *Proceedings of the National Academy of Sciences,* 101**,** 17622-17627.

Bo-Linn, G. W., Davis, G. R., Buddrus, D. J., Morawski, S. G., Santa Ana, C. & Fordtran, J. S. 1984. An evaluation of the importance of gastric acid secretion in the absorption of dietary calcium. *Journal of Clinical Investigation,* 73**,** 640-647.

Bollen, M., Gijsbers, R., Ceulemans, H., Stalmans, W. & Stefan, C. 2000. Nucleotide pyrophosphatases/phosphodiesterases on the move. *Critical Reviews in Biochemistry and Molecular Biology,* 35**,** 393-432.

Bonewald, L. F. 2011. The Amazing Osteocyte. *Journal of Bone and Mineral Research,* 26**,** 229-238.

Bonewald, L. F. & Wacker, M. J. 2013. FGF23 Production by Osteocytes. *Pediatric nephrology (Berlin, Germany),* 28**,** 563-568.

Bonucci, E. 1967. Fine structure of early cartilage calcification. *Journal of Ultrastructural Research,* 20**,** 33-50.

Boskey, A. L. & Roy, R. 2008. Cell Culture Systems for Studies of Bone and Tooth Mineralization. *Chemical Reviews,* 108**,** 4716-4733.

Bourgine, A., Pilet, P., Diouani, S., Sourice, S., Lesoeur, J., Beck-Cormier, S., Khoshniat, S., Weiss, P., Friedlander, G., Guicheux, J. & Beck, L. 2013. Mice with Hypomorphic Expression of the Sodium-Phosphate Cotransporter PiT1/Slc20a1 Have an Unexpected Normal Bone Mineralization. *Plos One,* 8.

Brandi, M. L. 2009. Microarchitecture, the key to bone quality. *Rheumatology,* 48**,** iv3-iv8.

Britto, J. M., Fenton, A. J., Holloway, W. R. & Nicholson, G. C. 1994. Osteoblasts mediate thyroid hormone stimulation of osteoclastic bone resorption. *Endocrinology,* 134**,** 169-76.

Brown, E. M. 2015. Chapter 6 - Control of Parathyroid Hormone Secretion by its Key Physiological Regulators A2 - Bilezikian, John P. *The Parathyroids (Third Edition).* San Diego: Academic Press.

Calbet, L. J. A., Moysi, S. J., Dorado, C. & Rodríguez, P. L. 1998. Bone Mineral Content and Density in Professional Tennis Players. *Calcified Tissue International,* 62**,** 491-496.

Canalis, E. & Delany, A. M. 2002. Mechanisms of glucocorticoid action in bone. *Annals of the New York Academy of Science,* 966**,** 73-81.

Carter, D. R., Van Der Meulen, M. C. H. & Beaupré, G. S. 1996. Mechanical factors in bone growth and development. *Bone,* 18**,** S5-S10.

Chae, Y.-M., Heo, S.-H., Kim, J.-Y., Lee, J.-M., Ryoo, H.-M. & Cho, J.-Y. 2009. Upregulation of smpd3 via BMP2 stimulation and Runx2. *Bmb Reports,* 42**,** 86-90.

Chambers, J. C., Loh, M., Lehne, B., Drong, A., Kriebel, J., Motta, V., Wahl, S., Elliott, H. R., Rota, F., Scott, W. R., Zhang, W., Tan, S. T., Campanella, G., Chadeau-Hyam, M., Yengo, L., Richmond, R. C., Adamowicz-Brice, M., Afzal, U., Bozaoglu, K., Mok, Z. Y., Ng, H. K., Pattou, F., Prokisch, H., Rozario, M. A., Tarantini, L., Abbott, J., Ala-Korpela, M., Albetti, B., Ammerpohl, O., Bertazzi, P. A., Blancher, C., Caiazzo, R., Danesh, J., Gaunt, T. R., De Lusignan, S., Gieger, C., Illig, T., Jha, S., Jones, S., Jowett, J., Kangas, A. J., Kasturiratne, A., Kato, N., Kotea, N., Kowlessur, S., Pitkaniemi, J., Punjabi, P., Saleheen, D., Schafmayer, C., Soininen, P., Tai, E. S., Thorand, B., Tuomilehto, J., Wickremasinghe, A. R., Kyrtopoulos, S. A., Aitman, T. J., Herder, C., Hampe, J., Cauchi, S., Relton, C. L., Froguel, P., Soong, R., Vineis, P., Jarvelin, M. R., Scott, J., Grallert, H., Bollati, V., Elliott, P., Mccarthy, M. I. & Kooner, J. S. 2015. Epigenome-wide association of DNA methylation markers in peripheral blood from Indian Asians and Europeans with incident type 2 diabetes: a nested case-control study. *Lancet Diabetes Endocrinol,* 3**,** 526-34.

Chang, M. K., Raggatt, L.-J., Alexander, K. A., Kuliwaba, J. S., Fazzalari, N. L., Schroder, K., Maylin, E. R., Ripoll, V. M., Hume, D. A. & Pettit, A. R. 2008. Osteal tissue macrophages are

intercalated throughout human and mouse bone lining tissues and regulate osteoblast function in vitro and in vivo. *Journal of Immunology,* 181**,** 1232-1244.
Chang, Y. L., Stanford, C. M. & Keller, J. C. 2000. Calcium and phosphate supplementation promotes bone cell mineralization: Implications for hydroxyapatite (HA)-enhanced bone formation. *Journal of Biomedical Materials Research,* 52**,** 270-278.

Charles, J. F. & Aliprantis, A. O. 2014. Osteoclasts: more than just 'bone eaters'. *Trends in Molecular Medicine,* 20**,** 449-459.

Chen, Q., Bei, J. J., Liu, C., Feng, S. B., Zhao, W. B., Zhou, Z., Yu, Z. P., Du, X. J. & Hu, H. Y. 2016. HMGB1 Induces Secretion of Matrix Vesicles by Macrophages to Enhance Ectopic Mineralization. *Plos One,* 11.

Cheng, Z., Liang, N., Chen, T.-H., Li, A., Maria, C. S., You, M., Ho, H., Song, F., Bikle, D., Tu, C., Shoback, D. & Chang, W. 2013. Sex and Age Modify Biochemical and Skeletal Manifestations of Chronic Hyperparathyroidism by Altering Target Organ Responses to Ca(2+) and PTH in Mice. *Journal of bone and mineral research : the official journal of the American Society for Bone and Mineral Research,* 28**,** 1087-1100.

Chung, C.-H., Golub, E. E., Forbes, E., Tokuoka, T. & Shapiro, I. M. 1992. Mechanism of action of β-glycerophosphate on bone cell mineralization. *Calcified Tissue International,* 51**,** 305-311.

Ciancaglini, P., Yadav, M. C., Sper Simao, A. M., Narisawa, S., Pizauro, J. M., Farquharson, C., Hoylaerts, M. F. & Millan, J. L. 2010. Kinetic Analysis of Substrate Utilization by Native and TNAP-, NPP1-, or PHOSPHO1-Deficient Matrix Vesicles. *Journal of Bone and Mineral Research,* 25**,** 716-723.

Clarke, B. 2008. Normal Bone Anatomy and Physiology. *Clinical Journal of the American Society of Nephrology,* 3**,** S131-S139.

Clarke, C. J., Cloessner, E. A., Roddy, P. l. & Hannun, Y. A. 2011. Neutral sphingomyelinase 2 (nSMase2) is the primary neutral sphingomyelinase isoform activated by tumour necrosis factor-α in MCF-7 cells. *Biochemical Journal,* 435**,** 381-390.

Cole, L. K., Vance, J. E. & Vance, D. E. 2012. Phosphatidylcholine biosynthesis and lipoprotein metabolism. *Biochimica et Biophysica Acta (BBA) - Molecular and Cell Biology of Lipids,* 1821**,** 754-761.

Cotmore, J. M., Nichols, G. & Wuthier, R. E. 1971. Phospholipid—Calcium Phosphate Complex: Enhanced Calcium Migration in the Presence of Phosphate. *Science,* 172**,** 1339-1341.

Coxam, V., Miller, M. A., Bowman, M. B. & Miller, S. C. 1996. Ontogenesis of IGF regulation of longitudinal bone growth in rat metatarsal rudiments cultured in serum-free medium. *Archives of Physiology and Biochemistry,* 104**,** 173-9.

Cui, L., Houston, D. A., Farquharson, C. & Macrae, V. E. 2016. Characterisation of matrix vesicles in skeletal and soft tissue mineralisation. *Bone,* 87**,** 147-158.

Dallas, S. L., Prideaux, M. & Bonewald, L. F. 2013. The Osteocyte: An Endocrine Cell … and More. *Endocrine Reviews,* 34**,** 658-690.

Dambach, S., Fartmann, M., Kriegeskotte, C., Bruning, C., Hellweg, S., Wiesmann, H. P., Lipinsky, D. & Arlinghaus, H. F. 2004. ToF-SIMS and laser-SNMS analysis of apatite formation in extracellular protein matrix of osteoblasts in vitro. *Surface and Interface Analysis,* 36**,** 711-715.

Dayeh, T., Tuomi, T., Almgren, P., Perfilyev, A., Jansson, P. A., De Mello, V. D., Pihlajamaki, J., Vaag, A., Groop, L., Nilsson, E. & Ling, C. 2016. DNA methylation of loci within ABCG1 and PHOSPHO1 in blood DNA is associated with future type 2 diabetes risk. *Epigenetics,* 11**,** 482-8.

Dempster, D. W., Parisien, M., Silverberg, S. J., Liang, X. G., Schnitzer, M., Shen, V., Shane, E., Kimmel, D. B., Recker, R., Lindsay, R. & Bilezikian, J. P. 1999. On the mechanism of cancellous bone preservation in postmenopausal women with mild primary hyperparathyroidism. *Journal of Clinical Endocrinology & Metabolism,* 84**,** 1562-1566.

Dempster, D. W., Hughes-Begos, C. E., Plavetic-Chee, K., Brandao-Burch, A., Cosman, F., Nieves, J., Neubort, S., Lu, S. S., Iida-Klein, A., Arnett, T. & Lindsay, R. 2005. Normal human osteoclasts formed from peripheral blood monocytes express PTH type 1 receptors and are stimulated by PTH in the absence of osteoblasts. *Journal of Cellular Biochemistry,* 95**,** 139-48.

Dempster, D. W., Müller, R., Zhou, H., Kohler, T., Shane, E., Parisien, M., Silverberg, S. J. & Bilezikian, J. P. 2007. Preserved three-dimensional cancellous bone structure in mild primary hyperparathyroidism. *Bone,* 41**,** 19-24.

Dobnig, H. & Turner, R. T. 1995. Evidence that Intermittent Treatment with Parathyroid-Hormone Increases Bone-Formation in Adult-Rats by Activation of Bone Lining Cells. *Endocrinology,* 136**,** 3632-3638.

Ducy, P., Schinke, T. & Karsenty, G. 2000. The Osteoblast: A Sophisticated Fibroblast under Central Surveillance. *Science,* 289**,** 1501-1504.

Eaton, S. L., Roche, S. L., Hurtado, M. L., Oldknow, K. J., Farquharson, C., Gillingwater, T. H. & Wishart, T. M. 2013. Total Protein Analysis as a Reliable Loading Control for Quantitative Fluorescent Western Blotting. *Plos One,* 8.

Epker, B. N. & Frost, H. M. 1966. Periosteal appositional bone growth from age two to age seventy in man. A tetracycline evaluation. *The Anatomical Record,* 154**,** 573-577.

Eriksen, E. F. 2002. Primary hyperparathyroidism: Lessons from bone histomorphometry. *Journal of Bone and Mineral Research,* 17**,** N95-N97.

Farquharson, C. & Jefferies, D. 2000. Chondrocytes and longitudinal bone growth: The development of tibial dyschondroplasia. *Poultry Science,* 79**,** 994-1004.

Farquharson, C. & Staines, K. 2011. The skeleton: no bones about it. *Journal of Endocrinology,* 211**,** 107-108.

Fisher, L. W. & Fedarko, N. S. 2003. Six genes expressed in bones and teeth encode the current members of the SIBLING family of proteins. *Connective Tissue Research,* 44**,** 33-40.
Folch, J., Lees, M. & Sloane Stanley, G. H. 1957. A simple method for the isolation and purification of total lipides from animal tissues. *Journal of Biological Chemistry,* 226**,** 497-509.

Franceschi, R. T. & Xiao, G. Z. 2003. Regulation of the osteoblast-specific transcription factor, runx2: Responsiveness to multiple signal transduction pathways. *Journal of Cellular Biochemistry,* 88**,** 446-454.

Franz-Odendaal, T. A. 2011. Induction and patterning of intramembranous bone. *Frontiers in Bioscience (Landmark Ed),* 16**,** 2734-46.

Gallego-Ortega, D., De Molina, A. R., Ramos, M. A., Valdes-Mora, F., Barderas, M. G., Sarmentero-Estrada, J. & Lacal, J. C. 2009. Differential Role of Human Choline Kinase alpha and beta Enzymes in Lipid Metabolism: Implications in Cancer Onset and Treatment. *Plos One,* 4.

Gardella, T. J. 2015. Chapter 4 - Interactions of PTH with Receptors and Signaling A2 - Bilezikian, John P. *The Parathyroids (Third Edition).* San Diego: Academic Press.

Genge, B. R., Wu, L. N. Y. & Wuthier, R. E. 2003. Separation and quantification of chicken and bovine growth plate cartilage matrix vesicle lipids by high-performance liquid chromatography using evaporative light scattering detection. *Analytical Biochemistry,* 322**,** 104-115.

Giachelli, C. M. 2005. Inducers and inhibitors of biomineralization: lessons from pathological calcification. *Orthodontics & Craniofacial Research,* 8**,** 229-231.

Gibellini, F. & Smith, T. K. 2010. The Kennedy pathway—De novo synthesis of phosphatidylethanolamine and phosphatidylcholine. *IUBMB Life,* 62**,** 414-428.

Glanemann, C., Loos, A., Gorret, N., Willis, L. B., O'brien, X. M., Lessard, P. A. & Sinskey, A. J. 2003. Disparity between changes in mRNA abundance and enzyme activity in Corynebacterium glutamicum: implications for DNA microarray analysis. *Applied Microbiology and Biotechnology,* 61**,** 61-68.

Glimcher, M. J. 1987. The nature of the mineral component of bone and the mechanism of calcification. *Instructional course lectures,* 36**,** 49-69.

Golub, E. E. 2011. Biomineralization and matrix vesicles in biology and pathology. *Seminars in Immunopathology,* 33**,** 409-417.

Gotliv, B. A., Robach, J. S. & Veis, A. 2006. The composition and structure of bovine peritubular dentin: Mapping by time of flight secondary ion mass spectroscopy. *Journal of Structural Biology,* 156**,** 320-333.

Groenen, M. a. M., Archibald, A. L., Uenishi, H., Tuggle, C. K., Takeuchi, Y., Rothschild, M. F., Rogel-Gaillard, C., Park, C., Milan, D., Megens, H.-J., Li, S., Larkin, D. M., Kim, H., Frantz, L. a. F., Caccamo, M., Ahn, H., Aken, B. L., Anselmo, A., Anthon, C., Auvil, L., Badaoui, B., Beattie,

C. W., Bendixen, C., Berman, D., Blecha, F., Blomberg, J., Bolund, L., Bosse, M., Botti, S., Bujie, Z., Bystrom, M., Capitanu, B., Carvalho-Silva, D., Chardon, P., Chen, C., Cheng, R., Choi, S.-H., Chow, W., Clark, R. C., Clee, C., Crooijmans, R. P. M. A., Dawson, H. D., Dehais, P., De Sapio, F., Dibbits, B., Drou, N., Du, Z.-Q., Eversole, K., Fadista, J., Fairley, S., Faraut, T., Faulkner, G. J., Fowler, K. E., Fredholm, M., Fritz, E., Gilbert, J. G. R., Giuffra, E., Gorodkin, J., Griffin, D. K., Harrow, J. L., Hayward, A., Howe, K., Hu, Z.-L., Humphray, S. J., Hunt, T., Hornshoj, H., Jeon, J.-T., Jern, P., Jones, M., Jurka, J., Kanamori, H., Kapetanovic, R., Kim, J., Kim, J.-H., Kim, K.-W., Kim, T.-H., Larson, G., Lee, K., Lee, K.-T., Leggett, R., Lewin, H. A., Li, Y., Liu, W., Loveland, J. E., Lu, Y., Lunney, J. K., Ma, J., Madsen, O., Mann, K., Matthews, L., Mclaren, S., Morozumi, T., Murtaugh, M. P., Narayan, J., Truong Nguyen, D., Ni, P., Oh, S.-J., Onteru, S., Panitz, F., Park, E.-W., et al. 2012. Analyses of pig genomes provide insight into porcine demography and evolution. *Nature,* 491**,** 393-398.

Gronowicz, G., Woodiel, F. N., Mccarthy, M.-B. & Raisz, L. G. 1989. In vitro mineralization of fetal rat parietal bones in defined serum-free medium: Effect of β-glycerol phosphate. *Journal of Bone and Mineral Research,* 4**,** 313-324.

Haaijman, A., Dsouza, R. N., Bronckers, A., Goei, S. W. & Burger, E. H. 1997. OP-1 (BMP-7) affects mRNA expression of type 1, II, X collagen, and matrix Gla protein in ossifying long bones in vitro. *Journal of Bone and Mineral Research,* 12**,** 1815-1823.

Haaijman, A., Karperien, M., Lanske, B., Hendriks, J., Löwik, C. W. G. M., Bronckers, A. L. J. J. & Burger, E. H. 1999. Inhibition of terminal chondrocyte differentiation by bone morphogenetic protein 7 (OP-1) in vitro depends on the periarticular region but is independent of parathyroid hormone-related peptide. *Bone,* 25**,** 397-404.

Hadjidakis, D. J. & Androulakis, I. I. 2006. Bone Remodeling. *Annals of the New York Academy of Sciences,* 1092**,** 385-396.

Hahn, M., Vogel, M., Pompesius-Kempa, M. & Delling, G. 1992. Trabecular bone pattern factor—a new parameter for simple quantification of bone microarchitecture. *Bone,* 13**,** 327-330.

Hajjawi, M. O. R., Macrae, V. E., Huesa, C., Boyde, A., Millan, J. L., Arnett, T. R. & Orriss, I. R. 2014. Mineralisation of collagen rich soft tissues and osteocyte lacunae in Enpp1(-/-) mice. *Bone,* 69**,** 139-147.

Hakim, F. T., Cranley, R., Brown, K. S., Eanes, E. D., Harne, L. & Oppenheim, J. J. 1984. Hereditary joint disorder in progressive ankylosis (ank/ank) mice I. association of calcium hydroxyapatite deposition with inflammatory arthropathy. *Arthritis & Rheumatism,* 27**,** 1411-1420.

Harmey, D., Hessle, L., Narisawa, S., Johnson, K. A., Terkeltaub, R. & Millan, J. L. 2004. Concerted regulation of inorganic pyrophosphate and osteopontin by Akp2, Enpp1, and Ank - An integrated model of the pathogenesis of mineralization disorders. *American Journal of Pathology,* 164**,** 1199-1209.

Heilig, J., Paulsson, M. & Zaucke, F. 2016. Insulin-like growth factor 1 receptor (IGF1R) signaling regulates osterix expression and cartilage matrix mineralization during endochondral ossification. *Bone,* 83**,** 48-57.

Henthorn, P. S. & Whyte, M. P. 1992. Missense mutations of the tissue-nonspecific alkaline phosphatase gene in hypophosphatasia. *Clinical Chemistry,* 38**,** 2501-2505.

Hewison, M., Zehnder, D., Bland, R. & Stewart, P. 2000. 1alpha-Hydroxylase and the action of vitamin D. *Journal of Molecular Endocrinology,* 25**,** 141-148.

Hisa, I., Inoue, Y., Hendy, G. N., Canaff, L., Kitazawa, R., Kitazawa, S., Komori, T., Sugimoto, T., Seino, S. & Kaji, H. 2011. Parathyroid Hormone-responsive Smad3-related Factor, Tmem119, Promotes Osteoblast Differentiation and Interacts with the Bone Morphogenetic Protein-Runx2 Pathway. *Journal of Biological Chemistry,* 286**,** 9787-9796.

Ho, A. M., Johnson, M. D. & Kingsley, D. M. 2000. Role of the Mouse *ank* Gene in Control of Tissue Calcification and Arthritis. *Science,* 289**,** 265-270.

Hock, J. M. & Gera, I. 1992. Effects of continuous and intermittent administration and inhibition of resorption on the anabolic response of bone to parathyroid hormone. *Journal of Bone and Mineral Research,* 7**,** 65-72.

Hogan, B. L. 1996. Bone morphogenetic proteins: multifunctional regulators of vertebrate development. *Genes and Development,* 10**,** 1580-94.

Hoshi, K. & Ozawa, H. 2000. Matrix vesicle calcification in bones of adult rats. *Calcified Tissue International,* 66**,** 430-434.

Houston, B., Seawright, E., Jefferies, D., Hoogland, E., Lester, D., Whitehead, C. & Farquharson, C. 1999. Identification and cloning of a novel phosphatase expressed at high levels in differentiating growth plate chondrocytes. *Biochimica Et Biophysica Acta-Molecular Cell Research,* 1448**,** 500-506.

Houston, B., Stewart, A. J. & Farquharson, C. 2004. PHOSPHO1 - A novel phosphatase specifically expressed at sites of mineralisation in bone and cartilage. *Bone,* 34**,** 629-637.

Houston, D. A., Myers, K., Macrae, V. E., Staines, K. A. & Farquharson, C. 2016. The Expression of PHOSPHO1, nSMase2 and TNAP is Coordinately Regulated by Continuous PTH Exposure in Mineralising Osteoblast Cultures. *Calcified Tissue International, In press*.

Huesa, C., Yadav, M. C., Finnila, M. a. J., Goodyear, S. R., Robins, S. P., Tanner, K. E., Aspden, R. M., Milian, J. L. & Farquharson, C. 2011. PHOSPHO1 is essential for mechanically competent mineralization and the avoidance of spontaneous fractures. *Bone,* 48**,** 1066-1074.

Huesa, C., Houston, D., Kiffer-Moreira, T., Yadav, M. C., Luis Millan, J. & Farquharson, C. 2015. The functional co-operativity of tissue-nonspecific alkaline phosphatase (TNAP) and PHOSPHO1 during initiation of skeletal mineralization. *Biochemistry and Biophysics Reports,* 4**,** 196-201.

Iida-Klein, A., Lu, S. S., Kapadia, R., Burkhart, M., Moreno, A., Dempster, D. W. & Lindsay, R. 2005. Short-term continuous infusion of human parathyroid hormone 1-34 fragment is catabolic with decreased trabecular connectivity density accompanied by hypercalcemia in C57BL/J6 mice. *Journal of Endocrinology,* 186**,** 549-557.

Irving, J. T. 1959. A histological staining method for sites of calcification in teeth and bone. *Archives of Oral Biology,* 1**,** 89-IN2.

Ishizuya, T., Yokose, S., Hori, M., Noda, T., Suda, T., Yoshiki, S. & Yamaguchi, A. 1997. Parathyroid hormone exerts disparate effects on osteoblast differentiation depending on exposure time in rat osteoblastic cells. *Journal of Clinical Investigation,* 99**,** 2961-2970.

Isogai, Y., Akatsu, T., Ishizuya, T., Yamaguchi, A., Hori, M., Takahashi, N. & Suda, T. 1996. Parathyroid hormone regulates osteoblast differentiation positively or negatively depending on the differentiation stages. *Journal of Bone and Mineral Research,* 11**,** 1384-1393.

Jacobson, B. C., Ferris, T. G., Shea, T. L., Mahlis, E. M., Lee, T. H. & Wang, T. C. 2003. Who is using chronic acid suppression therapy and why? *American Journal of Gastroenterology,* 98**,** 51-8.

James, A. W. 2013. Review of Signaling Pathways Governing MSC Osteogenic and Adipogenic Differentiation. *Scientifica,* 2013**,** 17.

Jang, M.-G., Lee, J. Y., Yang, J.-Y., Park, H., Kim, J. H., Kim, J.-E., Shin, C. S., Kim, S. Y. & Kim, S. W. 2015. Intermittent PTH treatment can delay the transformation of mature osteoblasts into lining cells on the periosteal surfaces. *Journal of Bone and Mineral Metabolism***,** 1-8.

Jansen, R. S., Küçükosmanoğlu, A., De Haas, M., Sapthu, S., Otero, J. A., Hegman, I. E. M., Bergen, A. a. B., Gorgels, T. G. M. F., Borst, P. & Van De Wetering, K. 2013. ABCC6 prevents ectopic mineralization seen in pseudoxanthoma elasticum by inducing cellular nucleotide release. *Proceedings of the National Academy of Sciences,* 110**,** 20206-20211.

Javaheri, B., Carriero, A., Staines, K. A., Chang, Y. M., Houston, D. A., Oldknow, K. J., Millan, J. L., Kazeruni, B. N., Salmon, P., Shefelbine, S., Farquharson, C. & Pitsillides, A. A. 2015. Phospho1 deficiency transiently modifies bone architecture yet produces consistent modification in osteocyte differentiation and vascular porosity with ageing. *Bone,* 81**,** 277-291.

Jilka, R. L., Weinstein, R. S., Bellido, T., Roberson, P., Parfitt, A. M. & Manolagas, S. C. 1999. Increased bone formation by prevention of osteoblast apoptosis with parathyroid hormone. *Journal of Clinical Investigation,* 104**,** 439-446.

Jilka, R. L., O'brien, C. A., Bartell, S. M., Weinstein, R. S. & Manolagas, S. C. 2010. Continuous Elevation of PTH Increases the Number of Osteoblasts via Both Osteoclast-Dependent and -Independent Mechanisms. *Journal of Bone and Mineral Research,* 25**,** 2427-2437.

Jonason, J. H. & O'keefe, R. J. 2014. Isolation and Culture of Neonatal Mouse Calvarial Osteoblasts. *In:* HILTON, J. M. (ed.) *Skeletal Development and Repair: Methods and Protocols.* Totowa, NJ: Humana Press.

Kakoi, H., Maeda, S., Shinohara, N., Matsuyama, K., Imamura, K., Kawamura, I., Nagano, S., Setoguchi, T., Yokouchi, M., Ishidou, Y. & Komiya, S. 2014. Bone Morphogenic Protein (BMP) Signaling Up-regulates Neutral Sphingomyelinase 2 to Suppress Chondrocyte Maturation via the Akt Protein Signaling Pathway as a Negative Feedback Mechanism. *Journal of Biological Chemistry,* 289**,** 8135-8150.

Kaneki, H., Takasugi, I., Fujieda, M., Kiriu, M., Mizuochi, S. & Ide, H. 1999. Prostaglandin E-2 stimulates the formation of mineralized bone nodules by a cAMP-independent mechanism in the culture of adult rat calvarial osteoblasts. *Journal of Cellular Biochemistry,* 73**,** 36-48.

Kano, J., Sugimoto, T., Fukase, M. & Chihara, K. 1994. Direct Involvement of cAMP-Dependent Protein Kinase in the Regulation of Alkaline Phosphatase Activity by Parathyroid Hormone (PTH) and PTH-Related Peptide in Osteoblastic UMR-106 Cells. *Biochemical and Biophysical Research Communiations,* 199**,** 271-276.

Kapustin, A. N., Davies, J. D., Reynolds, J. L., Mcnair, R., Jones, G. T., Sidibe, A., Schurgers, L. J., Skepper, J. N., Proudfoot, D., Mayr, M. & Shanahan, C. M. 2011. Calcium Regulates Key Components of Vascular Smooth Muscle Cell-Derived Matrix Vesicles to Enhance Mineralization. *Circulation Research,* 109**,** E1-U41.

Kapustin, A. N., Chatrou, M. L. L., Drozdov, I., Zheng, Y., Davidson, S. M., Soong, D., Furmanik, M., Sanchis, P., De Rosales, R. T. M., Alvarez-Hernandez, D., Shroff, R., Yin, X., Muller, K., Skepper, J. N., Mayr, M., Reutelingsperger, C. P., Chester, A., Bertazzo, S., Schurgers, L. J. & Shanahan, C. M. 2015. Vascular Smooth Muscle Cell Calcification Is Mediated by Regulated Exosome Secretion. *Circulation Research,* 116**,** 1312-1323.

Karsenty, G. 2006. Convergence between bone and energy homeostases: Leptin regulation of bone mass. *Cell Metabolism,* 4**,** 341-348.

Kato, K., Nishimasu, H., Okudaira, S., Mihara, E., Ishitani, R., Takagi, J., Aoki, J. & Nureki, O. 2012. Crystal structure of Enpp1, an extracellular glycoprotein involved in bone mineralization and insulin signaling. *Proceedings of the National Academy of Sciences,* 109**,** 16876-81.

Kato, Y., Shimazu, A., Nakashima, K., Suzuki, F., Jikko, A. & Iwamoto, M. 1990. Effects of Parathyroid Hormone and Calcitonin on Alkaline Phosphatase Activity and Matrix Calcification in Rabbit Growth-Plate Chondrocyte Cultures. *Endocrinology,* 127**,** 114-118.

Keller, H. & Kneissel, M. 2005. SOST is a target gene for PTH in bone. *Bone,* 37**,** 148-158.

Khavandgar, Z., Poirier, C., Clarke, C. J., Li, J. J., Wang, N., Mckee, M. D., Hannun, Y. A. & Murshed, M. 2011. A cell-autonomous requirement for neutral sphingomyelinase 2 in bone mineralization. *Journal of Cell Biology,* 194**,** 277-289.

Khavandgar, Z., Alebrahim, S., Eimar, H., Tamimi, F., Mckee, M. D. & Murshed, M. 2013. Local Regulation of Tooth Mineralization by Sphingomyelin Phosphodiesterase 3. *Journal of Dental Research,* 92**,** 358-364.

Khavandgar, Z. & Murshed, M. 2015. Sphingolipid metabolism and its role in the skeletal tissues. *Cellular and Molecular Life Sciences,* 72**,** 959-969.

Khouja, H. I., Bevington, A., Kemp, G. J. & Russell, R. G. G. 1990. Calcium and orthophosphate deposits in vitro do not imply osteoblast-mediated mineralization: Mineralization by betaglycerophosphate in the absence of osteoblasts. *Bone,* 11**,** 385-391.

Kiffer-Moreira, T., Yadav, M. C., Zhu, D., Narisawa, S., Sheen, C., Stec, B., Cosford, N. D., Dahl, R., Farquharson, C., Hoylaerts, M. F., Macrae, V. E. & Millan, J. L. 2013. Pharmacological Inhibition of PHOSPHO1 Suppresses Vascular Smooth Muscle Cell Calcification. *Journal of Bone and Mineral Research,* 28**,** 81-91.

Kim, K. M. 1976. Calcification of matrix vesicles in human aortic valve and aortic media. *Federation Proceedings,* 35**,** 156-62.

Kim, S. W., Pajevic, P. D., Selig, M., Barry, K. J., Yang, J. Y., Shin, C. S., Baek, W. Y., Kim, J. E. & Kronenberg, H. M. 2012. Intermittent parathyroid hormone administration converts quiescent lining cells to active osteoblasts. *Journal of Bone and Mineral Research,* 27**,** 2075-2084.

Kirsch, T., Wang, W. & Pfander, D. 2003. Functional differences between growth plate apoptotic bodies and matrix vesicles. *Journal of Bone and Mineral Research,* 18**,** 1872-1881.

Komori, T., Yagi, H., Nomura, S., Yamaguchi, A., Sasaki, K., Deguchi, K., Shimizu, Y., Bronson, R. T., Gao, Y. H., Inada, M., Sato, M., Okamoto, R., Kitamura, Y., Yoshiki, S. & Kishimoto, T. 1997. Targeted Disruption of Cbfa1 Results in a Complete Lack of Bone Formation owing to Maturational Arrest of Osteoblasts. *Cell,* 89**,** 755-764.

Komori, T. 2010. Regulation of bone development and extracellular matrix protein genes by RUNX2. *Cell and Tissue Research,* 339**,** 189-195.

Kousteni, S. & Bilezikian, J. P. 2008. The cell biology of parathyroid hormone in osteoblasts. *Current Osteoporosis Reports,* 6**,** 72-6.

Kozhemyakina, E., Lassar, A. B. & Zelzer, E. 2015. A pathway to bone: signaling molecules and transcription factors involved in chondrocyte development and maturation. *Development,* 142**,** 817-831.

Kramer, I., Keller, H., Leupin, O. & Kneissel, M. 2010. Does osteocytic SOST suppression mediate PTH bone anabolism? *Trends in Endocrinology and Metabolism,* 21**,** 237-244.

Krishnan, V., Moore, T. L., Ma, Y. F. L., Helvering, L. M., Frolik, C. A., Valasek, K. M., Ducy, P. & Geiser, A. G. 2003. Parathyroid hormone bone anabolic action requires Bbfa1/Runx2-dependent signaling. *Molecular Endocrinology,* 17**,** 423-435.

Kronenberg, H. M. 2003. Developmental regulation of the growth plate. *Nature,* 423**,** 332-336.

Kronenberg, H.M. 2005. How PTHrP controls growth plate chondrocytes. *BoneKEy-Osteovision,* 2, 7-15.

Kronenberg, H.M. 2006. PTHrP and Skeletal Development. *Annals of the New York Academy of Sciences*, 1068, 1-13.

Krug, H.E., Mahowald M.L. & Clark C. 1989. Progressive ankylosis (ank/ank) in mice: an animal model of spondyloarthropathy. III. Proliferative spleen cell response to T cell mitogens. *Clinical and Experimental Immunology,* 78, 97-101.

Kular, J., Tickner, J. C., Pavlos, N. J., Viola, H. M., Abel, T., Lim, B. S., Yang, X., Chen, H., Cook, R., Hool, L. C., Zheng, M. H. & Xu, J. 2015. Choline Kinase beta Mutant Mice Exhibit Reduced Phosphocholine, Elevated Osteoclast Activity, and Low Bone Mass. *Journal of Biological Chemistry,* 290**,** 1729-1742.

Kuzynski, M., Goss, M., Bottini, M., Yadav, M. C., Mobley, C., Winters, T., Poliard, A., Kellermann, O., Lee, B., Millan, J. L. & Napierala, D. 2014. Dual Role of the Trps1 Transcription Factor in Dentin Mineralization. *Journal of Biological Chemistry,* 289**,** 27481-27493.

Landis, W. J., Song, M. J., Leith, A., Mcewen, L. & Mcewen, B. F. 1993. Mineral and organic matrix interaction in normally calcifying tendon visualized in three dimensions by high-voltage electron microscopic tomography and graphic image reconstruction. *Journal of Structural Biology,* 110**,** 39-54.

Landis, W. J. 1999. An overview of vertebrate mineralization with emphasis on collagen-mineral interaction. *Gravitational and Space Biology Bulletin,* 12**,** 15-26.

Landis, W. J. & Silver, F. H. 2008. Mineral Deposition in the Extracellular Matrices of Vertebrate Tissues: Identification of Possible Apatite Nucleation Sites on Type I Collagen. *Cells, Tissues, Organs,* 189**,** 20-24.

Landis, W. J. & Jacquet, R. 2013. Association of Calcium and Phosphate Ions with Collagen in the Mineralization of Vertebrate Tissues. *Calcified Tissue International,* 93**,** 329-337.

Lang, T., Leblanc, A., Evans, H., Lu, Y., Genant, H. & Yu, A. 2004. Cortical and trabecular bone mineral loss from the spine and hip in long-duration spaceflight. *Journal of Bone and Mineral Research,* 19**,** 1006-1012.

Langdahl, B. L. & Harsløf, T. 2011. Medical treatment of osteoporotic vertebral fractures. *Therapeutic Advances in Musculoskeletal Disease*.

Lee, M.-H., Kim, Y.-J., Kim, H.-J., Park, H.-D., Kang, A.-R., Kyung, H.-M., Sung, J.-H., Wozney, J. M., Kim, H.-J. & Ryoo, H.-M. 2003. BMP-2-induced Runx2 Expression Is Mediated by Dlx5, and TGF-β1 Opposes the BMP-2-induced Osteoblast Differentiation by Suppression of Dlx5 Expression. *Journal of Biological Chemistry,* 278**,** 34387-34394.

Li, J. J., Manickam, G., Ray, S., Oh, C. D., Yasuda, H., Moffatt, P. & Murshed, M. 2016. Smpd3 expression in both chondrocytes and osteoblasts is required for normal endochondral bone development *Molecular and Cellular Biology, In press*.

Li, X., Zhang, Y., Kang, H., Liu, W., Liu, P., Zhang, J., Harris, S. E. & Wu, D. 2005. Sclerostin Binds to LRP5/6 and Antagonizes Canonical Wnt Signaling. *Journal of Biological Chemistry,* 280**,** 19883-19887.

Li, Y., Chen, S.-K., Li, L., Qin, L., Wang, X.-L. & Lai, Y.-X. 2015. Bone defect animal models for testing efficacy of bone substitute biomaterials. *Journal of Orthopaedic Translation,* 3**,** 95-104.

Li, Z., Wu, G., Sher, R. B., Khavandgar, Z., Hermansson, M., Cox, G. A., Doschak, M. R., Murshed, M., Beier, F. & Vance, D. E. 2014a. Choline kinase beta is required for normal endochondral bone formation. *Biochimica Et Biophysica Acta-General Subjects,* 1840**,** 2112-2122.

Li, Z., Wu, G., Van Der Veen, J. N., Hermansson, M. & Vance, D. E. 2014b. Phosphatidylcholine metabolism and choline kinase in human osteoblasts. *Biochimica Et Biophysica Acta-Molecular and Cell Biology of Lipids,* 1841**,** 859-867.

Lillico, S. G., Proudfoot, C., Carlson, D. F., Stverakova, D., Neil, C., Blain, C., King, T. J., Ritchie, W. A., Tan, W., Mileham, A. J., Mclaren, D. G., Fahrenkrug, S. C. & Whitelaw, C. B. 2013. Live pigs produced from genome edited zygotes. *Scientific Reports,* 3**,** 2847.

Lindsay, R., Krege, J. H., Marin, F., Jin, L. & Stepan, J. J. 2016. Teriparatide for osteoporosis: importance of the full course. *Osteoporosis International,* 27**,** 2395-2410.

Liu, Q., Wan, Q., Yang, R., Zhou, H. & Li, Z. 2012. Effects of intermittent versus continuous parathyroid hormone administration on condylar chondrocyte proliferation and differentiation. *Biochemical Biophysical Research Communications,* 424**,** 182-188.

Livak, K. J. & Schmittgen, T. D. 2001. Analysis of relative gene expression data using real-time quantitative PCR and the 2(T)(-Delta Delta C) method. *Methods,* 25**,** 402-408.

Locklin, R. M., Khosla, S., Turner, R. T. & Riggs, B. L. 2003. Mediators of the biphasic responses of bone to intermittent and continuously administered parathyroid hormone. *Journal of Cellular Biochemistry,* 89**,** 180-190.

Lorenz-Depiereux, B., Schnabel, D., Tiosano, D., Häusler, G. & Strom, T. M. 2010. Loss-of-Function ENPP1 Mutations Cause Both Generalized Arterial Calcification of Infancy and Autosomal-Recessive Hypophosphatemic Rickets. *American Journal of Human Genetics,* 86**,** 267-272.

Lotinun, S., Sibonga, J. D. & Turner, R. T. 2002. Differential effects of intermittent and continuous administration of parathyroid hormone on bone histomorphometry and gene expression. *Endocrine,* 17**,** 29-36.

Ma, B., Leijten, J. C. H., Wu, L., Kip, M., Van Blitterswijk, C. A., Post, J. N. & Karperien, M. 2013. Gene expression profiling of dedifferentiated human articular chondrocytes in monolayer culture. *Osteoarthritis and Cartilage,* 21**,** 599-603.

Ma, Y. F. L., Cain, R. L., Halladay, D. L., Yang, X. H., Zeng, Q. Q., Miles, R. R., Chandrasekhar, S., Martin, T. J. & Onyia, J. E. 2001. Catabolic effects of continuous human PTH (1-38) in vivo is associated with sustained stimulation of RANKL and inhibition of osteoprotegerin and gene-associated bone formation. *Endocrinology,* 142**,** 4047-4054.

Mackenzie, N. C. W., Huesa, C., Rutsch, F. & Macrae, V. E. 2012a. New insights into NPP1 function: Lessons from clinical and animal studies. *Bone,* 51**,** 961-968.

Mackenzie, N. C. W., Zhu, D., Milne, E. M., Van 'T Hof, R., Martin, A., Quarles, D. L., Millan, J. L., Farquharson, C. & Macrae, V. E. 2012b. Altered Bone Development and an Increase in FGF-23 Expression in Enpp1(-/-) Mice. *Plos One,* 7.

Mackie, E. J., Ahmed, Y. A., Tatarczuch, L., Chen, K. S. & Mirams, M. 2008. Endochondral ossification: How cartilage is converted into bone in the developing skeleton. *International Journal of Biochemistry & Cell Biology,* 40**,** 46-62.

Mackie, E. J., Tatarczuch, L. & Mirams, M. 2011. The skeleton: a multi-functional complex organ. The growth plate chondrocyte and endochondral ossification. *Journal of Endocrinology,* 211**,** 109-121.

Macnabb, C., Patton, D. & Hayes, J. S. 2016. Sclerostin Antibody Therapy for the Treatment of Osteoporosis: Clinical Prospects and Challenges. *Journal of Osteoporosis*.

Macrae, V. E., Farquharson, C. & Ahmed, S. F. 2006. The restricted potential for recovery of growth plate chondrogenesis and longitudinal bone growth following exposure to pro-inflammatory cytokines. *Journal of Endocrinology,* 189**,** 319-328.

Macrae, V. E., Davey, M. G., Mcteir, L., Narisawa, S., Yadav, M. C., Millan, J. L. & Farquharson, C. 2010. Inhibition of PHOSPHO1 activity results in impaired skeletal mineralization during limb development of the chick. *Bone,* 46**,** 1146-1155.

Maes, C., Kobayashi, T. & Kronenberg, H. M. 2007. A Novel Transgenic Mouse Model to Study the Osteoblast Lineage in Vivo. *Annals of the New York Academy of Sciences,* 1116**,** 149-164.

Mannstadt, M., Juppner, H. & Gardella, T. J. 1999. Receptors for PTH and PTHrP: their biological importance and functional properties. *American Journal of Physiology-Renal Physiology,* 277**,** F665-F675.

Marcinowska-Suchowierska, E. B., Talalaj, M. J., Wlodarcyzk, A. W., Bielecki, K., Zawadzki, J. J. & Brzozowski, R. 1995. Calcium/phosphate/vitamin D homeostasis and bone mass in patients after gastrectomy, vagotomy, and cholecystectomy. *World Journal of Surgery,* 19**,** 597-601; discussion 601-2.

Marino, S., Staines, K. A., Brown, G., Howard-Jones, R. A. & Adamczyk, M. 2016. Models of ex vivo explant cultures: applications in bone research. *BoneKEy Reports,* 5.

Martin, A., David, V., Laurence, J. S., Schwarz, P. M., Lafer, E. M., Hedge, A. M. & Rowe, P. S. N. 2008. Degradation of MEPE, DMP1, and release of SIBLING ASARM-peptides (minhibins): ASARM-Peptide(s) are directly responsible for defective mineralization in HYP. *Endocrinology,* 149**,** 1757-1772.

Mckee, M. D., Yadav, M. C., Foster, B. L., Somerman, M. J., Farquharson, C. & Millán, J. L. 2013. Compounded PHOSPHO1/ALPL Deficiencies Reduce Dentin Mineralization. *Journal of Dental Research*.

Mcmahon, D. 1975. Cycloheximide is not a Specific Inhibitor of Protein-Synthesis In vivo. *Plant Physiology,* 55**,** 815-821.

Mcnally, E. A., Schwarcz, H. P., Botton, G. A. & Arsenault, A. L. 2012. A model for the ultrastructure of bone based on electron microscopy of ion-milled sections. *Plos One,* 7**,** e29258.

Mebarek, S., Abousalham, A., Magne, D., Le Duy, D., Bandorowicz-Pikula, J., Pikula, S. & Buchet, R. 2013. Phospholipases of Mineralization Competent Cells and Matrix Vesicles: Roles in Physiological and Pathological Mineralizations. *International Journal of Molecular Sciences,* 14**,** 5036-5129.

Merrill, A. H., Sullards, M. C., Allegood, J. C., Kelly, S. & Wang, E. 2005. Sphingolipidomics: High-throughput, structure-specific, and quantitative analysis of sphingolipids by liquid chromatography tandem mass spectrometry. *Methods,* 36**,** 207-224.

Merrill, A. H. 2011. Sphingolipid and Glycosphingolipid Metabolic Pathways in the Era of Sphingolipidomics. *Chemical Reviews,* 111**,** 6387-6422.

Millan, J. L. 2006. Alkaline Phosphatases : Structure, substrate specificity and functional relatedness to other members of a large superfamily of enzymes. *Purinergic Signalling,* 2**,** 335-41.

Millán, J. 2012. The Role of Phosphatases in the Initiation of Skeletal Mineralization. *Calcified Tissue International***,** 1-8.

Millán, J. L. & Whyte, M. P. 2015. Alkaline Phosphatase and Hypophosphatasia. *Calcified Tissue International***,** 1-19.

Momeni, P., Glockner, G., Schmidt, O., Von Holtum, D., Albrecht, B., Gillessen-Kaesbach, G., Hennekam, R., Meinecke, P., Zabel, B., Rosenthal, A., Horsthemke, B. & Ludecke, H. J. 2000. Mutations in a new gene, encoding a zinc-finger protein, cause tricho-rhino-phalangeal syndrome type I. *Nature Genetics,* 24**,** 71-4.

Muriel, M. P., Bonaventure, J., Stanescu, R., Maroteaux, P., Guénet, J. L. & Stanescu, V. 1991. Morphological and biochemical studies of a mouse mutant (fro/fro) with bone fragility. *Bone,* 12**,** 241-248.

Nakashima, T., Hayashi, M., Fukunaga, T., Kurata, K., Oh-Hora, M., Feng, J. Q., Bonewald, L. F., Kodama, T., Wutz, A., Wagner, E. F., Penninger, J. M. & Takayanagi, H. 2011. Evidence for

osteocyte regulation of bone homeostasis through RANKL expression. *Nature Medicine,* 17**,** 1231-4.

Napierala, D., Sam, K., Morello, R., Zheng, Q., Munivez, E., Shivdasani, R. A. & Lee, B. 2008. Uncoupling of chondrocyte differentiation and perichondrial mineralization underlies the skeletal dysplasia in tricho-rhino-phalangeal syndrome. *Human Molecular Genetics,* 17**,** 2244-2254.

Narisawa, S., Frohlander, N. & Millan, J. L. 1997. Inactivation of two mouse alkaline phosphatase genes and establishment of a model of infantile hypophosphatasia. *Developmental Dynamics,* 208**,** 432-446.

Narisawa, S., Yadav, M. C. & Millán, J. L. 2013. In Vivo Overexpression of Tissue-Nonspecific Alkaline Phosphatase Increases Skeletal Mineralization and Affects the Phosphorylation Status of Osteopontin. *Journal of Bone and Mineral Research,* 28**,** 1587-1598.

Neer, R. M., Arnaud, C. D., Zanchetta, J. R., Prince, R., Gaich, G. A., Reginster, J. Y., Hodsman, A. B., Eriksen, E. F., Ish-Shalom, S., Genant, H. K., Wang, O. H. & Mitlak, B. H. 2001. Effect of parathyroid hormone (1-34) on fractures and bone mineral density in postmenopausal women with osteoporosis. *New England Journal of Medicine,* 344**,** 1434-1441.

Nishimura, R., Wakabayashi, M., Hata, K., Matsubara, T., Honma, S., Wakisaka, S., Kiyonari, H., Shioi, G., Yamaguchi, A., Tsumaki, N., Akiyama, H. & Yoneda, T. 2012. Osterix Regulates Calcification and Degradation of Chondrogenic Matrices through Matrix Metalloproteinase 13 (MMP13) Expression in Association with Transcription Factor Runx2 during Endochondral Ossification. *Journal of Biological Chemistry,* 287**,** 33179-33190.

Nitschke, Y., Baujat, G., Botschen, U., Wittkampf, T., Du Moulin, M., Stella, J., Le Merrer, M., Guest, G., Lambot, K., Tazarourte-Pinturier, M. F., Chassaing, N., Roche, O., Feenstra, I., Loechner, K., Deshpande, C., Garber, S. J., Chikarmane, R., Steinmann, B., Shahinyan, T., Martorell, L., Davies, J., Smith, W. E., Kahler, S. G., Mcculloch, M., Wraige, E., Loidi, L., Höhne, W., Martin, L., Hadj-Rabia, S., Terkeltaub, R. & Rutsch, F. 2012. Generalized arterial calcification of infancy and pseudoxanthoma elasticum can be caused by mutations in either ENPP1 or ABCC6. *American Journal of Human Genetics,* 90**,** 25-39.

Nudelman, F., Pieterse, K., George, A., Bomans, P. H. H., Friedrich, H., Brylka, L. J., Hilbers, P. a. J., De With, G. & Sommerdijk, N. a. J. M. 2010. The role of collagen in bone apatite formation in the presence of hydroxyapatite nucleation inhibitors. *Nature Materials,* 9**,** 1004-1009.

Okawa, A., Nakamura, I., Goto, S., Moriya, H., Nakamura, Y. & Ikegawa, S. 1998. Mutation in Npps in a mouse model of ossification of the posterior longitudinal ligament of the spine. *Nature Genetics,* 19**,** 271-273.

Oldknow, K. J., Macrae, V. E. & Farquharson, C. 2015. Endocrine role of bone: recent and emerging perspectives beyond osteocalcin. *Journal of Endocrinology,* 225**,** R1-R19.

Onyia, J. E., Helvering, L. M., Gelbert, L., Wei, T., Huang, S. G., Chen, P. N., Dow, E. R., Maran, A., Zhang, M. Z., Lotinun, S., Lin, X., Halladay, D. L., Miles, R. R., Kulkarni, N. H., Ambrose, E.

M., Ma, Y. L., Frolik, C. A., Sato, M., Bryant, H. U. & Turner, R. T. 2005. Molecular profile of catabolic versus anabolic treatment regimens of parathyroid hormone (PTH) in rat bone: An analysis by DNA microarray. *Journal of Cellular Biochemistry,* 95**,** 403-418.

Orimo, H. & Shimada, T. 2006. Effects of phosphates on the expression of tissue-nonspecific alkaline phosphatase gene and phosphate-regulating genes in short-term cultures of human osteosarcoma cell lines. *Molecular and Cellular Biochemistry,* 282**,** 101-108.

Pazianas, M. 2015. Anabolic effects of PTH and the 'anabolic window'. *Trends in Endocrinology & Metabolism,* 26**,** 111-113.

Pioszak, A. A. & Xu, H. E. 2008. Molecular recognition of parathyroid hormone by its G protein-coupled receptor. *Proceedings of the National Academy of Sciences,* 105**,** 5034-5039.

Poole, K. E. S. & Reeve, J. 2005. Parathyroid hormone - a bone anabolic and catabolic agent. *Current Opinion in Pharmacology,* 5**,** 612-617.

Potts Jr, J. T., Kronenberg, H. M. & Rosenblatt, M. 1982. Parathyroid Hormone: Chemistry, Biosynthesis, and Mode of Action. *In:* C.B. ANFINSEN, J. T. E. & FREDERIC, M. R. (eds.) *Advances in Protein Chemistry.* Academic Press.

Potts, J. T. 2005. Parathyroid hormone: past and present. *Journal of Endocrinology,* 187**,** 311-325.

Prideaux, M., Loveridge, N., Pitsillides, A. A. & Farquharson, C. 2012. Extracellular Matrix Mineralization Promotes E11/gp38 Glycoprotein Expression and Drives Osteocytic Differentiation. *Plos One,* 7**,** e36786.

Provot, S. & Schipani, E. 2005. Molecular mechanisms of endochondral bone development. *Biochemical Biophysical Research Communications,* 328**,** 658-665.

Qin, L., Qiu, P., Wang, L. Q., Li, X., Swarthout, J. T., Soteropoulos, P., Tolias, P. & Partridge, N. C. 2003. Gene expression profiles and transcription factors involved in parathyroid hormone signaling in osteoblasts revealed by microarray and bioinformatics. *Journal of Biological Chemistry,* 278**,** 19723-19731.

Qin, L., Raggatt, L. J. & Partridge, N. C. 2004. Parathyroid hormone: a double-edged sword for bone metabolism. *Trends in Endocrinology and Metabolism,* 15**,** 60-65.

Rashid, F., Shiba, H., Mizuno, N., Mouri, Y., Fujita, T., Shinohara, H., Ogawa, T., Kawaguchi, H. & Kurihara, H. 2003. The effect of extracellular calcium ion on gene expression of bone-related proteins in human pulp cells. *Journal of Endodontics,* 29**,** 104-107.

Reeve, J., Hesp, R., Williams, D., Hulme, P., Klenerman, L., Zanelli, J., Darby, A. J., Tregear, G. W. & Parsons, J. A. 1976a. Anabolic effect of low doses of a fragment of human parathyroid hormone on the skeleton in postmenopausal osteoporosis. *The Lancet,* 307**,** 1035-1038.

Reeve, J., Tregear, G. W. & Parsons, J. A. 1976b. Preliminary trial of low-doses of human parathyroid-hormone 1-34 peptide in treatment of osteoporosis. *Calcified Tissue Research,* 21**,** 469-477.

Register, T. C., Mclean, F. M., Low, M. G. & Wuthier, R. E. 1986. Roles of Alkaline-Phosphatase and Labile Internal Mineral in Matrix Vesicle-Mediated Calcification - Effect of Selective Release of Membrane-Bound Alkaline-Phosphatase and Treatment with Isosmotic pH-6 Buffer. *Journal of Biological Chemistry,* 261**,** 9354-9360.

Reinholt, F. P. & Wernerson, A. 1988. Septal distribution and the relationship of matrix vesicle size to cartilage mineralization. *Bone and Mineral,* 4**,** 63-71.

Revollo, L. & Civitelli, R. 2015. Chapter 7 - Molecular Actions of Parathyroid Hormone A2 - Bilezikian, John P. *The Parathyroids (Third Edition).* San Diego: Academic Press.

Rey, A., Manen, D., Rizzoli, R., Ferrari, S. L. & Caverzasio, J. 2007. Evidences for a role of p38 MAP kinase in the stimulation of alkaline phosphatase and matrix mineralization induced by parathyroid hormone in osteoblastic cells. *Bone,* 41**,** 59-67.

Rico, H., Revilla, M., Arribas, I., Villa, L. F. & Debuergo, M. A. 1994. Total and regional bone-mineral content in primary hyperparathyroidism - sex-differences. *Mineral and Electrolyte Metabolism,* 20**,** 112-116.

Roach, H. I., Aigner, T. & Kouri, J. B. 2004. Chondroptosis: a variant of apoptotic cell death in chondrocytes? *Apoptosis,* 9**,** 265-77.

Roberts, S., Narisawa, S., Harmey, D., Millan, J. L. & Farquharson, C. 2007. Functional involvement of PHOSPHO1 in matrix vesicle-mediated skeletal mineralization. *Journal of Bone and Mineral Research,* 22**,** 617-627.

Roberts, S. J., Stewart, A. J., Sadler, P. J. & Farquharson, C. 2004. Human PHOSPH01 exhibits high specific phosphoethanolamine and phosphocholine phosphatase activities. *Biochemical Journal,* 382**,** 59-65.

Robison, R. 1923. The possible significance of hexosephosphoric esters in ossification. *Biochemical Journal,* 17**,** 286-293.

Robling, A. G., Niziolek, P. J., Baldridge, L. A., Condon, K. W., Allen, M. R., Alam, I., Mantila, S. M., Gluhak-Heinrich, J., Bellido, T. M., Harris, S. E. & Turner, C. H. 2008. Mechanical stimulation of bone in vivo reduces osteocyte expression of Sost/sclerostin. *Journal of Biological Chemistry,* 283**,** 5866-75.

Rodriguez-Florez, N., Garcia-Tunon, E., Mukadam, Q., Saiz, E., Oldknow, K. J., Farquharson, C., Millan, J. L., Boyde, A. & Shefelbine, S. J. 2015. An Investigation of the Mineral in Ductile and Brittle Cortical Mouse Bone. *Journal of Bone and Mineral Research,* 30**,** 786-795.

Rowe, P. S. N. 2012. The chicken or the egg: PHEX, FGF23 and SIBLINGs unscrambled. *Cell Biochemistry and Function,* 30**,** 355-375.

Rubin, R. M., Cosman, F., Lindsay, R. & Bilezikian, P. J. 2002. The Anabolic Effects of Parathyroid Hormone. *Osteoporosis International,* 13**,** 267-277.

Rubin, M. R., Manavalan, J. S., Dempster, D. W., Shah, J., Cremers, S., Kousteni, S., Zhou, H., Mcmahon, D. J., Kode, A., Sliney, J., Shane, E., Silverberg, S. J. & Bilezikian, J. P. 2011. Parathyroid Hormone Stimulates Circulating Osteogenic Cells in Hypoparathyroidism. *The Journal of Clinical Endocrinology and Metabolism,* 96**,** 176-186.

Russell, R. G. G. & Fleisch, H. 1975. Pyrophosphate and Diphosphonates in Skeletal Metabolism - Physiological, Clinical and Therapeutic Aspects. *Clinical Orthopaedic Related Research***,** 241-263.

Rutsch, F., Schauerte, P., Kalhoff, H., Petrarulo, M., August, C. & Diekmann, L. 2000. Low levels of urinary inorganic pyrophosphate indicating systemic pyrophosphate deficiency in a boy with idiopathic infantile arterial calcification. *Acta Paediatrica, International Journal of Paediatrics,* 89**,** 1265-1269.

Sakagami, H., Aoki, J., Natori, Y., Nishikawa, K., Kakehi, Y., Natori, Y. & Arai, H. 2005. Biochemical and Molecular Characterization of a Novel Choline-specific Glycerophosphodiester Phosphodiesterase Belonging to the Nucleotide Pyrophosphatase/Phosphodiesterase Family. *Journal of Biological Chemistry,* 280**,** 23084-23093.

Samee, N., Geoffroy, V., Marty, C., Schiltz, C., Vieux-Rochas, M., Levi, G. & De Vernejoul, M.-C. 2008. Dlx5, a Positive Regulator of Osteoblastogenesis, is Essential for Osteoblast-Osteoclast Coupling. *The American Journal of Pathology,* 173**,** 773-780.

Sander, J. D. & Joung, J. K. 2014. CRISPR-Cas systems for editing, regulating and targeting genomes. *Nature Biotechnology,* 32**,** 347-355.

Sayegh, F. S., Solomon, G. C. & Davis, R. W. 1974. Ultrastructure of intracellular mineralization in the deer's antler. *Clinical Orthopaedic Related Research***,** 267-84.

Scheven, B. A. & Hamilton, N. J. 1991. Longitudinal bone growth in vitro: effects of insulin-like growth factor I and growth hormone. *Acta Endocrinology (Copenh),* 124**,** 602-7.

Schindeler, A., Mcdonald, M. M., Bokko, P. & Little, D. G. 2008. Bone remodeling during fracture repair: The cellular picture. *Seminars in Cell and Developmental Biology,* 19**,** 459-66.

Schluter, K. D. 1999. PTH and PTHrP: Similar structures but different functions. *News in Physiological Sciences,* 14**,** 243-249.

Sela, J. & Bab, I. A. 1979. The relationship between extracellular matrix vesicles and calcospherities in primary mineralization of neoplastic bone tissue. TEM and SEM studies on osteosarcoma. *Virchows Archive A. Pathological Anatomy and Histology,* 382**,** 1-9.

Shah, V. N., Bhadada, S. K., Bhansali, A., Behera, A., Mittal, B. R. & Bhavin, V. 2012. Influence of age and gender on presentation of symptomatic primary hyperparathyroidism. *Journal of Postgraduate Medicine,* 58**,** 107-111.

Sher, R. B., Aoyama, C., Huebsch, K. A., Ji, S., Kerner, J., Yang, Y., Frankel, W. N., Hoppel, C. L., Wood, P. A., Vance, D. E. & Cox, G. A. 2006. A Rostrocaudal Muscular Dystrophy Caused by a Defect in Choline Kinase Beta, the First Enzyme in Phosphatidylcholine Biosynthesis. *Journal of Biological Chemistry,* 281**,** 4938-4948.

Shimada, T., Kakitani, M., Yamazaki, Y., Hasegawa, H., Takeuchi, Y., Fujita, T., Fukumoto, S., Tomizuka, K. & Yamashita, T. 2004. Targeted ablation of Fgf23 demonstrates an essential physiological role of FGF23 in phosphate and vitamin D metabolism. *Journal of Clinical Investigation,* 113**,** 561-8.

Shore, E. M., Xu, M., Feldman, G. J., Fenstermacher, D. A., Cho, T.-J., Choi, I. H., Connor, J. M., Delai, P., Glaser, D. L., Lemerrer, M., Morhart, R., Rogers, J. G., Smith, R., Triffitt, J. T., Urtizberea, J. A., Zasloff, M., Brown, M. A. & Kaplan, F. S. 2006. A recurrent mutation in the BMP type I receptor ACVR1 causes inherited and sporadic fibrodysplasia ossificans progressiva. *Nature Genetics,* 38**,** 525-527.

Silva, B. C. & Bilezikian, J. P. 2015. Parathyroid hormone: anabolic and catabolic actions on the skeleton. *Current Opinion in Pharmacology,* 22**,** 41-50.

Silva, B. C. & Kousteni, S. 2015. Chapter 8 - Cellular Actions of PTH: Osteoblasts, Osteoclasts, and Osteocytes A2 - Bilezikian, John P. *The Parathyroids (Third Edition).* San Diego: Academic Press.

Simonet, W. S., Lacey, D. L., Dunstan, C. R., Kelley, M., Chang, M. S., Lüthy, R., Nguyen, H. Q., Wooden, S., Bennett, L., Boone, T., Shimamoto, G., Derose, M., Elliott, R., Colombero, A., Tan, H. L., Trail, G., Sullivan, J., Davy, E., Bucay, N., Renshaw-Gegg, L., Hughes, T. M., Hill, D., Pattison, W., Campbell, P., Sander, S., Van, G., Tarpley, J., Derby, P., Lee, R. & Boyle, W. J. 1997. Osteoprotegerin: A Novel Secreted Protein Involved in the Regulation of Bone Density. *Cell,* 89**,** 309-319.

Sisca, R. F. & Provenza, D. V. 1972. Initial dentin formation in human deciduous teeth. An electron microscope study. *Calcified Tissue Research,* 9**,** 1-16.

Sommerfeldt, D. W. & Rubin, C. T. 2001. Biology of bone and how it orchestrates the form and function of the skeleton. *European Spine Journal,* 10 Suppl 2**,** S86-95.

Sousa, S. B., Jenkins, D., Chanudet, E., Tasseva, G., Ishida, M., Anderson, G., Docker, J., Ryten, M., Sa, J., Saraiva, J. M., Barnicoat, A., Scott, R., Calder, A., Wattanasirichaigoon, D., Chrzanowska, K., Simandlová, M., Van Maldergem, L., Stanier, P., Beales, P. L., Vance, J. E. & Moore, G. E. 2014. Gain-of-function mutations in the phosphatidylserine synthase 1 (PTDSS1) gene cause Lenz-Majewski syndrome. *Nature Genetics,* 46**,** 70-76.

Speer, M. Y., Mckee, M. D., Guldberg, R. E., Liaw, L., Yang, H. Y., Tung, E., Karsenty, G. & Giachelli, C. M. 2002. Inactivation of the osteopontin gene enhances vascular calcification of matrix Gla protein-deficient mice: Evidence for osteopontin as an inducible inhibitor of vascular calcification in vivo. *Journal of Experimental Medicine,* 196**,** 1047-1055.

St John, H. C., Meyer, M. B., Benkusky, N. A., Carlson, A. H., Prideaux, M., Bonewald, L. F. & Pike, J. W. 2015. The parathyroid hormone-regulated transcriptome in osteocytes: Parallel

actions with 1,25-dihydroxyvitamin D-3 to oppose gene expression changes during differentiation and to promote mature cell function. *Bone,* 72**,** 81-91.

Staines, K. A., Mackenzie, N. C. W., Clarkin, C. E., Zelenchuk, L., Rowe, P. S., Macrae, V. E. & Farquharson, C. 2012. MEPE is a novel regulator of growth plate cartilage mineralization. *Bone,* 51**,** 418-430.

Staines, K. A., Prideaux, M., Allen, S., Buttle, D. J., Pitsillides, A. A. & Farquharson, C. 2016. E11/Podoplanin Protein Stabilization Through Inhibition of the Proteasome Promotes Osteocyte Differentiation in Murine in Vitro Models. *Journal of Cellular Physiology,* 231**,** 1392-1404.

Stenbeck, G. & Horton, M. A. 2004. Endocytic trafficking in actively resorbing osteoclasts. *Journal of Cell Science,* 117**,** 827-836.

Stern, P. H. & Vance, D. E. 1987. Phosphatidylcholine metabolism in neonatal mouse calvaria. *Biochemical Journal,* 244**,** 409-415.

Stewart, A. J., Schmid, R., Blindauer, C. A., Paisey, S. J. & Farquharson, C. 2003. Comparative modelling of human PHOSPHO1 reveals a new group of phosphatases within the haloacid dehalogenase superfamily. *Protein Engineering,* 16**,** 889-895.

Stewart, A. J., Roberts, S. J., Seawright, E., Davey, M. G., Fleming, R. H. & Farquharson, C. 2006. The presence of PHOSPHO1 in matrix vesicles and its developmental expression prior to skeletal mineralization. *Bone,* 39**,** 1000-1007.

Stoffel, W., Jenke, B., Block, B., Zumbansen, M. & Koebke, J. 2005. Neutral sphingomyelinase 2 (smpd3) in the control of postnatal growth and development. *Proceedings of the National Academy of Sciences,* 102**,** 4554-4559.

Stoffel, W., Jenke, B., Holz, B., Binczek, E., Guenter, R. H., Knifka, J., Koebke, J. & Niehoff, A. 2007. Neutral sphingomyelinase (SMPD3) deficiency causes a novel form of chondrodysplasia and dwarfism that is rescued by Col2A1-driven smpd3 transgene expression. *American Journal of Pathology,* 171**,** 153-161.

Sudo, H., Kodama, H. A., Amagai, Y., Yamamoto, S. & Kasai, S. 1983. In vitro differentiation and calcification in a new clonal osteogenic cell line derived from newborn mouse calvaria. *Journal of Cellular Biology,* 96**,** 191-198.

Sugiyama, T., Saxon, L. K., Zaman, G., Moustafa, A., Sunters, A., Price, J. S. & Lanyon, L. E. 2008. Mechanical loading enhances the anabolic effects of intermittent parathyroid hormone (1–34) on trabecular and cortical bone in mice. *Bone,* 43**,** 238-248.

Suzuki, A., Ghayor, C., Guicheux, J., Magne, D., Quillard, S., Kakita, A., Ono, Y., Miura, Y., Oiso, Y., Itoh, M. & Caverzasio, J. 2006. Enhanced expression of the inorganic phosphate transporter Pit-1 is involved in BMP-2-Induced matrix mineralization in osteoblast-like cells. *Journal of Bone and Mineral Research,* 21**,** 674-683.

Targownik, L. E., Lix, L. M., Metge, C. J., Prior, H. J., Leung, S. & Leslie, W. D. 2008. Use of proton pump inhibitors and risk of osteoporosis-related fractures. *Canadian Medical Association Journal,* 179**,** 319-26.

Teitelbaum, S. L. 2000. Bone Resorption by Osteoclasts. *Science,* 289**,** 1504-1508.

Terakado, A., Tagawa, M., Goto, S., Yamazaki, M., Moriya, H. & Fujimura, S. 1995. Elevation of alkaline phosphatase activity induced by parathyroid hormone in osteoblast-like cells from the spinal hyperostotic mouse TWY (twy/twy). *Calcified Tissue International,* 56**,** 135-139.

Terkeltaub, R. 2006. Physiologic and pathologic functions of the NPP nucleotide pyrophosphatase/phosphodiesterase family focusing on NPP1 in calcification. *Purinergic Signalling,* 2**,** 371-377.

Thouverey, C., Malinowska, A., Balcerzak, M., Strzelecka-Kiliszek, A., Buchet, R., Dadlez, M. & Pikula, S. 2011. Proteomic characterization of biogenesis and functions of matrix vesicles released from mineralizing human osteoblast-like cells. *Journal of Proteomics,* 74**,** 1123-1134.
Thouverey, C., Strzelecka-Kiliszek, A., Balcerzak, M., Buchet, R. & Pikula, S. 2009. Matrix vesicles originate from apical membrane microvilli of mineralizing osteoblast-like Saos-2 cells. *Journal of Cellular Biochemistry,* 106**,** 127-138.

Tintut, Y., Parhami, F., Le, V., Karsenty, G. & Demer, L. L. 1999. Inhibition of Osteoblast-specific Transcription Factor Cbfa1 by the cAMP Pathway in Osteoblastic Cells: Ubiquitin/Proteosome-dependent regulation. *Journal of Biological Chemistry,* 274**,** 28875-28879.

Uchida, T. 1994. Regulation of choline kinase r: Analyses of alternatively spliced choline kinases and the promoter region. *Journal of Biochemistry,* 116**,** 508-518.

Ueno, Y., Shinki, T., Nagai, Y., Murayama, H., Fujii, K. & Suda, T. 2003. In vivo administration of 1,25-dihydroxyvitamin D3 suppresses the expression of RANKL mRNA in bone of thyroparathyroidectomized rats constantly infused with PTH. *Journal of Cellular Biochemistry,* 90**,** 267-77.

Uzawa, T., Hori, M., Ejiri, S. & Ozawa, H. 1995. Comparison of the effects of intermittent and continuous administration of human parathyroid hormone(1–34) on rat bone. *Bone,* 16**,** 477-484.

Valentin-Opran, A., Wozney, J., Csimma, C., Lilly, L. & Riedel, G. E. 2002. Clinical evaluation of recombinant human bone morphogenetic protein-2. *Clin Orthop Relat Res***,** 110-20.

Van Der Horst, G., Farih-Sips, H., Lowik, C. & Karperien, M. 2005. Multiple mechanisms are involved in inhibition of osteoblast differentiation by PTHrP and PTH in KS483 cells. *Journal of Bone and Mineral Research,* 20**,** 2233-2244.

Vestergaard, P., Rejnmark, L. & Mosekilde, L. 2006. Proton pump inhibitors, histamine H2 receptor antagonists, and other antacid medications and the risk of fracture. *Calcified Tissue Interntional,* 79**,** 76-83.

Walsh, J. S. 2015. Normal bone physiology, remodelling and its hormonal regulation. *Surgery (Oxford),* 33**,** 1-6.

Wan, M., Yang, C. Z., Li, J., Wu, X. W., Yuan, H. L., Ma, H. R., He, X., Nie, S. Y., Chang, C. B. & Cao, X. 2008. Parathyroid hormone signaling through low-density lipoprotein-related protein 6. *Genes & Development,* 22**,** 2968-2979.

Wang, D., Christensen, K., Chawla, K., Xiao, G. Z., Krebsbach, P. H. & Franceschi, R. T. 1999. Isolation and characterization of MC3T3-E1 preosteoblast subclones with distinct in vitro and in vivo differentiation mineralization potential. *Journal of Bone and Mineral Research,* 14**,** 893-903.

Wang, W., Xu, J., Du, B. & Kirsch, T. 2005. Role of the Progressive Ankylosis Gene (ank) in Cartilage Mineralization. *Molecular and Cellular Biology,* 25**,** 312-323.

Wang, Y., Ho, C. C., Bang, E., Rejon, C. A., Libasci, V., Pertchenko, P., Hébert, T. E. & Bernard, D. J. 2014. Bone Morphogenetic Protein 2 Stimulates Noncanonical SMAD2/3 Signaling via the BMP Type 1A Receptor in Gonadotrope-Like Cells: Implications for FSH Synthesis. *Endocrinology,* 155**,** 1970-1981.

Weiss, M. J., Cole, D. E., Ray, K., Whyte, M. P., Lafferty, M. A., Mulivor, R. A. & Harris, H. 1988. A missense mutation in the human liver/bone/kidney alkaline phosphatase gene causing a lethal form of hypophosphatasia. *Proceedings of the National Academy of Sciences,* 85**,** 7666-7669.

White, A. P., Vaccaro, A. R., Hall, J. A., Whang, P. G., Friel, B. C. & Mckee, M. D. 2007. Clinical applications of BMP-7/OP-1 in fractures, nonunions and spinal fusion. *International Orthopaedics,* 31**,** 735-41.

Whyte, M. P. 2010. Physiological role of alkaline phosphatase explored in hypophosphatasia. *In:* ZAIDI, M. (ed.) *Skeletal Biology and Medicine.*

Whyte, M. P., Zhang, F., Wenkert, D., Mcalister, W. H., Mack, K. E., Benigno, M. C., Coburn, S. P., Wagy, S., Griffin, D. M., Ericson, K. L. & Mumm, S. 2015. Hypophosphatasia: Validation and expansion of the clinical nosology for children from 25 years experience with 173 pediatric patients. *Bone,* 75**,** 229-239.

Williams, G. R. 2013. Thyroid Hormone Actions in Cartilage and Bone. *European Thyroid Journal,* 2**,** 3-13.

Wolf, M., Jaeger, A., Abuduwali, N., Goetz, W. & Lossdoerfer, S. 2013. Continuous PTH modulates alkaline phosphatase activity in human PDL cells via protein kinase C dependent pathways in vitro. *Annals of Anatomy-Anatomischer Anzeiger,* 195**,** 455-460.

Woo, S. M., Rosser, J., Dusevich, V., Kalajzic, I. & Bonewald, L. F. 2011. Cell Line IDG-SW3 Replicates Osteoblast-to-Late-Osteocyte Differentiation In Vitro and Accelerates Bone Formation In Vivo. *Journal of Bone and Mineral Research,* 26**,** 2634-2646.

Wu, G., Aoyama, C., Young, S. G. & Vance, D. E. 2008. Early Embryonic Lethality Caused by Disruption of the Gene for Choline Kinase α, the First Enzyme in Phosphatidylcholine Biosynthesis. *Journal of Biological Chemistry,* 283**,** 1456-1462.

Wu, G., Sher, R. B., Cox, G. A. & Vance, D. E. 2010. Differential expression of choline kinase isoforms in skeletal muscle explains the phenotypic variability in the rostrocaudal muscular dystrophy mouse. *Biochimica et Biophysica Acta (BBA) - Molecular and Cell Biology of Lipids,* 1801**,** 446-454.

Wu, L. N. Y., Genge, B. R., Kang, M. W., Arsenault, A. L. & Wuthier, R. E. 2002. Changes in phospholipid extractability and composition accompany mineralization of chicken growth plate cartilage matrix vesicles. *Journal of Biological Chemistry,* 277**,** 5126-5133.

Wu, L. N. Y., Genge, B. R. & Wuthier, R. E. 2009. Differential effects of zinc and magnesium ions on mineralization activity of phosphatidylserine calcium phosphate complexes. *Journal of Inorganic Biochemistry,* 103**,** 948-962.

Wuthier, R. E. & Lipscomb, G. F. 2011. Matrix vesicles: structure, composition, formation and function in calcification. *Frontiers in Bioscience,* 16**,** 2812-+.

Xiao, Y. T., Xiang, L. X. & Shao, J. Z. 2007. Bone morphogenetic protein. *Biochemical and Biophysical Research Communications,* 362**,** 550-3.

Xiao, Z., Blonder, J., Zhou, M. & Veenstra, T. D. 2009. Proteomic analysis of extracellular matrix and vesicles. *Journal of Proteomics,* 72**,** 34-45.

Yadav, M. C., Simao, A. M. S., Narisawa, S., Huesa, C., Mckee, M. D., Farquharson, C. & Millan, J. L. 2011. Loss of Skeletal Mineralization by the Simultaneous Ablation of PHOSPHO1 and Alkaline Phosphatase Function: A Unified Model of the Mechanisms of Initiation of Skeletal Calcification. *Journal of Bone and Mineral Research,* 26**,** 286-297.

Yadav, M. C., De Oliveira, R. C., Foster, B. L., Fong, H., Cory, E., Narisawa, S., Sah, R. L., Somerman, M., Whyte, M. P. & Millan, J. L. 2012. Enzyme replacement prevents enamel defects in hypophosphatasia mice. *Journal of Bone and Mineral Research,* 27**,** 1722-1734.

Yadav, M. C., Huesa, C., Narisawa, S., Hoylaerts, M. F., Moreau, A., Farquharson, C. & Millan, J. L. 2014. Ablation of osteopontin improves the skeletal phenotype of phospho1(-/-) mice. *Journal of Bone and Mineral Research,* 29**,** 2369-81.

Yadav, M. C., Bottini, M., Cory, E., Bhattacharya, K., Kuss, P., Narisawa, S., Sah, R. L., Beck, L., Fadeel, B., Farquharson, C. & Millán, J. L. 2016. Skeletal Mineralization Deficits and Impaired Biogenesis and Function of Chondrocyte-Derived Matrix Vesicles in Phospho1-/- and Phospho1/Pit1 Double Knockout Mice. *Journal of Bone and Mineral Research***,** n/a-n/a.

Yamashita, T., Takahashi, N. & Udagawa, N. 2012. New roles of osteoblasts involved in osteoclast differentiation. *World Journal of Orthopedics,* 3**,** 175-181.

Yang, Y. X., Lewis, J. D., Epstein, S. & Metz, D. C. 2006. Long-term proton pump inhibitor therapy and risk of hip fracture. *Journal of the American Medical Association,* 296**,** 2947-53.

Yee, J. A. 1985. Stimulation of alkaline phosphatase activity in cultured neonatal mouse calvarial bone cells by parathyroid hormone. *Calcified Tissue International,* 37**,** 530-538.

Yoshiko, Y., Candeliere, G. A., Maeda, N. & Aubin, J. E. 2007. Osteoblast Autonomous Pi Regulation via Pit1 Plays a Role in Bone Mineralization. *Molecular and Cellular Biology,* 27**,** 4465-4474.

Zaidi, M., Blair, H. C., Moonga, B. S., Abe, E. & Huang, C. L. H. 2003. Osteoclastogenesis, Bone Resorption, and Osteoclast-Based Therapeutics. *Journal of Bone and Mineral Research,* 18**,** 599-609.

Zerega, B., Cermelli, S., Bianco, P., Cancedda, R. & Cancedda, F. D. 1999. Parathyroid hormone PTH(1-34) and parathyroid hormone-related protein PTHrP(1-34) promote reversion of hypertrophic chondrocytes to a prehypertrophic proliferating phenotype and prevent terminal differentiation of osteoblast-like cells. *Journal of Bone and Mineral Research,* 14**,** 1281-1289.

Zhu, D., Mackenzie, N. C., Shanahan, C. M., Shroff, R. C., Farquharson, C. & Macrae, V. E. 2015. BMP-9 regulates the osteoblastic differentiation and calcification of vascular smooth muscle cells through an ALK1 mediated pathway. *Journal of Cellular and Molecular Medicine,* 19**,** 165-74.

Zhu, W., Chen, T., Ding, S., Yang, G., Xu, Z., Xu, K., Zhang, S., Ma, T. & Zhang, J. 2016. Metabolomic study of the bone trabecula of osteonecrosis femoral head patients based on UPLC–MS/MS. *Metabolomics,* 12**,** 1-14.

Zweifler, L. E., Ao, M., Yadav, M., Kuss, P., Narisawa, S., Kolli, T. N., Wimer, H. F., Farquharson, C., Somerman, M. J., Millan, J. L. & Foster, B. L. 2016. Role of PHOSPHO1 in Periodontal Development and Function. *Journal of Dental Research,* 95**,** 742-51.

Appendix

Appendix I – Buffers and solutions

Cell and organ culture media

Maintenance medium

αMEM supplemented with 10% foetal bovine serum (FBS) and 0.05mg/mL gentamicin.

MC3T3 mineralisation medium

αMEM supplemented with: 10% FBS; 0.05mg/mL gentamicin; 50µg/mL L-ascorbic acid; 1.5mM calcium chloride.

Primary osteoblast mineralisation medium

αMEM supplemented with: 10% FBS; 0.05mg/mL gentamicin; 50µg/mL L-ascorbic acid; 6.0mM calcium chloride.

Human osteoblast culture medium

DMEM supplemented with: 20% FBS; 0.6mg/mL L-glutamine; 100U/mL / 100µg/mL penicillin-streptomycin; 1.25µg/ml fungizone.

IDG-SW3 proliferation medium

αMEM supplemented with: 10% FBS; 0.05mg/mL gentamicin; 25U/mL recombinant mouse Interferon-γ.

IDG-SW3 differentiation medium

αMEM supplemented with: 10% FBS; 0.05mg/mL gentamicin; 50µg/mL L-ascorbic acid; 4mM βGP.

Metatarsal preparation medium

0.8ml αMEM medium (without ribonucleosides), 10.45ml sterile PBS, 22.5mg BSA (Fraction V)

Metatarsal culture medium/ Calvariae culture media

αMEM medium (without ribonucleosides) supplemented with: 0.2% w/v BSA (Fraction V); 5µg/mL L-ascorbic acid phosphate; 0.05mg/ml gentamicin; 1.25µg/ml fungizone.

Freezing mix

60% DMEM/F-12, 20% FBS, 20% DMSO

Immunohistochemistry

Citrate buffer

1.92g/L citric acid in dH_2O at pH 6.0

Western Blotting

RIPA buffer

20mM Tris-HCl (pH8), 135mM NaCl, 10% Glycerol, 1% IGEPAL, 0.1% SDS, 0.5% Na Deoxycholate, 2mM EDTA

LDS Sample reducing agent

40% glycerol, 4% LDS, 4% Ficoll*-400, 0.8 M triethanolamine-Cl pH 7.6, 0.025% phenol red, 0.025% coomassie G250, 2mM EDTA disodium

1X Transfer buffer

100ml 10X transfer buffer, 200ml 98% Ethanol, 700ml dH2O.

10X Transfer buffer

29.3mg/ml glycine, 58mg/ml Tris Base (trismethylamine), 18.8µl/ml 20% SDS in dH2O

MOPS running buffer

5% v/v MOPS (50mM MOPS, 50mM Tris, 0.1% SDS, 1mM EDTA, pH 7.7) in dH_2O

Appendix II - qPCR primers

Gene	Source		Sequence (5'-3')
Phospho1	Primer Design	F	TTCTCATTTCGGATGCCAACA
		R	TGAGGATGCGGCGGAATAA
PHOSPHO1 (Human)	MWG Eurofins	F	CTCCCGGGCATTTAAAGGGG
		R	CAAGGGGTGCTTACGGGAAT
Smpd3	MWG Eurofins	F	CTAACCACCCACTCCCACTT
		R	CCAATAGACTCCAAACCTGAAGA
Alpl	MWG Eurofins	F	GGGACGAATCTCAGGGTACA
		R	AGTAACTGGGGTCTCTCTCTTT
Chkα	Primer Design	F	TTCTCATTTCGGATGCCAACA
		R	TGAGGATGCGGCGGAATAA
Chkβ	Primer Design	F	GATGCCACTAGAGCGAGAAG
		R	TCAGAAGTTACGAGACAAGACC
Enpp1	MWG Eurofins	F	GCTAATCATCAGGAGGTCAAG
		R	GCTAATCATCAGGAGGTCAAG
Pth1r	MWG Eurofins	F	CCAACCCTAAGCATCCCAAA
		R	TCCTCGGAGACTGGTAATGG
Runx2	MWG Eurofins	F	TTCTTCACACGCATTCCATCT
		R	GCCAACAGTAAAGTCACAATCC
Sp7	MWG Eurofins	F	CGGTTTGGGTCAGACGATG
		R	GCTTGCCTTTCTTCTTCTTC
Atf4	MWG Eurofins	F	ACTGGTATTTGAGGATTTTGCTAAC
		R	TGTTGTTGACGGTAACTGACTC
Sost	Primer Design	F	ATACCACAATACTGAATCTGAAAGC
		R	CACTATTTGCCTGTCCCTCTG
Trps1	MWG Eurofins	F	GAGCCCAATCACGTTTCAGTT
		R	TCCTTCCTGCTTCTTGCTAGC

Gene	**Source**		**Sequence (5'-3')**
Atp5b	Primer Design	F	Not disclosed
		R	Not disclosed
Gapdh	Primer Design	F	Not disclosed
		R	Not disclosed
GAPDH (Human)	Primer Design	F	Not disclosed
		R	Not disclosed

Appendix III - Antibodies

Primary antibodies

Antibody	Species	Source	Use	Dilution
PHOSPHO1	Human	Abd Serotec, Bio-Rad	Western blotting	1:1000
nSMase2	Rabbit	Santa Cruz Biotech	Western blotting / Immunohistochemistry	1:500 / 1:400
TNAP	Rat	R & D Systems	Western blotting / Immunohistochemistry	1:500 / 1:200
β-actin	Rabbit	Cell signalling technology	Western blotting	1:1000

Secondary antibodies

Antibody	Source	Use	Dilution
Goat anti-rat	Dako	Immunohistochemistry	1:100
Goat anti-rat IRDye 800CW	LI-COR Biosciences	Western Blotting	1:1250
Donkey anti-rabbit IRDye 680RD	LI-COR Biosciences	Western Blotting	1:1250
Goat anti-human IRDye 800CW	LI-COR Biosciences	Western Blotting	1:1250

Appendix IV – Genotyping

DNA extraction solutions

Solution 1

100mL dH_2O, 40µL of 0.5M EDTA, 0.1g NaOH.

Solution 2

96mL dH_2O, 4mL of 1M Tris, pH 5.5.

Genotyping primers

Genotyping assay	Source		Sequence (5'-3')
Phospho1 R74X	INGENOtyping	F	TCCTCCTCACCTTCGACTTC
		R	ATGCGGCGGAATAAACTGT

PCR fragment (355bp)

TCCTCCTCACCTTCGACTTCGATGAGACCATCGTGGACGAGAACAGCGAC
GACTCGATCGTGCGTGCCGCGCCAGGCCAGCAACTGCCCGAGAGCCTGC
GTGCCACCTATCGCGAGGGCTACTACAATGAGTACATGCAA**C/T**GAGTCT
TTAAGTACCTGGGTGAGCAGGGTGTACGGCCCCGGGACCTGCGCGCTGTC
TACGAGACCATCCCCCTGTCGCCAGGCATGGGCGATTTGTTGCAGTTCAT
AGCCAAACAGGGCTCCTGCTTCGAGGTTATTCTCATTTCGGATGCCAACA
CCTTCGGTGTGGAGAGTGCCCTGCGTGCCGCTGGCCACCACAGTTTATTC
CGCCGCAT

WT: C

Phospho1$^{-/-}$: T

Phospho1 genotyping PCR thermal conditions

1. 94°C for 3 min
2. (94°C for 30s, 61°C for 30s 72°C for 90s) x 2
3. (94°C for 30s, 59°C for 30s, 72°C for 30s) x 2
4. (94°C for 30s, 57°C for 30s, 72°C for 90s) x 2
5. (94°C for 30s, 55°C for 30s, 72°C for 30s) x 28
6. 94°C for 30s, 61°C for 30s and 72°C for 10 min

Restriction digest master mix

0.15µL BSA (purified, 100x), 1.5µL NEB buffer 2, 2.85µL dH_2O, 0.5µL BsrD1 restriction enzyme

To 10µL of PCR reaction add 5µL of the restriction digest master mix and incubate at 65°C for 1 h.

Appendix V – Mass spectrometry chromatograms

i) Phosphatidylcholines / Lysophosphatidylcholines

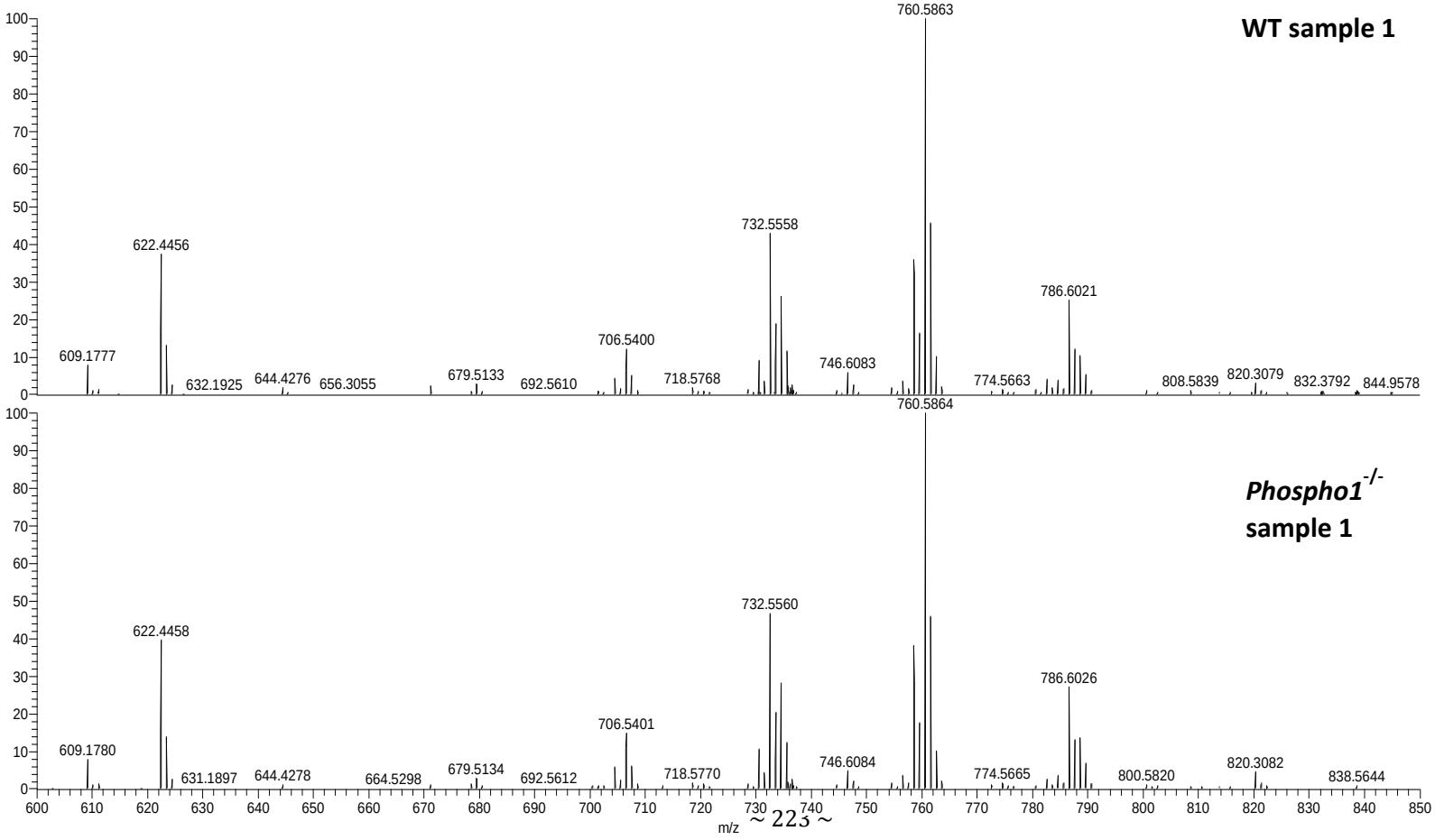

ii) Sphingomyelins

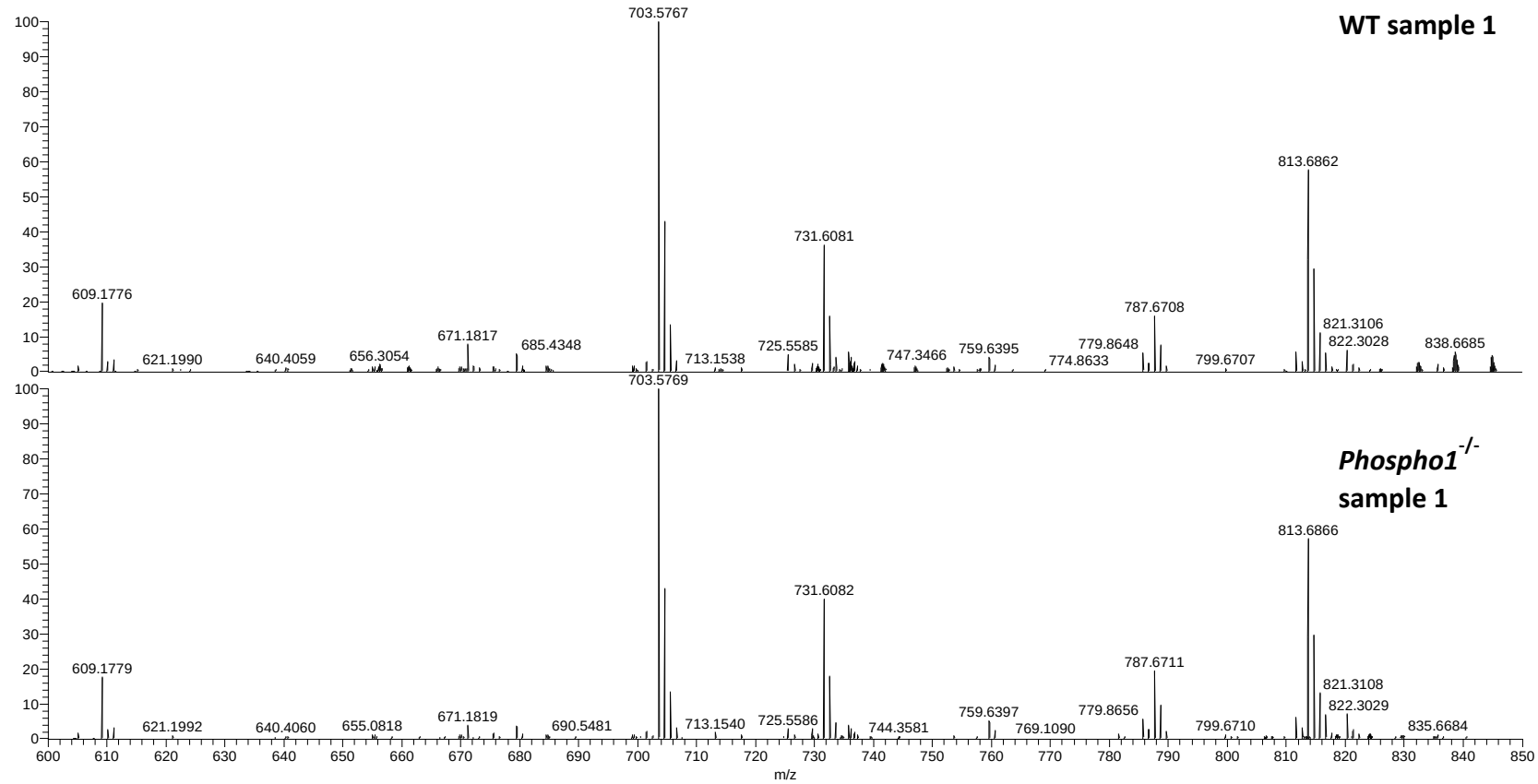

iii) Phosphatidylethanolaines/ Lysophosphatidylethanolamines

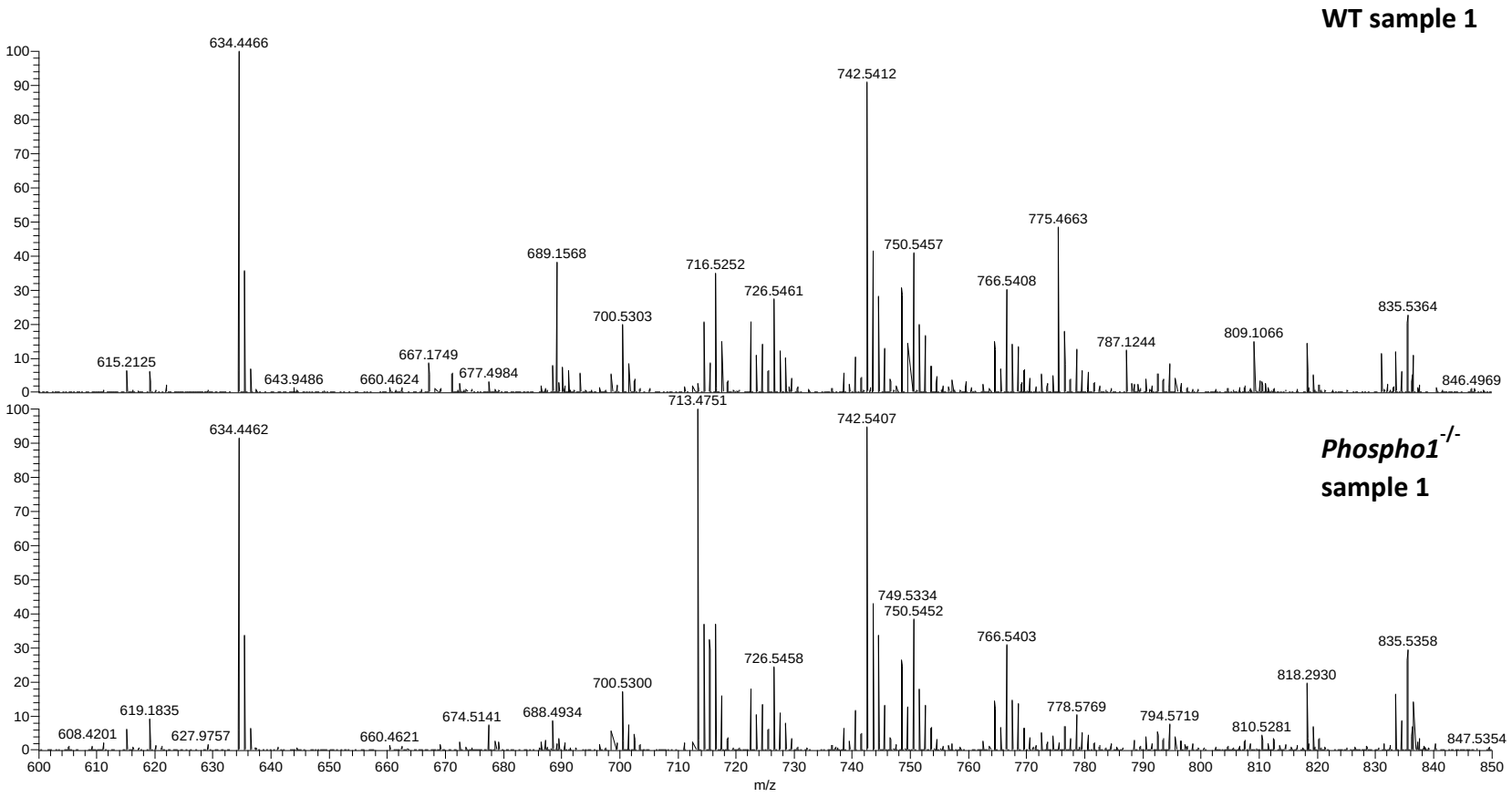

iv) Phosphatidylglycerols

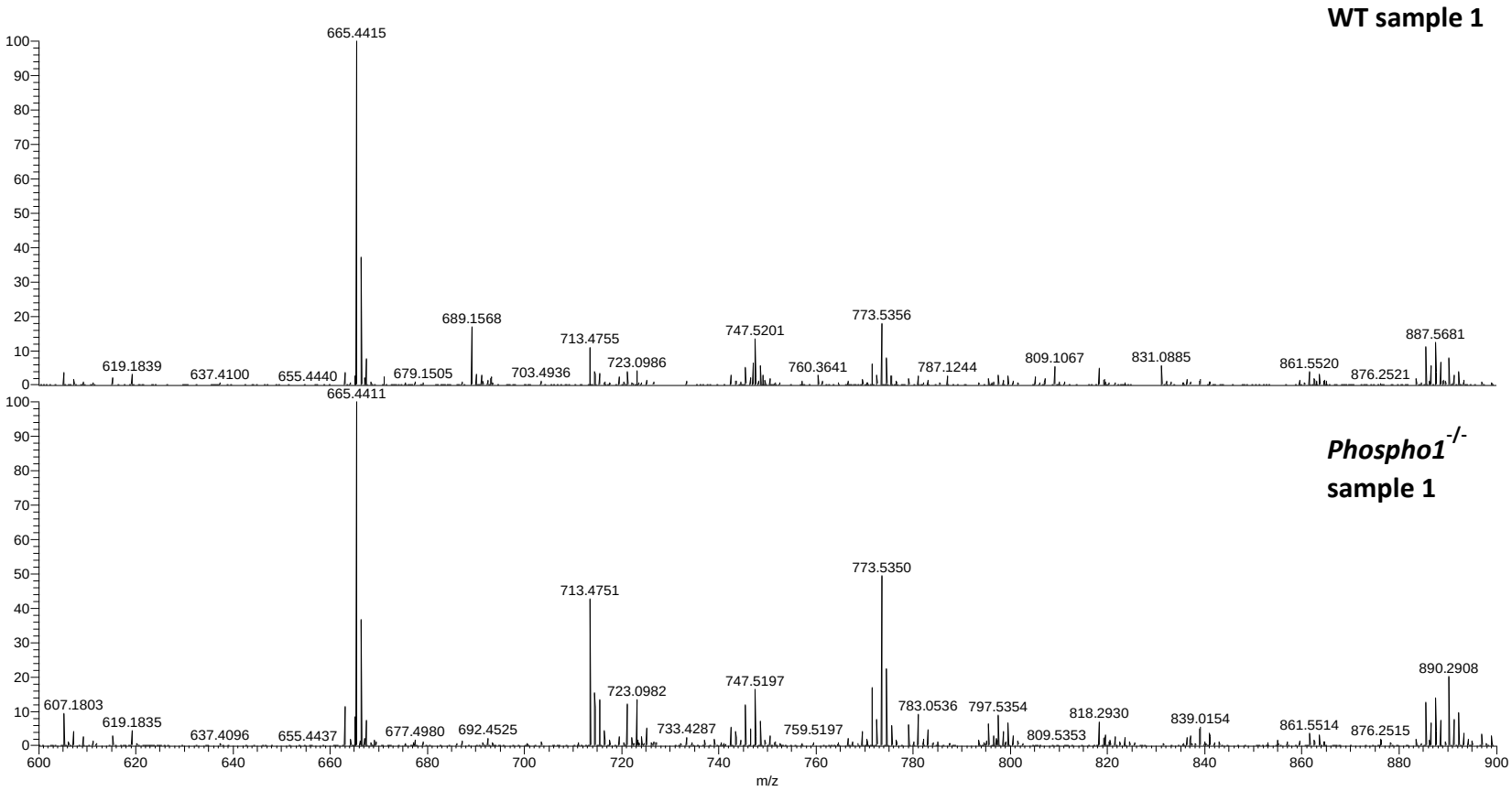

v) Phosphatidylinositols

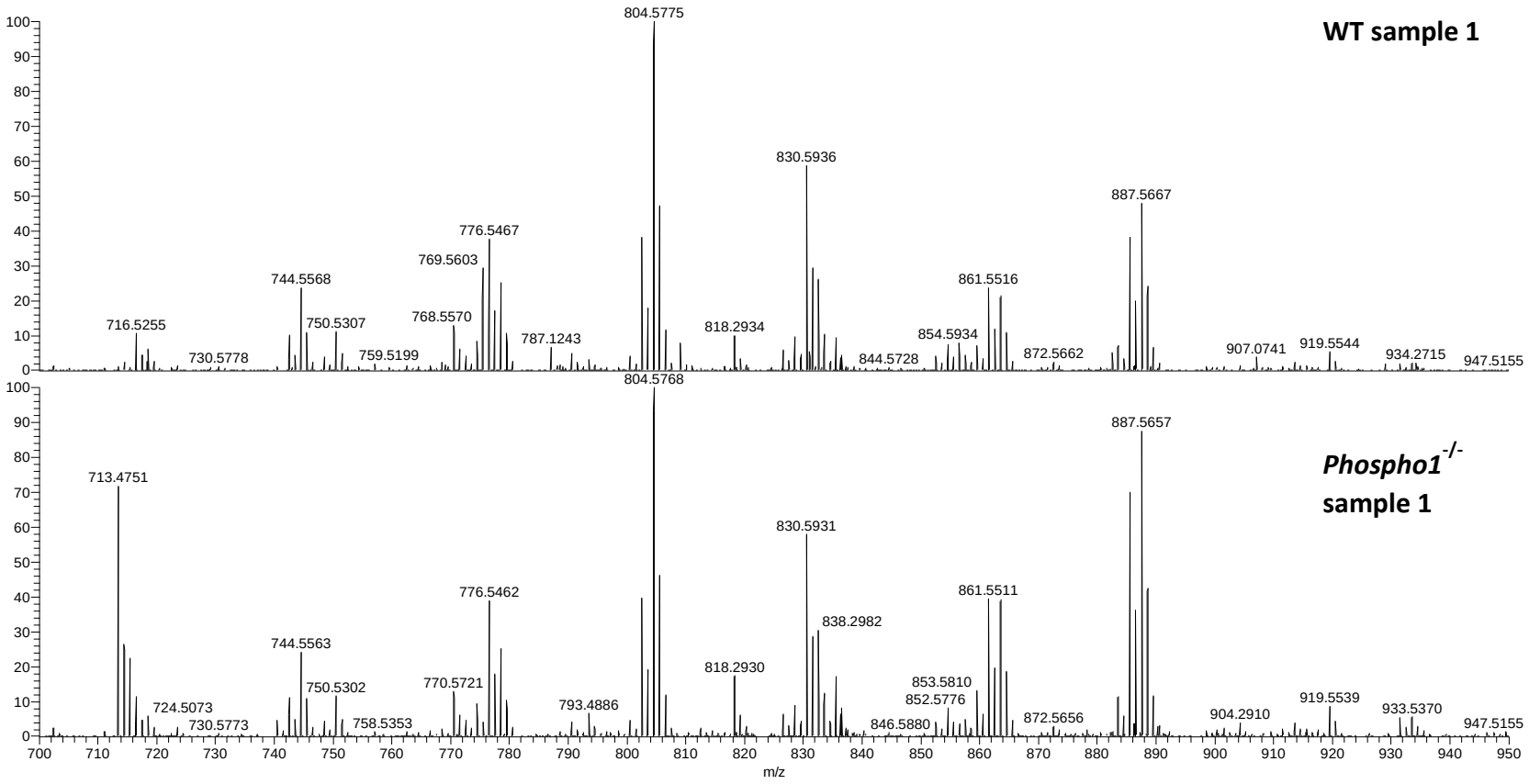

vi) Phosphatidylserines